Structural Behaviour of Hybrid Stainless Steel I-sections

-a Finite Element Study

A thesis submitted for the degree of

Doctor of Philosophy

by

Ricky Lalthazuala

Department of Civil Engineering

Indian Institute of Technology Guwahati

Guwahati-781039, India

August 2019

DECLARATION

I, Ricky Lalthazuala, a PhD Scholar of Indian Institute of Technology Guwahati declares that the content of this thesis entitled "***Structural Behaviour of Hybrid Stainless Steel I-sections – a Finite Element Study***" submitted here is a partial fulfillment for the requirement of awarding the Degree for **Doctor of Philosophy** and submitted in Indian Institute of Technology Guwahati, India. This thesis is the documentation of the research work carried out by me at the institute in a period of July, 2016 to August, 2019 under the supervision of ***Prof. Konjengbam Darunkumar Singh***, Professor, Department of Civil Engineering, Indian Institute of Technology Guwahati. I certify that the content of this thesis is the original work and has not been used for awarding any other degree, and is not published by any other person.

Date: **(Mr. Ricky Lalthazuala)**
Reg. No: 166104042

Place: IIT Guwahati

CERTIFICATE

This is to certify that the work content in the thesis entitled "***Structural Behaviour of Hybrid Stainless Steel I-sections – a Finite Element Study***" being submitted here by Mr**. Ricky Lalthazuala** to Indian Institute of Technology Guwahati, India for the award of degree of **Doctor of Philosophy** is a record of genuine research work carried out by the candidate as a research scholar under my supervision and guidance.

The Thesis work is worthy of considering for the award of degree of **Doctor of Philosophy** in accordance with the regulation of the Institute.

(Prof. Konjengbam Darunkumar Singh)
Professor
Department of Civil Engineering
Indian Institute of Technology Guwahati

Date:

Place: IIT Guwahati

to the Lord Almighty

to my dearest parents

Lallungawii and R. Lalhlira

ABSTRACT

Structural application of stainless steel members has been increased, especially when there is a demand for supreme aesthetic, high strength to weight ratio, good corrosion resistance, high ductility, low maintenance cost, impact and fire resistances etc. Despite its attractive advantages, its uses in the construction industry have been slow, owing to higher material cost as compared to carbon steel. However, it has become possible to present cost-effective stainless steel material, with the development of relatively newer grades of stainless steel such as Duplex stainless steel (DSS) and Lean duplex stainless steel (LDSS), which have lesser nickel content of ~ 4-5% and ~ 1.5% respectively. As compared with austenitic grades, DSS offers better corrosion resistances, higher strength and better wear resistances. On the other hand, LDSS is relatively a newer breed of stainless steel alloy (relative to DSS), with lesser nickel content, and hence resulted in considerably material cost reduction. Also, LDSS has better corrosion resistance, higher temperature properties, adequate weldability and fracture toughness properties, than the austenitic variety.

In steel structures having large spans and heavy loads, efficient and economic design is achieved by adopting hybrid girders. A hybrid steel girder/beam is basically a welded steel girder having higher strength steel grade in the flanges with relatively lower strength steel web. Thus, the aim of this research is to investigate the structural behaviour of hybrid stainless steel I-sections. Study is initiated on the flexural and shear behaviour of Hybrid stainless steel (HSS) adopting LDSS and DSS in the web and flanges respectively. In addition, study is further extended to cover the structural performance of hybrid stainless steel stub columns under axial compression load.

Flexural behaviour of Hybrid stainless steels (HSS) plate girders using the commercial finite element (FE) software, Abaqus is presented based on cross-sectional parameters such as flange and web slenderness study. The FE results are presented in the form of bending strength (M_u) and failure modes. Based on the investigation, significant improvement in M_u was observed for HSS I-beams as compared to homogenous sections such as LDSS and DSS I-beams. Also, EN 1993-1-4 was found to be reliable and applicable to LDSS, DSS and HSS I-beams, and hence, for the purpose of efficiency and economy, new slenderness limits has been proposed. In addition, new DSM formulation for HSS I-beams was proposed.

Parametric study on the shear behaviour (e.g. failure modes and shear capacity) of HSS plate girders using the FE software, Abaqus is presented, considering various parameters such as: (1) flange-to-web thickness ratio (t_f /t_w) by varying t_f and t_w, (2) flange slenderness (b_f /t_f) by varying b_f. Based on the study, it has been observed that web thickness (t_w) has higher positive influence on the shear capacity as compared to flange thickness (t_f). In addition, based on the present FE results, new design formulations in European code and DSM have been proposed.

Further, investigations on the behaviour of hybrid I-sections have been extended to determine the structural performance of hybrid stainless steel stub columns, using FE software, Abaqus. The hybrid stub columns considered consists of two configurations: (1) Hybrid stainless steel (HSS) stub column adopting DSS and LDSS on the flanges and web respectively; and (2) Hybrid stainless steel (HSS^a) stub column using DSS and LDSS on the web and flanges respectively. The FE results are presented in terms of column capacity (P_u) and failure modes. As observed from FE results, both flange thickness (t_f) and flange width (b_f) have more influence on the column capacity for HSS stub column as compared to HSS^a stub column. In general, EN 1993-1-4 Class 3 limit for internal web in compression was found to be applicable for all stainless steel stub columns. Based on the FE results, new DSM formulation for HSS and HSS^a stub columns has been proposed.

ACKNOWLEDGEMENT

My acknowledgement goes to all the persons who help me out in the progress of my research work. Their support and knowledge facilitated me to complete my work. I shall ever remain indebted to all of them. First of all, I would to thank Department of Civil Engineering, IIT Guwahati for providing the required facilities to complete my research work.

First and foremost, I would like to express my sincere gratitude to my supervisor Prof. ***Konjengbam Darunkumar Singh,*** Department of Civil Engineering, IIT Guwahati for taking me as a research scholar under his supervision. His continuous support, valuable guidance, encouragement and motivation throughout the course of my research work will remain indebted to me. Most prominently, he has facilitated me with the best research environment, and helped me out in every steps of my career right from the day I joined him as my M.Tech supervisor. This outstanding support I have received from him would be remembered in my life.

I am thankful to Prof. Sudip Talukdar, Prof. K.S.R. Krishna Murthy and Dr. Amit Shelke, my doctoral committee members, who have supported me and contributed precious suggestions in the development of my research work.

I am also thankful to my research associates, Tekcham Gishan Singh, Sanasam Vipej Devi, Narendra Babu, Suman and Prashant for helping me out in carrying out my

research activities. I would like to express my sincere gratitude to my friend Tekcham Gishan Singh for his valuable support in my research activities.

I am also very thankful to all my family members – R. Lalhlira (Father), Lallungawii (Mother) Malsawmzuala Royte (Brother), Mary Lalduhawmi (Sister) and R. Lalramnghaki (Wife). I would like to contribute my thesis to my parents – R. Lalhlira and Lallungawii, as I am very lucky to have them as parents. Also, I am forever indebted to them for their valuable support and guidance right from my early days, which has enabled me to reach this stage of my life.

Last but not the least, I express my truthful thankfulness to Almighty God for his guidance, blessing and enduring me with good health to accomplish my research work.

Ricky Lalthazuala

CONTENTS

LIST OF FIGURES

LIST OF TABLES

NOTATIONS

$\sigma_{0.2}$	proof stress at 0.2% offset strain
$\sigma_{1.0}$	proof stress at 0.1% offset strain
$\varepsilon_{t0.2}$	total strains at $\sigma_{0.2}$
$\varepsilon_{t0.1}$	total strains at $\sigma_{0.1}$
E	Young's modulus
$E_{0.2}$	tangent modulus at 0.2% offset strain
m	second strain hardening parameter
ε_u	ultimate total strain
σ_u	ultimate stress
b_f	flange width
t_f	flange thickness
h_w	web height
t_w	web thickness
L	specimen length

σ_{cr}	elastic critical buckling stress of plated elements
σ_{engg}	engineering stress
ε_{engg}	engineering strain
n *and* $n'_{0.2,\,1.0}$	strain hardening exponents
$\omega_{D\&W}$	Dawson and Walker imperfection amplitude
3PB	3-point bending
4PB	4-point bending
σ_{true}	true stress
$\varepsilon_{\ln}^{pl}$	log plastic strain
LDSS	Lean Duplex Stainless Steel
DSS	Duplex Stainless Steel
HSS	Hybrid Stainless Steel
M-θ	moment-rotation
FE	finite element
M_u	bending strength
θ_u	rotation at M_u
DSM	Direct Strength Method
HAZ	heat affected zone
c_f	flat element width of outstand flange

c_w	flat element width of web
ε	material factor
M_p	plastic moment
M_{el}	elastic moment
R	rotation capacity
θ_{pu}	total rotation at mid-span when moment curve drops below M_p
θ_{pl}	elastic component of rotation when moment curve reach M_p
κ_{pu}	total curvature at plastic hinge when moment curve drops below M_p
κ_{pl}	elastic curvature when moment curve reach M_p
I	second moment of area
M_{EN}	Eurocode 3 bending moment resistance
W_{pl}	major axis plastic section modulus
W_{el}	major axis elastic section modulus
W_{eff}	major axis effective section modulus for Class 4 sections
γ_{M0}	partial safety factor for cross-section resistance
M_{eff}	effective moment capacity for Class 4 sections
W_{eltf}	elastic section modulus of top flange
W_{elbf}	elastic section modulus of bottom flange
W_{eltw}	elastic section modulus of top web

W_{elbw}	elastic section modulus of bottom web
W_{pltf}	plastic section modulus of top flange
W_{plbf}	plastic section modulus of bottom flange
W_{pltw}	plastic section modulus of top web
W_{plbw}	plastic section modulus of bottom web
W_{efftf}	effective section modulus of top flange
W_{efftw}	effective section modulus of top web
$W_{effpltf}$	effective plastic section modulus of top flange
$W_{effplbf}$	effective plastic section modulus of bottom flange
$\sigma_{0.2tf}$	yield stress of top flange
$\sigma_{0.2bf}$	yield stress of bottom flange
$\sigma_{0.2tw}$	yield stress of top web
$\sigma_{0.2bw}$	yield stress of bottom web
$\sigma_{0.2f}$	yield stress of flange
$\sigma_{0.2w}$	yield stress of web
M_{crl}	critical elastic local buckling moment
M_v	DSM bending moment resistance
$M_{v,RR}$	modified DSM bending resistance proposed by Rossi and Rasmussen
$M_{v,ARR}$	modified DSM bending resistance proposed by Arrayago *et al.*

σ_{utf}	ultimate stress of top flange
σ_{ubf}	ultimate stress of bottom flange
σ_{utw}	ultimate stress of top web
σ_{ubw}	ultimate stress of bottom web
σ_{uf}	ultimate stress of flange
σ_{uw}	ultimate stress of web
A_{tf}	area of top flange
A_{bf}	area of bottom flange
A_{tw}	area of top web
A_{bw}	area of bottom web
A_f	area of flange
A_w	area of web
A	total area
φ	resistance factor
DL	Dead Load
LL	Live Load
M_m	mean for material properties
V_M	coefficient of variation for material properties
F_m	mean for fabrication factors

V_F	coefficient of variation for fabrication factors
P_m	mean values of the ratio of FE results to the design predictions
V_p	coefficient of variation of the ratio of FE results to the design predictions
PH	plastic hinge
LB	local buckling
WB	web buckling
$M_{v,P}$	proposed modified DSM bending resistance for HSS I-beams
a	shear span
t_s	stiffener or end post thickness
e	distance between end post and internal stiffener
V_u	shear capacity
δ_u	mid-span deflection at V_u
$V_{b,Rd}$	ultimate shear buckling resistance
χ_w	web buckling reduction factor
$\bar{\lambda}_w$	web slenderness
$V_{bf,Rd}$	shear resistances contributed by flange
$V_{bw,Rd}$	shear resistances contributed by web
η	web contribution factor
γ_{M1}	shear partial safety factor

k_τ	minimum shear buckling coefficient
M_{Ed}	design bending moment
$M_{f,Rd}$	design plastic moment of resistance of effective flange areas
c	distance between stiffener and plastic hinge location
V_{Ed}	design shear resistance
$M_{pl,Rd}$	design plastic moment of resistance of effective flange areas and fully effective web irrespective of cross-section class
V_{yw}	yield shear capacity of web
V_{cr}	elastic shear buckling resistance
V_v	original DSM shear resistance
$V_{v,KM}$	modified DSM shear resistance proposed by Keerathan and Mahendran
V_{EN}	Eurocode 3 design shear resistance
$V_{EN,P}$	proposed Eurocode 3 design shear resistance
$\chi_{w,P}$	proposed web buckling reduction factor
$V_{v,P}$	proposed DSM shear resistance
RP	reference point
BC	boundary condition
P_u	column capacity
δ_{Lu}	axial deformation at P_u

P_y	yield load
P_{EN}	Eurocode compression resistance
P_{crl}	critical elastic local buckling load
P_v	DSM compression strength
P_{nl}	local buckling resistance
P_{ne}	axial strength for yielding and global buckling
P_{cre}	critical elastic buckling load in flexure buckling
K	effective length factor
r_y	radius of gyration about minor axis of buckling
$P_{v,RR}$	modified DSM compression strength proposed by Rossi and Rasmussen
$P_{v,ARR}$	modified DSM compression strength proposed by Arrayago *et al.*
β_o	target reliability index of 2.5
β	reliability index of the ratio of FE results to the design predictions
$P_{v,P}$	proposed DSM compression strength

CHAPTER 1

1 INTRODUCTION

1.1 BACKGROUND

Stainless steel belongs to the family of corrosion resistant iron alloys with a minimum chromium content of ~10.5% by mass. Its significant advantages include excellent mechanical properties such as high strength to weight ratio, low maintenance cost, high corrosion resistance, significant strain hardening, high impact and fire resistances, etc. (Gardner, 2005; Gardner *et al.*, 2006; SCI-P413, 2017). Additionally, stainless steel offers aesthetically pleasing look, thereby making it attractive, especially for exposed applications. Since, the beginning of the twentieth century, designers and architects have been using stainless steel in various non-structural applications such as handrails, countertops, backsplashes, cladding, etc. The structural application of stainless steel in construction dated back to 1925 as early as the renovation of St Paul's Cathedral in London, the crown cladding of Chrysler Building in New York in 1929 (Figure 1.1), the exterior surface of the Gateway Arch in St Louis, Missouri which was completed in 1965 (Figure 1.2) and the cladding of the Walt Disney Concert Hall in Los Angeles which was finished in 2003 (Figure 1.3). In recent times, stainless steel also gains an increasing use as the primary structural material. Figures 1.4 and 1.5 show the Helix pedestrian bridge in Singapore and the Cloud Gate sculpture in Chicago, Illinois, respectively, both of which shows the use of stainless steel as a primary construction material.

1.2 DUPLEX AND LEAN DUPLEX STAINLESS STEEL

Stainless steel is mainly grouped into four types such as austenitic, ferritic, martenisitic and duplex grades (Gardner 2005). Amongst these grades, austenitic stainless steel is the most commonly adopted stainless steel. However, the high initial cost resulted from the high nickel content (~8-11% by mass) has hindered its widespread uses. This has led to the development of other relatively economical grades of stainless steel such as Duplex stainless steel (DSS) and Lean duplex stainless steel (LDSS), which have lesser nickel content of ~ 4-5% and ~ 1.5% respectively (EN 10088-4, 2009; EN 1993-1-4:2006 + A1, 2015). DSS is generally considered as high strength stainless steel and compared to austenitic grades, DSS provides better corrosion resistances, higher strength and better wear resistances (Gardner, 2005). Structural application of DSS can be seen in the *Celtic Gateway footbridge* in Anglesey, Wales (see Figure 1.6). LDSS on the other hand, is relatively a newer breed of stainless steel alloy, with lesser nickel content (thus relatively lower cost); and has higher strength, better corrosion resistance, high temperature properties, adequate weldability and fracture toughness as compared to austenitic grades (Sieurin *et al.*, 2006; Gardner *et al.*, 2010). Figure 1.7 shows the structural application of LDSS in *Likholefossen Bridge* in Norway.

1.3 HYBRID SECTIONS

In steel structures having large spans and heavy loads such as bridges, industrial and power plant buildings, steel plate girders/beams are generally adopted (Chacón *et al.*, 2011). For such long span and heavy structures, efficient and economic design is achieved by adopting hybrid steel plate girders (with higher strength steel flanges), as the flexural strength of a beam/girder is primarily attributed by the flanges (Greco, 2000). A hybrid steel beam/girder is basically a welded steel girder having higher strength steel grade in the flanges with relatively lower strength steel web. Figure 1.8

shows the structural application of hybrid steel girder in the State Route 52 over the Clear Fork River, USA (Wasserman *et al.*, 2003).

In the literature, although studies have been reported on the structural behaviour of hybrid carbon steels such as beams and columns, to the best of author's knowledge, no study has been reported, on the structural behaviour of stainless steel hybrid (consisting of DSS and LDSS elements) beams (e.g. (Frost and Schilling, 1964; Greco and Earls, 2003; Veljkovic and Johansson, 2004; Azizinamini *et al.*, 2007; Shokouhian and Shi, 2014, 2015; Shokouhian *et al.*, 2016)) and column members (e.g. (Zhao *et al.*, 2004; Heidarpour *et al.*, 2013)). Therefore, the aim of this research is identified as the numerical investigation of structural behaviour (shear, flexural and compression) of Hybrid stainless steel (HSS) I-members (i.e. plated I-sections), considering LDSS and DSS in the web and flanges respectively.

1.4 OBJECTIVES

The primary objective of the thesis is to study the structural behaviour of Hybrid stainless steel I-sections, using validated finite element (FE) analyses. Also, this study aims to assess the applicability of current design codes to HSS I-sections. The key objectives of the present study are then identified and enlisted below:

1. To study the effect of cross-sectional parameters such as flange thickness, web thickness and effect of flange width, on the structural behaviour of hybrid stainless steel (HSS) I-beams (with DSS and LDSS as plate elements) under bending and shear.

2. To study the structural performance of HSS stub columns (with DSS and LDSS as plate elements) based on cross-sectional parameters such as effect of flange thickness, web thickness and effect of flange width, under axial compression load.

1.5 THESIS OUTLINE

The content of the thesis is divided into six chapters and are briefly summarized below:

Brief background and introduction to the current research is presented in **Chapter 1**, focusing on stainless steel as structural material, with special attention made on the stainless steel grades such as Lean Duplex Stainless Steel (LDSS) and Duplex Stainless Steel (DSS). This is followed by an introduction on hybrid structural steel members. At the end, the objectives of the present research have been highlighted.

Chapter 2 presents the literature review related to the current study. The literature review has been divided into sub-topics *viz.*, stainless steel members under bending and shear, stub columns, and hybrid structural steel members. Stainless steel design standard (Eurocode 3) and design method (Direct Strength Method, DSM). Also, literatures pertaining to FE modelling of stainless steel members are also added.

Chapter 3 presents finite element (FE) study on the flexural behaviour of hybrid stainless steel (HSS) I-beams adopting LDSS and DSS on the web and flanges respectively. The effects of flange and web slenderness on the flexure behavior (moment capacity and failure/deformed modes) of HSS I-sections have been studied and the applicability of codified cross-section slenderness limits for, HSS I-beams under both 3PB and 4PB analyses have been assessed. In addition, FE results have also been compared with European code (EN 1993-1-4:2006 + A1, 2015) and Direct Strength Method (DSM) (Becque *et al.*, 2008; Rossi and Rasmussen, 2012; Arrayago *et al.*, 2017). Based on the FE results, for both Class 1 flange-critical section and web-critical section, it has been observed that LDSS I-beams have higher rotation capacity (R) as compared to HSS and DSS I-beams. Also, significant increase in flexural capacity (M_u) has been seen in case of HSS I-beams although the proportion of DSS material is maintained in HSS I-beams. In general, EN 1993-1-4 is found to be reliable and applicable for LDSS, HSS and DSS I-beams. Furthermore, for the purpose of efficient and economic designs, the following limits: 20, 16 and 11 have been proposed

for Class 3, Class 2 and Class 1 limits respectively for welded outstand flanges in compression (flange-critical section). Also, for internal webs in bending (web-critical section), the following limits: *viz.*, 110 and 100 have been proposed for Class 3 and Class 2 limits respectively. New DSM equation for HSS I-beams has been proposed based on the full-range modified DSM formulation for carbon steel given by Arrayago *et al.* (2017).

In **Chapter 4,** FE investigation on the shear behaviour of HSS plate girders has been presented adopting LDSS and DSS on the web and flanges respectively. The effects of the following parameters: (1) flange-to-web thickness ratio (t_f/t_w) by varying t_f and t_w, (2) flange slenderness (b_f/t_f) by varying b_f; on the shear capacity (V_u) and failure/deformed shapes, have been investigated. Furthermore, FE results have also been compared with the results given by European code (EN 1993-1-4:2006 + A1, 2015) and Direct Strength Method (DSM) (Keerthan and Mahendran, 2015; AISI, 2016b). Based on the FE investigations, three different failure mechanisms were observed in the FE specimens such as: shear dominant, bending dominant and combined shear and bending dominant failure modes. Increase in t_f and t_w has been seen to increase in shear capacity, however, the effect of t_w has been found to be relatively higher than that of t_f. On the other hand, increase of t_w has been observed to result in reduced ductility in contrast to the increase in t_f. In general, European code (EN 1993-1-4:2006 + A1, 2015), DSM (AISI, 2016b) and modified DSM (Keerthan and Mahendran, 2015) have been found to be overly conservative. Therefore, for the purpose of economic and efficient design, modified design formulations were proposed in EN 1993-1-4 and DSM for HSS plate girders.

Chapter 5 presents FE study on the structural behaviour of hybrid stainless steel stub columns having two configurations: (1) HSS stub column adopting DSS and LDSS on the flanges and web respectively; and (2) HSS^a stub column utilising DSS and LDSS on the web and flanges respectively. The effects of t_f, t_w and b_f on the column resistance (P_u) and deformed shapes, have been studied. Furthermore, a comparative study has

been presented between FE results and design specifications by EN 1993-1-4 (2006 + A1, 2015) and DSM (Rossi and Rasmussen, 2012; AISI, 2016b; Arrayago *et al.*, 2017). Based on the FE results, increase in flange thickness (t_f) has been seen to have significant improvement on P_u for HSS as compared to HSS^a stub columns. Whereas, increase in web thickness (t_w) is found to provide an enhancement in column capacity for HSS^a compared to HSS stub column. Also, an increase in flange width (b_f) has been seen to have more effect on HSS as compared to HSS^a stub columns. In general, EN 1993-1-4 (2006 + A1, 2015) Class 3 limit for internal webs in compression has been found to be reliable and applicable for HSS and HSS^a stub columns. However, for the purpose of efficient and economic designs, a new limit i.e. $c_w/t_w\varepsilon$ = 48, has been proposed as Class 3 limit. Additionally, new DSM formulations for HSS and HSS^a stub columns have been proposed based on the full-range modified DSM specification for carbon steel given by Arrayago *et al.*, (2017).

In **Chapter 6**, the main conclusions drawn from the current investigation on structural behaviour of hybrid stainless steel I-beams, plate girders and stub columns have been presented. Possible future works on the structural performance of hybrid stainless steel I-sections have also been added.

At the end of the thesis, supplementary appendices are presented. Design sample of HSS I-beams was given in **Appendix A**. Also, sample design calculation of HSS plate girders and hybrid stainless steel stub columns were presented in **Appendix B and C** respectively.

Figure 1.1**:** Chrysler Building (*static1.squarespace.com*)

Figure 1.2: Gateway Arch in St Louis, Missouri (*onmilwaukee.com*)

Figure 1.3: Walt Disney Concert Hall (*www.archdaily.com*)

Figure 1.4: Helix pedestrian bridge in Singapore (*essentialhome.eu)*

Figure 1.5: Cloud Gate sculpture in Chicago (*traveljapanblog.com*)

Figure 1.6: Celtic Gateway footbridge in Anglesey, Wales (*www.stayinwales.co.uk*)

Figure 1.7: Likholefossen Bridge in Norway (*amazonaws.com*)

Figure 1.8: State Route 52 over the Clear Fork River (Wasserman *et al.*, 2003)

CHAPTER 2

2 LITERATURE REVIEW

2.1 INTRODUCTION

Literature review pertaining to the present research work on stainless steel girders and stub columns are presented in this chapter, under four sub-topics viz., a) stainless steel beams, plate girders and stub columns, b) hybrid sections c) design standards for stainless steel members, and d) general numerical (i.e. finite element method) modelling procedures for thin walled metallic members. A brief summary of the literature review is presented at the end, highlighting key research gap areas.

2.2 STAINLESS STEEL MEMBERS

2.2.1 In-plane bending

This section presents literatures on the flexural behaviour of stainless steel beams (e.g. (Yamada. and Kato, 1988; Mirambell and Real, 2000; Kiymaz, 2005; Real and Mirambell, 2005a; Zhou and Young, 2005; Theofanous *et al.*, 2009a; Huang and Young, 2013; Saliba and Gardner, 2013a; Arrayago and Real, 2016; Gkantou *et al.*, 2019)). The first bending test on welded stainless steel I-section was conducted by Yamada and Kato (1988), which was followed by the test conducted on duplex stainless steel I-girder by ECSC WP2 (Kouhi *et al.*, 2000).

Several bending tests and numerical simulations on simply supported and continuous stainless steel beams were performed by Real and Mirambell (2000), considering rectangular and square hollow sections as well as H-sections. The deflections acquired by experimental and numerical tests were compared to those predicted by EN 1993-1-4 (1996). Hence, it was observed that the deflection obtained from EN 1993-1-4 (1996) predicted over-conservative results as compared to both experimental and numerical results. However, it was found that the deflections proposed by Rasmussen and Hancock (1993) provided accurate results upto yield stress.

Zhou and Young (2005) conducted bending tests on austenitic and duplex stainless steel beams. The test results were compared with the theoretical elastic and plastic moment resistances. It was observed that these theoretical moments predicted conservatively as compared to experimental results. In addition, the test results were further compared to the flexural strengths predicted by design specifications such as American Specification (ASCE, 2002), North American Specification (NAS, 2001) and Australian/New Zealand Standard (AS/NZS, 2001). It was found that the American (ASCE, 2002) and North American (NAS, 2001) standards are conservative for normal and high strength stainless steel beams, whereas Australian/New Zealand (AS/NZS, 2001) specification are observed to be conservative for normal strength stainless steel beams.

Real and Mirambell (2005) performed numerical and experimental investigations on austenitic and duplex stainless steel beams of square, rectangular and H-sections. The test and numerical results were compared to the design values given by the linear simplified method (ENV 1993-1-4, 1996). It was observed that the deflection values obtained by linear simplified methods predicted overestimated results. Hence, a new equation was proposed, based on moment-curvature relationship of stainless steel cross-sections, for determining the deflection values.

Kiymaz (2005) carried out experimental investigation on austenitic and duplex stainless steel beams of circular hollow cross-sections. The experimental values were compared

with the design specifications predicted by American (ASCE, 2002), Australian (AS/NZS, 2001) and European codes (ENV 1993-1-4, 1996). It was observed that the moment capacity given by American specification (ASCE, 2002) predicted conservative results as compared to Australian and Eurpoean specifications. Also, it was found that the cross-section slenderness limits given by the current specifications were inappropriate, and based on the test results, improvement on cross-section slenderness limits were shown.

Theofanous *et al.*, (2009a) conducted 3-point bending tests on austenitic stainless steel of oval hollow cross-sections. Numerical study was carried out to cover a wide range of cross-section slenderness. The numerical and test results were compared to the design resistances given by EN 1993-1-4 (2006). It was found that the current slenderness limits for stainless steel circular hollow sections may be adopted for stainless steel oval sections with a proposed equivalent diameter.

Saliba and Gardner (2013a) carried out bending tests on LDSS welded I-section. Numerical investigation was also conducted. The results obtained from test and numerical models were compared to EN 1993-1-4 (2006) design specification. It was observed that the cross-section classification in EN 1993-1-4 (2006) was safely applicable and conservative, and new limit was suggested for LDSS beams by adopting the proposed limits of Gardner and Theofanous (2009a). In addition, the test results were also compared to other grades of stainless steel such as duplex, ferritic and austenitic grades. It was found that the structural behaviour of LDSS was similar to other grades of stainless steel.

Huang and Young (2013) conducted numerical and experimental studies on lean duplex stainless steel beams of square and rectangular hollow cross-sections. The test and FE results were compared to design specifications given by American (ASCE 8-02, 2002), Australian/New Zealand (AS/NZS, 2001), European (EN 1993-1-4, 2006), direct strength method (AISI, 2007) and continuous strength method (Saliba and Gardner, 2013a). Based on this study, it was observed that the continuous strength

method provided accurate prediction as compared to other design specifications. Also, a new modified direct strength method (DSM) was proposed for LDSS beams of rectangular and square hollow cross-sections.

Arrayago and Real (2016) carried out an experimental investigation on ferritic stainless simply supported and continuous steel beams of square and rectangular hollow cross-sections. The test results were used to check the appropriateness of cross-section classification limits given in European code (EN 1993-1-4, 2006) and those given by Gardner and Theofanous (2008). Based on the study, it was observed that the slenderness limits given by Gardner and Theofanous (2008) predicted more accurately than European (EN 1993-1-4, 2006) code for Class 2 and Class 3 ferritic stainless steel sections.

Gkantou *et al.,* (2019) conducted numerical and experimental investigations on austenitic and duplex stainless steel beams of rectangular cross sections. The study consisted of simply supported beams and two span continuous beams. The results obtained from this study were compared to the design specifications predicted by European code (EN 1993-1-4:2006 + A1, 2015) and continuous strength method (Afshan and Gardner, 2013). Based on this study, it was found that the European code (EN 1993-1-4:2006 + A1, 2015) predicted over conservative results for stainless steel continuous beams. On the other hand, the continuous strength method (CSM) considering moment redistribution was found to give most accurate predictions.

2.2.2 Members under shear

This section presents the literature on structural behaviour of stainless steel plate girders under shear loading (e.g. (Carvalho *et al.*, 1990; Olsson, 2001; Estrada *et al.*, 2007a, 2007b; Real *et al.*, 2007; Hassanein, 2010, 2011; Saliba and Gardner, 2013b; Saliba *et al.*, 2014; Sonu and Singh, 2017)).

The first experimental investigation on the shear capacity of short span cold-formed stainless steel beams was carried out by Carvalho *et al.*, (1990), which was followed

by Olsson (2001). Olsson (2001) investigated the shear performance of stainless steel plate girders by varying the flange thickness and shear span. It was observed that the shear capacity decreased with increasing shear span. Also, new slenderness and shear buckling factors have been proposed for EN 1993-1-4 (1996).

Estrada *et al.,* (2007a) conducted experimental investigation on shear performance of stainless steel plate girders. It was observed that the shear resistance given by EN 1993-1-4 (1996), which was based on simple post critical method was found to predict extremely conservative results. Hence, for improving the shear capacity predictions, rotated stress field method incorporated in EN 1993-1-5 (1997) was also adopted for stainless steel plate girders. Also, this method was observed to give conservative results and found to provide more accurate predictions as compared to simple post-critical method.

Real *et al.*, (2007) conducted the shear tests on austenitic stainless steel plate girders. Based on their study, it was observed that increase in shear span reduces the shear capacity. Also, decrease in web slenderness was found to enhance the shear capacity for similar flange thicknesses considered. In addition, EN 1993-1-4 (1996) is found to predict conservative results for stainless steel plate girders.

Hassanein (2010) performed a numerical study on shear characteristics of austenitic stainless steel plate girders. Based on the study, it was observed that increasing flange width and flange thickness enhanced shear capacity. Conversely, shear capacity was found to reduce with increase in web slenderness. Also, shear failure was seen in specimens having $t_f / t_w > 2$ (where t_f and t_w are the flange and web thicknesses respectively) and 1.5 for an initial imperfection of $h_w/100$ and $h_w/100000$ respectively (i.e. h_w is the web height).

Hassanein (2011) carried out numerical investigation on the shear behaviour of LDSS (Grade EN 1.4162) plate girders. For constant web thickness (t_w), it was observed that higher t_f/t_w or t_f specimens failed by shear. However, for lower t_f/t_w or t_f specimens, the

failure was found to be governed by bending. In addition, it was observed that EN 1993-1-4 (2006) predicted more accurate shear capacity (i.e. lesser conservative) results as compared to EN 1993-1-4 (2007) for LDSS plate girders. Hence, for enhanced economy and efficiency, a new design formulation was proposed based on EN 1993-1-4 (2006).

Saliba and Gardner (2013b) performed shear tests on LDSS plate girders. Based on their study, three failure mechanisms have been observed: a) shear dominant failure, b) bending dominant failure and c) combined shear and bending dominant failure mechanisms. It was observed that shear design equations given in EN 1993-1-4 (2006) are applicable to LDSS plate girders.

Saliba *et al.,* (2014) carried out a comparative study of experimental results of stainless steel plate girders reported by Olsson (2001), Real *et al.,* (2007), Estrada *et al.,* (2007a) and Saliba and Gardner (2013b) with the design formulations predicted by EN 1993-1-4 (2006), EN 1993-1-5 (2007) and Estrada *et al.,* (2007b). Based on the comparative study, the design shear equations given by EN 1993-1-5 (2007) and proposed by Estrada *et al.,* (2007b) were found to give more accurate results as compared to those predicted by EN 1993-1-4 (2006). Therefore, a new design formulation was proposed to predict the shear capacity for stainless steel plate girders. Also, these design equations have been included in the latest amendment to EN 1993-1-4 (2006) i.e. EN 1993-1-4:2006 + A1, 2015.

Sonu and Singh (2017) conducted numerical investigation on shear behaviour of LDSS beams. It was observed the shear capacity is enhanced with increase in flange thickness. However, increase in web slenderness and shear span has shown to result reduction in shear resistance. Also, three failure modes have been observed: a) shear dominant failure mode, b) bending dominant failure mode and c) combined shear and bending dominant failure mode. In addition, EN 1993-1-4 (2006) and DSM are observed to be applicable and conservative for shear design calculation of LDSS

beams. New design equations in line with EN 1993-1-4 (2006) and DSM have been proposed.

2.2.3 Stub columns

Literature on the structural performance of stainless steel I-section stub columns subjected to axial compression load is presented in this section (e.g. (Bredenkamp and Van den Berg, 1995; Kuwamura, 2003; Ashraf *et al.*, 2006a; Saliba and Gardner, 2013a; H.X. Yuan *et al.*, 2014)).

The first test on stainless steel I-section stub columns was carried out by Bredenkamp and Van den Berg (1995), followed by an experimental study conducted by Kuwamura (2003). Kuwamura (2003) carried out experimental investigation on stainless steel stub columns of cross-sections such as angle, H-shaped, channel, lipped channel, square and circular hollow sections. Based on the study, equations were proposed for the effective width to thickness ratios of the sections considered.

Ashraf *et al.*, (2006a) conducted numerical study on stainless steel stub columns of different cross-sections such as angle, I-section, channel and lipped channel. Based on the study, FE modeling techniques applicable for stainless steel sections were developed. Also, it was observed that the residual stresses developed due to welding was found to have very less effect on column capacity and hence, can be ignored.

Saliba and Gardner (2013a) performed experimental and numerical studies on LDSS welded I-section stub columns. The test and FE results in terms of column resistance were compared with European specification (EN 1993-1-4, 2006). Based on the comparison, it was found that design slenderness limits for Class 3 sections given by EN 1993-1-4 (2006) predicted very conservative results and therefore, economical design, the limits given by Theofanous and Gardner (2008) was suggested for Class 3 slenderness limits of LDSS welded I-sections.

Yuan *et al.,* (2014b) carried out experimental study on stainless steel stub columns of cross-sections such as I-section, rectangular and square hollow sections. The test results in terms of column capacity were compared with design specifications given by European code (EN 1993-1-4, 2006), direct strength method (DSM) (Rossi and Rasmussen, 2012) and continuous strength method (CSM) (Afshan and Gardner, 2013). Based on the comparison, the direct strength method (DSM) was found to present accurate predictions for all the specimens. However, the continuous strength method (CSM) was observed to give accurate predictions only for non-slender sections.

2.2.4 Hybrid sections

Study of structural behaviour of hybrid steel section are presented in this section (e.g. (Frost and Schilling, 1964; Greco and Earls, 2003; Veljkovic and Johansson, 2004; Zhao *et al.*, 2004; Azizinamini *et al.*, 2007; Heidarpour *et al.*, 2013; Shokouhian and Shi, 2014, 2015; Shokouhian *et al.*, 2016)). A review on the investigations on steel hybrid sections, consisting of various steels such as mild carbon steel, high strength carbon steel and high performance steel (HPS), subjected to both bending and compression are presented herein.

Application of hybrid steel section dated back to 1940s, the first research work was carried out in 1964 by Frost and Schilling (1964). Frost and Schilling (1964) conducted a theoretical and experimental investigation on hybrid sections at the Applied Research Laboratory of the United States Steel Corporation. The tests were performed on three hybrid beams utilizing high strength steel A514 of yield strength (690MPa) in the flanges and varying steel grades in the web which are made of A7 (228MPa), A242 (345MPa) and A514 (690MPa). Based on their study, it was found that the plastic moment for homogenous beam (i.e. A514 steel beam) is larger than hybrid beam because of larger web contribution from homogenous sections to the ultimate flexural strength.

Study on hybrid beams was carried out by Greco and Earls (2003) which focuses on the flexural ductility of hybrid high performance steel (HPS) I-shaped beams. They performed bending tests on hybrid beams which employed high strength steel HPS483W of yield strength (552MPa) in the flanges and mild carbon steel of grade Gr.276 (276MPa), Gr.345 (345MPa) and Gr.414 (414MPa) in the web. Based on their study, improvement in rotation capacity can be observed in hybrid section of unbraced length equal to depth of section. Also, in order to achieve the rotation capacity of three or more, it was observed that the slenderness to be maintained between 5 and 3.5.

Veljkovic and Johansson (2004) conducted experimental study on hybrid steel girders, fabricated by welding high strength steel (HSS) flanges and relatively lower strength web. Based on the study, hybrid girders were seen to be more economical and efficient as compared to homogenous sections. Also, it was suggested that for serviceability requirement, the strength of flanges to be maintained within twice the strength of the web.

The AASHTO LRFD Bridge Design Specifications in versions prior to 2004 restricted the use of tension field action for shear resistance of hybrid high performance steel I-girders. Based on these limitations, an experimental investigation on shear behaviour of hybrid steel plate girders was conducted by Azizinamini et al. (2007). Based on the experimental study, it was observed that the tested girders shows higher shear reistances as compared to those predicted with inclusion of tension field action. This study, has led to the inclusion of tension field action in shear resistance estimation in the revised AASHTO (2004) LRFD Bridge Design Specifications. Also, the tested shear capacity exceeded the predicted strength with no shear moment interaction, and hence, based on this finding, the shear and moment interaction provisions have been removed from AASHTO (2004).

Shokouhian and Shi (2014) conducted numerical investigation on hybrid steel beams. Two types of carbon steel grades Q345 and Q460 (GB/T1591, 2008). Three types of sections were considered in the current study, designated as a) ST1, homogenous steel

section using Q345 in both flanges and web b) ST2, homogenous high strength steel section using Q460 in both flanges and web c) ST3, high strength steel hybrid section using Q460 in flanges and Q345 in web. It was observed that for all the sections, ductility reduces with increase in flange and web slenderness. Also, it was seen that when a significant amount of compression flange were not restrained laterally, lateral torsional buckling occured which forbade achievement of plastic moment. In addition, it was reported that the flange slenderness limit of ST1, ST2 and ST3 and web slenderness limit of ST1 according to GB50017 (2003) cannot fulfill the ductility requirement of compact section (i.e. rotation capacity >3).

Shokouhian and Shi (2015) performed numerical and experimental investigations on hybrid and homogenous high-strength steel (Q345 and Q460) (GB/T1591, 2008). Based on their study, equation for calculation of flexural resistance of hybrid and homogenous sections were proposed. This proposed equation was compared with those of AISC (2010), EN 1993-1-1 (2005) and GB 50017 (2003) steel design specifications. It was observed that EN 1993-1-1 (2005) provided most accurate predictions. Also, it was suggested that the proposed equation can be adopted in a new version of Chinese Code for Design of Steel Structures (GB50017, 2003).

Shokouhian *et al.,* (2016) carried out numerical investigation on flexural behaviour of hybrid I-beams. Numerical study on hybrid sections was carried out based on the experiments conducted by Shokouhian and Shi (2015). Based on their study, equations were proposed for hybrid steel I-beams for determination of shear and shear-moment capacity. Also, significant reduction in flexural capacity was observed when interaction of modes involving lateral torsional buckling modes were considered.

Zhao *et al.,* (2004) carried out experimental study on hybrid stub columns of square and triangular fabricated mild steel sections, formed by welding very high strength circular carbon steel tubes to the corners of square and triangular fabricated sections. The compression strength of the current hybrid stub column was found to predict 3.5 times higher than the nominal column strength of corresponding welded triangular and

square hollow section without tubes. Also, design equations were proposed for determination of column capacity for hybrid sections adopted in the study.

Heidarpour *et al.*, (2013) conducted numerical and experimental investigations on hybrid stub column. The hybrid stub column employs square and triangular mild steel cross-sections with stainless steel circular tubes welded to its corners. An improvement in column capacity and ductility were observed in the current hybrid stub column as compared to corresponding welded square and triangular sections without tubes. Also, it was seen that hybrid sections resulted better structural performance at elevated temperature as compared to corresponding conventional sections.

2.3 STAINLESS STEEL DESIGN STANDARDS

2.3.1 European standards

Eurocode 3 (EN 1993-1-4, 1996) pre-standard was developed in 1996 by European Standards organization (CEN) with the supplementary guidelines for stainless steel. Based on this pre-standard, the full European standard EN 1993-1-4 (2006) was developed and published in 2006. This European standard provides guidelines for design of stainless steel members. However, newer stainless steel breeds such as 'Lean duplex stainless steel (LDSS)' has not been included in this design specification. Further, this specification has been upgraded (see (EN 1993-1-4:2006 + A1, 2015)) with the inclusion of various grades of stainless steel such as EN 1.4062, EN 1.4162, EN 1.4662 and EN 1.4482. This newly upgraded specification has made certain improvement in the class classification limits for flat elements subjected to bending (e.g. $c/t\varepsilon$ values updated from 124 to 90 (Class 3 limit); and 83 to 76 (Class 2 limit)) and compression (e.g. $c/t\varepsilon$ values updated from 42 to 37 (Class 3 limit); and 38 to 35 (Class 2 limit)). Also, the reduction factor for slender sections (i.e. Class 4 sections) was also changed.

The shear design approach for stainless steel members given in EN 1993-1-4 (1996) was Simple Post-Critical method, based on Höglunds (1971, 1973) rotated stress field theory. The design shear capacity adopting Simple Post-Critical method was observed to predict overly conservative results. This is due to the fact that this method did not consider the shear resistance contributed by the flanges. Due to the shortcoming of the Simple Post-Critical method, Olsson (2001) performed experimental investigations on stainless steel plate girders. Based on the study, new design methods based on Höglunds rotated stress field theory was proposed. This proposed method incorporated both the flange and web contribution in calculation of design shear capacity and was found to predict accurate results as compared to Simple Post-Critical method. Hence, this method was incorporated in EN 1993-1-4 (2006). Further, test results from Saliba and Gardner (2013b), Estrada *et al.,* (2007b), Real *et al.,* (2007) were compared with those predicted by EN 1993-1-4 (2006). It was found that EN 1993-1-4 (2006) predicted conservative results. Therefore, for the purpose of improvement on shear design predictions, Saliba *et al.,* (2014) proposed new design equation which was included in the recent amendment to EN 1993-1-4 (2006) i.e. EN 1993-1-4 (2006 + A1, 2015).

2.3.2 Direct Strength method

The direct strength method (DSM) was first proposed by Schafer and Pekoz (1998) for the design of cold formed steel members. It is a simple non-iterative design method which is an alternative to the traditional 'effective width method'. Later, DSM was included in Appendix 1 of North American Specification (NAS) for the design of cold-formed carbon steel structural members in 2004 (Schafer, 2008). DSM considered elastic instabilities such as local, distortional and global flexure or flexural-torsional modes along with the interaction between the modes. Application of DSM can be seen for several structural members such as beams, columns, etc. (e.g. (Schafer and Pekoz, 1998; Pham and Hancock, 2012; Pham *et al.,* 2014)). DSM has also been extended to stainless steel members (Becque *et al.,* 2008). In addition, this method was extended to

investigate the shear behaviour of LiteSteel beams (Keerthan and Mahendran, 2011) and LDSS beams reported by Sonu and Singh (2017)

2.4 NUMERICAL MODELLING

2.4.1 General

Numerical procedures such as FE analysis have been adopted to study the structural behaviour of thin-walled metallic members, steel members, etc. (see Theofanous and Gardner, 2009; Patton and Singh, 2012; Hassanein and Silvestre, 2013; Huang and Young, 2013; Saliba and Gardner, 2013a; Sonu and Singh, 2017). Large scale experimental tests, covering a range of parameters, may not be very feasible and convenient, as it the cost involved would be prohibitive. Hence, FE analysis can suitably be carried out to cover large structural parameters, when calibrated against the reliable experimental results. Thus, FE analysis serves as a relatively efficient and economical solution technique. Also, the accuracy and efficiency of FE analysis depends on several factors such as material modelling, boundary conditions, types of elements, loading, imperfection, etc. and are discussed in the following sections.

2.4.2 Material modelling

Accurate material modelling plays a vital role in studying the structural behaviour of thin-walled structural members. Several material models for steels (such as carbon steel, stainless steel etc.) have been proposed as early as 1940s (e.g.(Ramberg and Osgood, 1943; Hill, 1944)). Since then, various material models have been developed for stainless steel material (e.g. (Mirambell and Real, 2000; Rasmussen, 2003)). The proposed model for aluminum alloys given by Ramberg and Osgood (1943) was observed to be suitable for modelling stainless steel material upto yield stress (Mirambell and Real, 2000; Rasmussen, 2003). Hence, for stainless steel material before attainment of yield stress (i.e. $\sigma \leq \sigma_{0.2}$), Ramberg and Osgood model (Ramberg

and Osgood, 1943) given in Equation 2.1 is generally adopted in the literature and is known to provide good agreement with experiments for steel up to $\sigma_{0.2}$.

$$\varepsilon = \frac{\sigma}{E} + K\left(\frac{\sigma}{\sigma_{0.2}}\right)^{n} \tag{2.1}$$

where ε, σ and E are the strain, stress and Young's modulus respectively, n and K are the material nonlinearity indices obtained from experiments. The value of K = 0.002 has been reported to predict good agreement for stress-strain behaviour of stainless steel up to $\sigma_{0.2}$. However, for strains exceeding $\varepsilon_{t0.2}$ (total strains at $\sigma_{0.2}$), the model was found to give higher stress values. Hence, for stress beyond $\sigma_{0.2}$, an expression was proposed by Rasmussen (2003) which is valid for the full stress-strain range. Rasmussen (2003) adopted Mirambell and Real (2000) modified Ramberg-Osgood model for stresses beyond $\sigma_{0.2}$ to propose the full stress-strain curve (see Equation 2.2).

$$\varepsilon = \frac{\sigma - \sigma_{0.2}}{E_{0.2}} + \varepsilon_u\left(\frac{\sigma - \sigma_{0.2}}{\sigma_{1.0} - \sigma_{0.2}}\right)^{m} + \varepsilon_{t0.2} \tag{2.2}$$

$$\varepsilon_u = 1 - \frac{\sigma_{0.2}}{\sigma_u} \tag{2.3}$$

$$E_{0.2} = \frac{\sigma_{0.2} E}{\sigma_{0.2} + 0.002nE} \tag{2.4}$$

where $\sigma_{1.0}$ and ε_u (Equation 2.3) are the proof stress at 1% offset strain and ultimate total strain respectively; m and $E_{0.2}$ (Equation 2.4) are the second strain hardening parameter and tangent modulus at 0.2% offset strain respectively. Also, the ultimate tensile strength is determined by Equation 2.5.

$$\frac{\sigma_{0.2}}{\sigma_u} = \frac{0.2 + 185\left(\frac{\sigma_{0.2}}{E}\right)}{1 - 0.0375(n-5)} \tag{2.5}$$

Therefore, the full stress strain curve developed by Rasmussen takes the following form (see Equation 2.6)

$$\varepsilon = \begin{cases} \dfrac{\sigma}{E} + K\left(\dfrac{\sigma}{\sigma_{0.2}}\right)^{n} & \text{for } \sigma \le \sigma_{0.2} \\ \dfrac{\sigma - \sigma_{0.2}}{E_{0.2}} + \varepsilon_u\left(\dfrac{\sigma - \sigma_{0.2}}{\sigma_u - \sigma_{0.2}}\right)^{m} + \varepsilon_{t0.2} & \text{for } \sigma > \sigma_{0.2} \end{cases} \tag{2.6}$$

Gardner and Nethercot (2001) found that necking is absent in compressive coupons. Thus, the stress-strain equation given in Equation 2.2 may not be applicable for compressive coupons since this equation depends on ultimate stress (σ_u) and strain (ε_u). Therefore, Gardner (2002) proposed for the use of 1% proof stress ($\sigma_{1.0}$) and strain ($\varepsilon_{t1.0}$) instead of ultimate stress (σ_u) and strain (ε_u). Based on this proposal, Gardner and Ashraf (2006a) developed a new method for stresses exceeding $\sigma_{0.2}$ given in Equation 2.7.

$$\varepsilon = \frac{\sigma - \sigma_{0.2}}{E_{0.2}} + \left(\varepsilon_{t1.0} - \varepsilon_{t0.2} - \frac{\sigma_{1.0} - \sigma_{0.2}}{E_{0.2}}\right) \times \left(\frac{\sigma - \sigma_{0.2}}{\sigma_{1.0} - \sigma_{0.2}}\right)^{n'_{0.2,1.0}} + \varepsilon_{t0.2} \tag{2.7}$$

where $\varepsilon_{t1.0}$ and $n'_{0.2,\ 1.0}$ are the total strain at $\sigma_{1.0}$ and strain hardening exponent respectively. It was observed that Gardner and Ashraf (2006a) model given in Equation 2.7 provides accurate results for both compressive and tensile coupons, and is widely adopted for modelling stainless steel materials.

2.4.3 Element type

In the literature, thin-walled metallic structures were generally modelled using shell FE elements. Four-noded doubly curved shell FE element with reduced integration (S4R) available in Abaqus has been reported suitable for modelling thin-walled metallic members and has been adopted by various researchers (e.g. (Ellobody and Young, 2005; Theofanous and Gardner, 2009; Patton and Singh, 2012; Saliba and Gardner, 2013a; Sonu and Singh, 2017)). Also, FE modeling using S4R elements has shown

accurate predictions as compared to compression, bending and shear test results (e.g. (Theofanous and Gardner, 2009; Hassanein, 2010; Saliba and Gardner, 2013b; Huang and Young, 2014)). Further, in many studies (e.g. (Patton and Singh, 2012; Ellobody *et al.*, 2013; Sachidananda and Singh, 2015; Sonu and Singh, 2017)), an element aspect ratio of ~1 has been adopted as ~1 in order to provide reliable accurate results.

2.4.4 Geometric imperfections

Geometric imperfections are the variation of shape from the perfect geometry which may occur during production, manufacturing, transportation, fabrication processes, etc. Two types of initial geometric imperfections are generally considered such as local and global imperfections. The imperfection that occurred in the form of deformation on the inner and outer surface are termed as local imperfection whereas the deformation acting along the whole member globally in any direction (e.g. bowing, warping and twisting) is termed as global imperfection. Presence of geometric imperfection greatly affects the structural behaviour (i.e. load carrying capacity, ductility, post buckling behaviour, etc.) of structures. The magnitudes of initial imperfection in FE modelling are generally seeded based on the least eigen mode obtained from elastic eigen value buckling analysis. This method has been adopted for stainless steel members under bending (Theofanous and Gardner, 2010), compression (e.g. (Ellobody and Young, 2005; Patton and Singh, 2012)) and shear (Saliba and Gardner, 2013b). The imperfection amplitude for steel members can be determined from direct experiments or *via* models developed by Dawson and Walker (1972) (see Equation 2.8) with further modification ((Gardner and Nethercot, 2004; Cruise and Gardner, 2006; M. Ashraf *et al.*, 2006b)).

$$\omega_{D\&W} = 0.023\left(\frac{\sigma_{0.2}}{\sigma_{cr}}\right)t \tag{2.8}$$

where, σ_{cr} is the elastic critical buckling stress obtained from buckling analysis, and t is the thickness. Also, this imperfection amplitude has been successfully adopted in LDSS I-section (e.g. (Saliba and Gardner, 2013a, 2013b)).

2.4.5 Residual stress

The stresses that are developed in the absence of external load in a structural member are generally called residual stress. They are formed in a structural member from different mechanisms such as cold-forming, welding processes, etc. In the literature, the residual stress effect has been reported to have lesser influence on the structural behaviour of members under compression (e.g. (Gardner and Nethercot, 2004; Ellobody and Young, 2005; Huang and Young, 2014)), bending (e.g. (Huang and Young, 2012; Hassanein and Silvestre, 2013; Saliba and Gardner, 2013a)) and shear (Saliba and Gardner, 2013b) and hence, residual stresses were neglected in FE models (e.g. (Saliba and Gardner, 2013a, 2013b)).

2.5 SUMMARY

This chapter presented a review on the literature on stainless steel flexural members subjected to bending and shear. Also, a brief review on stainless steel columns was reported. Further, previous works conducted on hybrid sections were also presented. Design considerations (e.g. Eurocode, Direct Strength Method) that are relevant for stainless steel design were summarized. In addition, details for FE modelling of thin-walled stainless steel members have been presented. Based on the literature review, it has been seen that to the best of author's knowledge, no studies have been reported on the bending and shear; and compression performances of hybrid (consisting of duplex stainless steel (DSS) and lean duplex stainless steel (LDSS)) plate girders and I-section stub columns. This forms the background of the present thesis work.

CHAPTER 3

3 FLEXURAL BEHAVIOUR OF HYBRID STAINLESS STEEL I-BEAMS

3.1 INTRODUCTION

In building civil engineering structures with large spans such as bridges, steel buildings, etc welded I-sections are commonly adopted. Also, considering the benefits and advantages of using stainless steel as a structural material (Gardner, 2005; Baddoo, 2008; SCI-P413, 2017), nowadays studies have been carried out on the flexural behaviour of stainless steel I-sections (e.g. (Yamada. and Kato, 1988; Carvalho *et al.*, 1990; Kouhi *et al.*, 2000; Olsson, 2001; Real and Mirambell, 2005b; Real *et al.*, 2007; Saliba and Gardner, 2013a; 2013b)). Fabricated sections akin to welded I-section are built up sections made by welding (e.g. laser welding (Gardner *et al.*, 2016), shielded metal arc welding (SMAW) (Gardner and Cruise, 2009; Yuan *et al.*, 2014a)) together hot-rolled plates.

In addition to the family of homogenous steel I-section which are traditionally used in the construction industries, newer Hybrid steel I-section are being explored both in research and construction (e.g. (Frost and Schilling, 1964; Greco and Earls, 2003; Azizinamini *et al.*, 2007; Shokouhian and Shi, 2014, 2015; Shokouhian *et al.*, 2016)). Hybrid steel I-sections are fabricated sections having high strength steel flanges and relatively lower strength steel web. Flexural resistance of a beam is primarily attributed by the flanges, and hence for a member under pure bending, the concept of hybrid provides more economical and efficient design (Shokouhian and Shi, 2014). This

concept is true since the longitudinal flexural stress are more critical than the shear stress in typical I-section beams under constant moment loading (Greco, 2000). Furthermore, it has been reported that use of hybrid steel sections can result in cost savings up to ~15% as compared to homogenous steel girders (Veljkovic and Johansson, 2004).

Numerous studies on the flexural behaviour of homogeneous steel I-sections have been carried out (e.g. (Haaijer, 1957; Haaijer and Thürlimann, 1958; McDermott, 1969; Kemp, 1985; Schilling, 1988; Kuhlmann, 1989; Barth and White, 1998; Green *et al.*, 2002; Wilkerson, 2005; Topkaya, 2006; White and Jung, 2007)). Despite the advantages and benefits of utilizing hybrid steel I-sections, relatively lesser work has been carried out as compared to homogeneous sections. Studies on the structural performance of hybrid sections include investigations by Frost and Schilling (1964), Greco and Earls (2003), Azizinamini *et al.*, (2007), Shokouhian and Shi (2014, 2015), Shokouhian *et al.*, (2016). According to the author's knowledge, study on structural behaviour of hybrid I-beams using stainless steel materials have not been conducted. Therefore, in the light of expanding the knowledge of structural behaviour of hybrid I-beams, study is initiated on the flexural performance of Hybrid Stainless Steel (HSS) I-beams utilizing Duplex Stainless Steel (DSS) and Lean Duplex Stainless Steel (LDSS) on the flanges and web respectively based on parametric study of flange and web slenderness. Furthermore, for the purpose of direct comparison with HSS I-beams, similar study will also be carried out in homogenous section such as LDSS I-beams following Saliba and Gardner (2013a) and DSS I-beams for the same section. The FE bending strength (M_u) results are also compared with those predicted by European code (EN 1993-1-4:2006 + A1, 2015) and Direct Strength Method (DSM) (Becque *et al.*, 2008; Rossi and Rasmussen, 2012; Arrayago *et al.*, 2017), in order to assess their applicability. Finally, attempts are made to modify both the European code and DSM design equations, for a possible improvement in the design predictions, for HSS I-beams.

3.2 NUMERICAL MODELLING

3.2.1 General

Numerical study was carried out utilizing the commercial finite element software, Abaqus (2009) by employing similar modelling procedure adopted in a number of previous studies (e.g. (Theofanous and Gardner, 2009; Patton and Singh, 2012; Hassanein and Silvestre, 2013; Huang and Young, 2013; Saliba and Gardner, 2013a; Sonu and Singh, 2017)) and are known to provide accurate results. Initially, the experimental results: 3-point bending (3PB) and 4-point bending (4PB) tests on LDSS welded I-beams (Saliba and Gardner, 2013a) and 4PB tests on hybrid high-strength steel (Gr.Q345 and Gr.Q460) welded I-beams (Shokouhian *et al.*, 2016) are used for validating the FE models. Hence, the validated FE models are further utilized for parametric studies to cover a wide range of slenderness study on LDSS, HSS and DSS I-beams.

3.2.2 Geometry

The cross-sectional geometry of the I-beam is shown in Figure 3.1a, where b_f, t_f, h_w and t_w are the flange width, flange thickness, web height and web thickness respectively. The specimen designation system is given by section type, followed by web height × flange width × flange thickness × web thickness. The schematic diagram of 3PB and 4PB specimens of constant length (L= 2800 mm) are shown in Figures 3.1b and c respectively.

3.2.3 FE modelling

The finite element type S4R, reduced integration four-noded doubly curved shell element with six degrees of freedom per node (three displacements and three rotations per node) was adopted in the current investigation to discretize FE models as shown in Figure 2. This element is reported suitable for modelling a wide range of shell thickness and was successfully used in similar type of investigations conducted in thin-

walled structures (e.g. (Ellobody and Young, 2005; Patton and Singh, 2012; Saliba and Gardner, 2013a; Sonu and Singh, 2017)). FE elements with aspect ratio of S4R element equal to ~1.0 were adopted. Element size of ~10 mm × 10 mm has been chosen based on mesh convergence study (by performing linear elastic eigen value buckling analysis). The number of S4R elements used in the current study ranges from ~ 12,000 to 25,000. Boundary conditions for bending tests were chosen to match up the experimental test conducted by Saliba and Gardner (2013a). Vertical and lateral displacements were restrained at both the support ends (bottom flange) similar to simply supported condition and lateral displacement was restrained at mid span where vertical concentrated load is applied (top flange) in order to avoid lateral torsional buckling following Saliba and Gardner (2013a) as shown in Figure 3. The loads were applied as static uniform loads in increments at the loaded points using the modified RIKS method, which is reported to be suitable for static and non-linear analysis (Hassanein, 2011). Intermediate stiffeners and end posts are also provided at the loaded points and supports respectively as shown in Figure 1 following Saliba and Gardner (2013a) in order to prevent local buckling of web and flanges particularly at loaded points and supports due to heavy concentrated loads.

3.2.4 Material modelling

The material properties of LDSS, HSS and DSS I-beams used in the present study consist of LDSS material (Table 3.1) based on the experimental study of LDSS plates by Saliba and Gardner (2013a) and DSS material (Table 3.2) based on the experimental study conducted on DSS sheet by Arrayago *et al.*, (2015). LDSS material and DSS material are used for LDSS and DSS I-beams respectively, and exceptionally for HSS I-beams, LDSS material (Tables 3.1a and b) and DSS material (Table 3.2) are used in the web and flanges respectively. Equation 3.1 represents the Ramberg and Osgood model (1943) for $\sigma \leq \sigma_{0.2}$ ($\sigma_{0.2}$ is the 0.2% proof stress) which provide good agreement with stress-strain curve obtained from experiments for steel up to $\sigma_{0.2}$ and for strains exceeding $\varepsilon_{t0.2}$ (total strains at $\sigma_{0.2}$), it gives higher values of stress as compared to

experimental data. Therefore, for strains exceeding $\varepsilon_{t0.2}$, Gardner and Ashraf (2006) proposed a modified version of Ramberg-Osgood model (Equation 3.2) which are utilized for LDSS material and similarly a modified Ramberg-Osgood model (Equation 3.3) given by Rasmussen (2003) are used for DSS material which were based on Mirambell and Real's two-stage model (Mirambell and Real, 2000).

$$\varepsilon = \frac{\sigma}{E} + 0.002\left(\frac{\sigma}{\sigma_{0.2}}\right)^{n} \tag{3.1}$$

$$\varepsilon = \frac{\sigma - \sigma_{0.2}}{E_{0.2}} + \left(\varepsilon_{t1.0} - \varepsilon_{t0.2} - \frac{\sigma_{1.0} - \sigma_{0.2}}{E_{0.2}}\right) \times \left(\frac{\sigma - \sigma_{0.2}}{\sigma_{1.0} - \sigma_{0.2}}\right)^{n'_{0.2,1.0}} + \varepsilon_{t0.2} \tag{3.2}$$

$$\varepsilon = \frac{\sigma - \sigma_{0.2}}{E_{0.2}} + \varepsilon_{u}\left(\frac{\sigma - \sigma_{0.2}}{\sigma_{1.0} - \sigma_{0.2}}\right)^{m} + \varepsilon_{t0.2} \tag{3.3}$$

$$E_{0.2} = \frac{\sigma_{0.2} E}{\sigma_{0.2} + 0.002nE} \tag{3.4}$$

$$\varepsilon_{u} = 1 - \frac{\sigma_{0.2}}{\sigma_{u}} \tag{3.5}$$

where $\sigma_{0.2}$ and $\sigma_{1.0}$ are the proof stresses at 0.2% and 1% offset strains respectively; $\varepsilon_{t0.2}$ and $\varepsilon_{t1.0}$ are the total strains at $\sigma_{0.2}$ and $\sigma_{1.0}$ respectively; n and $n'_{0.2,\ 1.0}$ are strain hardening exponents; E and $E_{0.2}$ (Equation 3.4) are the Young's modulus and tangent modulus at 0.2% offset strain respectively; m and ε_u (Equation 3.5) are the second strain hardening parameter and ultimate total strain respectively; σ_u is the ultimate stress which are obtained from experimental results. The two stage non-linear stress-strain relationship given in Eqs. (1), (2) and (3) are further modified into a multi-linear model defined in terms of true stress and log plastic strain for input into Abaqus model (2009). The relationship between true stress (σ_{true}) and engineering stress (σ_{engg}) is given by Equation 3.6, and the relationship between log plastic strain ($\varepsilon_{\ln}^{pl}$) and engineering strain (ε_{engg}) is given by Equation 3.7.

$$\sigma_{true} = \sigma_{engg}\left(1+\varepsilon_{engg}\right) \tag{3.6}$$

$$\varepsilon_{\ln}^{pl} = \ln\left(1+\varepsilon_{engg}\right) - \frac{\sigma_{true}}{E} \tag{3.7}$$

3.2.5 Geometric imperfection

Most of the engineering structures have initial imperfections, which occurred mostly during the production, fabrication and transportation stages. These imperfections affect the structural performance to a great extent, and it is necessary to account these imperfections in validation of FE models. Two types of geometric imperfections are mainly considered in structures; global and local geometric imperfections. In the present study, only local geometric imperfections were considered in the FE models, since global buckling of the beam is prevented (lateral displacement was restrained at mid span top flange) following Saliba and Gardner (2013a). The method used to incorporate initial geometric imperfections into FE model is to determine the amplitude of the lowest eigen mode by performing elastic buckling analysis, using the Subspace method which will be further used in the subsequent nonlinear analysis (Theofanous and Gardner, 2010; Saliba and Gardner, 2013a). The imperfection amplitude given by Dawson and Walker (1972) (Equation 3.8) which was modified by Gardner and Nethercot (2004) for stainless steel was chosen to determine the imperfection amplitude for the parametric studies as it has shown least deviation in ultimate loads between test and FE model as compared to other imperfection amplitudes performed by Saliba and Gardner (2013a).

$$\omega_{D\&W} = 0.023\left(\frac{\sigma_{0.2}}{\sigma_{cr}}\right)t \tag{3.8}$$

Where t is the thickness of plates and σ_{cr} is the elastic critical buckling stress of plated elements.

3.2.6 Validation of FE models

A validation study was carried out based on the results of experimental tests performed on homogeneous LDSS welded I-beams from the work of Saliba and Gardner (2013a) and hybrid high-strength steel (Gr.Q345 and Gr.Q460) welded I-beams conducted by Shokouhian *et al.* (2016). This study aims at validation of current FE model considering similar cross-sections and loading conditions followed in the experimental tests. For homogeneous LDSS welded I-beams, 3PB and 4PB tests conducted on the beam (I-200×140×10×8) were validated using the material properties given in Table 1, the average stress-strain relationship of tensile coupons for 8 mm (Table 3.1a) and 10 mm (Table 3.1c) thicknesses were applied to the lower halves (below neutral axis) of the beam at the web and flange respectively. Also, the average stress-strain relationship of compressive coupons for 8 mm (Table 3.1b) and 10 mm (Table 3.1d) thicknesses were applied to the upper halves (above neutral axis) at the web and flange respectively following Saliba and Gardner (2013a). For hybrid high strength steel welded I-beams, 4PB test conducted on the beam (I-360×168×12×8) was validated using the material properties given in Table 3.3: the stress-strain relationship of the tensile coupons for 8 mm thick (Gr.Q345) and 12 mm thick (Gr.Q460) high strength steel were applied to the web and flanges respectively. FE failure modes for 3PB and 4PB specimens of LDSS welded I-beams (I-200×140×10×8) are shown in Figures 3.4 and 3.5 and FE failure mode for 4PB test of hybrid high strength steel welded I-beams (I-360×168×12×8) is shown in Figure 3.6. Figures 3.7 and 3.8 show the comparison of FE and experimental normalized moment-rotation (M-θ) curve for 3PB and 4PB specimens of LDSS welded I-beams (I-200×140×10×8) respectively. It can be observed from Figures 3.7, 3.8 and 3.9 that the percentage errors in flexural strength are ~2.70%, ~1.67% and ~1.87% respectively, which may be considered minimal. Figure 3.9 shows the comparison of FE and experimental normalized M-θ curve for 4PB specimen of hybrid high strength steel welded I-beams (I-360×168×12×8) and the percentage error in flexural strength is ~1.87%. It can be seen from Figures 3.7, 3.8 and 3.9 that a good agreement between FE and experimental models was achieved (i.e. bending strength (M_u) and rotation at M_u

(θ_u) are well predicted). Therefore, FE modeling approach adopted in the current study are found to predict the experimental results accurately and hence can be adopted for further parametric studies. Also, it is understood that LDSS, HSS and DSS I-beams having different thicknesses and materials (in case of HSS I-beams) of flange and web plates would be formed by welding, following similar procedure carried out by Saliba and Gardner (2013a). However, the effect of residual stress developed due to welding near the heat affected zone (HAZ) may be neglected in all FE models, since the effect of considering residual stresses seen in the study conducted by Saliba and Gardner (2013a) for LDSS welded I-sections was found to be insignificant.

3.2.7 Parametric study

Upon successful calibration of FE models with experimental results, numerical investigation on the flexural behaviour of LDSS, HSS and DSS I-beams are carried out. The material properties adopted for the parametric study are given in Tables 3.1 and 3.2. The material properties incorporated for homogenous LDSS I-beams are similar to the material properties (see Table 3.1) which are used in validation study of LDSS I-beams (i.e. I-200×140×10×8). The material properties used for homogenous DSS I-beams are given in Table 3.2. In case of HSS I-beams, the DSS material properties given in Table 3.2 are used in both flanges and the LDSS material properties given in Table 3.1a and b are used for the bottom web (below neutral axis) and top web (above neutral axis) respectively. The flange and web slenderness are considered as key parameters which include flange-critical section and web-critical section and also the applicability of codified cross-section slenderness limits for three types of sections: LDSS, HSS and DSS I-beams. 3PB and 4PB tests were chosen for the current investigation. The flange and web slenderness were studied by varying flange thickness (t_f) and web thickness (t_w) respectively keeping flange width (b_f = 140 mm) and web height (h_w= 200 mm) as constant. The ranges of various parameters adopted in the current study are: t_f = 4-18 mm and t_w = 2-12 mm and a total of about 110 FE models have been analysed. The FE results are plotted in the form of moment capacity and

failure/deformed shapes. In addition, FE results are also compared with the results given by European code (EN 1993-1-4:2006 + A1, 2015) and Direct Strength Method (DSM) (Becque *et al.*, 2008; Rossi and Rasmussen, 2012; Arrayago *et al.*, 2017).

3.3 CURRENT DESIGN CODES

3.3.1 General

The numerical bending strength (M_u) are compared with unfactored design bending resistance predicted by European code (EN 1993-1-4:2006 + A1, 2015) and Direct Strength Method (DSM) (Becque *et al.*, 2008; Rossi and Rasmussen, 2012; Arrayago *et al.*, 2017) for LDSS, DSS and HSS I-beams. Comparison of numerical results with design moment resistances are shown in Tables 3.4 to 3.6.

3.3.2 European code

In order to check the applicability of the current flange and web slenderness limits of European code (EN 1993-1-4:2006 + A1, 2015), the FE results of three different sections: LDSS, HSS and DSS I-beams are plotted for the various response characteristics: M_u/M_{el}, M_u/M_p and R against the flange slenderness ($c_f/t_f\varepsilon$) for the flange-critical case and web slenderness ($c_w/t_w\varepsilon$) for the web-critical case of the cross-section following Saliba and Gardner (2013a), where M_p and M_{el} are the plastic moment and elastic moment respectively; R is the rotation capacity which is calculated based on rotation (Equation 3.9) and curvature (Equation 3.10) for 3PB and 4PB specimens respectively following Saliba and Gardner (2013a); c_w and c_f are the flat element width of web and outstand flange width respectively; t_f and t_w are the flange thickness and web thickness respectively and ε is the material factor (Equation 3.11). The section slenderness limits for stainless steel sections given in EN 1993-1-4 (2006 + A1, 2015) are based on the width-to-thickness ratios of the critical elements which are grouped in four cross-section classes (Class 1, 2, 3 and 4) in bending. Stainless steel sections

which are capable of achieving their full plastic moment (M_p) and sufficient amount of rotation capacity (R) = 3 are considered as Class 1 similar to carbon steel (EN 1993-1-1, 2005). Sections that are capable of reaching their full plastic moment (M_p) are considered as Class 2. Cross-sections that are capable of attaining their elastic moment (M_{el}) are considered as Class 3. Class 4 cross-sections are those sections which are incapable of attaining their elastic moment (M_{el}) due to occurrence of local buckling (LB).

$$R = \frac{\theta_{pu}}{\theta_{pl}} - 1 \tag{3.9}$$

$$R = \frac{\kappa_{pu}}{\kappa_{pl}} - 1 \tag{3.10}$$

$$\varepsilon = \left[\frac{235}{\sigma_{0.2}} \frac{E}{210000} \right]^{0.5} \tag{3.11}$$

where θ_{pu} is the total rotation at mid-span when moment curve drops below M_p; θ_{pl} is the elastic component of rotation when moment curve reach M_p given as $\theta_{pl} = M_pL/2EI$; κ_{pu} is the total curvature at plastic hinge when moment curve drops below M_p; κ_{pl} is the elastic curvature when moment curve reach M_p given as $\kappa_{pl} = M_p/EI$; I is the second moment of area. According to Clause 5.1 given in European code (EN 1993-1-4:2006 + A1, 2015), the provisions given in Section 5 and 6 of EN 1993-1-1 (2005) should be applied for stainless steels, except where modified or superseded by the special provisions given in European code (EN 1993-1-4:2006 + A1, 2015). Classification of the cross-sections were carried out according to Table 5.2 in EN 1993-1-4 (2006 + A1, 2015), and consequently the EC3 bending moment resistance (M_{EN}) was calculated by the Equations 6.13 to 6.15 of Clause 6.2.5 in EN 1993-1-1 (2005) given in Equation 3.12.

$$M_{EN} = \begin{cases} \dfrac{W_{pl}\sigma_{0.2}}{\gamma_{M0}} \\ \dfrac{W_{el}\sigma_{0.2}}{\gamma_{M0}} \\ \dfrac{W_{eff}\sigma_{0.2}}{\gamma_{M0}} \end{cases} \tag{3.12}$$

where W_{pl} and W_{el} are the major axis plastic and elastic section modulii respectively; W_{eff} is the major axis effective section modulus for Class 4 sections; γ_{M0} is a partial safety factor for cross-section resistance. For Class 4 sections, the effective widths are calculated using Table 4.1 and Clause 4.4 in EN 1993-1-5 (2007). In case of HSS I-beams, the EC3 bending moment resistance (M_{EN}) was calculated by Equation 3.13.

$$M_{EN} = \begin{cases} M_p & M_p = W_{pltf}\sigma_{0.2tf} + W_{plbf}\sigma_{0.2bf} + W_{pltw}\sigma_{0.2tw} + W_{plbw}\sigma_{0.2bw} \\ M_{el} & M_{el} = W_{eltf}\sigma_{0.2tf} + W_{elbf}\sigma_{0.2bf} + W_{eltw}\sigma_{0.2tw} + W_{elbw}\sigma_{0.2bw} \\ M_{eff} & M_{eff} = W_{efftf}\sigma_{0.2tf} + W_{elbf}\sigma_{0.2bf} + W_{efftw}\sigma_{0.2tw} + W_{elbw}\sigma_{0.2bw} \end{cases} \tag{3.13}$$

where W_{eltf} , W_{elbf}, W_{eltw} and W_{elbw} are the elastic section modulus of top flange, bottom flange, top web and bottom web respectively; W_{pltf} , W_{plbf}, W_{pltw} and W_{plbw} are the plastic section modulus of top flange, bottom flange, top web and bottom web respectively; W_{efftf} and W_{efftw} are the effective section modulus of top flange and top web respectively for Class 4 sections, $\sigma_{0.2tf}$, $\sigma_{0.2bf}$, $\sigma_{0.2tw}$ and $\sigma_{0.2bw}$ are the yield stress of top flange, bottom flange, top web and bottom web respectively (see Tables 3.1 and 3.2); M_{eff} is the effective moment capacity for Class 4 sections.

3.3.3 Direct strength method

Direct Strength Method (DSM) is a simple non-iterative design method which is an alternative for the traditional 'effective width method'. It was first developed by Schafer and Pekoz (1998) and further implemented in the North American

Specifications AISI (2016b) for carbon steel structures. The DSM procedure adopted in the current study utilizes the full cross-section slenderness ratio (λ_l) which measures the susceptibility of the cross-section to local buckling through the critical elastic local buckling moment (M_{crl}) which can be obtained from software programs based on finite element and finite strip methods (Equation 3.14) (Arrayago *et al.*, 2017).

$$\lambda_l = \sqrt{\frac{M_{el}}{M_{crl}}} \tag{3.14}$$

All stainless steel grades show a non-linear rounded stress-strain curve, with no sharp yield point and significant strain hardening (Gardner, 2005) which makes them different from carbon steel. Due to the significant strain hardening, DSM predicts overly-conservative design results for stainless steel sections. An alternative design approach for stainless steel sections employing strain hardening effects into the DSM formulation was proposed by Rossi and Rasmussen (2012) particularly for compression members. Later, DSM design rules for different loading conditions including bending, compression and combined loading were developed for stainless steel Rectangular and Square Hollow Sections (RHS and SHS) (Arrayago *et al.*, 2017). The DSM bending moment resistance (M_v) for stainless steel sections can be calculated from Equation 3.15 which shows slenderness limits of 0.474 for slender and stocky sections (Becque *et al.*, 2008). It may be noted that, in Equation 3.15, the inelastic reserved strength in flexure (M_n) (as mentioned in Procedure II adopted by SEI/ASCE 8-02 (ASCE, 2002)) becomes M_{el}, as the compression strain factor (C_y) becomes 1, in the present case.

$$\frac{M_v}{M_{el}} = \begin{cases} 1 & for \lambda_l \leq 0.474 \\ \frac{0.95}{\lambda_l^{0.8}} - \frac{0.22}{\lambda_l^{1.6}} & for \lambda_l > 0.474 \end{cases} \tag{3.15}$$

The DSM bending moment resistance (M_v) for stainless steel stocky sections given in Equation 3.15 is limited to M_{el} (see Equation 3.13) which results in overly-conservative

design as the beneficial strain hardening effect has not been incorporated. An alternative modified DSM formulation ($M_{v,RR}$) including strain hardening effect for stainless steel sections which was proposed by Rossi and Rasmussen (2012) is given in Equation 3.16.

$$\frac{M_{v,RR}}{M_{el}} = \begin{cases} 1+\left(1-2.11\lambda_l\right)\left(\frac{\sigma_u}{\sigma_{0.2}}-1\right) & for\ \lambda_l \le 0.474 \\ \frac{0.95}{\lambda_l^{0.8}} - \frac{0.22}{\lambda_l^{1.6}} & for\ \lambda_l > 0.474 \end{cases} \tag{3.16}$$

Furthermore, Arrayago *et al.* (2017) proposed a full-range modified DSM formulation ($M_{v,ARR}$) based on carbon steel strength curve following similar procedure proposed by Rossi and Rasmussen (2012) which is given in Equation 3.17. For HSS I-beams, σ_u (Equation 3.18) and $\sigma_{0.2}$ (Equation 3.19) are taken as weighted average values in the DSM formulation given in Equations 3.16 and 3.17.

$$\frac{M_{v,ARR}}{M_{el}} = \begin{cases} 1+(1-1.29\lambda_l)\left(\frac{\sigma_u}{\sigma_{0.2}}-1\right) & for\ \lambda_l \le 0.776 \\ \frac{1}{\lambda_l^{0.8}} - \frac{0.15}{\lambda_l^{1.6}} & for\ \lambda_l > 0.776 \end{cases} \tag{3.17}$$

$$\sigma_{0.2} = \frac{A_{tf}\sigma_{0.2tf} + A_{bf}\sigma_{0.2bf} + A_{tw}\sigma_{0.2tw} + A_{bw}\sigma_{0.2bw}}{A} \tag{3.18}$$

$$\sigma_u = \frac{A_{tf}\sigma_{utf} + A_{bf}\sigma_{ubf} + A_{tw}\sigma_{utw} + A_{bw}\sigma_{ubw}}{A} \tag{3.19}$$

where σ_{utf}, σ_{ubf}, σ_{utw} and σ_{ubw} are the ultimate stress of top flange, bottom flange, top web and bottom web respectively (see Tables 3.1 and 3.2); A_{tf}, A_{bf}, A_{tw}, A_{bw} and A are the areas of top flange, bottom flange, top web, bottom web and total area of cross-section respectively.

3.3.4 Reliability analysis

A reliability analysis following the principles given by Lin *et al.*, (1992) as the basis of LRFD design for stainless steel members was conducted to check the applicability of present design standard adopted in the current study. The reliability analysis procedure given in the Commentary of the ASCE Specifications for the design of cold-formed stainless steel structural members (ASCE 8-02, 2002) was adopted in the present study. A target reliability index (β_o) of 2.5 is used as a lower limit for stainless steel structural members. The design specification given by EC3 (EN 1993-1-1, 2005), DSM in AISI standard (AISI, 2016b) and modified DSM (Rossi and Rasmussen, 2012; Arrayago *et al.*, 2017) which were used in the current study are considered to be reliable if the reliable index is greater than or equal to 2.5. The resistance factor (φ) of 0.90 for stiffened and partially stiffened compression flanges subjected to bending was recommended for DSM (AISI, 2016b) and resistance factor (φ) of 0.91 was adopted for EC3 (EN 1993-1-1, 2005). The load combination of 1.35 DL +1.5 LL was used for EC3 and 1.2 DL + 1.6 LL for DSM following Huang and Young (2013). The dead load (DL) to live load (LL) ratio of 1/5 was recommended in AISI specification (AISI, 2016b). The statistical parameters which includes the mean and coefficients of variation for material properties (M_m = 1.10, V_M = 0.10) and fabrication factors (F_m = 1.0 and V_F = 0.05) for flexural members detailed in Clause 3.3.1.1 of the commentary of ASCE specification (ASCE 8-02, 2002) were adopted. The reliability index (β) was calculated using the Eq. C-2 given in the commentary of ASCE specification (ASCE 8-02, 2002). The mean values (P_m), coefficient of variation (V_p) and reliability index (β) of the ratio of FE results to the design predictions for LDSS, HSS and DSS I-beams were computed and shown in Tables 3.4, 3.5 and 3.6 respectively. Direct comparison adopting similar resistance factor (φ_o) of 0.90 and load combination of 1.2 DL +1.6 LL following Huang and Young (2013) were used to compute the reliability index (β) and the values are given in Tables 3.4-3.6.

3.4 RESULTS AND DISCUSSIONS

3.4.1 Flange-critical section

The results obtained from the FE models are categorized into three section types as discussed earlier LDSS, HSS and DSS I-beams subjected to 3PB and 4PB. Figure 3.10 shows normalized moment-rotation (M-θ) curve for Class 1 section (i.e. $c_f/t_f\varepsilon \leq 9$) of flange slenderness ratios ($c_f/t_f = 4.7$) for LDSS, HSS and DSS I-beams in 3PB and 4PB. For 3PB specimen (see Figure 3.10), it can be seen that rotation capacity (R) is maximum for LDSS I-beams, and a reduction of ~34% and ~48% can be seen from HSS and DSS I-beams respectively. Similar observations can also be seen for the case of 4PB specimen as compared to that of 3PB specimen with R being maximum for LDSS I-beams with a reduction of around ~36% and ~38% for HSS and DSS I-beams respectively (see Figure.10). The increase of R clearly shows that LDSS I-beams have higher ductility as compared to HSS and DSS I-beams thus indicating that use of LDSS results in enhanced ductility. However, M_u is found to be minimum for LDSS I-beams. In comparison with LDSS I-beams, an increase of around ~22% and ~26% in case of 3PB specimen (Tables 3.4-3.6), and ~27% and ~31% in case of 4PB specimen (Tables 3.4-3.6) can be seen for HSS and DSS I-beams respectively. From this observation, significant increase in M_u can be seen in case of HSS I-beams although the proportion of DSS material is maintained in HSS I-beams. Though, it is known that incase of HSS I-beams, DSS material is used only in the flanges which are relatively of higher strength as compared to LDSS material and consistent with M_u being primarily contributed by the flanges for a member subjected to pure bending (Shokouhian and Shi, 2014). Figure 3.11 shows Von-Mises stress contours for HSS Class 1 section (c_f/t_f = 4.7) in 3PB and 4PB corresponding to θ_u (rotation at M_u) and $2\theta_u$. The values of Von-Mises stress (hereafter referred to as stress) ≥ 652 MPa (i.e. $\sigma_{0.2f}$) are grey-coloured, in order to identify areas which have exceeded yield stress of flange (i.e. $\sigma_{0.2f}$). The stress exceeding yield stress can be the effect of strain hardening. It can be observed from 3PB specimen (Figures 3.11a and b) that at θ_u, the top and bottom flanges in the mid

span have yielded and further at $2\theta_u$ the beam initiates to bend without any signs of plastic hinge (PH). In case of 4PB specimen (Figures 3.11c and d), relatively larger area compared to 3PB specimen at the top and bottom flanges near the mid span have yielded at θ_u. At $2\theta_u$, the beam initiates to bend with occurrence of PH on top flange near the mid span. In both cases (i.e. 3PB and 4PB specimens), shown in Figure 3.10, it can be seen that 3PB specimen shows higher M_u as compared to 4PB specimen for Class 1 sections .This is a commonly observed phenomenon and the reason may be due to lesser possibility of occurrence of local buckling (LB) in case of 3PB specimen (Saliba and Gardner, 2013a).

Figure 3.12 shows normalized M-θ curve for Class 4 sections (i.e. $c_f/t_f\varepsilon > 14$) of flange slenderness ratios ($c_f/t_f = 16.8$) for LDSS, HSS and DSS I-beams in 3PB and 4PB. As seen in Class 1 section, similar behaviour in M_u is also observed for Class 4 section. Minimum M_u is observed for LDSS I-beams with an increase of around ~18% and ~22% in case of 3PB specimens (Tables 3.4-3.6), and ~29% and ~23% in case of 4PB specimens (Tables 3.4-3.6) for HSS and DSS I-beams respectively. Significant improvement in M_u can also be seen for HSS I-beams in Class 4 sections similar to Class 1 sections (see Figure 3.12). Figure 3.13 shows stress contours for HSS I-beams Class 4 sections ($c_f/t_f = 16.8$) in 3PB and 4PB corresponding to θ_u and $2\theta_u$. For 3PB specimen (Figures 3.13a and b) at θ_u, only the top flange near the mid span has yielded and further at $2\theta_u$, occurrence of LB in the yielded region can be observed. However, in 4PB specimen (Figures 3.13c and d) at θ_u, a relatively larger area compared to 3PB specimen has yielded at the top flange near the mid span and also initiation of LB in the yielded region can be observed. At $2\theta_u$, in contrast to 3PB specimen, multiple LB can be seen in the yielded region at the top flange near the mid span. Additionally, a similar observation with Class 1 sections can also be observed in both cases i.e. 3PB and 4PB specimens shown in Figure 3.12, and likewise it can be seen that 3PB specimen shows higher M_u as compared to 4PB specimen for Class 4 sections. Also, it can be observed that increasing the flange slenderness (c_f/t_f) decreases the amount of R in all three

sections: LDSS, HSS and DSS I-beams similar to the observations made by Shokouhian and Shi (2014).

3.4.2 Web-critical section

Normalized M-θ curve for Class 1 sections ($c_w/t_w\varepsilon \leq 72$) of web slenderness ratios (c_w/t_w= 41.7) for LDSS, HSS and DSS I-beams in 3PB and 4PB are shown in Figure 3.14. It can be observed that increasing the web slenderness (c_w/t_w) decreases the amount of R for the three cases considered (see Figure 3.14) similar to the observations made by Shokouhian and Shi (2014). It can be seen that R is generally high for LDSS I-beams when compared with HSS and DSS I-beams in case of Class 1 sections (c_w/t_w = 41.7) similar to the case of flange-critical section (see Section 3.4.1). Reduction of ~36% and ~39% can be seen for HSS and DSS I-beams respectively in 4PB. However, in contrast to 4PB specimen, opposite behaviour can be observed in the case of 3PB specimen. R is found to be maximum for DSS I-beams with a reduction of around ~6% and ~20% for HSS and LDSS I-beams respectively in 3PB. Normally, M_u is found to be minimum for LDSS I-beams with an increase of around ~31% and ~36% in case of 3PB specimens (Tables 3.4-3.6), and ~28% and ~31% in case of 4PB specimens (Tables 3.4-3.6) for HSS and DSS I-beams respectively. This comparison shows that the concept of using hybrid section has significantly improved M_u which was mentioned earlier in flange-critical section (see Section 3.4.1). Figure 3.15 shows stress contours for HSS I-beams Class 1 sections (c_w/t_w = 41.7) in 3PB and 4PB corresponding to θ_u and $2\theta_u$. In case of 3PB specimens (Figures 3.15a and b), it can be seen that at θ_u, the top and bottom flanges around the mid span have yielded. At $2\theta_u$, bending can be seen without any signs of PH similar to the case observed in flange-critical section (see Section 3.4.1). However, in 4PB specimens (Figures 3.15c and d), it can be seen that a larger area compared with the case of 3PB specimens at the top and bottom flanges in the mid span have yielded at θ_u. At $2\theta_u$, initiation of bending can be seen due to buckling of web (WB) in the mid span which enhances occurrence of PH in the top flange around mid span.

Figure 3.16 shows normalized M-θ curve for Class 4 sections ($c_w/t_w\varepsilon$ > 90) of web slenderness ratios (c_w/t_w= 125) in 3PB and 4PB for LDSS, HSS and DSS I-beams. M_u is found to be minimum for LDSS I-beams with an increase of around ~18% and ~22% in case of 3PB specimens (Tables 3.4-3.6), and ~29% and ~23% in case of 4PB specimens (Tables 3.4-3.6) for HSS and DSS I-beams respectively. An improvement in M_u similar to flange-critical section can also be seen for HSS I-beams Class 4 sections (see Section 3.4.1). Figure 3.17 shows stress contours for HSS I-beams Class 4 section (c_w/t_w = 125) in 3PB and 4PB corresponding to θ_u and $2\theta_u$. In case of 3PB specimens (Figures 3.17a and b), it can be seen that at θ_u, the top flange around the mid span has yielded. However in contrast to the flange-critical section (see Section 3.4.1), at $2\theta_u$, it can be observed that the web buckled (WB) diagonally around the mid span with occurrence of LB within the yielded region in top flange. Also, in case of 4PB specimens (Figures 3.17c and d), it can be seen that a larger area at the top flange around the mid span and at the web between the support and loaded points is highly stressed (but not yielded) at θ_u. At $2\theta_u$, the web buckled (WB) diagonally between the support and loaded points. Similar observations in case of flange-critical section (see Section 3.4.1) can be seen that increasing the web slenderness (c_w/t_w) decreases the amount of R in all three sections: LDSS, HSS and DSS I-beams and also consistent to the observations made by Shokouhian and Shi (2014).

3.4.3 Comparison of FE results with European code

The FE results of LDSS, HSS and DSS I-beams in 3PB and 4PB are collected and plotted for the various response characteristics such as M_u/M_{el}, M_u/M_p and R vs the flange slenderness ($c_f/t_f\varepsilon$) for the flange-critical section and web slenderness ($c_w/t_w\varepsilon$) for the web-critical section shown in Figures 3.18-3.23. First considering the case for flange-critical section shown in Figures 3.18-3.20, it can be seen that 3PB specimens give more resistance to bending as compared to 4PB specimens for the same cross-section and class similar to the observation seen in (Saliba and Gardner, 2013a). The flange slenderness limits ($c_f/t_f\varepsilon$) such as Class 3 limits (14), Class 2 limits (10) and

Class 1 limits (9) given in EN 1993-1-4 (2006 + A1, 2015) for welded outstand flanges in compression are found to be safe and overly-conservative and hence to allow for economic designs, the following limits ($c_f/t_f\varepsilon$): 20, 16 and 11 are proposed for Class 3, Class 2 and Class 1 limits respectively. It can also be seen that HSS and DSS I-beams predicted overly-conservative results as compared to LDSS I-beams.

In case of web-critical section shown in Figures 3.21-3.23, it can be seen that 3PB specimens also predict higher bending resistance as compared to 4PB specimens similar to the observations mentioned in flange-critical section. The web slenderness limits ($c_w/t_w\varepsilon$) such as Class 3 limits (90) and Class 2 limits (76) given in EN 1993-1-4 (2006 + A1, 2015) for internal webs in bending are found to be safe and conservative and hence to allow for economic designs, the following limits ($c_w/t_w\varepsilon$): 110 and 100 are also proposed for Class 3 and Class 2 limits respectively. Similar conclusions are also obtained for the case of Class 1 sections, where the limit of 1993-1-4 (2006 + A1, 2015) are found to be safe and conservative for internal webs in bending. The values of mean (P_m), coefficient of variance (V_p) and reliability index (β) for LDSS, HSS and DSS I-beams are found to be 1.11, 0.12, 2.75; 1.08, 0.12, 2.62; and 1.10, 0.13, 2.61 respectively (see Tables 3.4-3.6). Hence, it can be seen that for all the three cases, the reliability index (i.e. β) were observed to be greater than the target reliability index (β_o=2.5) and hence it is reliable.

3.4.4 Direct strength method

This section evaluates the applicability of DSM for the design of LDSS, HSS and DSS I-beams shown in Figures 3.24-3.26. First the DSM formulation (DSM) developed for stainless steel section (Becque *et al.*, 2008) shown in Equation 3.13 has been plotted for all the three sections and it can be seen that the results predicted are too conservative particularly for stocky sections since the DSM flexural capacity (M_v) is limited to M_{el}. The values of mean (P_m), coefficient of variance (V_p) and reliability index (β) for LDSS, HSS and DSS I-beams are found to be 1.17, 0.09, 3.09; 1.14, 0.09, 3.00; and 1.18, 0.09, 3.06 respectively (see Tables 3.4-3.6). From the results of reliability

analysis, the values of β is found to be greater than the target reliability index (β_o=2.5) and hence reliable.

Furthermore, the modified DSM incorporating the beneficial strain hardening effect proposed by Rossi and Rasmussen (DSM-RR) (2012) given in Equation 3.14 was plotted (see Figures 3.24-3.26) and it can be observed that the predicted results are overly-conservative particularly for HSS and DSS I-beams. However, the formulation given in Equation 3.14 predicted accurate results and can be adopted for LDSS I-beams (see Figure 3.24). The values of P_m, V_p and β for LDSS, HSS and DSS I-beams are found to be 1.06, 0.06, 2.80; 1.07, 0.07, 2.81; and 1.11, 0.07, 2.90 respectively (see Tables 3.4-3.6). The values of β is also found to be greater than the target reliability index (β_o =2.5), and in comparison with the DSM formulation (DSM) given in Equation 3.13, the modified DSM formulation (DSM-RR) given in Equation 3.14 predicts more accurate results for all three sections and hence reliable.

The modified full-range DSM formulation (Equation 3.14) based on carbon steel by Arrayago et al. (DSM-ARR) (Arrayago *et al.*, 2017) were also plotted (Figures 3.24-3.26) and it can be seen in Figure 3.24 that the predicted results are unconservative for LDSS I-beams since most of the data points are below the predicted curve. The value of P_m, V_p and β for LDSS I-beams are 0.93, 0.06 and 2.26 respectively, and hence it is found unreliable (see Tables 3.4). Therefore the modified full-range DSM formulation (Equation 3.14) given by Arrayago et al. (DSM-ARR) is not applicable for LDSS I-beams since it is unconservative and not reliable (i.e. β < 2.5). But, this formulation predicted accurate results for DSS I-beams as shown in Figure 3.25. The value of P_m, V_p and β for DSS I-beams are 1.00, 0.09 and 2.52 (see Table 3.6). It can be observed that for DSS I-beams, β is observed to be greater than the target reliability index (β_o=2.5) and hence it is reliable.

3.4.5 Proposed Direct strength method

A new DSM formulation for HSS I-beams is proposed based on the full-range DSM formulation for carbon steel given by Arrayago *et al.*, (2017), in which the ultimate stress (σ_u) and the yield stress ($\sigma_{0.2}$) given in Equation 3.17 are replaced by their weighted average values which are given in Equations 3.18 and 3.19 respectively. After incorporating these weighted average values in Equation 3.17, a simplified equation is obtained and is given in Equation 3.20 which was found to predict conservative results as shown in Figure 3.26. The proposed modified DSM formulation ($M_{v,P}$) for HSS I-beams is given in Equation 3.20 and they predicted accurate results as shown in Figure 3.26.

$$\frac{M_{v,P}}{M_{el}} = \begin{cases} \frac{1}{P_y}\left[\begin{matrix}\left\{2A_f\sigma_{uf} + 2.58\lambda_l\left(A_f\sigma_{0.2f} - A_f\sigma_{uf}\right)\right\}+ \\ \left\{A_w\sigma_{uw} + 1.29\lambda_l\left(A_w\sigma_{0.2w} - A_w\sigma_{uw}\right)\right\}\end{matrix}\right] & for\,\lambda_l \le 0.776 \\ \frac{1}{\lambda_l^{0.8}} - \frac{0.15}{\lambda_l^{1.6}} & for\,\lambda_l > 0.776 \end{cases} \quad (3.20)$$

$$P_y = 2A_f\sigma_{0.2f} + A_w\sigma_{0.2w} \quad (3.21)$$

where A_f and A_w are the cross-sectional area of flange and web respectively; $\sigma_{0.2f}$ and $\sigma_{0.2w}$ are the yield stress of flange and web respectively; σ_{uf} and σ_{uw} are the ultimate stress of flange and web respectively and P_y is the yield load (Equation 3.21). Comparison of the bending strength predicted by the proposed modified DSM (i.e. Equation 3.20) and FE results are shown in Figure 3.26 and Table 3.5. It can be seen that the value of P_m, COV and β for HSS I-beams are 0.99, 0.07 and 2.51 (see Table 3.5). The proposed modified DSM ($M_{v,P}$) given in Equation 3.20 is reliable as β is found to be greater than the target value of 2.5 as shown in Table 3.5.

3.4.6 Conclusion

Numerical study investigating the flexural behaviour of HSS I-beams along with LDSS and DSS I-beams for both flange-critical and web-critical section were conducted in this paper, through a parametric study. Furthermore, the FE results were used to evaluate the applicability of existing design approaches predicted by European code (EN 1993-1-4:2006 + A1, 2015) and Direct Strength Method (DSM) (Becque *et al.*, 2008; Rossi and Rasmussen, 2012; Arrayago *et al.*, 2017). The conclusions drawn from the numerical investigations are presented below:

1) For both Class 1 flange-critical section of c_f/t_f = 4.7 ($c_f/t_f\varepsilon$ = 7.86) and web-critical section of c_w/t_w= 41.7 ($c_w/t_w\varepsilon$ = 62.52), it can be observed that LDSS I-beams has a higher R as compared to HSS and DSS I-beams.

2) Significant increase in M_u can be seen in case of HSS I-beams although the proportion of DSS material is maintained in HSS I-beams. Also, 3PB specimens show higher M_u as compared to 4PB specimens.

3) An increase in flange slenderness ($c_f/t_f\varepsilon$) and web slenderness ($c_w/t_w\varepsilon$) decreases the amount of R for all sections.

4) In general, EN 1993-1-4 is found to be reliable and applicable for LDSS, HSS and DSS I-beams. Additionally, for the purpose of efficient and economic designs, the following limits: 20, 16 and 11 were proposed for Class 3, Class 2 and Class 1 limits respectively for welded outstand flanges in compression (flange-critical section). Also, for internal webs in bending (web-critical section), the following limits: 110 and 100 are proposed for Class 3 and Class 2 limits respectively.

5) New DSM formulation for HSS I-beams has been proposed based on the full-range modified DSM formulation for carbon steel given by Arrayago et al. (2017).

Table 3.1: Lean Duplex Stainless Steel (LDSS) material properties (Saliba and Gardner, 2013a)

Plate thickness (mm)	E (N/mm^2)	$\sigma_{0.2}$ (N/mm^2)	$\sigma_{1.0}$ (N/mm^2)	σ_u (N/mm^2)	Modified R-O coefficients	
					n	$n'_{0.2,\,1.0}$
(a) Average tensile coupon tests						
8	203000	504	545.5	727.5	12.2	2.2
(b) Average compressive coupon tests						
8	206825	525.5	593.8	-	9.2	1.7
(c) Average tensile coupon tests						
10	216500	501	557	768.5	11.8	2.2
(d) Average compressive coupon tests						
10	200975	488.2	557.5	-	7.4	1.6

Table 3.2: Duplex Stainless Steel (DSS) material properties (Arrayago *et al.*, 2015)

Sheet thickness (mm)	Orientation to rolling direction	E (N/mm^2)	$\sigma_{0.2}$ (N/mm^2)	$\sigma_{1.0}$ (N/mm^2)	σ_u (N/mm^2)	Strain hardening exponents	
						n	m
Tensile coupon tests							
3	Longitudinal	208800	652	-	854	8.1	3.9

Table 3.3: High strength steel material properties (Shokouhian *et al.*, 2016)

Sheet thickness (mm)	Steel grade	E (N/mm^2)	$\sigma_{0.2}$ (N/mm^2)	σ_u (N/mm^2)	$\varepsilon_{st}/\varepsilon_y$	$\varepsilon_u/\varepsilon_y$
8	Q345	197600	442.8	555.3	8.1	38.4
12	Q460	206800	545.1	627.2	11.4	32.8

Table 3.4: Comparison of FE results with design predictions for LDSS I-beams

	Section (c/t)	M_u (kNm)	M_{EN} (kNm)	M_v (kNm)	$M_{v,RR}$ (kNm)	$M_{v,ARR}$ (kNm)	$\frac{M_u}{M_{EN}}$	$\frac{M_u}{M_v}$	$\frac{M_u}{M_{v,RR}}$	$\frac{M_u}{M_{v,ARR}}$
3PB specimen	**Flange-critical section (c_f/t_f)**									
	I-200×140×18×11 (3.6)	371.60	328.35	289.32	354.29	383.15	1.13	1.28	1.05	0.97
	I-200×140×14×8.4 (4.7)	288.89	250.70	223.83	272.07	295.18	1.15	1.29	1.06	0.98
	I-200×140×11×6.6 (6.1)	227.01	194.70	175.55	211.83	230.56	1.17	1.29	1.07	0.98
	I-200×140×9.5×5.7 (7.1)	194.76	151.49	151.49	179.84	197.15	1.29	1.29	1.08	0.99
	I-200×140×8×4.8 (8.4)	161.98	127.49	127.49	144.43	161.69	1.27	1.27	1.12	1.00
	I-200×140×7×4.2 (9.7)	135.19	107.27	111.51	120.75	138.01	1.26	1.21	1.12	0.98
	I-200×140×6×3.6 (11.4)	115.89	91.92	95.55	97.16	114.40	1.26	1.21	1.19	1.01
	I-200×140×5.5×3.3 (12.4)	94.97	84.24	86.50	86.50	102.59	1.13	1.10	1.10	0.93
	I-200×140×4.5×2.7 (15.2)	72.14	68.91	66.32	66.32	78.99	1.05	1.09	1.09	0.91
	I-200×140×4.1×2.4 (16.8)	59.58	62.58	57.88	57.88	69.20	0.95	1.03	1.03	0.86
	I-200×140×3.5×2.1 (19.7)	46.11	53.13	46.20	46.20	55.34	0.87	1.00	1.00	0.83
	Web-critical section (c_w/t_w)									
	I-200×140×20×6.4 (31.2)	373.00	337.63	302.03	369.35	399.67	1.10	1.23	1.01	0.93
	I-200×140×16×6.4 (31.2)	308.36	272.26	245.18	298.64	323.72	1.13	1.26	1.03	0.95

	I-200×140×12×4.8 (41.7)	230.22	200.87	183.38	220.26	240.22	1.15	1.26	1.05	0.96
	I-200×140×11×4.4 (45.4)	211.94	183.37	168.00	198.35	217.97	1.16	1.26	1.07	0.97
	I-200×140×10×4 (50)	192.07	152.64	152.64	175.92	195.42	1.26	1.26	1.09	0.98
	I-200×140×9×3.6 (55.6)	172.42	133.68	137.31	153.48	172.87	1.29	1.26	1.12	1.00
	I-200×140×8×3.2 (62.5)	148.93	118.77	122.00	131.05	150.34	1.25	1.22	1.14	0.99
	I-200×140×6×2.4 (83.3)	100.58	88.96	88.78	88.78	105.33	1.13	1.13	1.13	0.95
	I-200×140×5×2 (100)	76.65	73.56	69.45	69.45	82.85	1.04	1.10	1.10	0.93
	I-200×140×4×1.6 (125)	49.61	58.37	50.34	50.34	60.24	0.85	0.99	0.99	0.82
4PB specimen	**Flange-critical section (c_f/t_f)**									
	I-200×140×18×11 (3.6)	359.69	328.35	289.32	364.08	389.13	1.10	1.24	0.99	0.92
	I-200×140×14×8.4 (4.7)	270.41	250.70	223.83	280.93	300.60	1.08	1.21	0.96	0.90
	I-200×140×11×6.6 (6.1)	222.38	194.70	175.55	210.95	230.02	1.14	1.27	1.05	0.97
	I-200×140×10×6 (6.7)	201.09	176.30	159.50	187.34	206.35	1.14	1.26	1.07	0.97
	I-200×140×9×5.4 (7.5)	179.08	143.49	143.49	163.75	182.71	1.25	1.25	1.09	0.98
	I-200×140×8×4.8 (8.4)	152.75	127.49	127.49	140.21	159.10	1.20	1.20	1.09	0.96
	I-200×140×7×4.2 (9.7)	126.94	107.27	111.51	116.70	135.53	1.18	1.14	1.09	0.94
	I-200×140×6×3.6 (11.4)	102.43	91.92	94.42	94.42	111.99	1.11	1.08	1.08	0.91
	I-200×140×5.5×3.3 (12.4)	89.61	84.24	84.45	84.45	100.23	1.06	1.06	1.06	0.89
	I-200×140×5×3 (13.7)	81.28	76.57	74.34	74.34	88.47	1.06	1.09	1.09	0.92
	I-200×140×4.5×2.7 (15.2)	62.96	68.91	64.22	64.22	76.72	0.91	0.98	0.98	0.82

	I-200×140×4.1×2.4 (16.8)	51.66	62.58	55.89	55.89	66.97	0.83	0.92	0.92	0.77
	Web-critical section (c_w/t_w)									
	I-200×140×20×6.4 (31.25)	367.36	337.63	302.03	370.40	400.31	1.09	1.22	0.99	0.92
	I-200×140×16×6.4 (31.25)	293.29	272.26	245.18	305.01	327.61	1.08	1.20	0.96	0.90
	I-200×140×13×5.2 (38.5)	250.00	218.51	198.79	237.46	259.60	1.14	1.26	1.05	0.96
	I-200×140×12×4.8 (41.7)	216.41	200.87	183.38	214.95	236.97	1.08	1.18	1.01	0.91
	I-200×140×10.4×4.2 (47.6)	197.69	173.14	158.92	179.81	201.41	1.14	1.24	1.10	0.98
	I-200×140×8×3.2 (62.5)	147.40	118.77	122.00	125.17	146.75	1.24	1.21	1.18	1.00
	I-200×140×6×2.4 (83.3)	99.47	88.96	85.53	85.53	101.78	1.12	1.16	1.16	0.98
	I-200×140×5×2 (100)	71.83	73.56	65.86	65.86	78.89	0.98	1.09	1.09	0.91
	I-200×140×4×1.6 (125)	44.13	58.97	47.62	47.62	56.21	0.75	0.93	0.93	0.78
Mean (P_m)							1.11	1.17	1.06	0.93
COV(V_p)							0.12	0.09	0.06	0.06
Resistance factor (φ)							0.91	0.90	0.90	0.90
Reliability index (β)							2.56	3.09	2.80	2.29
Resistance factor (φ_o)							0.90	0.90	0.90	0.90
Reliability index (β)							2.75	3.09	2.80	2.26

Table 3.5: Comparison of FE results with design predictions for HSS I-beams

	Section (c/t)	M_u (kNm)	M_{EN} (kNm)	M_v (kNm)	$M_{v,RR}$ (kNm)	$M_{v,ARR}$ (kNm)	$\frac{M_u}{M_{EN}}$	$\frac{M_u}{M_v}$	$\frac{M_u}{M_{v,RR}}$	$\frac{M_u}{M_{v,P}}$
3PB specimen	**Flange-critical section (c_f/t_f)**									
	I-200×140×18×11 (3.6)	453.09	414.81	369.36	419.68	448.45	1.09	1.23	1.08	1.01
	I-200×140×14×8.4 (4.7)	351.62	316.71	285.87	322.84	345.81	1.11	1.23	1.09	1.02
	I-200×140×12×7.2 (5.5)	301.43	269.28	244.72	275.38	295.42	1.12	1.23	1.09	1.02
	I-200×140×9×5.4 (7.5)	225.89	183.24	183.24	200.69	217.84	1.23	1.23	1.13	1.04
	I-200×140×8×4.8 (8.4)	199.92	162.81	162.81	173.48	190.59	1.23	1.23	1.15	1.05
	I-200×140×7×4.2 (9.7)	167.75	138.17	142.40	146.26	163.36	1.21	1.18	1.15	1.03
	I-200×140×5.5×3.3 (12.4)	118.13	108.50	107.10	107.10	122.55	1.09	1.10	1.10	0.96
	I-200×140×5×3 (13.7)	102.83	98.62	93.81	93.81	108.72	1.04	1.10	1.10	0.95
	I-200×140×4.1×2.4 (16.8)	70.48	80.40	70.59	70.59	84.17	0.88	1.00	1.00	0.84
	Web-critical section (c_w/t_w)									
	I-200×140×20×6.4 (31.2)	453.08	434.58	391.14	444.26	472.12	1.04	1.16	1.02	0.96
	I-200×140×16×6.4 (31.2)	351.62	348.41	316.21	356.94	381.00	1.01	1.11	0.99	0.92
	I-200×140×12×4.8 (41.7)	299.90	256.92	236.48	266.01	284.38	1.17	1.27	1.13	1.06
	I-200×140×11×4.4 (45.4)	260.03	234.51	216.65	239.25	257.87	1.11	1.20	1.09	1.01
	I-200×140×10×4 (50)	225.88	196.84	196.84	215.45	233.14	1.15	1.15	1.05	0.97

	I-200×140×9×3.6 (55.6)	211.89	177.06	177.06	187.01	205.65	1.20	1.20	1.13	1.03
	I-200×140×6×2.4 (83.3)	142.36	115.16	115.78	115.78	131.17	1.24	1.23	1.23	1.09
	I-200×140×5×2 (100)	88.06	95.43	85.98	85.98	101.42	0.92	1.02	1.02	0.87
	I-200×140×4×1.6 (125)	58.39	76.61	61.84	61.84	73.11	0.76	0.94	0.94	0.80
4PB specimen	**Flange-critical section (c_f/t_f)**									
	I-200×140×19×11.4 (3.4)	476.73	438.50	389.49	456.89	483.62	1.09	1.22	1.04	0.99
	I-200×140×16.3×9.76 (4.0)	402.04	372.06	333.33	384.77	409.88	1.08	1.21	1.04	0.98
	I-200×140×14×8.4 (4.7)	343.54	316.71	285.87	329.53	351.24	1.08	1.20	1.04	0.98
	I-200×140×13×7.8 (5.1)	324.83	292.90	265.28	303.45	324.43	1.11	1.22	1.07	1.00
	I-200×140×9×5.4 (7.5)	218.29	183.24	183.24	195.67	215.15	1.19	1.19	1.12	1.01
	I-200×140×8×4.8 (8.4)	188.88	162.81	162.81	168.83	187.94	1.16	1.16	1.12	1.01
	I-200×140×6.5×3.9 (10.5)	147.19	128.27	129.16	129.16	146.87	1.15	1.14	1.14	1.00
	I-200×140×6×3.6 (11.4)	125.19	118.39	116.74	116.74	133.63	1.06	1.07	1.07	0.94
	I-200×140×4.1×2.4 (16.8)	66.74	80.40	76.07	76.07	88.82	0.83	0.88	0.88	0.75
	Web-critical section (c_w/t_w)									
	I-200×140×20×6.4 (31.2)	450.12	434.58	391.14	441.61	472.04	1.04	1.15	1.15	0.95
	I-200×140×16×6.4 (31.2)	387.09	348.41	316.21	361.53	385.11	1.11	1.22	1.07	1.01
	I-200×140×12×4.8 (41.7)	276.14	256.92	236.48	257.68	280.03	1.07	1.17	1.07	0.99
	I-200×140×11×4.4 (45.4)	260.22	234.51	216.65	231.80	253.86	1.11	1.20	1.12	1.03
	I-200×140×10×4 (50)	227.65	196.84	196.84	218.53	235.63	1.16	1.16	1.04	0.97

	I-200×140×9×3.6 (55.6)	203.90	177.06	177.06	180.06	201.58	1.15	1.15	1.13	1.01
	I-200×140×8×3.2 (62.5)	171.89	154.09	155.09	155.09	175.52	1.12	1.11	1.11	0.98
	I-200×140×6×2.4 (83.3)	104.01	115.16	105.44	105.44	123.43	0.90	0.99	0.99	0.84
	I-200×140×4×1.6 (125)	49.79	75.89	56.40	56.40	65.90	0.66	0.88	0.88	0.76
Mean (P_m)							1.08	1.14	1.07	0.99
COV(V_p)							0.12	0.09	0.07	0.07
Resistance factor (φ)							0.91	0.90	0.90	0.90
Reliability index (β)							2.50	3.00	2.81	2.51
Resistance factor (φ_o)							0.90	0.90	0.90	0.90
Reliability index (β)							2.62	3.00	2.81	2.51

Table 3.6: Comparison of FE results with design predictions for DSS I-beams

	Section (c/t)	M_u (kNm)	M_{EN} (kNm)	M_v (kNm)	$M_{v,RR}$ (kNm)	$M_{v,ARR}$ (kNm)	$\frac{M_u}{M_{EN}}$	$\frac{M_u}{M_v}$	$\frac{M_u}{M_{v,RR}}$	$\frac{M_u}{M_{v,ARR}}$
3PB specimen	**Flange-critical section (c_f/t_f)**									
	I-200×140×18×11 (3.6)	472.20	429.90	372.14	418.85	445.50	1.10	1.27	1.13	1.06
	I-200×140×14×8.4 (4.7)	364.84	328.24	289.08	323.41	344.87	1.11	1.26	1.13	1.06
	I-200×140×12×7.2 (5.5)	314.04	279.16	247.95	276.44	295.22	1.12	1.27	1.14	1.06
	I-200×140×9×5.4 (7.5)	235.26	186.24	186.24	202.43	218.57	1.26	1.26	1.16	1.08
	I-200×140×8×4.8 (8.4)	207.98	160.88	165.66	174.45	190.98	1.29	1.26	1.19	1.09
	I-200×140×7×4.2 (9.7)	179.40	140.71	145.05	148.44	164.59	1.27	1.24	1.21	1.09
	I-200×140×5.5×3.3 (12.4)	119.40	110.50	109.07	109.07	124.04	1.08	1.09	1.09	0.96
	I-200×140×5×3 (13.7)	102.53	100.44	95.86	95.86	110.49	1.02	1.07	1.07	0.93
	I-200×140×4.1×2.4 (16.8)	72.98	81.55	71.89	71.89	85.72	0.89	1.02	1.02	0.85
	Web-critical section (c_w/t_w)									
	I-200×140×20×6.4 (31.2)	472.21	443.36	392.36	441.61	469.71	1.07	1.18	1.18	1.04
	I-200×140×16×6.4 (31.2)	364.80	357.19	318.23	356.02	379.65	1.02	1.20	1.07	1.01
	I-200×140×12×4.8 (41.7)	312.80	263.51	238.64	266.05	284.13	1.19	1.15	1.02	0.96
	I-200×140×11×4.4 (45.4)	268.94	218.78	218.78	239.95	258.06	1.23	1.32	1.18	1.11

	I-200×140×10×4 (50)	243.99	198.92	198.92	214.23	232.23	1.23	1.23	1.12	1.04
	I-200×140×9×3.6 (55.6)	218.81	175.62	179.07	188.45	206.36	1.25	1.23	1.14	1.05
	I-200×140×6×2.4 (83.3)	145.33	116.54	117.29	117.29	132.12	1.25	1.24	1.24	1.10
	I-200×140×5×2 (100)	88.64	96.45	87.25	87.25	102.72	0.92	1.02	1.02	0.86
	I-200×140×4×1.6 (125)	60.31	77.50	62.80	62.80	74.24	0.78	0.96	0.96	0.81
4PB specimen	**Flange-critical section (c_f/t_f)**									
	I-200×140×18×11 (3.6)	478.75	429.90	372.14	434.35	454.98	1.11	1.29	1.10	1.05
	I-200×140×14×8.4 (4.7)	352.93	328.24	289.08	331.68	349.93	1.08	1.22	1.06	1.01
	I-200×140×12×7.2 (5.5)	310.50	279.16	247.95	278.94	296.75	1.11	1.25	1.11	1.05
	I-200×140×10.5×6.3 (6.4)	269.90	217.11	217.11	238.62	256.40	1.24	1.24	1.13	1.05
	I-200×140×8×4.8 (8.4)	196.27	160.88	165.66	171.38	189.10	1.22	1.18	1.15	1.04
	I-200×140×6.5×3.9 (10.5)	146.08	130.64	131.84	131.84	148.67	1.12	1.11	1.11	0.98
	I-200×140×6×3.6 (11.4)	127.68	120.57	120.78	120.78	136.57	1.06	1.06	1.06	0.93
	I-200×140×5.2×3.1 (13.2)	96.51	104.40	97.67	97.67	113.46	0.92	0.99	0.99	0.85
	I-200×140×4.1×2.4 (16.8)	63.73	81.55	66.85	66.85	79.43	0.78	0.95	0.95	0.85
	Web-critical section (c_w/t_w)									
	I-200×140×20×6.4 (31.2)	494.59	443.36	392.36	440.15	468.82	1.12	1.26	1.12	1.05
	I-200×140×16×6.4 (31.2)	397.79	357.19	318.23	360.08	382.13	1.11	1.25	1.10	1.04
	I-200×140×15.5×6.2 (32.2)	384.76	345.32	308.26	343.72	367.05	1.11	1.25	1.12	1.05
	I-200×140×12×4.8 (41.7)	282.86	263.51	238.64	257.11	278.67	1.07	1.19	1.10	1.02

	I-200×140×11×4.4 (45.4)	267.62	218.78	218.78	226.00	249.53	1.22	1.22	1.18	1.07
	I-200×140×10×4 (50)	241.82	198.92	197.35	197.35	221.58	1.22	1.23	1.23	1.09
	I-200×140×8×3.2 (62.5)	189.58	156.03	147.57	147.57	169.86	1.21	1.28	1.28	1.12
	I-200×140×6×2.4 (83.3)	119.93	116.54	101.34	101.34	120.77	1.03	1.18	1.18	0.99
	I-200×140×4×1.6 (125)	57.49	77.50	59.87	59.87	69.46	0.74	0.96	0.96	0.83
Mean (P_m)							1.10	1.18	1.11	1.00
COV(V_p)							0.13	0.09	0.07	0.09
Resistance factor (φ)							0.91	0.90	0.90	0.90
Reliability index (β)							2.50	3.06	2.90	2.52
Resistance factor (φ_o)							0.90	0.90	0.90	0.90
Reliability index (β)							2.61	3.06	2.90	2.52

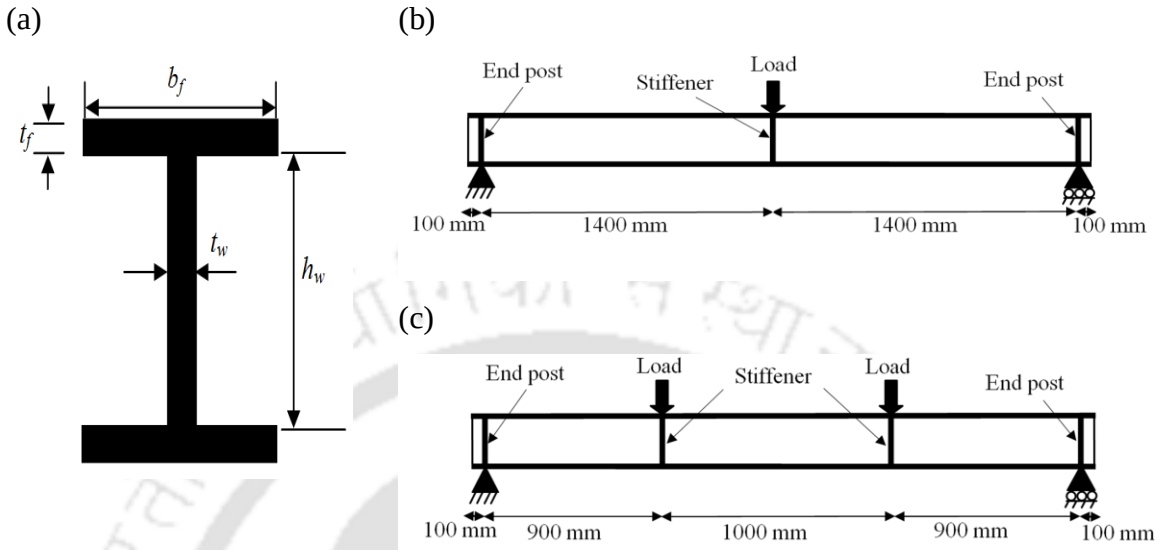

Figure 3.1: Schematic diagram showing (a) Cross-section notations (b) 3PB specimen (c) 4PB specimen

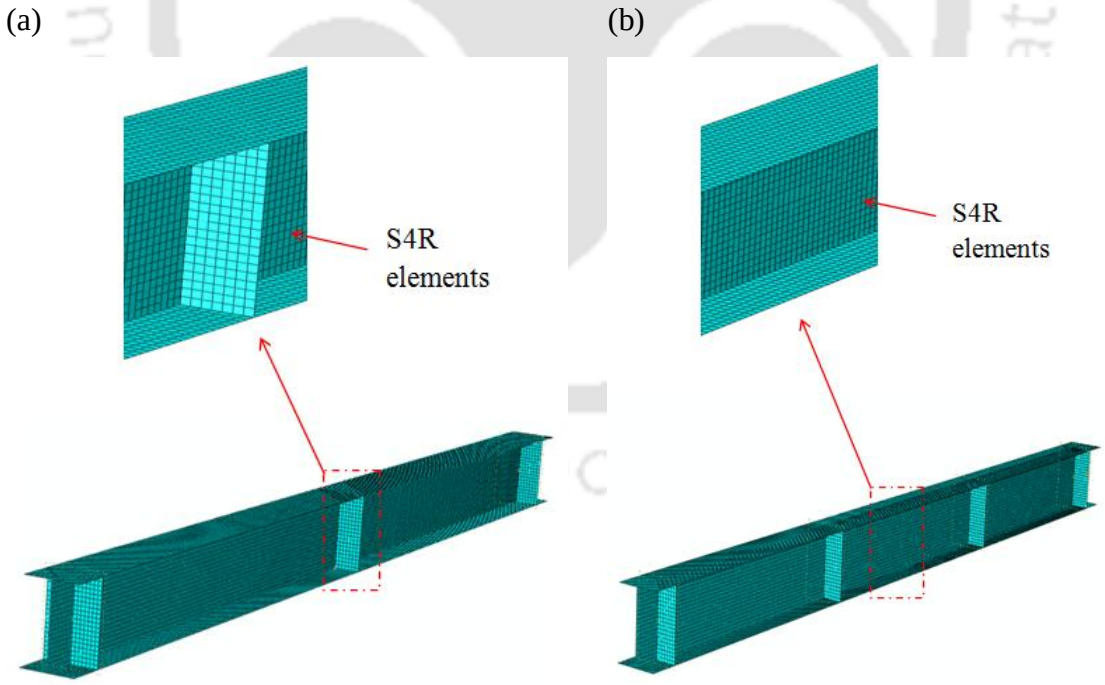

Figure 3.2: Schematic FE mesh diagram of (a) 3PB specimen (b) 4PB specimen

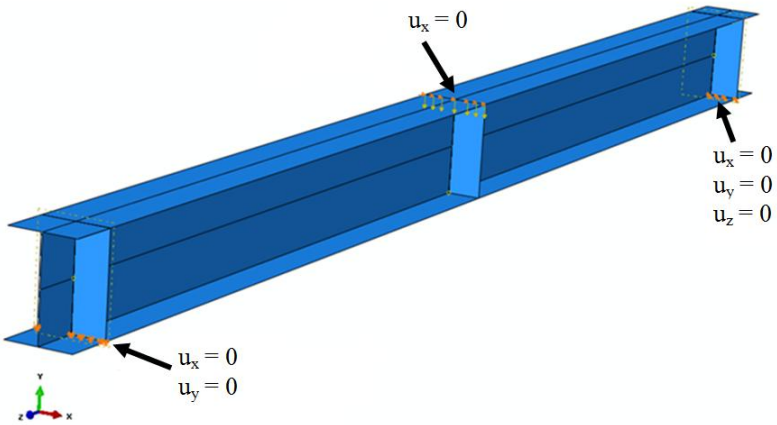

Figure 3.3: Schematic diagram showing boundary conditions of 3PB specimen

(a)

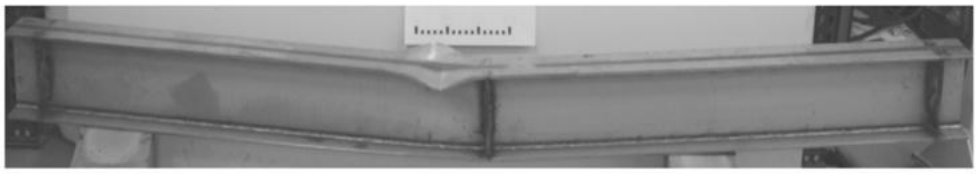

(b)

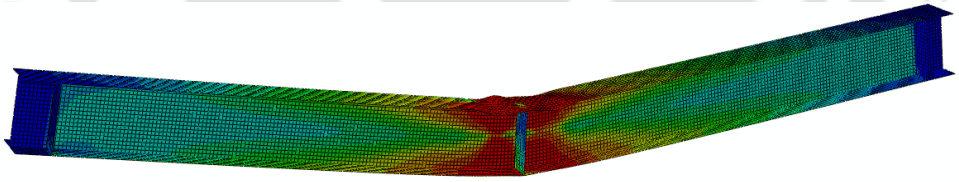

Figure 3.4: Typical failure mode of 3PB specimen of LDSS welded I-beams (I-200×140×10×8) showing (a) Experiment (Saliba and Gardner, 2013a) (b) FE

(a)

(b)

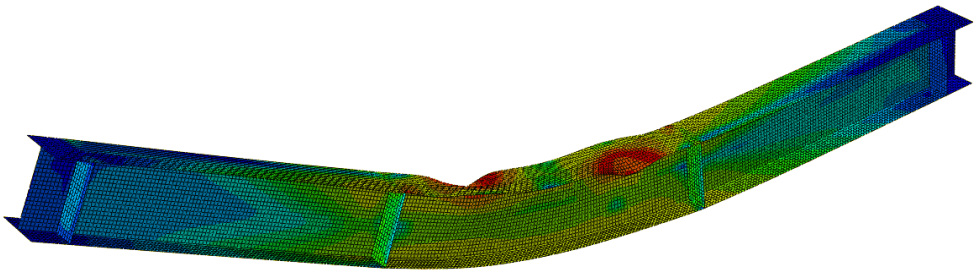

Figure 3.5: Typical failure mode of 4PB specimen of LDSS welded I-beams (I-200×140×10×8) showing (a) Experiment (Saliba and Gardner, 2013a) (b) FE

(a)

(b)

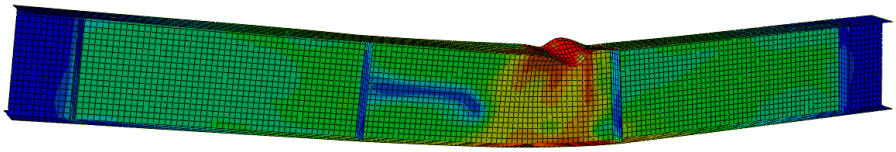

Figure 3.6: Typical failure mode of 4PB specimen of Hybrid high strength steel welded I-beams (I-360×168×12×8) showing (a) Experiment (Shokouhian *et al.*, 2016) (b) FE

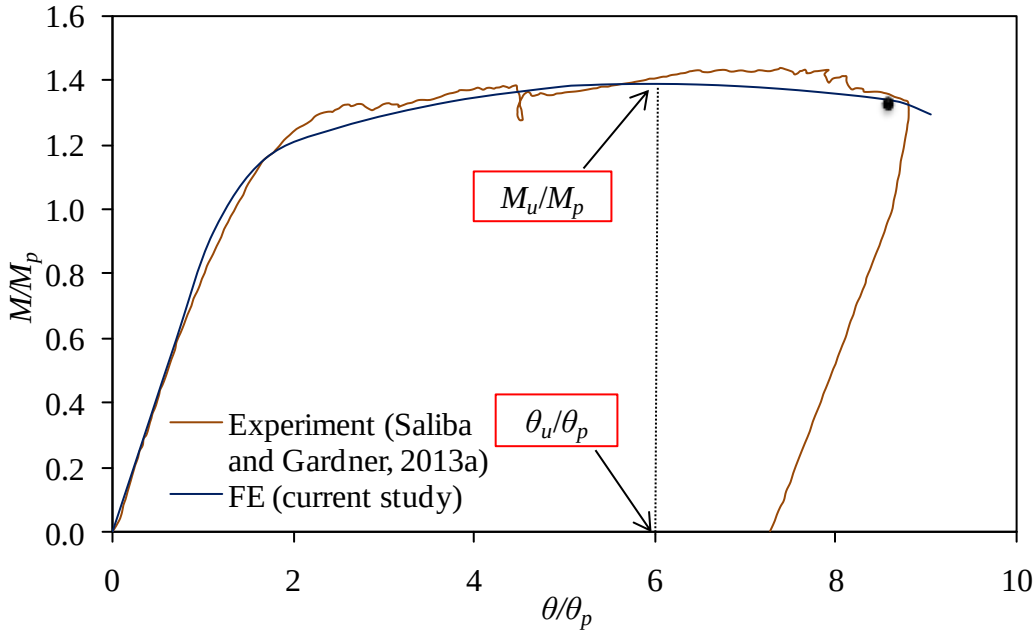

Figure 3.7: Comparison of experimental and FE results for 3PB specimen of LDSS welded I-beams (I-200×140×10×8)

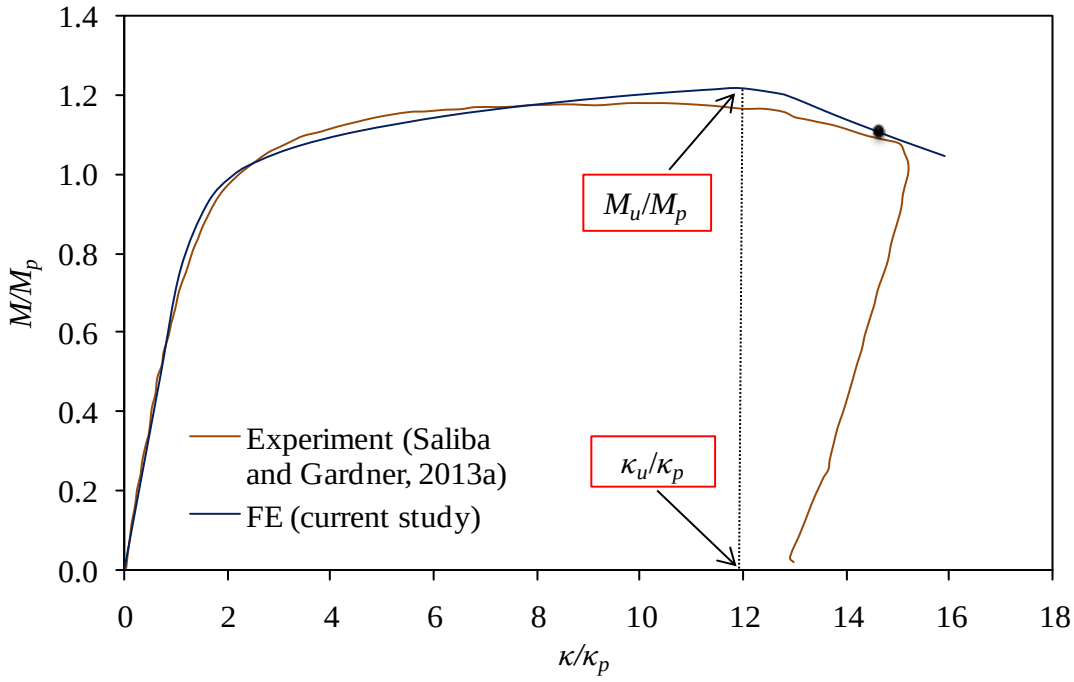

Figure 3.8: Comparison of experimental and FE results for 4PB specimen of LDSS welded I-beams (I-200×140×10×8)

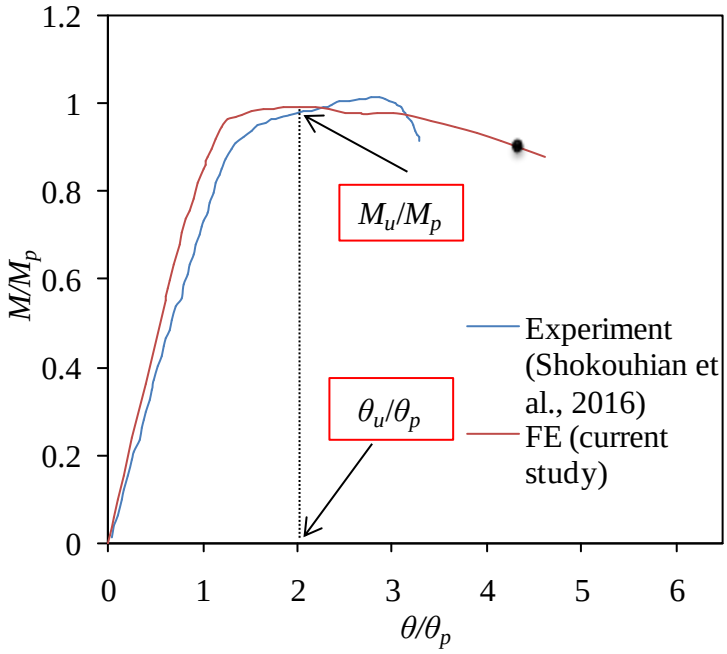

Figure 3.9: Comparison of experimental and FE results for 4PB specimen of Hybrid high strength steel welded I-beams (I-360×168×12×8)

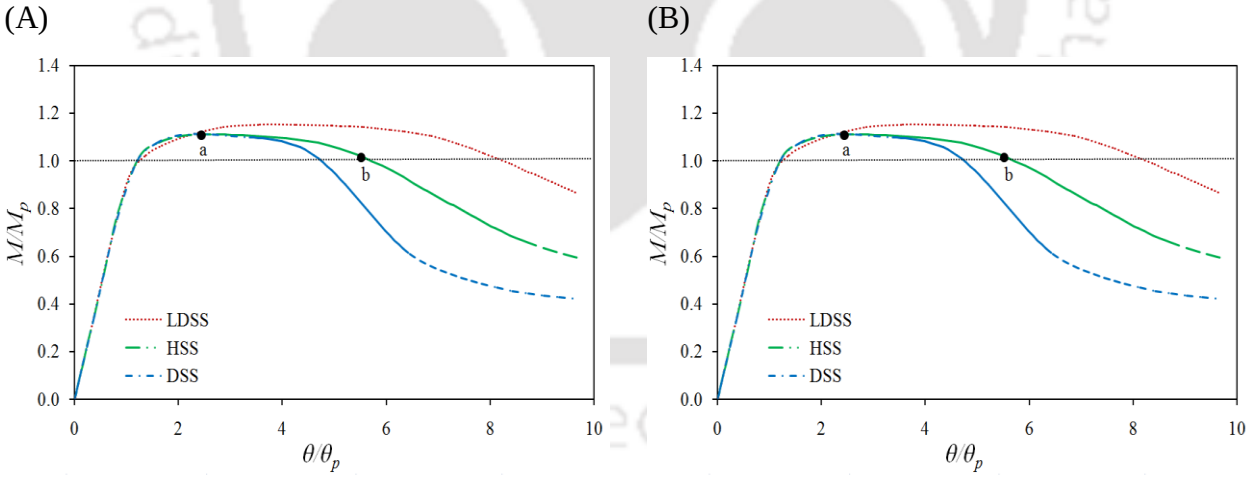

Figure 3.10: Normalised moment-rotation (M-θ) curve for Class 1 sections (c_f/t_f= 4.7): (A) 3PB specimens (B) 4PB specimens

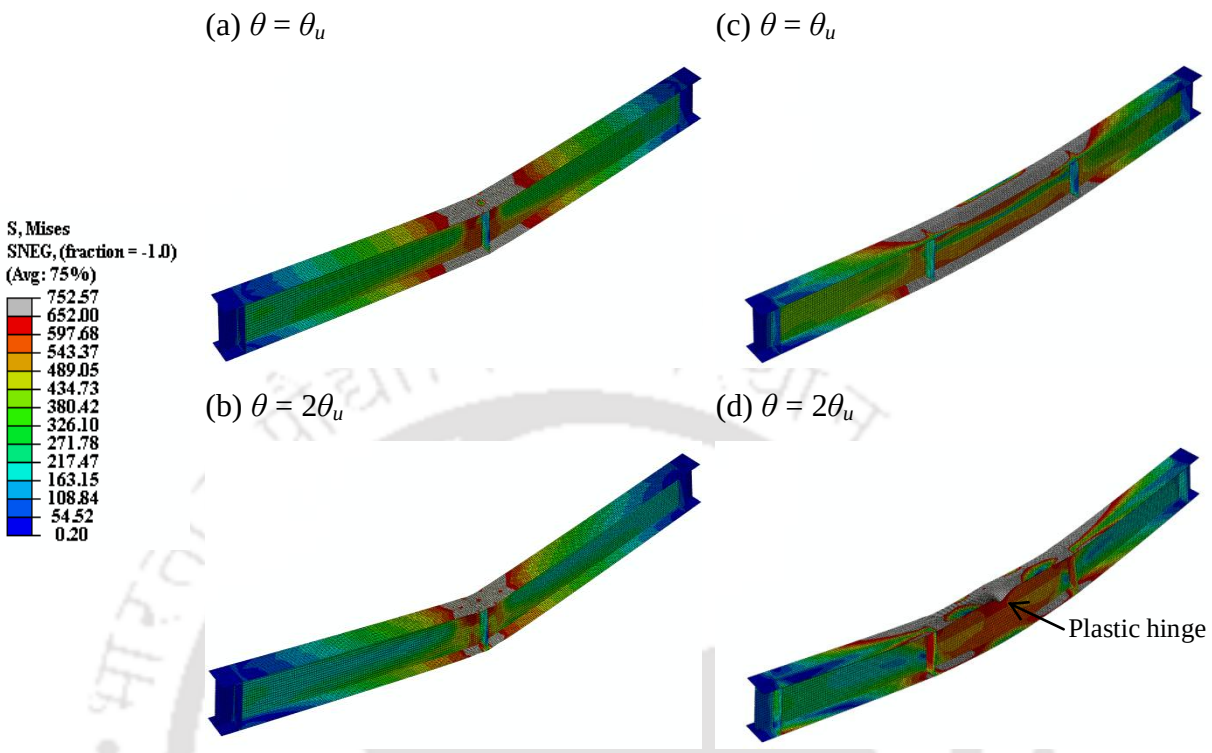

Figure 3.11: Schematic FE diagram of Class 1 HSS sections (c_f/t_f= 4.7): 3PB specimen (a,b) and 4PB specimen (c,d)

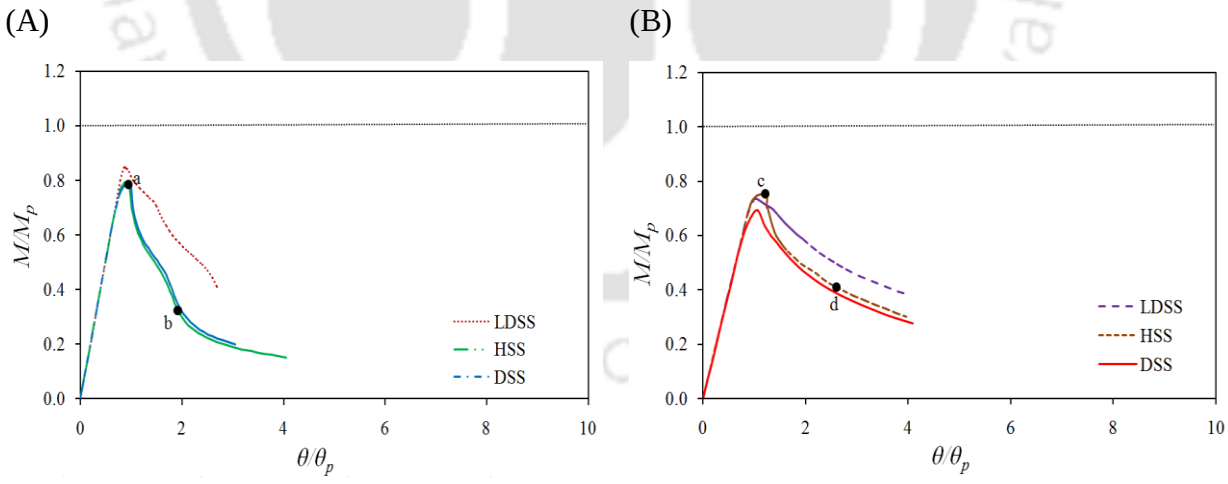

Figure 3.12: Normalised *M*-θ curve for Class 4 sections (c_f/t_f = 16.8): (A) 3PB specimens (B) 4PB specimens

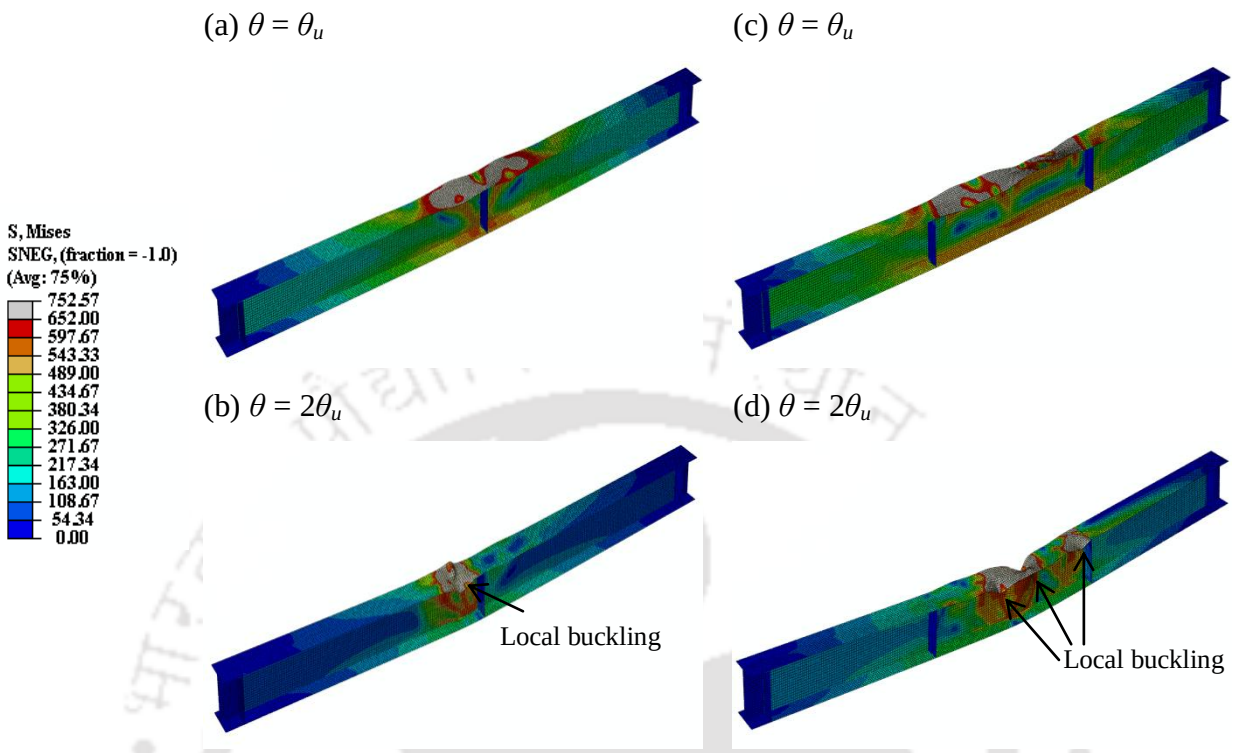

Figure 3.13: Schematic FE diagram of Class 4 HSS sections (c_f/t_f= 16.8): 3PB specimen (a,b) and 4PB specimen (c,d)

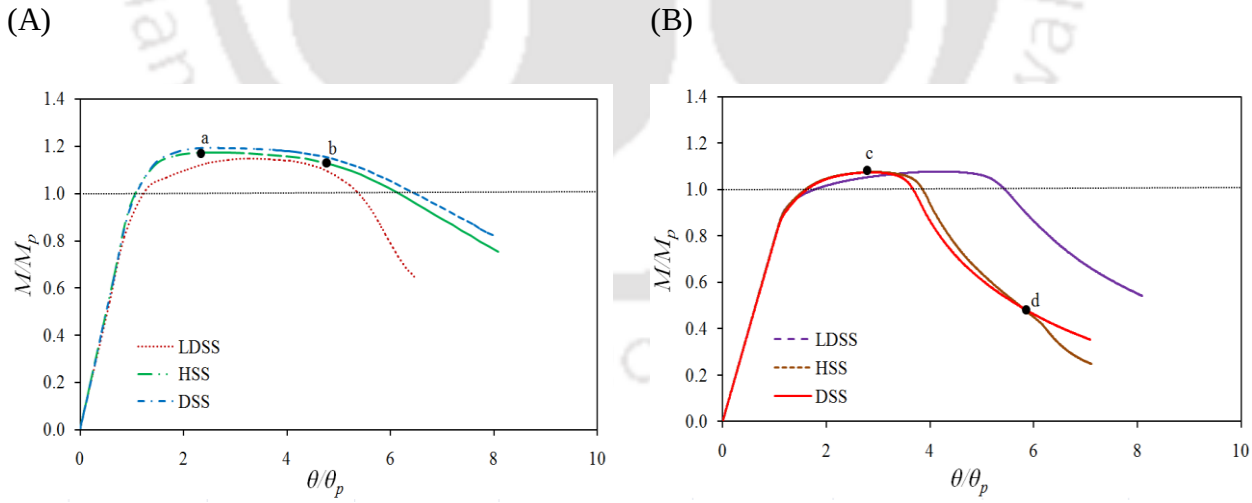

Figure 3.14: Normalised M-θ curve for Class 1 sections (c_w/t_w= 41.7): (A) 3PB specimens (B) 4PB specimens

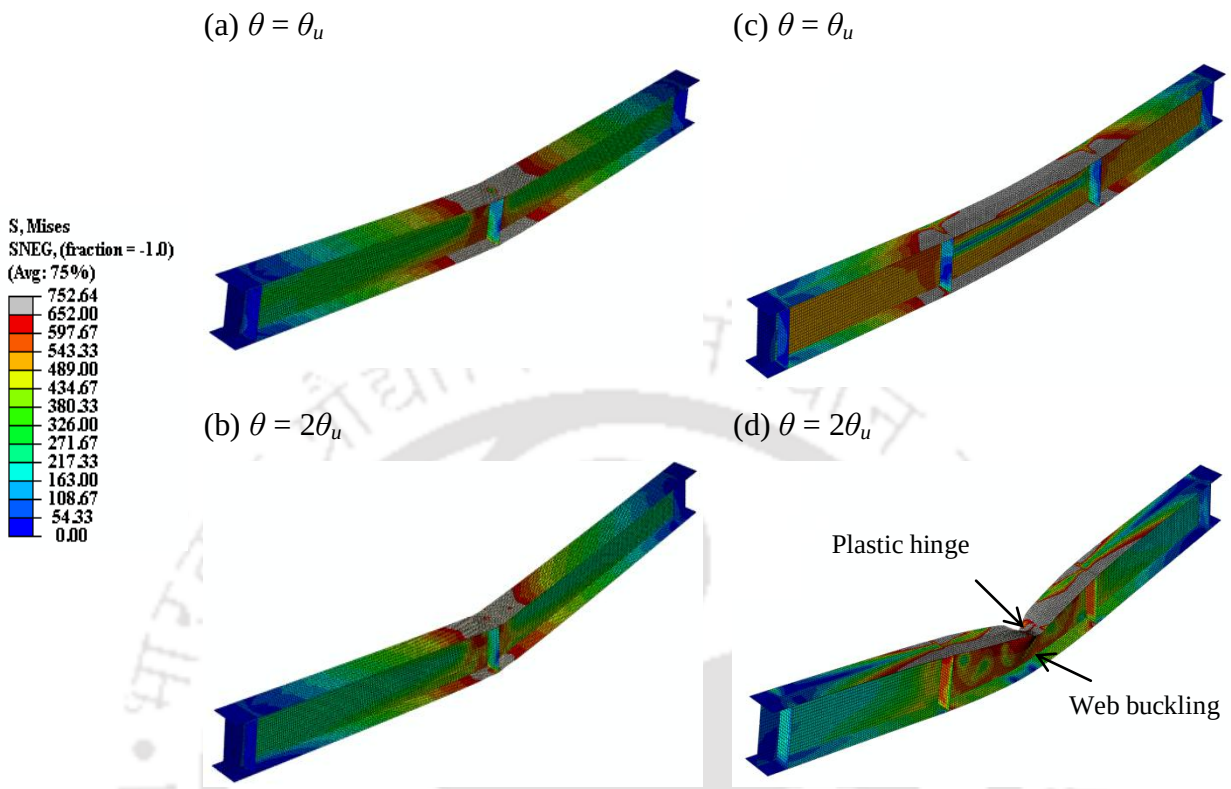

Figure 3.15: Schematic FE diagram of Class 1 HSS sections (c_w/t_w= 41.7): 3PB specimen (a,b) and 4PB specimen (c,d)

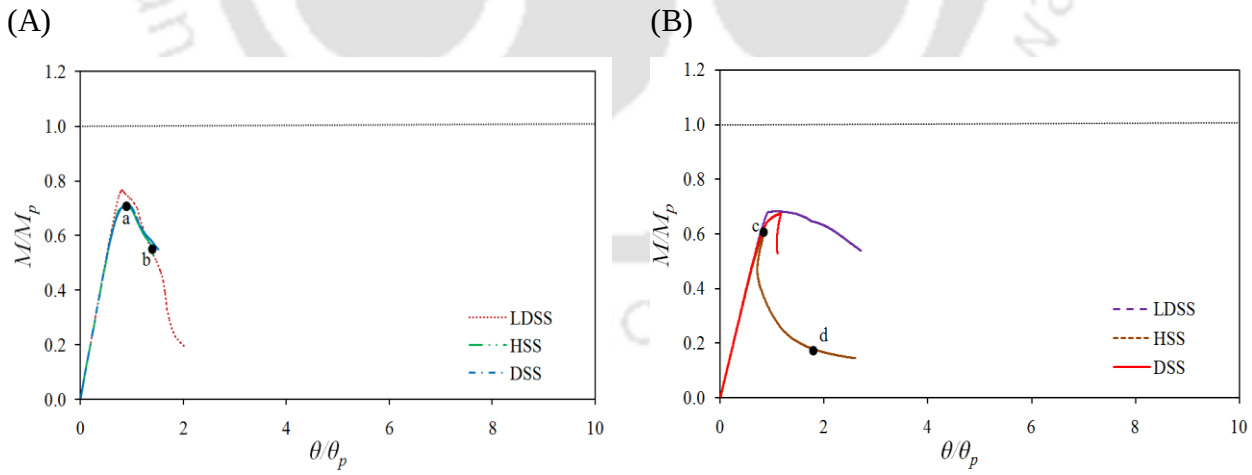

Figure 3.16: Normalised M-θ curve for Class 4 sections (c_w/t_w= 125): (A) 3PB specimens (B) 4PB specimens

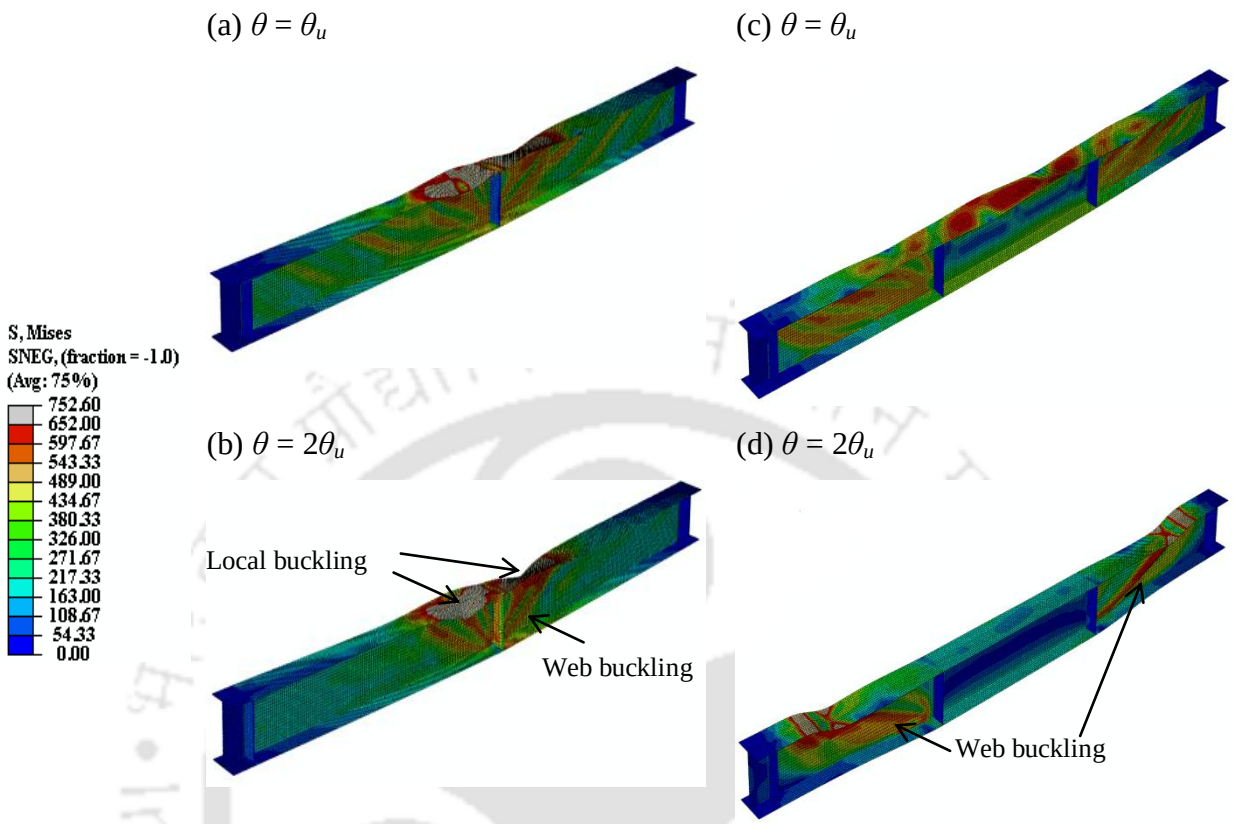

Figure 3.17: Schematic FE diagram of Class 1 HSS sections (c_w/t_w= 125): 3PB specimen (a,b) and 4PB specimen (c,d)

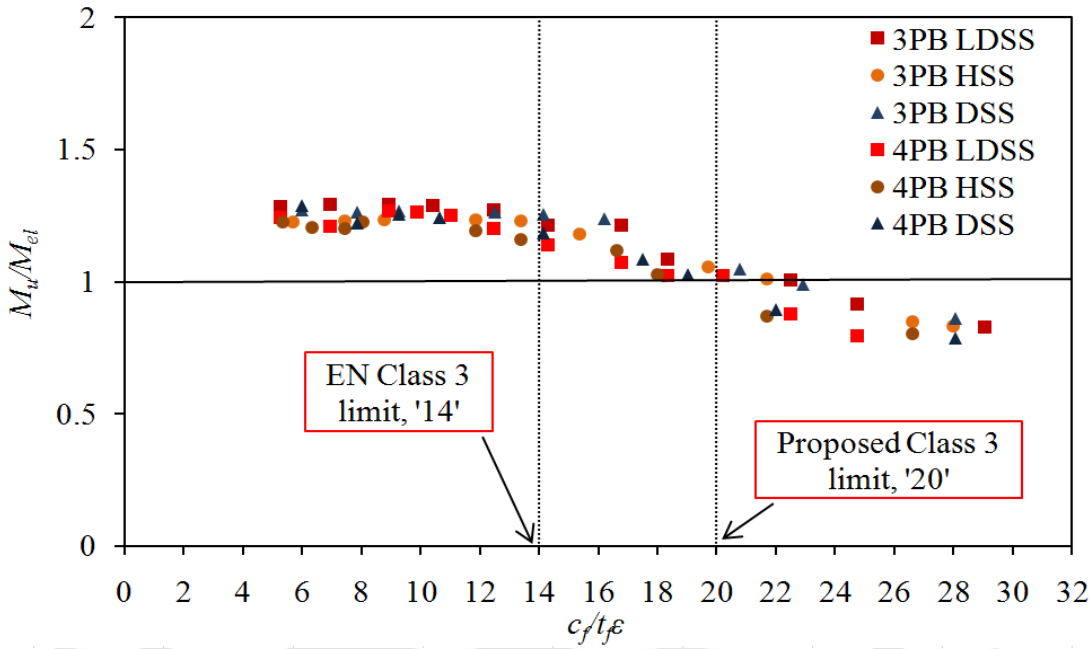

Figure 3.18: Assessment of Class 3 slenderness limits: LDSS, DSS and HSS I-beams of flange-critical sections

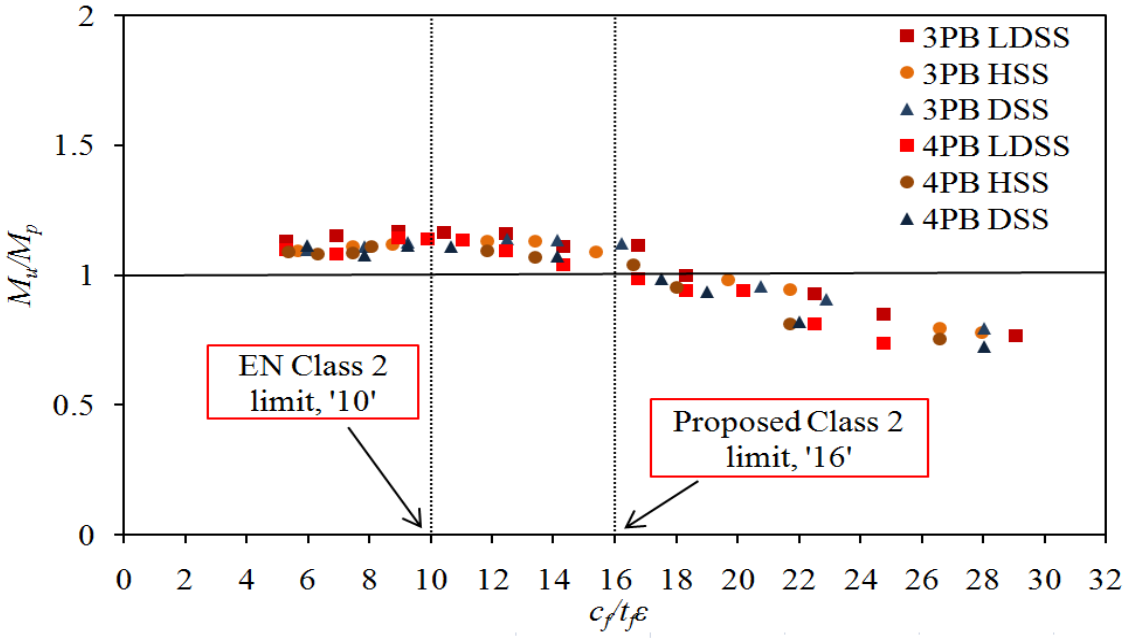

Figure 3.19: Assessment of Class 2 slenderness limits: LDSS, DSS and HSS I-beams of flange-critical sections

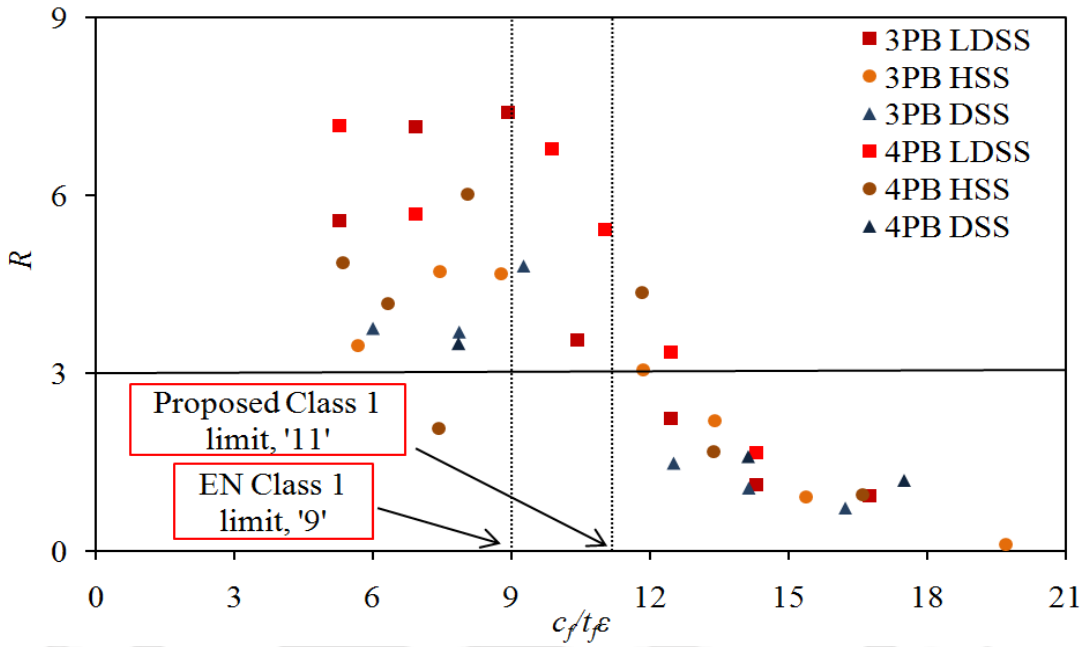

Figure 3.20: Assessment of Class 1 slenderness limits: LDSS, DSS and HSS I-beams of flange-critical sections

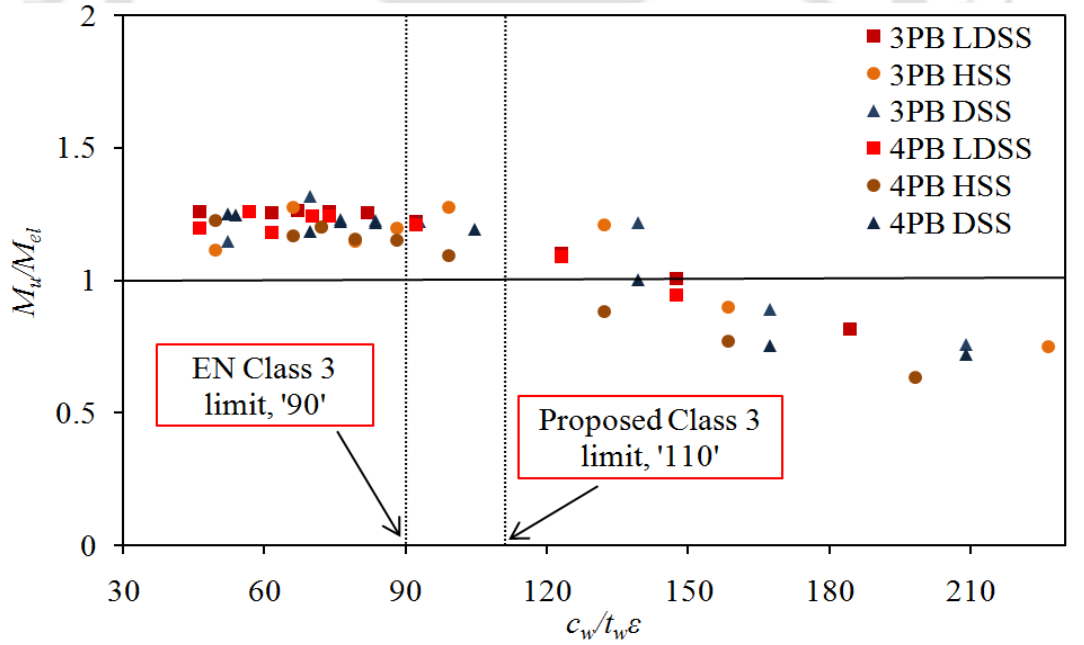

Figure 3.21: Assessment of Class 3 slenderness limits: LDSS, DSS and HSS I-beams of web-critical sections

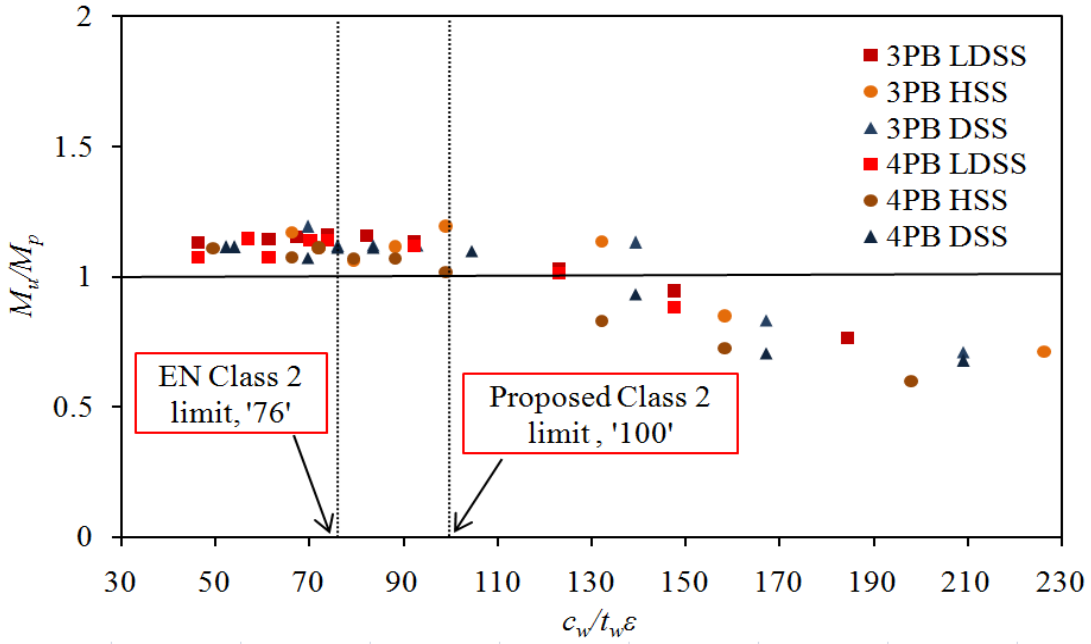

Figure 3.22: Assessment of Class 2 slenderness limits: LDSS, DSS and HSS I-beams of web-critical sections

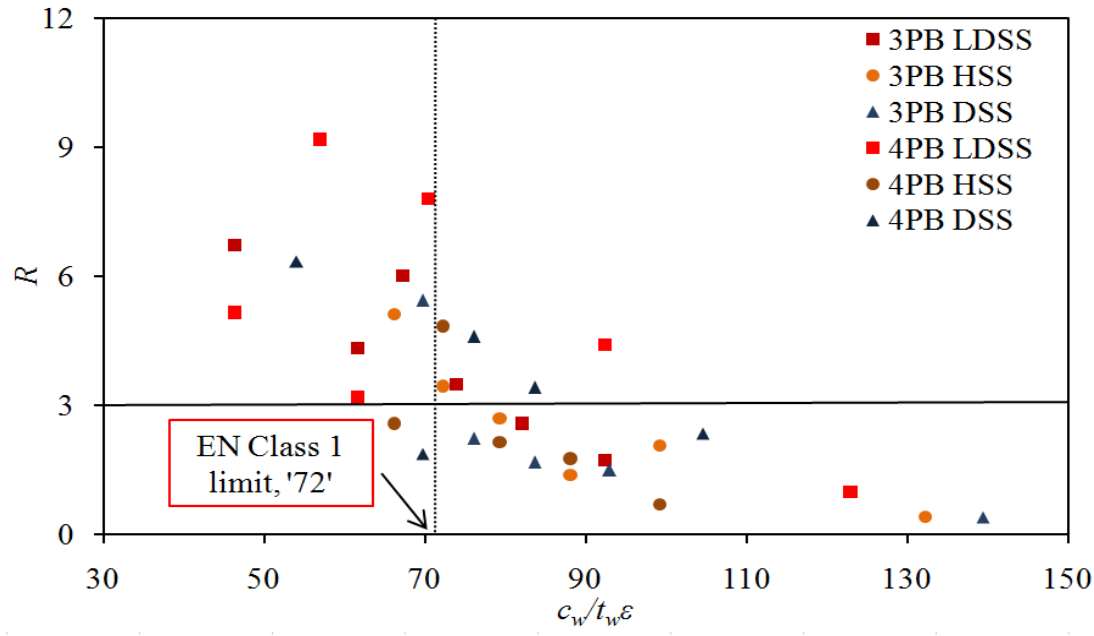

Figure 3.23: Assessment of Class 1 slenderness limits: LDSS, DSS and HSS I-beams of web-critical sections

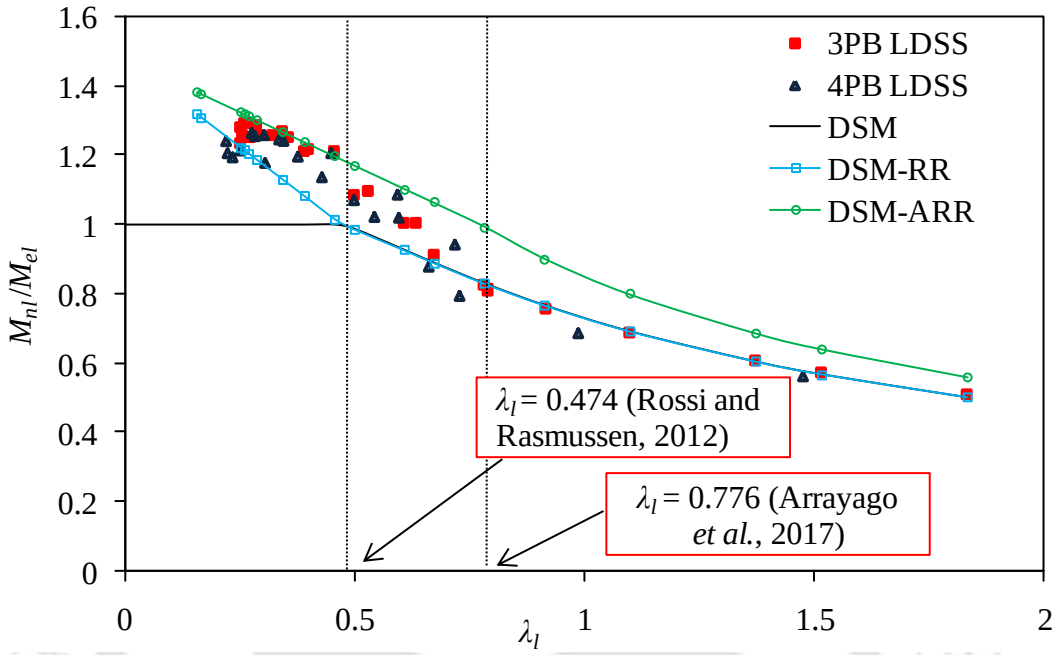

Figure 3.24: DSM approach for LDSS I-beams

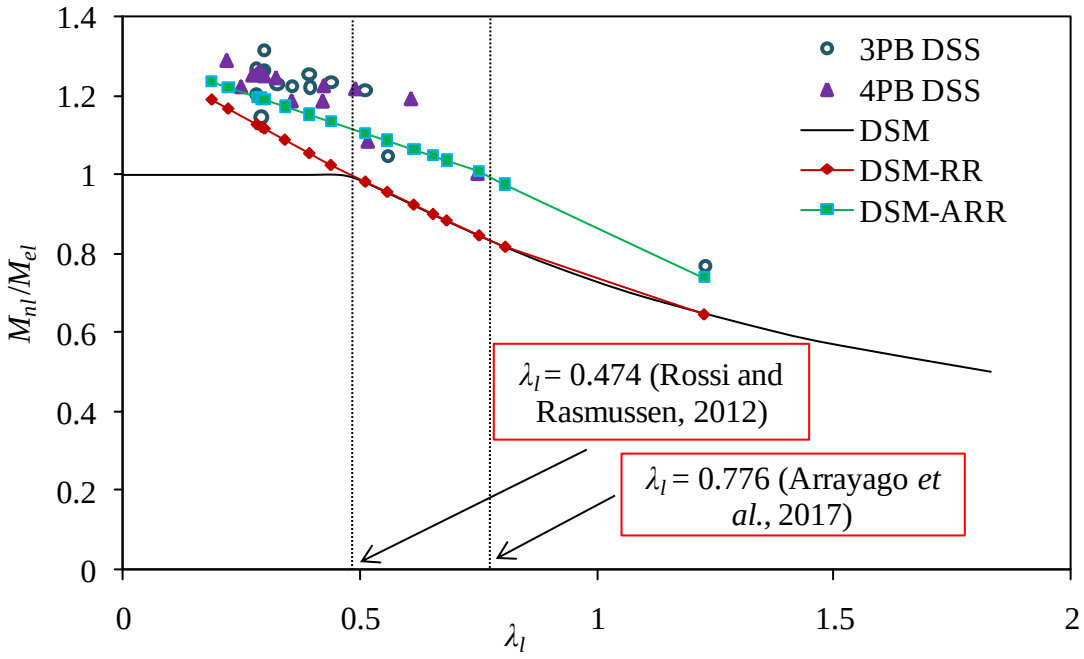

Figure 3.25: DSM approach for DSS I-beams

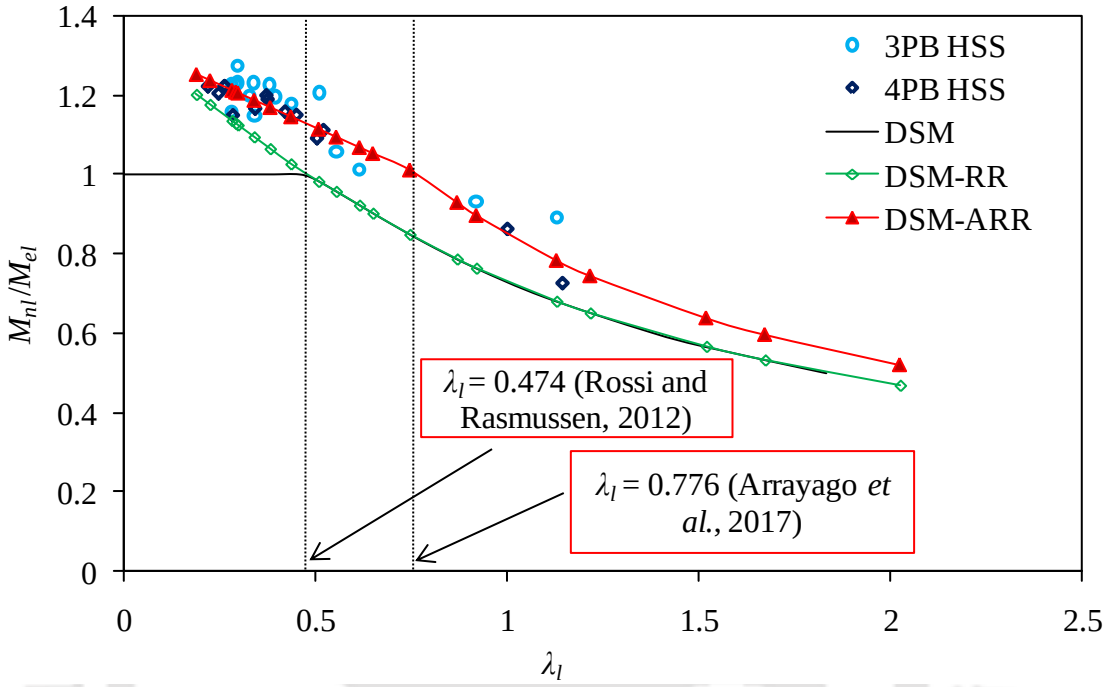

Figure 3.26: DSM approach for HSS I-beams

CHAPTER 4

4 SHEAR BEHAVIOUR OF HYBRID STAINLESS STEEL PLATE GIRDERS

4.1 INTRODUCTION

In this chapter, the previous study on the flexural behavior of hybrid stainless steel I-beams, has been extended, to assess the shear behavior of hybrid stainless steel plate-girders. Steel plate girders are generally adopted in steel structures having relatively larger spans and heavier loads (in comparison to steel beams, by general nomenclature) such as bridges, industrial and power plant buildings (Chacón *et al.*, 2011). With the development of stainless steel industry and considering the benefits of adopting stainless steel as a primary structural material (Gardner, 2005; Gardner *et al.*, 2006; SCI-P413, 2017), of late, an increasing interest amongst steel research community on the shear behaviour of stainless steel plate girders, can be seen (e.g.(Yamada. and Kato, 1988; Carvalho *et al.*, 1990; Kouhi *et al.*, 2000; Olsson, 2001; Real and Mirambell, 2005b; Real *et al.*, 2007; Saliba and Gardner, 2013a, 2013b)).

In addition to homogenous steel plate girders, newer Hybrid carbon steel sections are now being explored both in research and construction (Frost and Schilling, 1964; Greco, 2000; Greco and Earls, 2003; Azizinamini *et al.*, 2007; Shokouhian and Shi, 2014, 2015; Shokouhian *et al.*, 2016), to provide an economical option. However, in the literature, limited studies were reported on shear performance of carbon steel hybrid plate girders (Veljkovic and Johansson, 2004; Azizinamini *et al.*, 2007; Chacón *et al.*, 2011). To the best of authors' knowledge, there is an apparent lack of the study on

shear behaviour of hybrid stainless steel plate girders. With this as backdrop, in the light of understanding the shear performance of stainless steel plate girders, the current study is initiated on the shear behaviour of Hybrid Stainless Steel (HSS) plate girders adopting DSS and LDSS on the flanges and web respectively, using validated finite element (FE) modelling approach. The FE shear capacity (V_u) results are also compared with those predicted by European code (EN 1993-1-4:2006 + A1, 2015) and Direct Strength Method (DSM) (Keerthan and Mahendran, 2015; AISI, 2016b), to assess their applicability. Finally, attempts are made to modify both the European code and DSM design equations, for a possible improvement in the design predictions, for HSS plate girders.

4.2 NUMERICAL MODELLING

4.2.1 General

Numerical study is carried out using the commercial FE software, Abaqus (2009) by utilizing similar modeling methods adopted in a number of previous studies (e.g. (Theofanous and Gardner, 2009; Patton and Singh, 2012; Hassanein and Silvestre, 2013; Huang and Young, 2013; Saliba and Gardner, 2013a; Sonu and Singh, 2017)) which are known to provide accurate results. At first, the experimental results such as LDSS welded I-beam (Saliba and Gardner, 2013a) and hybrid high-strength steel beam (Shokouhian *et al.*, 2016) subjected to bending, LDSS plate girder (Saliba and Gardner, 2013b) subjected to shear are used for validating the FE models. After successful validation of FE models, parametric studies are carried out on LDSS, HSS and DSS plate girders.

4.2.2 Geometry

The cross-sectional geometry of plate girder is shown in Figure 4.1 where a, L, b_f, h_w, t_f and t_w are the shear span, length, flange width, web height, flange thickness and web

thickness respectively; t_s is the stiffener or end post thickness; e is the distance between end post and internal stiffener. The specimen designation system is given by section type, followed by web height × flange width × flange thickness × web thickness. For example, the label 'I-600×200×12×8' represents the girder having h_w = 600 mm, b_f = 200 mm, t_f = 12 mm and t_w = 8 mm. In the current study: a, L, h_w, t_s and e are fixed at 600 mm, 1360 mm, 600 mm, 20.6 mm and 80 mm respectively.

4.2.3 FE modelling

The four-noded doubly curved shell FE element with reduced integration S4R available in Abaqus (2009) was adopted in the current study to discretize the models as shown in Figure 4.2. The S4R element has six degrees of freedom per node (three displacements and three rotations per node). Also, this element is reported to give accurate results for modelling a wide range of shell thickness and was successfully employed in similar type of studies conducted in thin-walled structures (e.g. (Ellobody and Young, 2005; Patton and Singh, 2012; Saliba and Gardner, 2013a; Sonu and Singh, 2017)). The FE element size was chosen as ~10 mm × 10 mm based on mesh convergence study (by performing linear elastic eigen value buckling analysis) and element aspect ratio ~1.0 was adopted. A total of ~ 20,000 S4R elements were used in the analysis for all the FE models. Load was applied through a bearing plate at the centre of the top flange similar to 3-point bending (3PB) as shown in Figure 4.1b. The bearing plate has 100 mm length, 50 mm thick and width similar to width of plate girder (i.e. 200 mm) adopted in the current study. Loading was carried out as static uniform loads in increments utilizing the modified RIKS method. This method is often used in static analysis and was reported to be suitable for non-linear analysis (Hassanein, 2011). Boundary conditions were carefully chosen in FE model to match up the experimental test conducted by Saliba and Gardner (2013b). Lateral and vertical displacements were restrained at both the supports (bottom flange) similar to simply supported condition along with longitudinal displacement and rotation about horizontal axes were restrained at mid span following Saliba and Gardner (2013b) as shown in Figure 4.2b. Also,

intermediate stiffeners are provided at the center and supports in order to prevent local buckling of web and flanges. In addition, stiffners are provided at both ends of plate girder in case of rigid end post plate girder (see Figure 4.1). In every structural member, initial geometric imperfections occurred mostly during the fabrication, production and transportation stages. Therefore, it is necessary to account these imperfections since it affect the structural performance to a greater extent. In the current study, only local geometric imperfections were considered due to its short span nature and similar approach was also adopted by Saliba and Gardner (2013b). These initial local geometric imperfections were incorporated in the current FE model by considering the amplitude of the lowest eigen mode in elastic buckling analysis, using the Subspace method (Theofanous and Gardner, 2010; Saliba and Gardner, 2013a). The imperfection amplitude adopted in this study was given by Dawson and Walker (1972) (see Equation 3.8) which was modified by Gardner and Nethercot (2004) as it has shown least deviation in ultimate loads between test and FE model as compared to other imperfection amplitudes performed by Saliba and Gardner (2013a). Also, this imperfection amplitude has been successfully adopted in other similar applications such as ((Ashraf *et al.*, 2006b; Theofanous and Gardner, 2009, 2010; Saliba and Gardner, 2013a)).

4.2.4 Material modelling

The material properties of LDSS, HSS and DSS plate girders adopted in the current study consist of LDSS material (Table 3.1) and DSS material (Table 3.2) based on the experimental test of LDSS plates conducted by Saliba and Gardner (2013a) and DSS sheet carried out by Arrayago *et al.*, (2015) respectively. LDSS material (Table 3.1a) and DSS material (Table 3.2) are used for LDSS and DSS homogenous plate girders respectively. In case of HSS plate girders, LDSS material (Table 3.1a) and DSS material (Table 3.2) are used in the web and flanges respectively. Ramberg and Osgood (1943) model (Equation 3.1) has been adopted for non-linear stress strain curve for $\sigma \leq \sigma_{0.2}$ ($\sigma_{0.2}$ is the 0.2% proof stress) which provide good agreement with stress-strain

curve obtained from experiments for stainless steel up to $\sigma_{0.2}$. However, for strains exceeding $\varepsilon_{t0.2}$ (total strains at $\sigma_{0.2}$), it predicts higher stress values compared to experimental data and hence a modified version of Ramberg-Osgood model has been adopted in the current study. Therefore, the modified Ramberg-Osgood model proposed by Gardner and Ashraf (2006) (Equation 3.2) was adopted for LDSS material and also modified Ramberg-Osgood model given by Rasmussen (2003) (Equation 3.3) was employed for DSS material which were based on Mirambell and Real's two-stage model (Mirambell and Real, 2000).

4.2.5 Validation of FE models

The accuracy of FE models was assessed by comparing with the results of experimental tests conducted on homogeneous LDSS plate girder from the work of Saliba and Gardner (2013b) and hybrid high-strength steel (Gr.Q345 and Gr.Q460) beam conducted by Shokouhian *et al.* (2016). 3-point bending (3PB) tests conducted on homogenous LDSS I-beam (I-200×140×10×8) of L = 2800 mm and LDSS plate girder (I-600×200×12×8) of L = 1360 mm were validated using the material properties given in Table 3.1. The average stress-strain results of compressive coupons for 8 mm (Table 3.1b) and 10 mm (Table 3.1d) thicknesses were applied to the upper halves (above neutral axis) of the beam at the web and flange respectively. Similarly, the average stress-strain relationship of tensile coupons for 8 mm (Table 3.1a) and 10 mm (Table 3.1c) thicknesses were applied to the lower halves (below neutral axis) at the web and flange respectively following Saliba and Gardner (2013a). In case of hybrid high strength steel welded I-beams, 4-point bending (4PB) test performed on the beam (I-598×168×12×8) was validated using the material properties given in Table 3: the stress-strain results of tensile coupons for 8 mm thick (Gr.Q345) and 12 mm thick (Gr.Q460) high strength steel were applied to the web and flanges respectively. Figures 4.3 shows the failure mode for 3PB specimen of LDSS plate girder (I-600×200×12×8) and failure mode for 4PB specimen of hybrid high strength steel welded I-beams (I-598×168×12×8) is also shown in Figure 4.4. Normalized moment-rotation (M-θ) curve

for 3PB specimen of LDSS plate girder (I-600×200×12×8) are shown in Figure 4.5. Figure 4.6 shows the normalized M-θ curve for 4PB specimen of hybrid high strength steel welded I-beams (I-598×168×12×8). It can be observed that the percentage error in flexural strength from Figures 4.6 is ~1%. Also, the percentage error in shear capacity observed from Figure 4.5 is ~0.1%. Therefore, the percentage error in all the cases may be considered minimal and hence, the current FE models are considered to predict the experimental results accurately and can be used for further parametric studies. Also, in the study conducted by Saliba and Gardner (2013a), the effect of residual stress due to welding near the heat affected zone (HAZ) was ignored. The reason is due to insignificant variation in results when models with and without residual stresses were compared. Since, similar approach is adopted in the current study and hence, the effect of residual stress will not be considered.

4.2.6 Parametric study

Upon successful validation of FE models with the experimental results, numerical investigation on the shear performance of HSS plate girders are carried out in parallel with the homogenous sections such as LDSS and DSS plate girders. The material properties adopted for homogenous LDSS and DSS plate girders are given in Tables 3.1a and 3.2 respectively. In case of HSS plate girders, LDSS material properties given in Table 3.1a are used in the web and the DSS material properties given in Table 3.2 are used in both the flanges. For investigation of the shear behaviour of LDSS, HSS and DSS plate girders, a total of ~150 models are conducted covering the following parameters: (1) flange-to-web thickness ratio (t_f /t_w) by varying t_f and t_w, (2) flange slenderness (b_f /t_f) by varying b_f. 3PB test was selected for the current investigation. The FE results are plotted in the form of shear capacity and failure/deformed shapes. Furthermore, FE results are also compared with the results given by European code (EN 1993-1-4:2006 + A1, 2015) and Direct Strength Method (DSM) (Keerthan and Mahendran, 2015; AISI, 2016b).

4.3 DESIGN CODES

4.3.1 General

The FE results in the form of shear capacity (V_u) are compared with the unfactored design shear resistance given by EN 1993-1-4 (2006 + A1, 2015) and DSM (Keerthan and Mahendran, 2015; AISI, 2016b) for HSS plate girders. Comparison of FE results with design shear resistances are shown in Tables 4.1 and 4.2.

4.3.2 European code

The design method for calculation of shear resistance for stainless steel plate girders adopted in the current European code (EN 1993-1-4:2006 + A1, 2015) was based on Höglunds rotated stress field method (Höglund, 1971, 1973, 1997) which considers both flange and web contribution to ultimate shear resistance ($V_{b,Rd}$). In order to check the applicability of the present stainless steel design shear resistance given in European code (EN 1993-1-4:2006 + A1, 2015) to the current investigations of HSS plate girders, FE results are plotted in terms of web buckling reduction factor (χ_w) and web slenderness ($\overline{\lambda}_w$).

The ultimate shear resistance ($V_{b,Rd}$) of stainless steel plate girders including the flange and web contribution according to EN 1993-1-4 (2006 + A1, 2015) is given in Equation 4.1.

$$V_{b,Rd} = V_{bf,Rd} + V_{bw,Rd} \leq \frac{\eta \sigma_{0.2w} h_w t_w}{\sqrt{3}\gamma_{M1}} \tag{4.1}$$

where, $V_{bf,Rd}$ and $V_{bw,Rd}$ are the shear resistances contributed by flange and web respectively; η, γ_{M1} and $\sigma_{0.2w}$ are the web contribution factor, shear partial safety factor and yield strength of web respectively. The values of η and γ_{M1} are equal to 1.2 and 1 respectively (Saliba and Gardner, 2013b). The web shear resistance ($V_{bw,Rd}$) is given by:

$$V_{bw,Rd} = \frac{\chi_w \sigma_{0.2w} h_w t_w}{\sqrt{3}\gamma_{M1}} \tag{4.2}$$

in which χ_w is the web buckling reduction factor for rigid and non-rigid end post given in Equations 4.3 and 4.4.

$$\chi_w = \begin{cases} \eta & for\ \bar{\lambda}_w \le \dfrac{0.65}{\eta} \\ \dfrac{0.65}{\bar{\lambda}_w} & for\ \dfrac{0.65}{\eta} < \bar{\lambda}_w \le 0.65 \\ \dfrac{1.56}{0.91 + \bar{\lambda}_w} & for\ \bar{\lambda}_w \ge 0.65 \end{cases} \tag{4.3}$$

$$\chi_w = \begin{cases} \eta & for\ \bar{\lambda}_w \le \dfrac{0.65}{\eta} \\ \dfrac{0.65}{\bar{\lambda}_w} & for\ \dfrac{0.65}{\eta} < \bar{\lambda}_w \le 0.65 \\ \dfrac{1.19}{0.54 + \bar{\lambda}_w} & for\ \bar{\lambda}_w \ge 0.65 \end{cases} \tag{4.4}$$

where $\bar{\lambda}_w$ is the web slenderness and for transverse stiffeners at supports and mid-span, $\bar{\lambda}_w$ is defined as:

$$\bar{\lambda}_w = \frac{h_w}{37.4 t_w \varepsilon \sqrt{k_\tau}} \tag{4.5}$$

where k_τ and ε are the minimum shear buckling coefficient and material factor given in Equations 4.6 and 4.7 respectively.

$$k_\tau = \begin{cases} 5.34 + 4.00\left(\dfrac{h_w}{a}\right)^2 & for\ h_w/a \ge 1.0 \\ 4.00 + 5.34\left(\dfrac{h_w}{a}\right)^2 & for\ h_w/a < 1.0 \end{cases} \tag{4.6}$$

$$\varepsilon = \left[\frac{235}{\sigma_{0.2}}\frac{E}{210000}\right]^{0.5} \tag{4.7}$$

The flange shear resistance is also given by:

$$V_{bf,Rd} = \left(\frac{b_f t_f^2 \sigma_{0.2f}}{c\gamma_{M1}}\right)\left(1-\left(\frac{M_{Ed}}{M_{f,Rd}}\right)^2\right) \tag{4.8}$$

where M_{Ed} and $M_{f,Rd}$ are the design bending moment and design plastic moment of resistance of section consisting of effective area of flanges respectively; and c is the distance from the stiffener to plastic hinge location given by:

$$c = \left(0.17 + \frac{3.5 b_f t_f^2 \sigma_{0.2f}}{t_w h_w^2 \sigma_{0.2w}}\right) a \text{ with } \frac{c}{a} \le 0.65 \tag{4.9}$$

Shear-moment interaction occurs only when the design shear force (V_{Ed}) exceeds 50% of the web shear resistance ($V_{bw,Rd}$) or $\bar{\eta}_3 \ge 0.5$ for I or box girder according to EN-1993-1-5 (2007). Therefore, if $\bar{\eta}_3 \ge 0.5$, shear-moment interaction should satisfy:

$$\bar{\eta}_1 + \left(1-\frac{M_{f,Rd}}{M_{pl,Rd}}\right)\left(2\bar{\eta}_3 - 1\right)^2 \le 1 \quad for\ \bar{\eta}_1 \ge \frac{M_{f,Rd}}{M_{pl,Rd}} \tag{4.10}$$

where $M_{pl,Rd}$ is the design plastic moment of cross section consisting of effective area of the flanges and fully effective web irrespective of its section class (EN 1993-1-5, 2007). Also, $\bar{\eta}_1$ and $\bar{\eta}_3$ are given in Equations 4.11 and 4.12 respectively.

$$\bar{\eta}_1 = \frac{M_{Ed}}{M_{pl,Rd}} \tag{4.11}$$

$$\bar{\eta}_3 = \frac{V_{Ed}}{V_{bw,Rd}} \tag{4.12}$$

For HSS plate girders, $M_{f,Rd}$ and $M_{pl,Rd}$ was calculated by Equations 4.13 and 4.14 respectively.

$$M_{f,Rd} = \begin{cases} W_{pltf}\sigma_{0.2tf} + W_{plbf}\sigma_{0.2bf} & \text{Class 1, 2 and 3 sections} \\ W_{effpltf}\sigma_{0.2tf} + W_{effplbf}\sigma_{0.2bf} & \text{Class 4 section} \end{cases} \quad (4.13)$$

$$M_{pl,Rd} = \begin{cases} W_{pltf}\sigma_{0.2tf} + W_{plbf}\sigma_{0.2bf} + W_{pltw}\sigma_{0.2w} + W_{plbw}\sigma_{0.2w} & \text{Class 1, 2 and 3 sections} \\ W_{effpltf}\sigma_{0.2tf} + W_{effplbf}\sigma_{0.2bf} + W_{pltw}\sigma_{0.2w} + W_{plbw}\sigma_{0.2w} & \text{Class 4 section} \end{cases} \quad (4.14)$$

W_{pltf} , W_{plbf}, W_{pltw} and W_{plbw} are the plastic section modulus of top flange, bottom flange, top web and bottom web respectively; $W_{effpltf}$ and $W_{effplbf}$ are the effective plastic section modulus of top flange and bottom flange respectively for Class 4 sections, $\sigma_{0.2tf}$, $\sigma_{0.2bf}$, $\sigma_{0.2w}$ are the yield stress of top flange, bottom flange and web respectively (see Tables 3.1 and 3.2).

4.3.3 Direct strength method

Direct Strength Method (DSM) is an alternative method for the traditional 'effective width method'. It was first proposed by Schafer and Pekoz (1998) for design of cold-formed steel members and further implemented in the North American Specifications AISI (AISI, 2016b). The DSM procedure adopted here considers the full cross-section slenderness ratio (λ_l) rather than considering the slenderness ratio of the most slender constituent plate elements (see Equation 4.15).

$$\lambda_l = \sqrt{\frac{V_{yw}}{V_{cr}}} \quad (4.15)$$

where V_{yw} is the yield shear capacity of the web based on average web shear yield stress (i.e. $0.6\sigma_{0.2w}$) and V_{cr} is the elastic shear buckling resistance obtained through FE

analysis. Till date, more number of applications of DSM can be seen for members subjected to compression and bending. However, a relatively lesser applications of DSM have been observed for members subjected to shear and hence were reported in the study conducted by Pham *et al.*, (2014) and Keerathan and Mahendran (2011, 2015). Initially, FE results are compared with original DSM which ignores the effect of post-critical strength. Therefore, the DSM shear resistance (V_v) without considering the effect of post-critical strength (AISI, 2016b) can be calculated from Equation 4.16.

$$\frac{V_v}{V_{yw}} = \begin{cases} 1 & \lambda_l \le 0.815 \\ \dfrac{0.815}{\lambda_l} & 0.815 < \lambda_l \le 1.23 \\ \dfrac{1}{\lambda_l^2} & \lambda_l > 1.23 \end{cases} \tag{4.16}$$

In the current study, development of diagonal tension band can be seen in FE specimens indicating shear dominant failure mode. Therefore, the original DSM is further extended by incorporating the effect of post-buckling strength, as suggested by Keerathan and Mahendran (2011, 2015). Furthermore, the modified DSM shear resistance ($V_{v,KM}$) including the effect of post-buckling strength which was proposed by Keerathan and Mahendran (2015) is given in Equation 4.17.

$$\frac{V_{v,KM}}{V_{yw}} = \begin{cases} 1 & \lambda_l \le 0.815 \\ \dfrac{0.815}{\lambda_l} + 0.25\left[1 - \dfrac{0.815}{\lambda_l}\right] & 0.815 < \lambda_l \le 1.23 \\ \dfrac{1}{\lambda_l^2} + 0.25\left[1 - \dfrac{1}{\lambda_l^2}\right] & \lambda_l > 1.23 \end{cases} \tag{4.17}$$

4.3.4 Reliability analysis

The applicability of current European code (EN 1993-1-4:2006 + A1, 2015), DSM (AISI, 2016b), modified DSM (Keerthan and Mahendran, 2015) and the proposed design equations for the estimation of shear capacity of HSS plate girders have been assessed through reliability analysis. The reliability analysis methods given in the Commentary of the ASCE Specifications for the design of cold-formed stainless steel structural members (ASCE 8-02, 2002) was used in the present study. The resistance factor (φ) value of 0.85 is recommended for flexural members under shear buckling of web by ASCE 8-02 (ASCE 8-02, 2002) which is adopted in the current study for estimation of reliability index (β). Also, a target reliability index (β_o) of 2.5 has been adopted as per AISI-S100-16C (AISI, 2016a). Therefore, the design specification given by EN 1993-1-4 (2006 + A1, 2015), DSM (AISI, 2016b), modified DSM (Keerthan and Mahendran, 2015) and the proposed design equations which were used in the current study are considered to be reliable if $\beta \geq 2.5$. The dead load (DL) to live load (LL) ratio of 1/5 has been adopted following AISI-S100-16C (AISI, 2016a). The statistical parameters which includes mean for material properties (M_m = 1.10) and fabrication factors (F_m = 1.0); coefficients of variation for material properties (V_M = 0.10) and fabrication factors (V_F = 0.05) are considered and a load combination of 1.2DL + 1.6LL has been adopted in the current study (AISI, 2016a). The mean values (P_m), coefficient of variation (V_p) and reliability index (β) of the ratio of FE results to the design predictions for HSS plate girders were calculated and shown in Tables 4.1 and 4.2.

4.4 RESULTS AND DISCUSSIONS

4.4.1 Failure mechanisms

Three different failure modes have been identified from the FE results: (1) shear dominant failure mode indicating shear buckling of web, (2) bending dominant failure

mode showing buckling of top flange (i.e. compression flange) and (3) combined shear and bending failure mode indicating an interaction of (1) shear dominant failure mode and (2) bending dominant failure mode. These failure modes are discussed in the subsequent sections.

4.4.1.1 Shear dominant failure

Typical plot showing shear dominant failure mode of HSS plate girder (I-600×200×12×4) can be seen in Figure 4.7. It can be observed that the web buckled diagonally which indicates formation of diagonal tension band. Also, plastic hinge type deformation can be seen in top flange near the supports which provides anchorage to diagonal tension band (Hassanein, 2011; Sonu and Singh, 2017). Shear dominant failure mechanism are mainly observed in HSS plate girders of thick flange with relatively thinner web section. The moment-shear interaction diagram plotted for the same HSS specimen (i.e. I-600×200×12×4) as per EN 1993-1-4 (2006 + A1, 2015) can be seen in Figure 4.8. The FE specimen results are plotted using the coordinates ($V_u/V_{b,Rd}$, $M_u/M_{c,Rd}$), where V_u and M_u are the ultimate shear and moment capacity respectively. FE data points having a high value of $V_u/V_{b,Rd}$ and low value of $M_u/M_{c,Rd}$ are considered as shear dominant failure. Also, FE specimens satisfying (V_u/M_u) / ($V_{bw,Rd}$ /$M_{f,Rd}$) > 1 are considered as shear dominant failure. The HSS plate girder considered herein is having (V_u/M_u) / ($V_{bw,Rd}$ /$M_{f,Rd}$) = ~ 4.2, which is indicative of shear dominant failure mode.

4.4.1.2 Bending dominant failure

In case of HSS plate girder displaying bending dominant failure mode, formation of plastic hinge (or local buckling in case of thin section) can be seen at mid-span compression flange followed by web buckling around mid-span (Hassanein, 2011). Figure 4.9 shows HSS plate girder (I-600×200×12×12) exhibiting bending dominant failure mode. Bending dominant failure mechanism can be seen in sections having lower t_f/t_w (i.e. $t_f/t_w \leq 1$). Moment-shear interaction diagram for HSS plate girder (I-600×200×12×12) can be seen in Figure 4.10. It can be observed that the specimen

shows (V_u /M_u) / ($V_{bw,Rd}$ /$M_{f,Rd}$) < 1 (i.e. V_u/M_u / $V_{bw,Rd}$ /$M_{f,Rd}$ = ~ 0.77), which indicates bending dominant failure mode.

4.4.1.3 Combined shear and bending failure

A combined failure mode of HSS plate girder (I-600×200×12×10) involving both shear and bending dominant failure mode can be seen in Figure 4.11. It can be observed that formation of plastic hinge can be seen in mid-span compression flange which is similar to bending dominant failure mode (see Section 4.4.1.2). Also, the web buckled diagonally on one side indicating resemblance with shear dominant failure mode (see Section 4.4.2.1). The moment-shear interaction diagram plotted for HSS plate girder (i.e. I-600×200×12×10) can be seen in Figure 4.12. It can be observed that the specimen lies in the transition area of shear and moment interaction diagram (i.e. V_u /M_u / $V_{bw,Rd}$ /$M_{f,Rd}$ = ~ 0.98).

4.4.2 Effect of t_f/t_w

Typical plots showing the effect of t_f /t_w are shown in the form of variation of shear force (V) with mid-span deflection (δ). Figure 4.13 shows the variation of V-δ for HSS plate girders covering a range of t_f /t_w = 2-5 by varying t_f; keeping t_w and b_f as constant (i.e. t_w = 4 mm and b_f = 200 mm). It can be seen that the shear capacity (V_u) and mid-span deflection at ultimate load (δ_u) increases by increasing t_f /t_w and similar observation can be seen in the study conducted on LDSS members (e.g. (Hassanein, 2011; Sonu and Singh, 2017)). Also, an increase in t_f (4-20 mm) or t_f/t_w (1-5) by 400% results in increase in V_u of ~50%. It can be observed that the behaviour of V-δ curve changes by increasing t_f. At thinner flange thickness (i.e.t_f /t_w = 1), the curve is relatively sharper around V_u, and further with increase in t_f, the curve becomes increasingly flatter as shown in Figure 4.13. V-δ curve for two sections (i.e. t_f /t_w = 1 and 3.5) of LDSS, DSS and HSS plate girders can be seen in Figure 4.14. In case of thin flange sections (i.e. t_f /t_w = 1), increase in V_u of ~ 21% and ~ 4% can be seen in DSS and HSS plate girders respectively compared with LDSS plate girder. For thick

flange sections having t_f/t_w = 3.5, ~29% and ~ 4% increase in V_u can be seen in DSS and HSS plate girder respectively compared with LDSS plate girder. This clearly shows that shear capacity is mainly contributed by the web. Figure 4.15 shows Von-Mises stress contours for HSS plate girders of t_f/t_w = 1 and 3.5 corresponding to δ_u and 2.5δ_u. Von-Mises stress (hereafter refer to as stress) ≥ 652 Mpa (i.e. $\sigma_{0.2f}$) are grey-coloured, indicating areas which have crossed yield stress of flange (i.e. $\sigma_{0.2f}$). The stress exceeding yield stress can be related with strain hardening. For thinner flange sections of t_f/t_w = 1 (Figure 4.15a) at δ_u, initiation of local buckling (LB) can be seen in both compression flange (top flange) and web. Further at 2.5δ_u, LB is significantly enhanced which shows 'combined shear and bending' dominant failure mechanisms. For thick flange sections of t_f/t_w = 3.5, at δ_u, formation of diagonal tension band can be seen in the web. At 2.5δ_u, the diagonal tension band is more enhanced and plastic hinge deformation (anchorage of diagonal tension band) can be seen at the compression flange near the supports indicating shear dominant failure mechanisms. Therefore, it can be observed that increasing t_f (keeping constant t_w) improves both shear capacity and ductility. In addition, V-δ curve for two sections (i.e. t_f/t_w = 1 and 3.5) of rigid and non-rigid end post HSS plate girders can be seen in Figure 4.16. It can be observed that increase in V_u of ~ 7% and ~ 13% can be seen for thin (i.e. t_f/t_w = 1) and thick flange (i.e. t_f/t_w = 3.5) rigid end post specimens respectively as compared to non-rigid end post plate girders

The effect of varying t_w for HSS plate girders, keeping t_f and b_f as constant (i.e. t_f = 12 mm and b_f = 200 mm) can be seen in the form of variation of V-δ curve as shown in Figure 4.17 covering a range of t_f/t_w = 1-3. It can be seen that increase in t_w (4-12 mm) or t_f/t_w (3-1) by 200% results in increase in V_u of ~270%. In contrast to increase in t_f (i.e. constant t_w), it can be observed that the curve becomes increasingly sharper around V_u as t_w increases keeping t_f as constant (see Figure 4.17). A comparison of LDSS, HSS and DSS plate girders in the form of variation of V-δ curve for two sections (i.e. t_f/t_w = 3 and 1) can be seen in Figure 4.18. For thin web sections (i.e. t_f/t_w = 3), increase in V_u of ~ 30% and ~ 3% can be seen in DSS and HSS plate girder respectively compared

with LDSS plate girder. Also, in case of thick web sections of t_f/t_w = 1.2, ~ 18% and ~ 3.5% increase in V_u can be seen in DSS and HSS plate girder respectively compared with LDSS plate girder. Figure 4.19 shows stress contours for HSS plate girders of t_f/t_w = 1 and 3 corresponding to δ_u and 2.5δ_u. In case of thin web sections (i.e. t_f/t_w = 3) shown in Figure 4.19, initiation of diagonal tension band can be seen in the web at δ_u and further at 2.5δ_u, the web section is highly stressed with enhanced diagonal tension band, and also plastic hinge deformation can be seen in compression flange (Figures 4.19a and b), suggesting of 'shear dominant failure'. In contrast, for thick web sections of t_f/t_w = 1, it can be seen that areas near the loaded points in compression flange are highly stressed at δ_u. At post ultimate (i.e. 2.5δ_u), plastic hinge deformation can be seen at highly stressed region near the loaded points and in addition, web buckling can be seen on one side of the web section (Figures 4.19c and d), indicating 'combined shear and bending dominant failure'. It can be observed that increasing t_w (keeping constant t_f) significantly enhances shear capacity and decreases ductility. Also, it can be seen from Figure 4.20 that increase in V_u of ~ 12% and ~ 1% can be seen for thin (i.e. t_f/t_w = 3) and thick web (i.e. t_f/t_w = 1) rigid end post HSS plate girders respectively as compared to non-rigid end post sections. Hence, it can be observed that the effect of rigid and non-rigid end posts has shown higher influence on shear capacity for specimens with higher t_f/t_w.

4.4.3 Effect of b_f/t_f

Effect of b_f/t_f for HSS plate girders is given in the form of V-δ curve shown in Figure 4.21 which covers a range of b_f/t_f = 12.5-25 by varying b_f; keeping h_w, t_f and t_w as constant (i.e. h_w = 600 mm, t_f = 12 mm and t_w = 10 mm). It can be observed that the shear capacity (V_u) and δ_u increases by increasing the flange width (b_f) and a similar observation can be seen in the work conducted by Hassanein (2011). An increase in b_f (150-300 mm) or b_f/t_f (12.5-25) by ~100% results in increase in V_u of ~18%. Also, the behaviour of V-δ curve changes by increasing b_f. At smaller flange width (i.e. b_f/t_f = 12.5), the curve is sharper around the peak (i.e. V_u), and further with increase in b_f, the

curve becomes increasingly flatter as shown in Figure 4.21. *V*-δ curve for two sections (i.e. b_f/t_f = 12.5 and 25) in LDSS, HSS and DSS plate girders can be seen in Figure 4.22. For both sections (i.e. b_f/t_f = 12.5 and 25) in HSS plate girders, minimal increase in V_u of ~ ≤ 2% can be seen compared with LDSS plate girder for similar sections considered. Whereas, in case of DSS plate girders, an increase in V_u of ~17% and ~29% can be seen when compared with LDSS plate girders for b_f = 150 and 300 respectively. Figure 4.23 shows stress contours for HSS plate girders (i.e.b_f/t_f = 25 and 12.5) corresponding to δ_u and 2.5δ_u. For b_f/t_f = 25 shown in Figure 4.21, it can be seen that a larger area in the web is highly stressed at δ_u and further at 2.5δ_u, formation of diagonal tension band in the web section along with plastic hinge deformation can be seen in compression flange (Figures 4.23a and b), indicating of 'shear dominant failure'. In case of b_f/t_f = 12.5 shown in Figure 4.23, it can be seen that areas near the loaded points (i.e. mid-section) in compression flange are highly stressed at δ_u and at 2.5δ_u, plastic hinge deformation can be seen at highly stressed region near the loaded points (Figures 4.23c and d) which indicates bending dominant failure mode. In addition, it can be seen from Figure 4.24 that increase in V_u of ~ 0.1% and ~ 1% can be seen for b_f = 300 mm and 150 mm rigid end post HSS plate girders respectively as compared to non-rigid end post sections.

4.4.4 Comparison of FE results with European code

In order to check the applicability of the present stainless steel design shear resistance (V_{EN}) given in European code (EN 1993-1-4:2006 + A1, 2015) to the current investigations on HSS plate girders, FE results are plotted in terms of web buckling reduction factor (χ_w) and web slenderness ($\bar{\lambda}_w$) shown in Figures 4.25 and 4.27. Also, FE results exhibiting only shear dominant failure mode (i.e. (V_u/M_u) / ($V_{bw,Rd}/M_{f,Rd}$) > 1) are considered for comparison with EN 1993-1-4 (2006 + A1, 2015). In addition, the FE $\bar{\lambda}_w$ results are calculated as (V_u-$V_{bf,Rd}$) / V_{yw} i.e. flange shear resistance ($V_{bf,Rd}$) is deducted from the ultimate shear capacity (V_u) and is further normalized by yield shear capacity of web (V_{yw}). It can be seen from Figure 4.25 that for higher $\bar{\lambda}_w$ values (i.e.

thinner web), FE predicted higher values compared with EN 1993-1-4 (2006 + A1, 2015). The mean (P_m), coefficient of variance (V_p) and β of the ratio of FE shear capacity to design shear resistance (i.e. V_u /V_{EN}) are found to be 1.74, 0.34, 2.98 and 1.53, 0.23, 3.35 respectively (see Tables 4.1 and 4.2) for rigid and non-rigid HSS plate girders. Furthermore, it can be seen from Figures 4.25 and 4.27 that for thicker sections (i.e. $\bar{\lambda}_w \le 0.65$), FE results are not safe. But, for thin sections (i.e. $\bar{\lambda}_w > 1.5$), EN 1993-1-4 (2006 + A1, 2015) predicted overly-conservative results. Therefore, this indicates that EN 1993-1-4 (2006 + A1, 2015) design shear resistances can be conservatively applied to HSS plate girders for thin sections (i.e. $\bar{\lambda}_w > 1.5$). However, an improved design expression similar to EN 1993-1-4 (2006 + A1, 2015) is proposed for rigid and non-rigid end post HSS plate girders through a new modified web buckling reduction factor ($\chi_{w,P}$) given in Equations 4.18 and 4.19 respectively.

$$\chi_{w,P} = \begin{cases} 1 & for\ \bar{\lambda}_w \le 0.65 \\ \dfrac{1.8}{\bar{\lambda}_w + 1.15} & for\ 0.65 < \bar{\lambda}_w \le 1.5 \\ \dfrac{4}{\bar{\lambda}_w + 4.5} & for\ \bar{\lambda}_w > 1.5 \end{cases} \tag{4.18}$$

$$\chi_{w,P} = \begin{cases} 1 & for\ \bar{\lambda}_w \le 0.65 \\ \dfrac{1.65}{\bar{\lambda}_w + 1.1} & for\ 0.65 < \bar{\lambda}_w \le 1.5 \\ \dfrac{2.7}{\bar{\lambda}_w + 2.8} & for\ \bar{\lambda}_w > 1.5 \end{cases} \tag{4.19}$$

It can be seen from Figures 4.25 and 4.27 that the proposed design $\chi_{w,P}$ for HSS plate girders predicted accurate results. The P_m, V_p and β for rigid and non-rigid end post HSS plate girders are found to be 1.4, 0.2, 3.28 and 1.27, 0.13 and 3.40 (see Tables 4.1 and 4.2). Therefore, the proposed design formulation ($\chi_{w,P}$) for HSS plate girders was observed to be greater than target reliability index (β_o = 2.5) and hence it is

reliable. Also, V_{EN} and $V_{EN,P}$ are the design shear capacity and proposed shear capacity in European code (EN 1993-1-4:2006 + A1, 2015) for HSS plate girders.

4.4.5 Comparison of FE results with DSM

This section evaluates the applicability of DSM for the design of HSS plate girders given in Figures 4.26 and 4.28. Initially, the original DSM formulation which ignores the effect of post-critical strength (AISI, 2016b) given in Equation 4.16 has been plotted for HSS plate girder. It can be seen that the results predicted are too conservative for most of the sections. However, it is not safe and applicable for some sections (i.e. $0.65 < \lambda_l \leq 1.23$) as shown in Figures 4.26 and 4.28. The value of P_m, V_p and β for rigid and non-rigid end post plate girders are found to be 3.08, 0.85, 2.04 and 1.81, 0.71 and 1.70 respectively (see Tables 4.1 and 4.2). Also, β is found to be less than β_o and hence it is not reliable for HSS plate girders.

Furthermore, the modified DSM incorporating the effect of post-buckling strength which was proposed by Keerathan and Mahendran (2015) given in Equation 4.17 was plotted for HSS plate girder shown in Figures 4.26 and 4.28. It can be seen that the modified DSM predicted more accurate results compared to the original DSM (AISI, 2016b). However, it is also not safe and applicable for few data points (i.e. $0.65 < \lambda_l \leq 1.23$). The value of P_m, V_p and β for rigid and non-rigid end post HSS plate girders were found to be 1.52, 0.38, 2.45 and 1.14, 0.23, 2.45 respectively (see Tables 4.1 and 4.2). In addition, β was observed to be less than β_o and hence it is not reliable for HSS plate girders.

A new DSM formulation for HSS plate girder is proposed based on the modified DSM formulation incorporating the effect of post buckling strength given by Keerathan and Mahendran (2015). The proposed DSM shear capacity ($V_{v,P}$) for rigid and non-rigid end post HSS plate girders are given in Equations 4.20 and 4.21 respectively, and they predicted accurate results which are shown in Figures 4.26 and 4.28.

$$\frac{V_{v,P}}{V_{yw}} = \begin{cases} 1 & \lambda_l \le 0.65 \\ \dfrac{0.65}{\lambda_l} + 0.4\left[1 - \dfrac{0.65}{\lambda_l}\right] & 0.815 < \lambda_l \le 1.23 \\ \dfrac{0.9}{\lambda_l^2} + 0.35\left[1 - \dfrac{1}{\lambda_l^2}\right] & \lambda_l > 1.23 \end{cases} \quad (4.20)$$

$$\frac{V_{v,P}}{V_{yw}} = \begin{cases} 1 & \lambda_l \le 0.65 \\ \dfrac{0.65}{\lambda_l} + 0.3\left[1 - \dfrac{0.65}{\lambda_l}\right] & 0.65 < \lambda_l \le 1.23 \\ \dfrac{0.86}{\lambda_l^2} + 0.3\left[1 - \dfrac{1}{\lambda_l^2}\right] & \lambda_l > 1.23 \end{cases} \quad (4.21)$$

Also, the values of P_m, V_p and β for HSS plate girders were found to be 1.39, 0.28 and 2.75 respectively as shown in Table 4.1. The proposed DSM formulation ($V_{v,P}$) for HSS plate girders given in Equations 4.20 and 4.21 are reliable since the value of β is greater than the target reliability index (i.e. β_o = 2.5).

4.5 CONCLUSIONS

Numerical programme investigating the shear behaviour of HSS plate girders along with LDSS and DSS plate girders has been conducted through a parametric study such as: (1) flange-to-web thickness ratio (t_f /t_w) by varying t_f and t_w, (2) flange slenderness (b_f /t_f) by varying b_f using the commercial finite element software, Abaqus. The FE results in the form of shear capacity (V_u) are compared with the unfactored design shear resistances given by European code (EN 1993-1-4:2006 + A1, 2015) and Direct Strength Method (DSM) (Keerthan and Mahendran, 2015; AISI, 2016b) for HSS plate girders. The conclusions drawn from the FE investigations are presented below:

1) Three different modes of failure mechanisms were observed in the FE specimens such as: shear dominant failure mode, bending dominant failure mode and combined shear and bending dominant failure mode.

2) Increase in t_f (4-20 mm) or t_f/t_w (1-5) by 400% keeping t_w as constant results in increase in shear capacity (V_u) of ~50% and also enhances ductility for HSS plate girders. Also, increase in t_w (4-12 mm) or t_f/t_w (3-1.2) by 200% keeping t_f as constant significantly enhances shear capacity (V_u) of ~270% but reduces ductility.

3) Shear capacity (V_u) and ductility increases by increasing the flange width (b_f). An increase in b_f (150-300 mm) or b_f/t_f (12.5-25) by ~100% results in increase in V_u of ~ 18%.

4) Effect of rigid and non-rigid end posts have more influence on shear capacity for specimens having higher t_f/t_w.

5) In general, European (EN 1993-1-4) code (EN 1993-1-4:2006 + A1, 2015), DSM (AISI, 2016b) and modified DSM (Keerthan and Mahendran, 2015) are not applicable for shear design of HSS plate girders for few specimens. Also, for most common specimens of HSS plate girders, they predicted overly conservative results. Therefore, for the purpose of economic and efficient design, modified design formulations were proposed in EN 1993-1-4 and DSM for HSS plate girders.

Table 4.1: Comparison of FE results with design predictions for HSS plate girders.

Section		V_u (kN)	V_{EN} (kN)	$V_{EN,P}$ (kN)	V_v (kN)	$V_{v,KM}$ (kN)	$V_{v,P}$ (kN)	$\frac{V_u}{V_{EN}}$	$\frac{V_u}{V_{EN,P}}$	$\frac{V_u}{V_v}$	$\frac{V_u}{V_{v,KM}}$	$\frac{V_u}{V_{v,P}}$
3PB specimen												
	I-600×200×12×4	565.00	380.15	432.70	377.88	464.86	461.85	1.49	1.31	1.50	1.22	1.22
	I-600×200×12×6	924.66	738.15	768.41	982.64	1009.14	905.67	1.25	1.20	0.94	0.92	1.02
	I-600×200×12×8	1413.06	1154.14	1181.50	1451.52	1451.52	1421.76	1.22	1.20	0.97	0.97	0.99
	I-600×200×8×4	517.25	380.15	432.70	399.69	481.21	473.84	1.36	1.20	1.29	1.07	1.09
	I-600×200×10×4	535.94	380.15	432.70	388.79	473.03	467.85	1.41	1.24	1.38	1.13	1.15
	I-600×200×15×4	613.84	380.15	432.70	365.90	455.86	455.26	1.61	1.42	1.68	1.35	1.35
	I-600×200×18×4	665.71	380.15	432.70	356.09	448.50	449.86	1.75	1.54	1.87	1.48	1.48
	I-600×200×20×4	702.82	380.15	432.70	348.09	442.51	445.47	1.85	1.62	2.02	1.59	1.58
	I-600×200×12×4.5	640.57	462.77	503.75	545.03	612.90	587.41	1.38	1.27	1.18	1.05	1.09
	I-600×200×12×4.8	687.59	514.73	546.86	621.22	683.64	645.64	1.34	1.26	1.11	1.01	1.06
	I-600×200×12×5	721.28	550.31	575.77	676.06	733.85	686.39	1.31	1.25	1.07	0.98	1.05
	I-600×200×12×5.5	813.11	642.25	671.92	821.93	865.93	792.49	1.27	1.21	0.99	0.94	1.03
	I-600×200×12×6.5	1042.79	837.61	867.92	1156.17	1161.97	1025.00	1.24	1.20	0.90	0.90	1.02
	I-600×200×12×7	1177.26	940.29	970.12	1270.08	1270.08	1151.43	1.25	1.21	0.93	0.93	1.02
	I-600×200×12×7.5	1287.94	1045.89	1074.73	1360.80	1360.80	1284.00	1.23	1.20	0.95	0.95	1.00
	I-600×200×12×3.5	493.17	303.09	362.91	247.99	344.75	358.66	1.63	1.36	1.99	1.43	1.38

	I-600×200×12×2	296.42	112.98	166.05	43.60	123.42	150.99	2.62	1.79	6.80	2.40	1.96
	I-600×200×12×2.5	359.18	168.57	228.84	86.30	178.12	206.22	2.13	1.57	4.16	2.02	1.74
	I-600×200×12×3	424.77	232.28	294.76	155.33	252.58	275.95	1.83	1.44	2.73	1.68	1.54
	I-600×200×12×1.8	271.82	93.27	142.10	31.56	105.32	131.66	2.91	1.91	8.61	2.58	2.06
	I-600×200×12×1.9	284.12	102.93	153.98	37.28	114.14	141.16	2.76	1.85	7.62	2.49	2.01
	I-600×200×12×2.1	308.78	123.39	178.30	50.93	133.46	161.37	2.50	1.73	6.06	2.31	1.91
	I-600×200×12×2.2	321.21	134.17	190.71	58.75	143.86	172.02	2.39	1.68	5.47	2.23	1.87
	I-600×200×12×2.3	333.86	145.30	203.29	67.48	154.94	183.18	2.30	1.64	4.95	2.15	1.82
	I-600×200×12×2.4	346.73	156.77	216.00	76.30	166.09	194.38	2.21	1.61	4.54	2.09	1.78
	I-600×200×12×1.75	265.79	88.59	136.24	28.93	101.08	127.04	3.00	1.95	9.19	2.63	2.09
	I-600×200×15×2.1	352.29	123.39	178.30	49.60	132.45	160.64	2.86	1.98	7.10	2.66	2.19
	I-600×200×15×2.2	365.26	134.17	190.71	56.96	142.51	171.03	2.72	1.92	6.41	2.56	2.14
	I-600×200×15×2.3	378.35	145.30	203.29	65.39	153.37	182.03	2.60	1.86	5.79	2.47	2.08
	I-600×200×15×2.4	391.48	156.77	216.00	74.12	164.46	193.18	2.50	1.81	5.28	2.38	2.03
	I-600×200×15×2.5	404.74	168.57	228.84	84.71	176.93	205.35	2.40	1.77	4.78	2.29	1.97
	I-600×200×15×3	472.27	232.28	294.76	149.88	248.49	272.95	2.03	1.60	3.15	1.90	1.73
	I-600×200×15×3.5	541.87	303.09	362.91	241.63	339.98	355.16	1.79	1.49	2.24	1.59	1.53
	I-600×200×15×4.5	687.84	462.77	503.75	527.32	599.61	575.79	1.49	1.37	1.30	1.15	1.19
	I-600×200×15×4.8	733.86	514.73	546.86	610.99	675.97	640.74	1.43	1.34	1.20	1.09	1.15
	I-600×200×15×5	764.84	550.31	575.77	665.86	726.20	681.51	1.39	1.33	1.15	1.05	1.12

	I-600×200×15×5.5	845.09	642.25	671.92	809.76	856.80	786.66	1.32	1.26	1.04	0.99	1.07
	I-600×200×15×6.5	1058.61	837.61	867.92	1138.02	1148.36	1016.32	1.26	1.22	0.93	0.92	1.04
	I-600×200×15×7	1181.37	940.29	970.12	1270.08	1270.08	1141.81	1.26	1.22	0.93	0.93	1.03
	I-600×200×15×7.5	1326.09	1045.89	1074.73	1360.80	1360.80	1273.44	1.27	1.23	0.97	0.97	1.04
	I-600×200×12×1.6	247.46	75.14	119.00	21.95	89.04	113.68	3.29	2.08	11.27	2.78	2.18
	I-600×200×12×1.58	245.04	73.42	116.75	20.95	87.38	111.86	3.34	2.10	11.70	2.80	2.19
	I-600×200×60×20	4620.65	4190.18	3491.81	3628.80	3628.80	3628.80	1.10	1.32	1.27	1.27	1.27
	I-600×200×45×15	3394.82	3142.63	2618.86	2721.60	2721.60	2721.60	1.08	1.30	1.25	1.25	1.25
	I-600×200×30×10	2045.39	1609.40	1626.35	1814.40	1814.40	1814.40	1.27	1.26	1.13	1.13	1.13
	I-600×200×20×8	1443.47	1154.14	1181.50	1451.52	1451.52	1392.65	1.25	1.22	0.99	0.99	1.04
	I-600×200×80×30	6923.91	6285.27	5237.72	5443.20	5443.20	5443.20	1.10	1.32	1.27	1.27	1.27
	I-600×200×70×25	5745.11	5237.72	4364.77	4536.00	4536.00	4536.00	1.10	1.32	1.27	1.27	1.27
	I-600×200×7×3.5	430.28	303.09	362.91	267.06	359.06	369.15	1.42	1.19	1.61	1.20	1.17
	I-600×200×6×3	346.40	232.28	294.76	168.96	262.80	283.44	1.49	1.18	2.05	1.32	1.22
	I-600×200×5.6×2.8	314.77	205.89	268.09	137.35	230.02	253.35	1.53	1.17	2.29	1.37	1.24
	I-600×200×5×2.5	269.77	168.57	228.84	97.65	186.64	212.47	1.60	1.18	2.76	1.45	1.27
	I-600×200×5.5×3.5	418.26	303.09	362.91	273.42	363.83	372.65	1.38	1.15	1.53	1.15	1.12
	I-600×200×4.5×3	335.02	232.28	294.76	171.68	264.84	284.94	1.44	1.14	1.95	1.26	1.18
	I-600×200×4.2×2.8	304.01	205.89	268.09	139.89	231.93	254.75	1.48	1.13	2.17	1.31	1.19
	I-600×200×4.5×3.5	407.75	303.09	362.91	276.60	366.21	374.40	1.35	1.12	1.47	1.11	1.09

	I-600×200×3.9×3	329.22	232.28	294.76	174.41	266.89	286.44	1.42	1.12	1.89	1.23	1.15
	I-600×200×3.6×2.8	298.48	205.89	268.09	142.43	233.83	256.15	1.45	1.11	2.10	1.28	1.17
	I-600×200×3.2×2.5	254.43	168.57	228.84	99.92	188.34	213.72	1.51	1.11	2.55	1.35	1.19
	I-600×200×2.8×2.2	212.08	134.17	190.71	67.95	150.75	177.08	1.58	1.11	3.12	1.41	1.20
	I-600×200×2.5×2	184.19	112.98	166.05	50.87	128.87	154.99	1.63	1.11	3.62	1.43	1.19
	I-600×200×2.3×1.8	159.62	93.27	142.10	37.61	109.85	134.99	1.71	1.12	4.24	1.45	1.18
	I-600×200×2.2×1.7	147.40	84.00	130.44	30.89	100.28	124.94	1.75	1.13	4.77	1.47	1.18
	I-600×200×1.9×1.5	119.20	66.70	107.82	21.80	84.39	107.25	1.79	1.11	5.47	1.41	1.11
Mean (P_m)								**1.74**	**1.40**	**3.08**	**1.52**	**1.39**
COV(V_p)								**0.34**	**0.20**	**0.85**	**0.38**	**0.28**
Resistance factor (φ)								**0.85**	**0.85**	**0.85**	**0.85**	**0.85**
Reliability index (β)								**2.98**	**3.28**	**2.04**	**2.45**	**2.75**

Table 4.2: Comparison of FE results with design predictions for HSS plate girders (non-rigid).

Section		V_u (kN)	V_{EN} (kN)	$V_{EN,P}$ (kN)	V_v (kN)	$V_{v,KM}$ (kN)	$V_{v,P}$ (kN)	$\frac{V_u}{V_{EN}}$	$\frac{V_u}{V_{EN,P}}$	$\frac{V_u}{V_v}$	$\frac{V_u}{V_{v,KM}}$	$\frac{V_u}{V_{v,P}}$
3PB specimen												
	I-600×200×12×4	503.34	332.98	396.48	377.88	464.86	427.31	1.51	1.27	1.33	1.08	1.18
	I-600×200×12×6	896.44	676.07	719.03	982.64	1009.14	875.18	1.33	1.25	0.91	0.89	1.02
	I-600×200×12×8	1413.06	1095.00	1109.10	1451.52	1451.52	1416.80	1.29	1.27	0.97	0.97	1.00
	I-600×200×8×4	471.26	332.98	396.48	399.69	481.21	441.55	1.42	1.19	1.18	0.98	1.07
	I-600×200×10×4	482.48	332.98	396.48	388.79	473.03	435.45	1.45	1.22	1.24	1.02	1.11
	I-600×200×15×4	545.99	332.98	396.48	365.90	455.86	422.63	1.64	1.38	1.49	1.20	1.29
	I-600×200×18×4	598.65	332.98	396.48	356.09	448.50	417.14	1.80	1.51	1.68	1.33	1.44
	I-600×200×20×4	633.63	332.98	396.48	348.09	442.51	412.66	1.90	1.60	1.82	1.43	1.54
	I-600×200×12×4.5	586.95	410.33	467.40	545.03	612.90	549.23	1.43	1.26	1.08	0.96	1.07
	I-600×200×12×4.8	635.85	459.60	510.79	621.22	683.64	608.09	1.38	1.24	1.02	0.93	1.05
	I-600×200×12×5	671.65	493.58	540.02	676.06	733.85	649.59	1.36	1.24	0.99	0.92	1.03
	I-600×200×12×5.5	787.31	582.30	628.14	821.93	865.93	758.25	1.35	1.25	0.96	0.91	1.04
	I-600×200×12×6.5	1017.24	774.54	812.86	1156.17	1161.97	999.28	1.31	1.25	0.88	0.88	1.02
	I-600×200×12×7	1155.44	877.38	909.33	1270.08	1270.08	1131.65	1.32	1.27	0.91	0.91	1.02
	I-600×200×12×7.5	1264.56	984.29	1008.15	1360.80	1360.80	1271.20	1.28	1.25	0.93	0.93	0.99
	I-600×200×12×3.5	426.68	262.02	327.67	247.99	344.75	329.39	1.63	1.30	1.72	1.24	1.30

	I-600×200×12×1.9	231.08	84.76	129.48	37.28	114.14	124.30	2.73	1.78	6.20	2.02	1.86
	I-600×200×15×2.1	296.16	102.29	151.71	49.60	132.45	142.08	2.90	1.95	5.97	2.24	2.08
	I-600×200×15×4.5	623.77	410.33	467.40	527.32	599.61	540.24	1.52	1.33	1.18	1.04	1.15
	I-600×200×15×4.8	665.30	459.60	510.79	610.99	675.97	602.38	1.45	1.30	1.09	0.98	1.10
	I-600×200×15×5	701.06	493.58	540.02	665.86	726.20	643.90	1.42	1.30	1.05	0.97	1.09
	I-600×200×15×5.5	800.73	582.30	628.14	809.76	856.80	751.45	1.38	1.27	0.99	0.93	1.07
	I-600×200×15×6.5	1029.82	774.54	812.86	1138.02	1148.36	989.15	1.33	1.27	0.90	0.90	1.04
	I-600×200×15×7	1158.23	877.38	909.33	1270.08	1270.08	1120.43	1.32	1.27	0.91	0.91	1.03
	I-600×200×15×7.5	1286.14	984.29	1008.15	1360.80	1360.80	1258.88	1.31	1.28	0.95	0.95	1.02
	I-600×200×60×20	4556.01	4190.18	3491.81	3628.80	3628.80	3628.80	1.09	1.30	1.26	1.26	1.26
	I-600×200×45×15	3353.22	3142.63	2618.86	2721.60	2721.60	2721.60	1.07	1.28	1.23	1.23	1.23
	I-600×200×30×10	2041.22	1571.20	1530.42	1814.40	1814.40	1814.40	1.30	1.33	1.13	1.13	1.13
	I-600×200×80×30	6794.36	6285.27	5237.72	5443.20	5443.20	5443.20	1.08	1.30	1.25	1.25	1.25
	I-600×200×70×25	5641.37	5237.72	4364.77	4536.00	4536.00	4536.00	1.08	1.29	1.24	1.24	1.24
	I-600×200×7×3.5	391.89	262.02	327.67	267.06	359.06	340.07	1.50	1.20	1.47	1.09	1.15
	I-600×200×6×3	303.49	198.01	261.51	168.96	262.80	257.91	1.53	1.16	1.80	1.15	1.18
	I-600×200×5.6×2.8	276.40	174.49	235.95	137.35	230.02	229.32	1.58	1.17	2.01	1.20	1.21
	I-600×200×5×2.5	240.12	141.56	198.76	97.65	186.64	190.76	1.70	1.21	2.46	1.29	1.26
	I-600×200×5.5×3.5	379.84	262.02	327.67	273.42	363.83	343.63	1.45	1.16	1.39	1.04	1.11
	I-600×200×4.5×3	303.13	198.01	261.51	171.68	264.84	259.44	1.53	1.16	1.77	1.14	1.17

	I-600×200×4.2×2.8	276.00	174.49	235.95	139.89	231.93	230.75	1.58	1.17	1.97	1.19	1.20
	I-600×200×4.5×3.5	371.49	262.02	327.67	276.60	366.21	345.41	1.42	1.13	1.34	1.01	1.08
	I-600×200×3.9×3	288.55	198.01	261.51	174.41	266.89	260.97	1.46	1.10	1.65	1.08	1.11
	I-600×200×3.6×2.8	257.34	174.49	235.95	142.43	233.83	232.17	1.47	1.09	1.81	1.10	1.11
	I-600×200×3.2×2.5	218.23	141.56	198.76	99.92	188.34	192.04	1.54	1.10	2.18	1.16	1.14
	I-600×200×2.8×2.2	185.18	111.59	163.16	67.95	150.75	157.80	1.66	1.13	2.73	1.23	1.17
	I-600×200×2.5×2	161.02	93.34	140.47	50.87	128.87	137.35	1.73	1.15	3.17	1.25	1.17
	I-600×200×2.3×1.8	145.70	76.54	118.74	37.61	109.85	119.04	1.90	1.23	3.87	1.33	1.22
	I-600×200×2.2×1.7	128.50	68.69	108.27	30.89	100.28	109.83	1.87	1.19	4.16	1.28	1.17
	I-600×200×1.9×1.5	107.45	54.15	88.22	21.80	84.39	93.86	1.98	1.22	4.93	1.27	1.14
Mean (P_m)								**1.53**	**1.27**	**1.81**	**1.14**	**1.18**
COV(V_p)								**0.23**	**0.13**	**0.71**	**0.23**	**0.17**
Resistance factor (φ)								**0.85**	**0.85**	**0.85**	**0.85**	**0.85**
Reliability index (β)								**3.35**	**3.40**	**1.70**	**2.45**	**2.90**

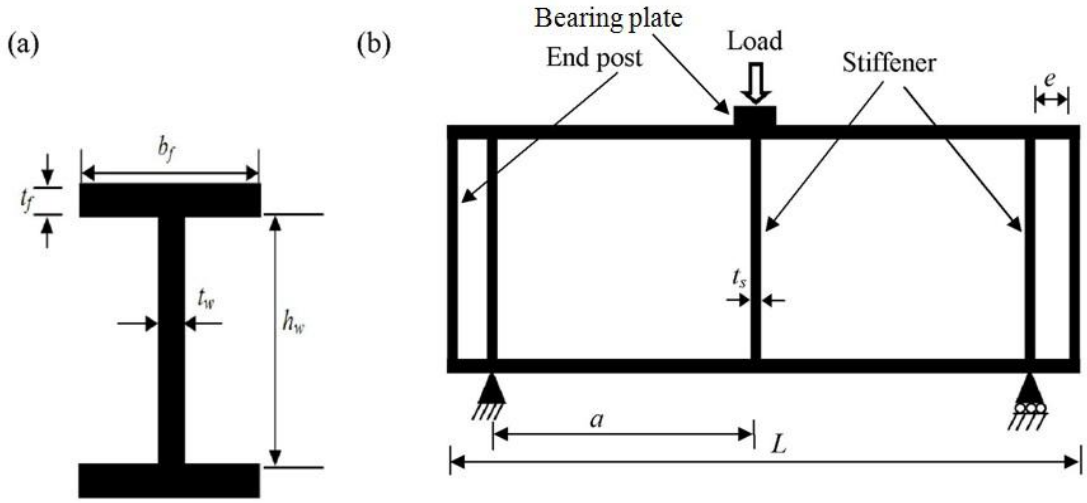

Figure 4.1: Schematic diagram showing (a) Cross-section notations (b) Geometry of rigid end post of plate girder

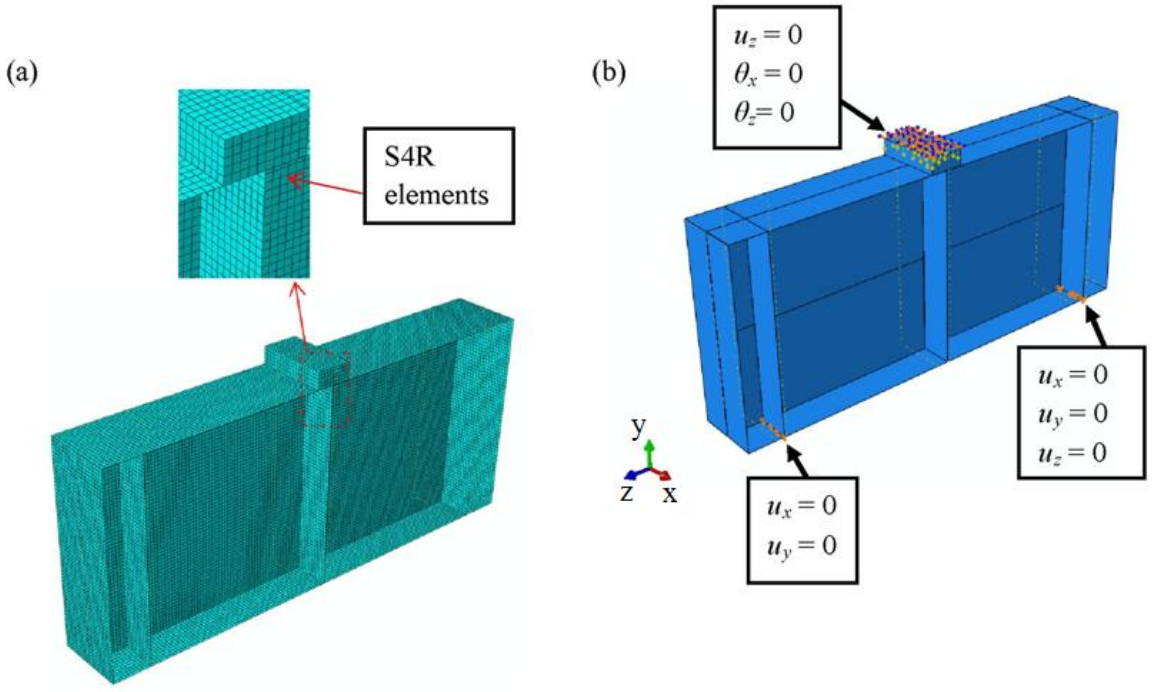

Figure 4.2: Schematic diagram showing (a) FE mesh (b) Boundary condition of plate girder

(a)

(b)

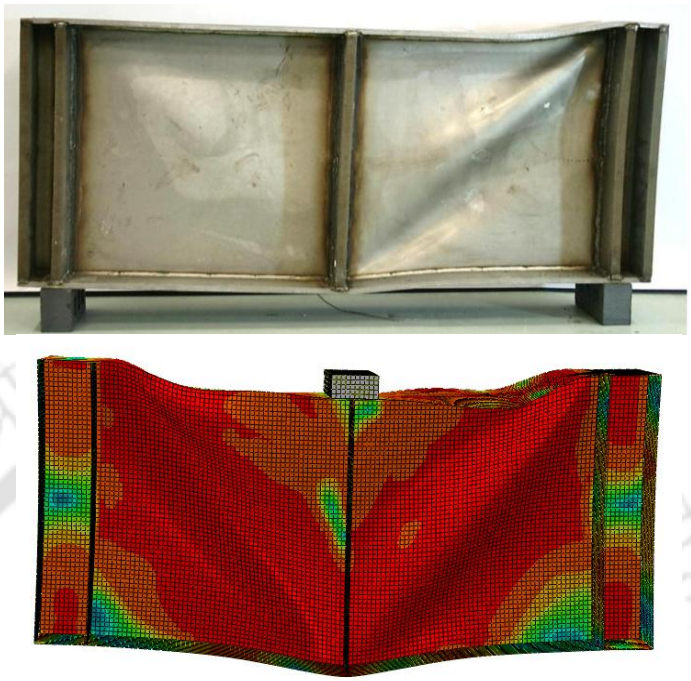

Figure 4.3: Typical failure mode of 3PB specimen of LDSS plate girder (I-600×200×12×8) showing (a) Experiment (Saliba and Gardner, 2013b) (b) FE

(a)

(b)

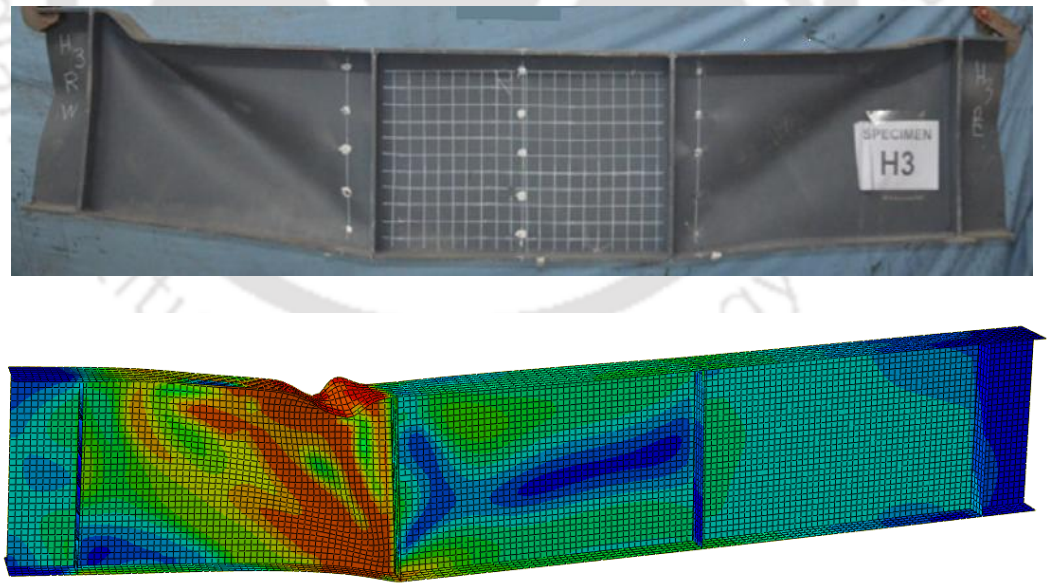

Figure 4.4: Typical failure mode of 4PB specimen of Hybrid high strength steel welded I-beams (I-598×168×12×8) showing (a) Experiment (Shokouhian *et al.*, 2016) (b) FE

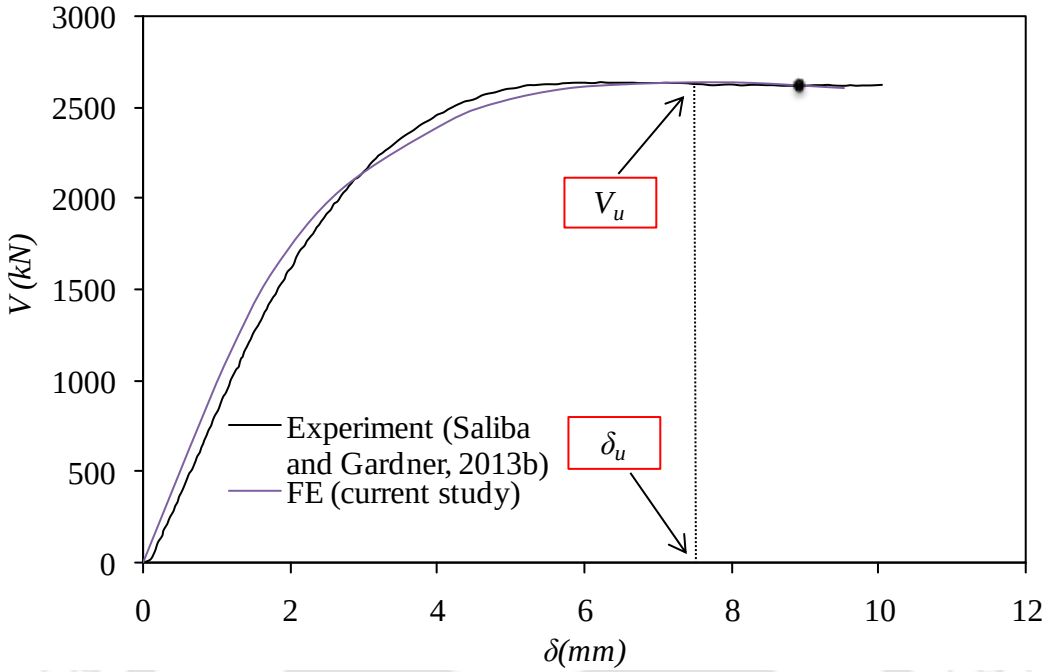

Figure 4.5: Comparison of experimental and FE results for LDSS plate girders (I-600×200×12×8)

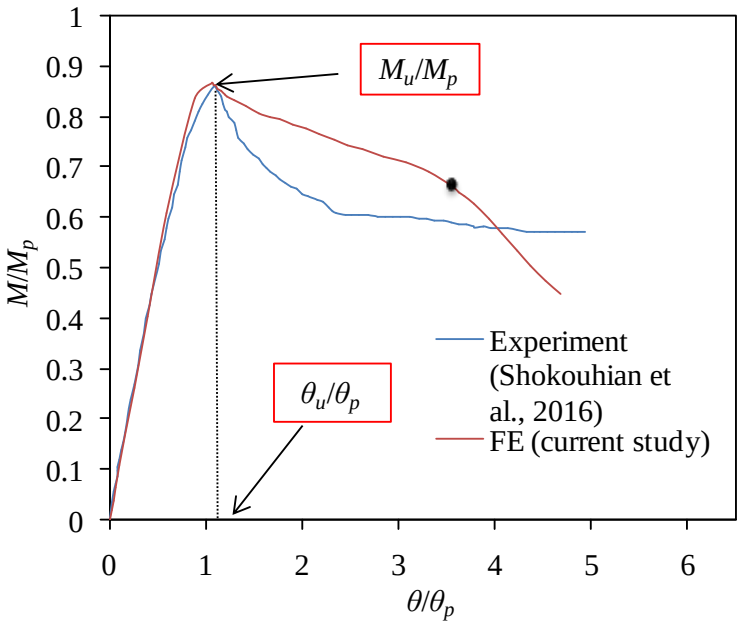

Figure 4.6: Comparison of experimental and FE results for 4PB specimen of Hybrid high strength steel welded I-beams (I-598×168×12×8)

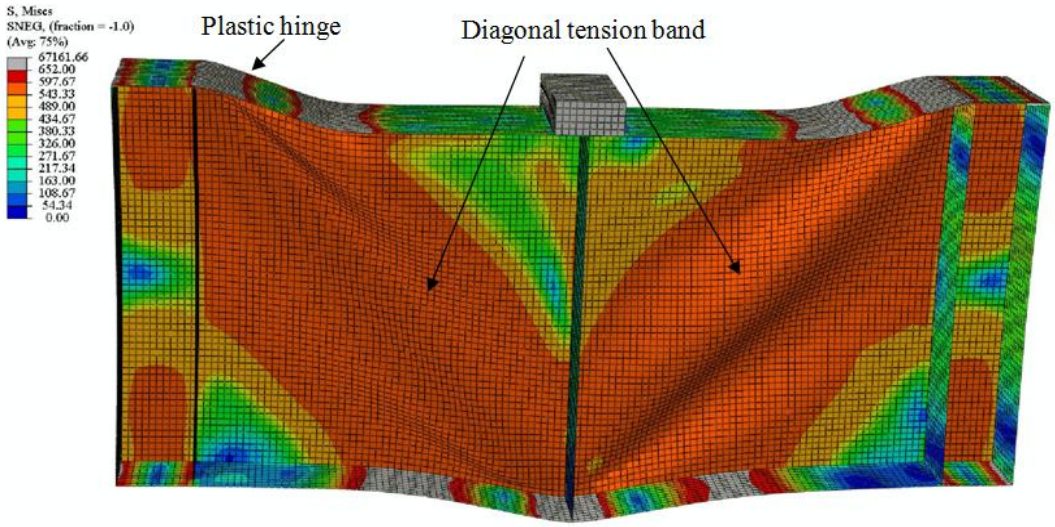

Figure 4.7: Schematic FE diagram of HSS plate girder (I-600×200×12×4) showing shear dominant failure mode

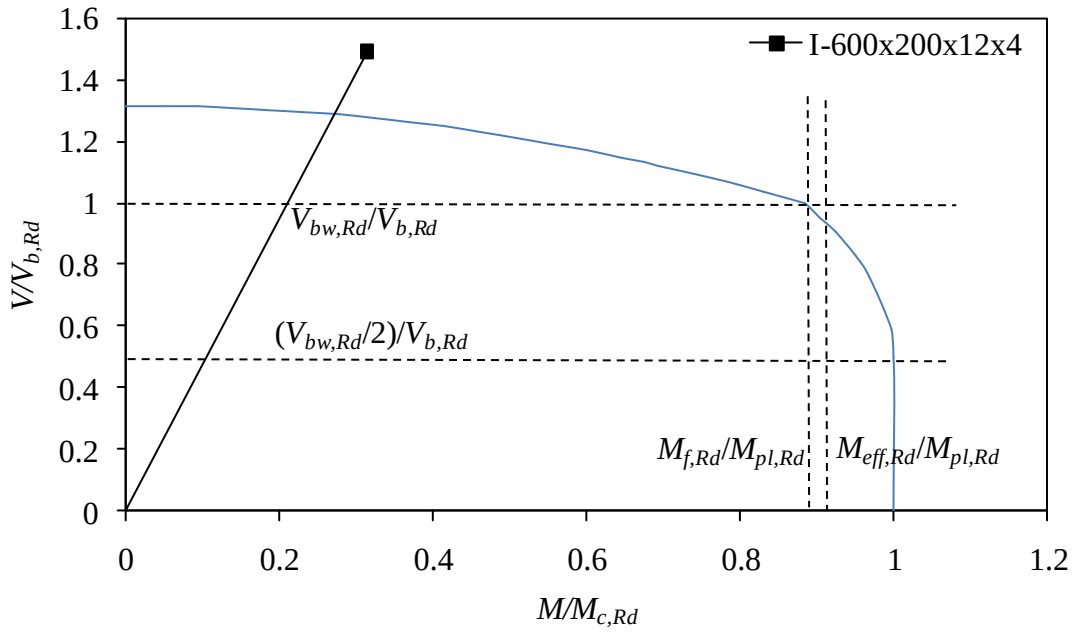

Figure 4.8: Moment-shear interaction diagram for HSS plate girder (I-600×200×12×4) showing shear dominant failure

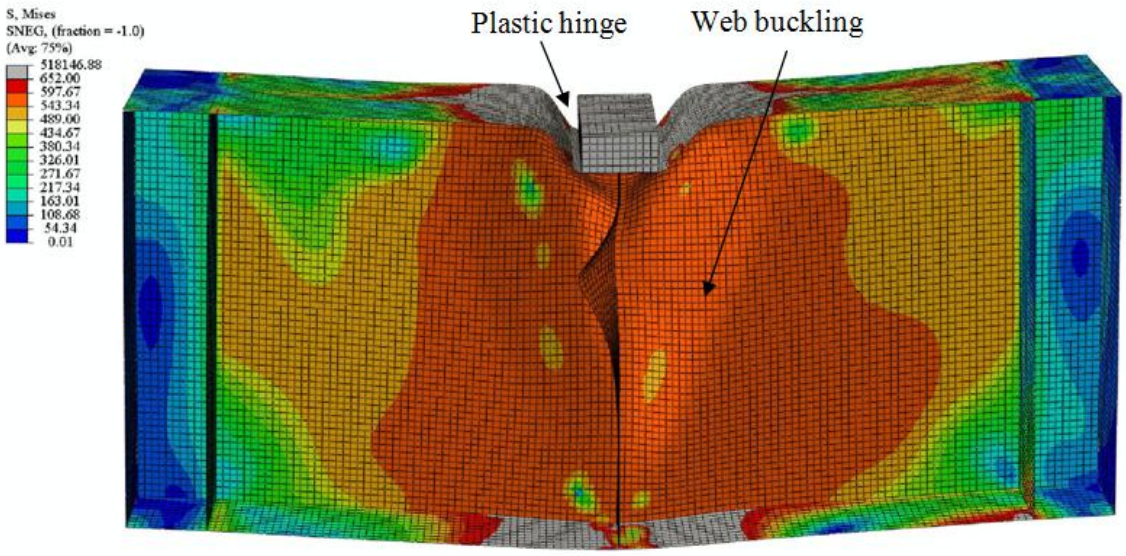

Figure 4.9: Schematic FE diagram of HSS plate girder (I-600×200×12×12) showing bending dominant failure mode

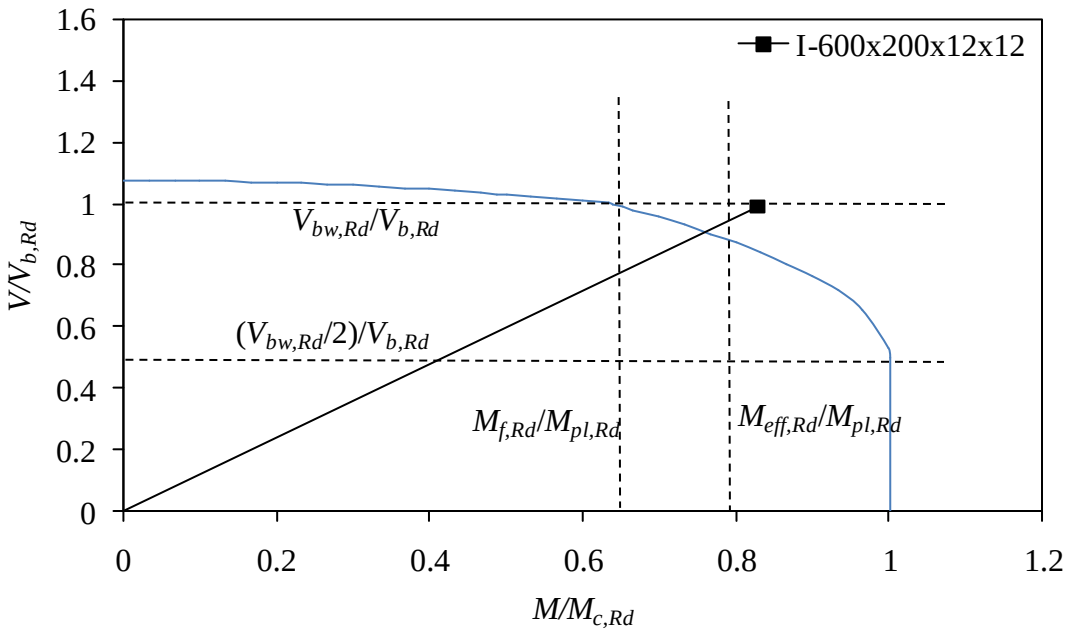

Figure 4.10: Moment-shear interaction diagram for HSS plate girder (I-600×200×12×12) showing bending dominant failure

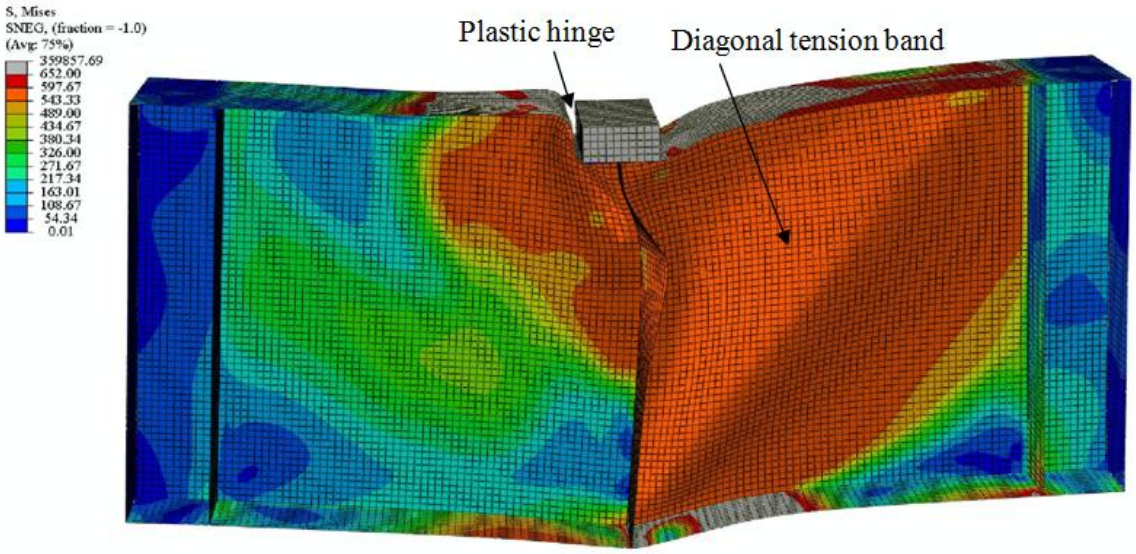

Figure 4.11: Schematic FE diagram of HSS plate girder (I-600×200×12×10) showing combined shear and bending dominant failure mode

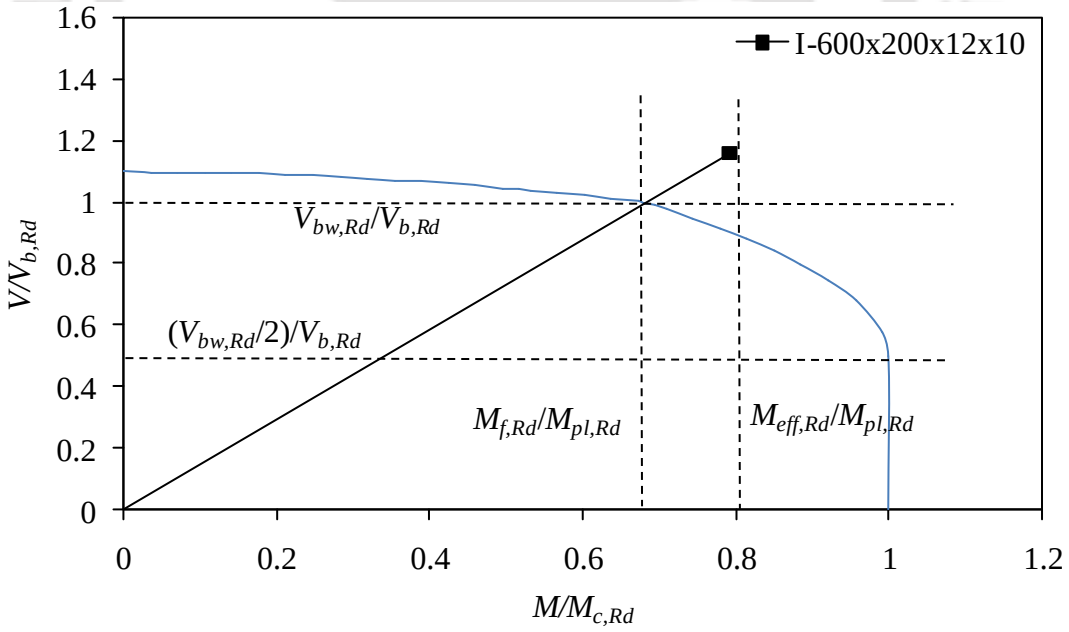

Figure 4.12: Moment-shear interaction diagram for HSS plate girder (I-600×200×12×10) showing combined shear-bending dominant failure

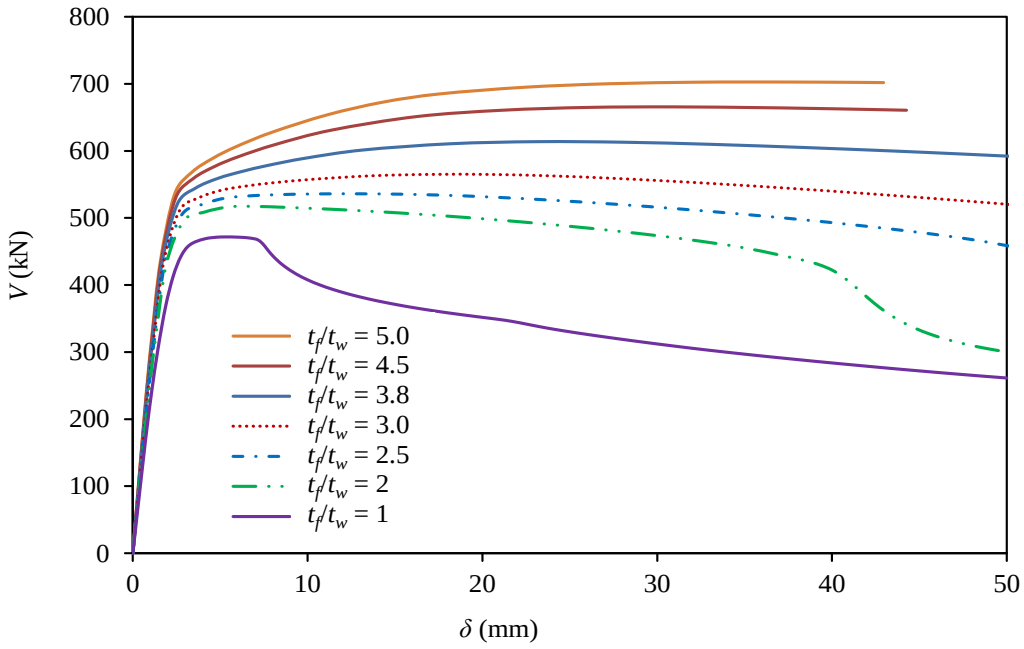

Figure 4.13: Effect of shear force (V) vs mid-span deflection (δ) by varying t_f (t_w = 4 mm, b_f = 200 mm) for HSS plate girders

(A) (B)

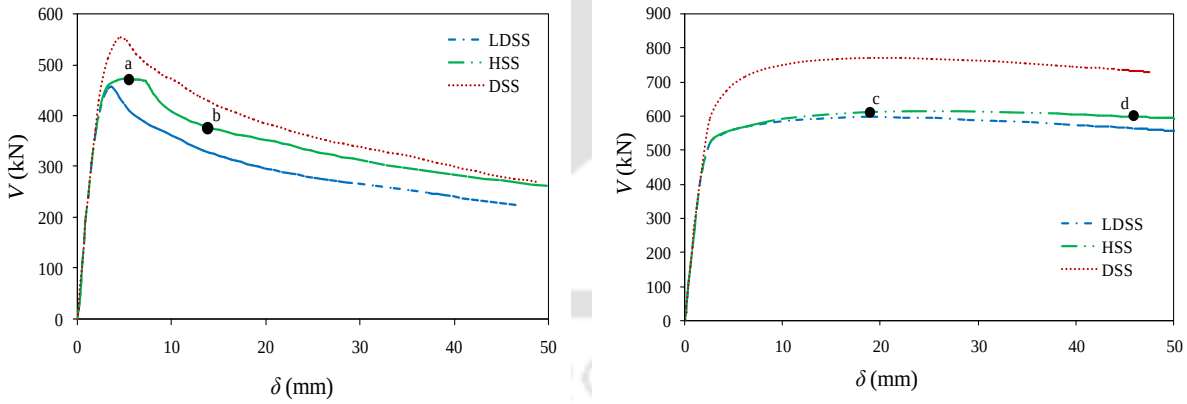

Figure 4.14: Variation of V vs δ by varying t_f: (A) I-600×200×4×4 (B) I-600×200×15×4

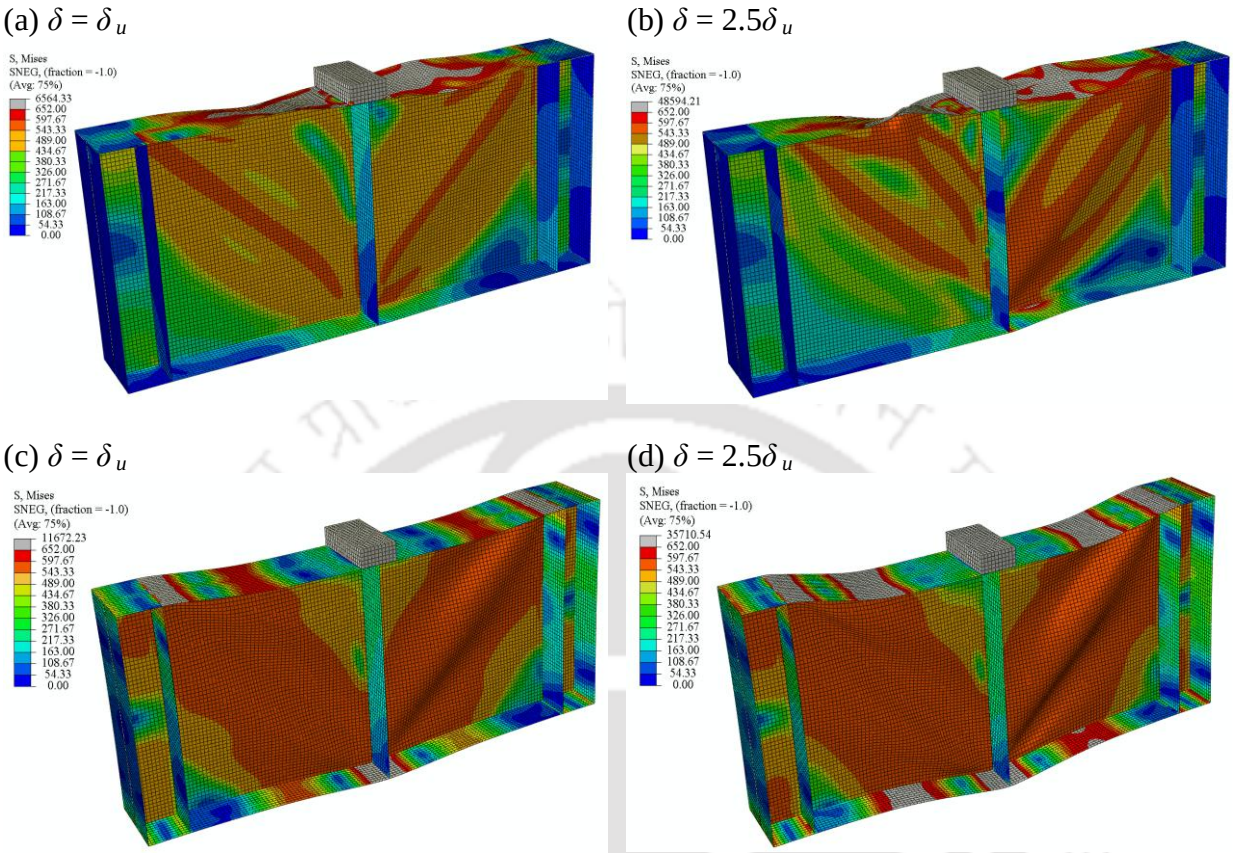

Figure 4.15: Schematic FE diagram of HSS plate girders: I-600×200×4×4 (a,b) and I-600×200×15×4 (c,d)

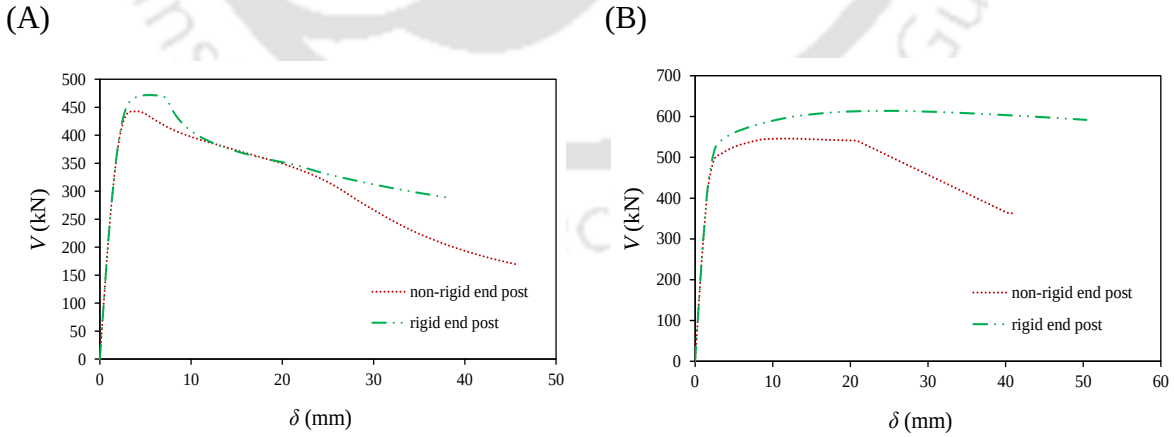

Figure 4.16: Variation of V vs δ by varying t_f for rigid and non-rigid end post HSS plate girders: (A) I-600×200×4×4 (B) I-600×200×15×4

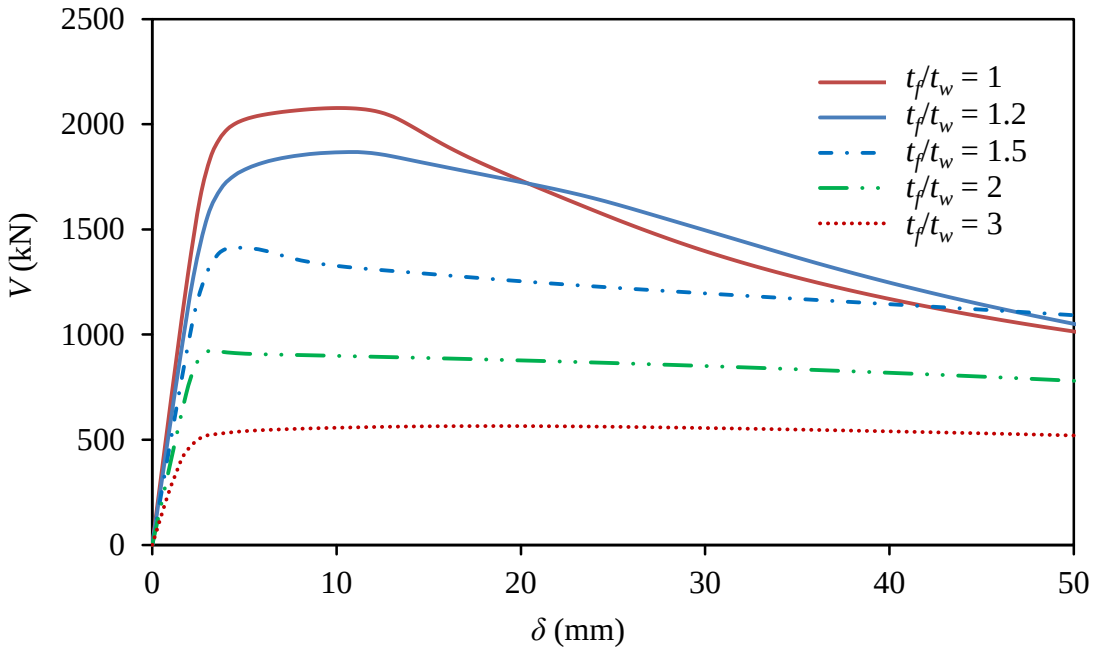

Figure 4.17: Effect of V vs δ by varying t_w (t_f = 12 mm, b_f = 200 mm) for HSS plate girders

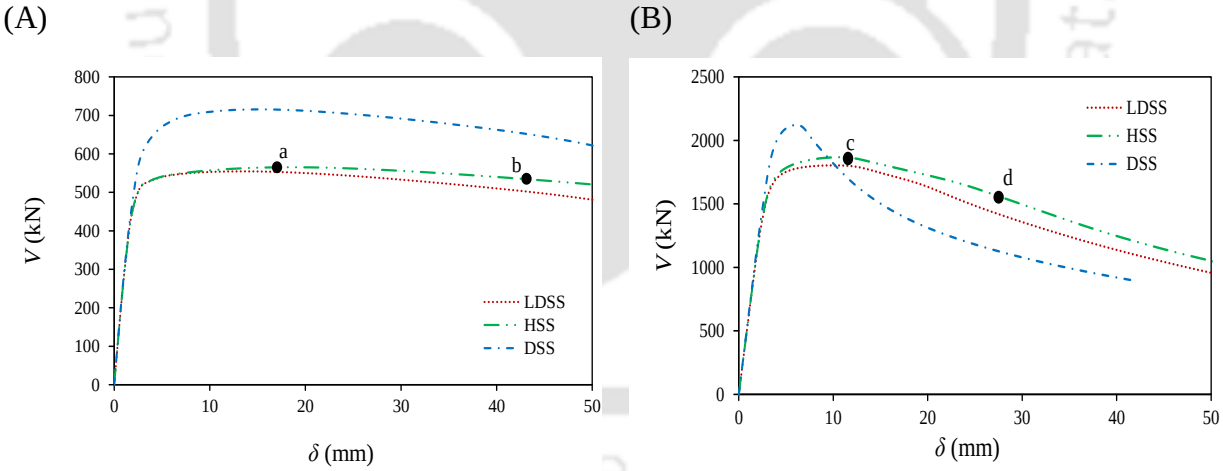

Figure 4.18: Variation of V vs δ by varying t_w: (A) I-600×200×12×4-1 (B) I-600×200×12×12-1

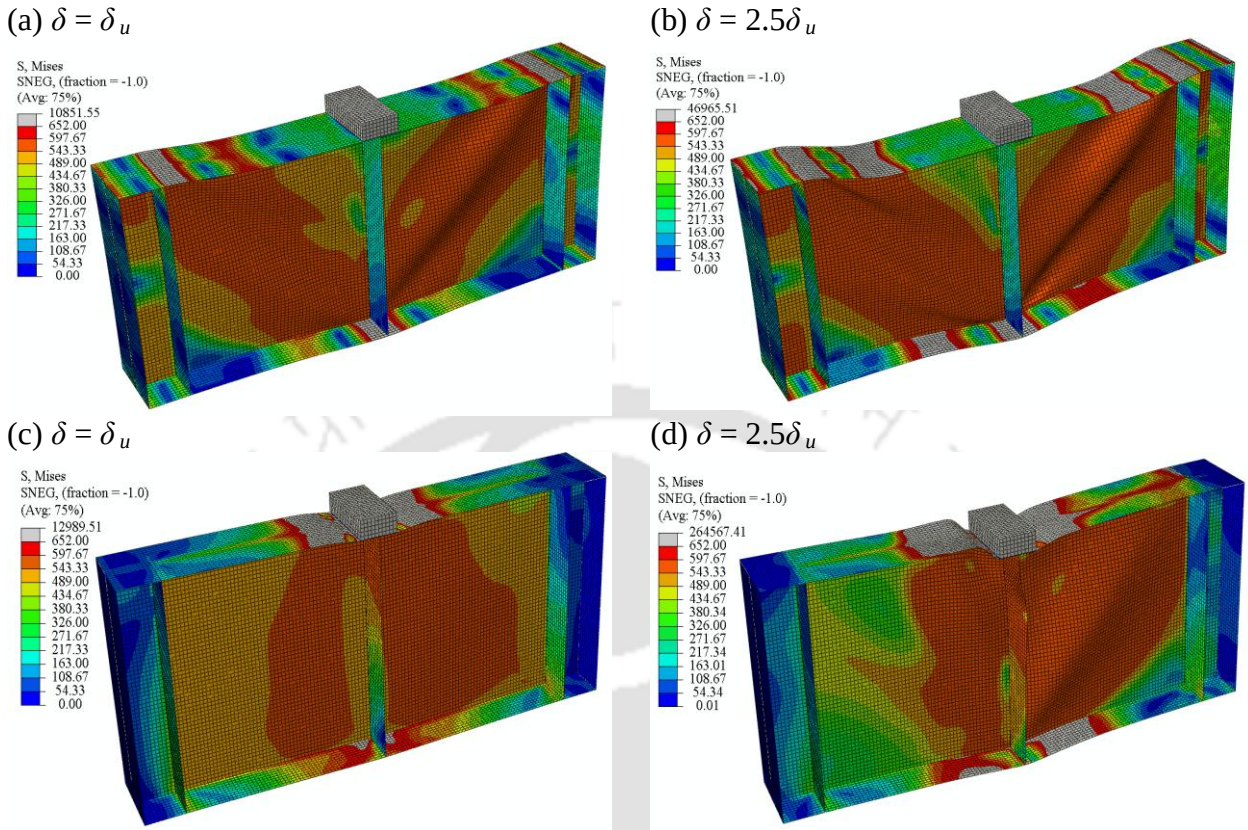

Figure 4.19: Schematic FE diagram of HSS plate girders: I-600×200×12×4-1 (a,b) and I-600×200×12×12-1 (c,d)

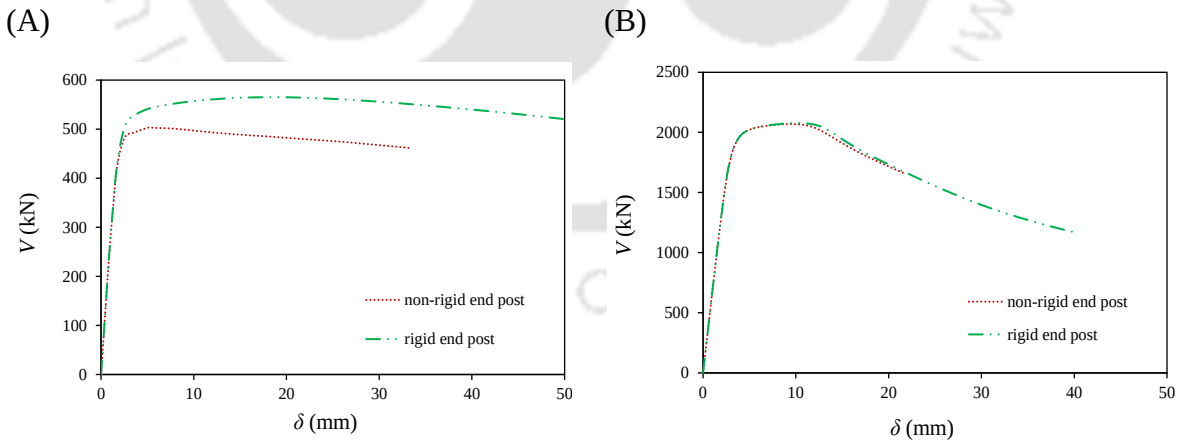

Figure 4.20: Variation of V vs δ by varying t_w for rigid and non-rigid end post HSS plate girders: (A) I-600×200×12×4 (B) I-600×200×12×12

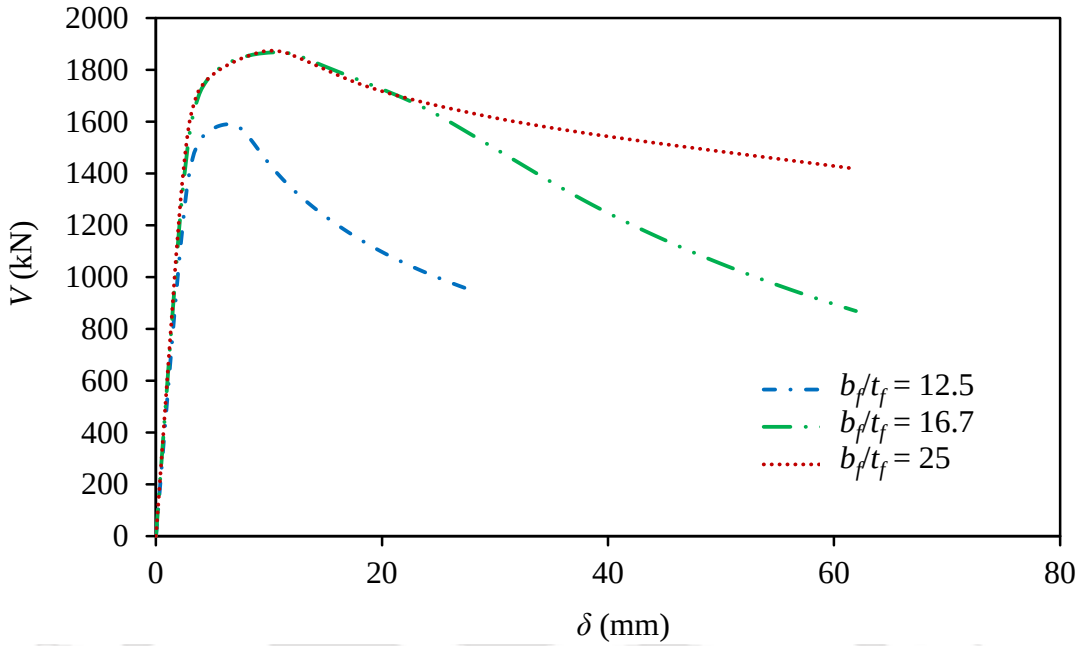

Figure 4.21: Effect of V vs δ by varying b_f (t_f = 12 mm, t_w = 10 mm) for HSS plate girders

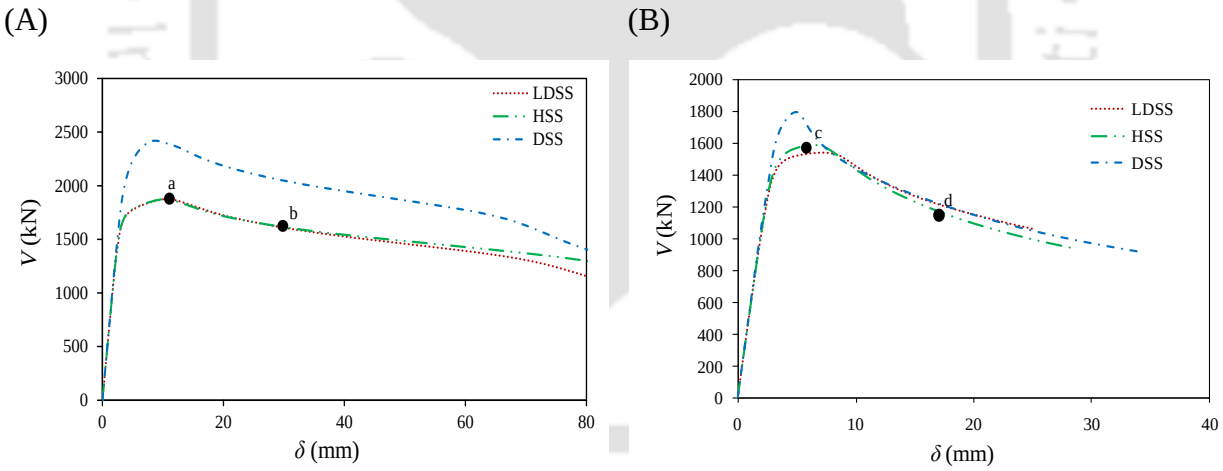

Figure 4.22: Variation of V vs δ by varying b_f (A) I-600×300×12×10-1 (B) I-600×150×12×10-1

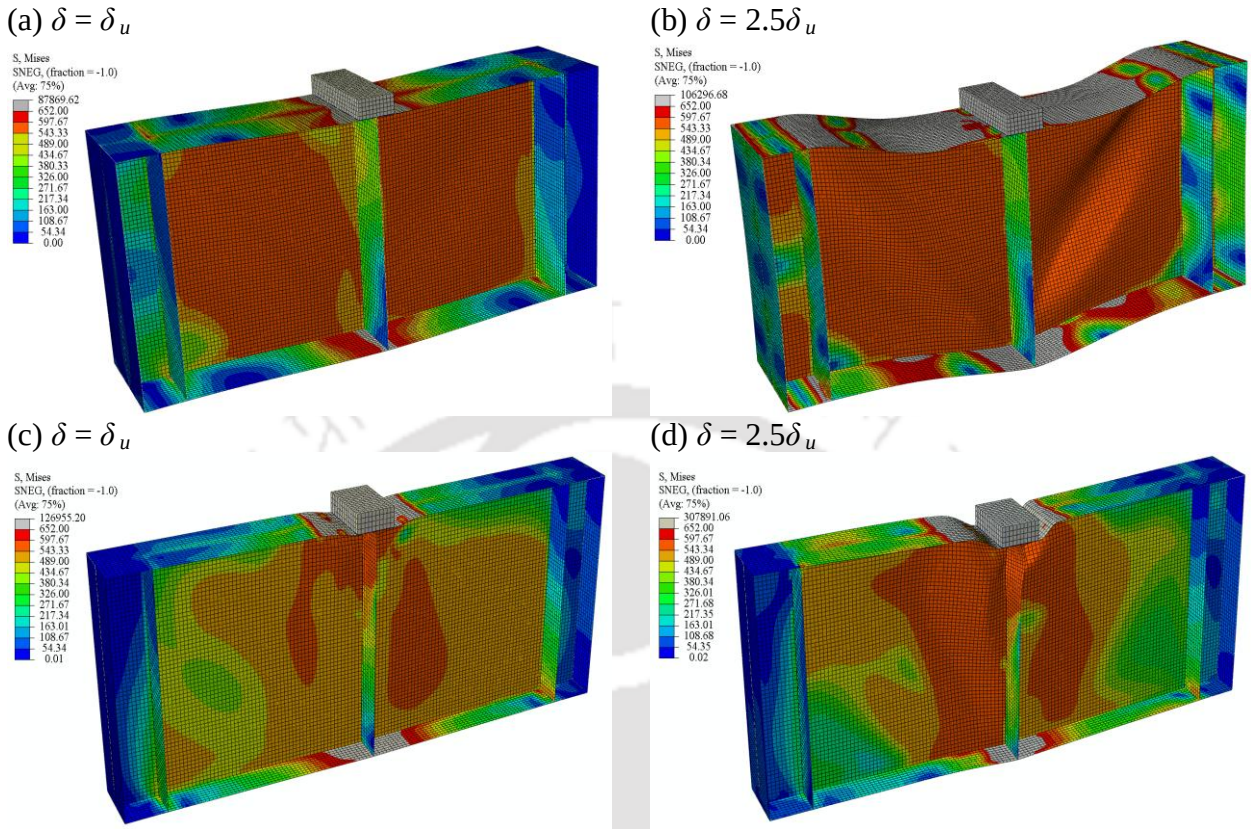

Figure 4.23: Schematic FE diagram of HSS plate girders: I-600×300×12×10-1 (a,b) and I-600×150×12×10-1 (c,d)

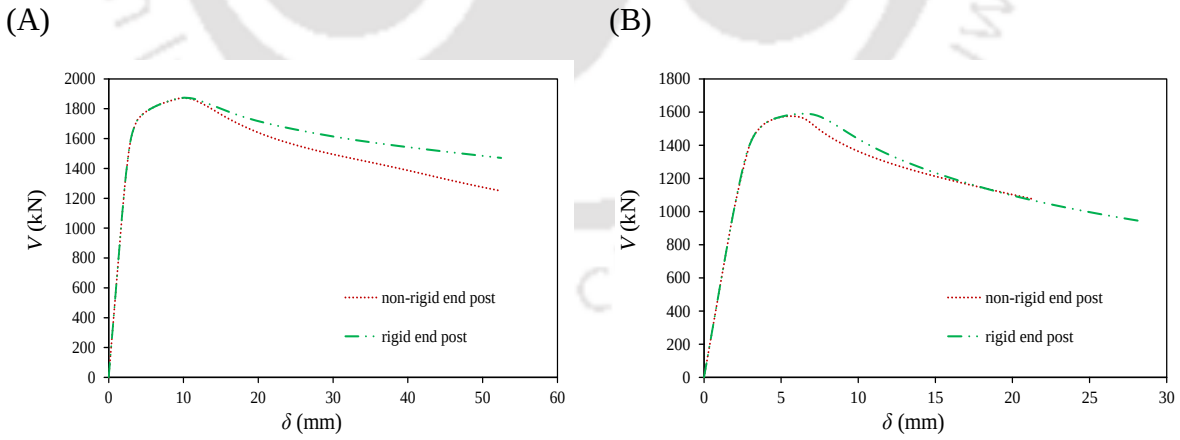

Figure 4.24: Variation of V vs δ by varying b_f for rigid and non-rigid end post HSS plate girders: (A) I-600×300×12×10 (B) I-600×150×12×10

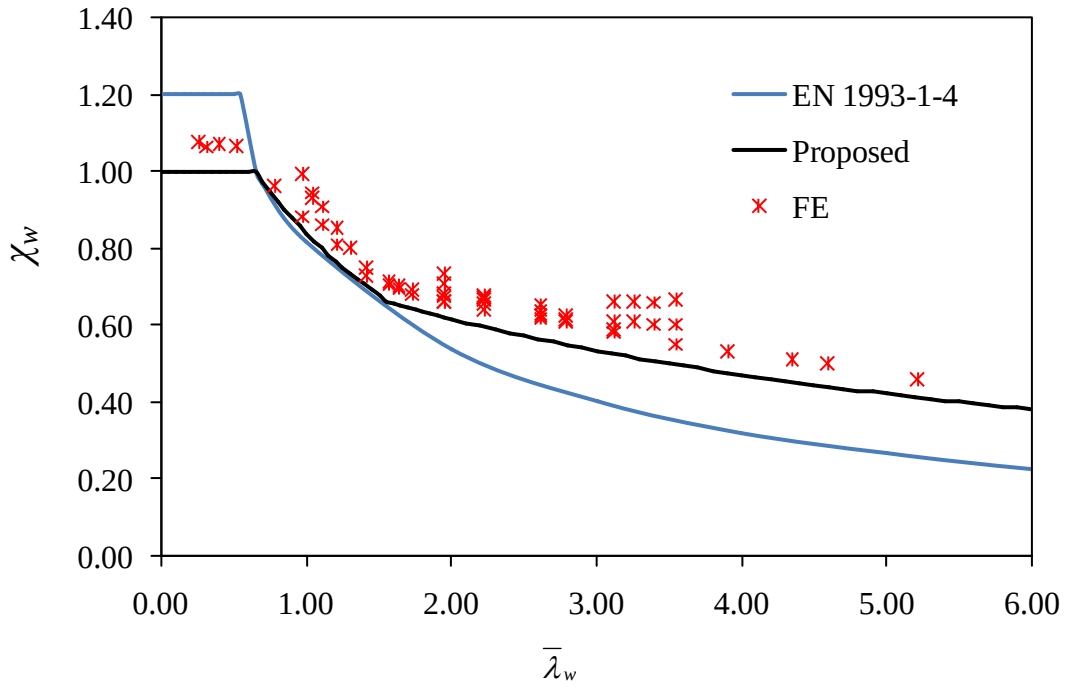

Figure 4.25: Comparison of FE results with EN 1993-1-4 shear design curve for HSS plate girders

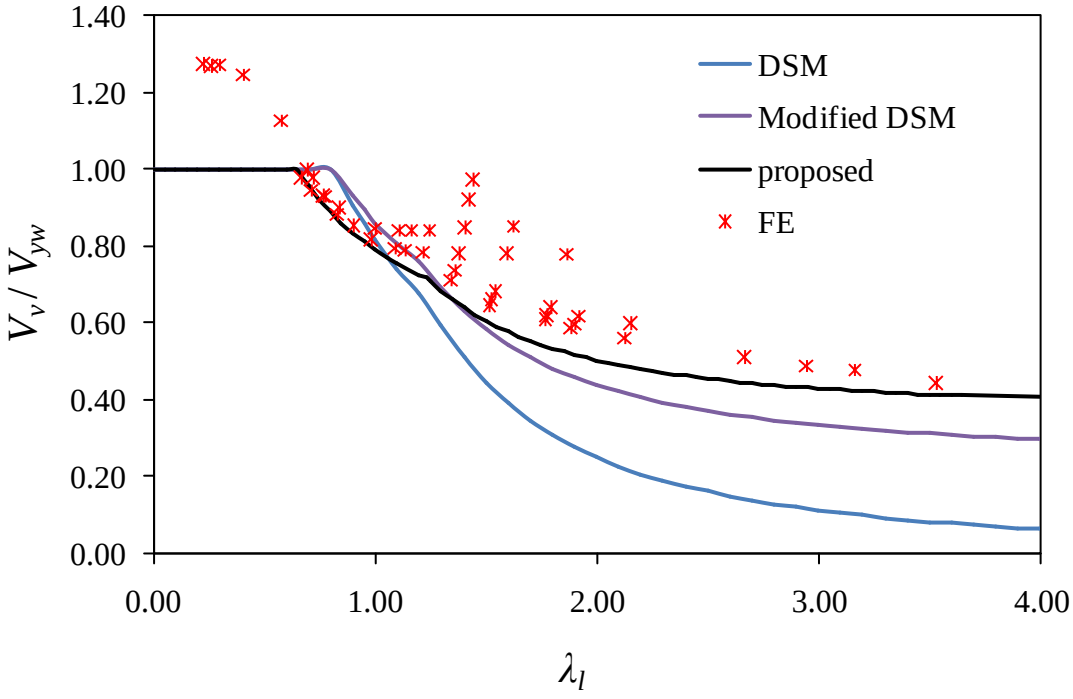

Figure 4.26: Comparison of FE results with DSM shear design curve for HSS plate girders

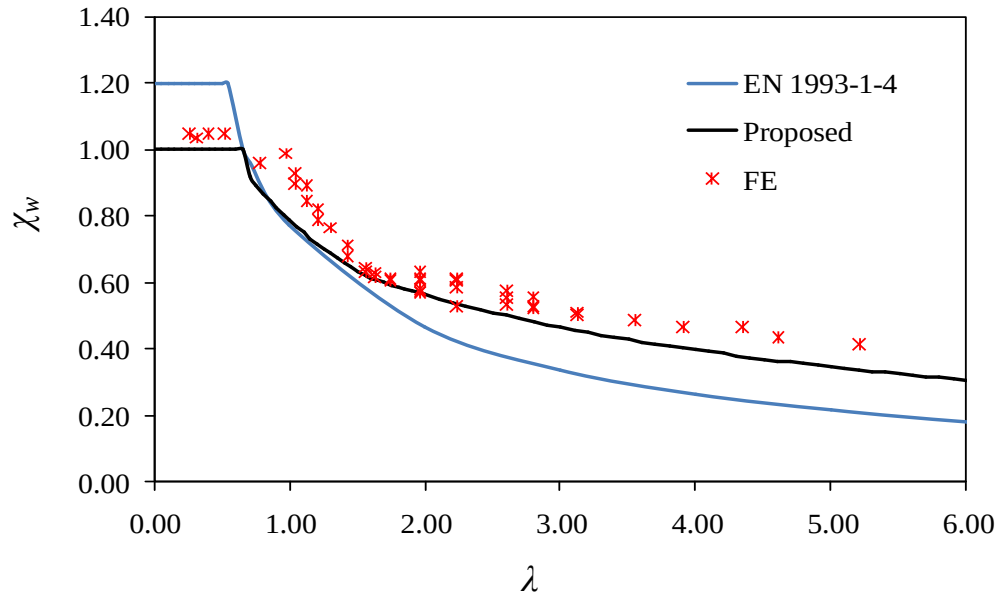

Figure 4.27: Comparison of FE results with EN 1993-1-4 shear design curve for non-rigid end post HSS plate girders

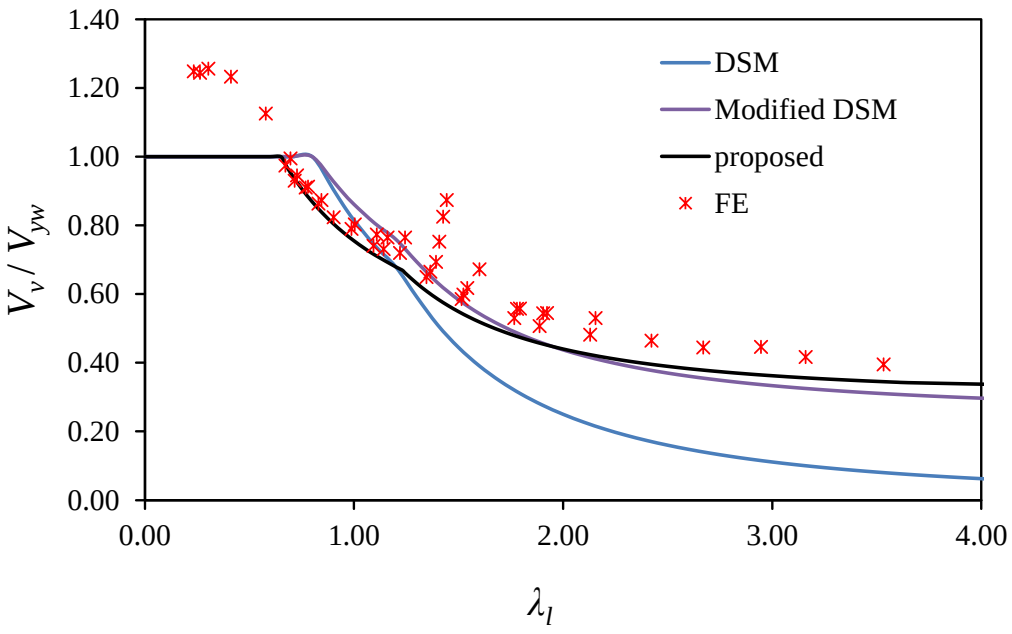

Figure 4.28: Comparison of FE results with DSM shear design curve for non-rigid end post HSS plate girders

CHAPTER 5

5 HYBRID STAINLESS STEEL STUB COLUMNS UNDER PURE AXIAL COMPRESSION

5.1 INTRODUCTION

Over the last few decades, researchers were mainly focussed on the commonly adopted stainless steel compression members such as square (Liu and Young, 2003; Theofanous and Gardner, 2009), rectangular (Theofanous *et al.*, 2012), circular (Ashraf *et al.*, 2008) and open sections such as I-sections (Ashraf *et al.*, 2006b; Saliba and Gardner, 2013a). Due to enhanced architecural demands, investigations were also carried out on elliptical hollow sections, flat oval sections, semi elliptical secions, etc. (e.g. (Theofanous *et al.*, 2009b; Patton and Singh, 2012; Zhu and Young, 2012; Silvestre *et al.*, 2013; Narendra and Singh, 2016; Sachidananda and Singh, 2017)). In addition, few studies were reported on built-up sections such as H-shaped columns, hybrid columns, etc. (e.g. (Nagarajarao *et al.*, 1972; Aoki and Ji, 2000; Kuwamura, 2003; Zhao *et al.*, 2004; Heidarpour *et al.*, 2013; Javidan *et al.*, 2016)). Studies on hybrid columns are very limited and the first work on hybrid I-section columns dated back to 1972 by Nagarajarao *et al.* (1972). This section utilizes high strength carbon steel flanges and relatively lower strength carbon steel in the web. Later, an investigation on innovative hybrid stub column which employs mild carbon steel circular tubes welded to the corners of triangular and square mild steel columns was carried out by Aoki and Ji (2000). This concept of employing circular tubes as corners was further investigated by

Zhao *et al.,* (2004) by employing very high strength carbon steel tubes. Also, similar hybrid section were further extended and investigated by Heidarpour *et al.,* (2013) adopting stainless steel tubes at the corners. However, to the best of author's knowledge, study conducted by Nagarajarao *et al.*, (1972) is the only work pertaining to hybrid carbon steel I-section columns. An investigation is further extended here on hybrid stub columns adopting stainless steel materials. With this as background, and in the light of understanding the behaviour of stainless steel columns, in this chapter, the structural performance of Hybrid stub columns having two configurations: (1) Hybrid stainless steel (HSS) stub column adopting DSS and LDSS on the flanges and web respectively; and (2) Hybrid stainless steel (HSS^a) stub column using DSS and LDSS on the web and flanges respectively, is presented. Further, the FE column capacity (P_u) are also compared with those design specifications predicted by European code (EN 1993-1-4:2006 + A1, 2015) and Direct strength method (DSM) (Rossi and Rasmussen, 2012; AISI, 2016b; Arrayago *et al.*, 2017), to assess their applicability. Finally, attempts are made to modify both the European code and DSM design predictions, for a possible improvement in the design specifications, for HSS and HSS^a stub columns.

5.2 NUMERICAL MODELLING

5.2.1 General

This section presents a numerical study on structural performance of hybrid stainless steel stub columns. This study was conducted utilizing the commercial FE software, Abaqus (2009). The FE modelling techniques currently adopted in this study are known to give accurate results and have been used in a number of similar studies conducted earlier (e.g. (Theofanous and Gardner, 2009; Patton and Singh, 2012; Hassanein and Silvestre, 2013; Huang and Young, 2013; Saliba and Gardner, 2013a; Sonu and Singh, 2017)). Initially, the FE models are validated using the experimental results of LDSS welded I-section stub columns (Saliba and Gardner, 2013a). Further, the validated FE

models are adopted to assess the structural performance of HSS, HSS[a], LDSS and DSS stub columns.

5.2.2 Geometry

Figure 5.1 shows the cross-section of I-section stub column, where b_f and h_w are the flange width and web height; t_f and t_w are the flange and web thicknesses, respectively. The stub column is designated by the section type, followed by web height × flange width × flange thickness × web thickness. For example, the label 'I-200×140×10×8' represents the stub column with h_w = 200 mm, b_f = 140 mm, t_f = 10 mm and t_w = 8 mm. The length (L) of stub column is taken as three times the larger cross section and less than 20 times the minimum radius of gyration to avoid flexural buckling (Heidarpour *et al.*, 2013). Therefore, in the current study: L and h_w are fixed at 600 mm and 200 mm respectively. The schematic diagram of stub column is shown in Figure 5.1b.

5.2.3 FE modelling

Four-noded doubly curved shell FE element with reduced integration (S4R) available in Abaqus (2009) has been used in the current study to discretize the models as shown in Figure 5.2. The S4R element has six degrees of freedom per node. This element has been adopted in numerous similar investigations conducted in thin-walled structures (e.g. (Ellobody and Young, 2005; Patton and Singh, 2012; Saliba and Gardner, 2013a; Sonu and Singh, 2017)) and is known to predict accurate results. The FE element size has been kept as ~9 mm × 9 mm based on mesh convergence study (by performing linear elastic eigen value buckling analysis) and element aspect ratio of ~1.0 was adopted. The number of S4R elements used in the current study ranges from ~ 3000 to 6000 for all FE models. Reference points (RP-1 and RP-2) were provided at both ends of the stub column which constraints column ends through kinematic coupling as shown in Figure. 2. Boundary conditions were provided through these reference points (i.e. Bottom and top BC's were applied through RP1 and RP2 respectively). Bottom end of stub column was fixed while top end (loaded end) is permitted to undergo only

free vertical translation (i.e. along the direction of application of load) as shown in Figure 5.2. A central concentrated load was applied statically at top end through RP2 using displacement control. Loading was carried out as static point loads in increments using the modified RIKS method available in Abaqus Library (Abaqus, 2009). This method is often used in static analysis and was reported to be a powerful method for non-linear analysis (Hassanein, 2011). Also, it is known that initial geometric imperfections occurred mostly during the fabrication and production stages for every structural member. Hence, it is required to take into account these imperfections since it affect the behaviour of structures to a greater extent. In the current study, only local geometric imperfections were considered due to its short length nature (i.e. stub column). The same approach was also adopted by Saliba and Gardner (2013a). These local geometric imperfections were used in the current FE model by adopting the amplitude of the lowest eigen mode in elastic buckling analysis (Theofanous and Gardner, 2010; Saliba and Gardner, 2013a). The imperfection amplitude provided by Dawson and Walker (Dawson and Walker, 1972) (see Equation 3.8) which was further modified by Gardner and Nethercot (2004) has been chosen in the current study since it has shown least deviation in ultimate loads between test and FE model as compared to other imperfection amplitudes (Saliba and Gardner, 2013a). Also, this imperfection amplitude has been successfully employed in other similar applications (e.g. (Ashraf *et al.*, 2006b; Theofanous and Gardner, 2009, 2010; Saliba and Gardner, 2013a)).

5.2.4 Material modelling

Stainless steel properties adopted in the current investigation consists of LDSS material (see Table 3.1a) which are developed from LDSS test results given by Saliba and Gardner (2013a) and DSS material (see Table 3.2) which are obtained from test results performed on DSS sheets carried out by Arrayago *et al.*, (2015). LDSS (see Table 3.1a) and DSS (see Table 3.2) materials are adopted for the homogenous sections such as LDSS and DSS stub columns respectively. For hybrid sections such as HSS stub columns, LDSS material (Tables 3.1a) and DSS material (Table 3.2) are adopted in the

web and flanges respectively, whereas for HSS[a] stub columns, LDSS material (Table 3.1a) is adopted in the flanges and DSS material (Table 3.2) is used in the web. In the current investigation, for stainless steel material having $\sigma \leq \sigma_{0.2}$, Ramberg and Osgood model (1943) given in Equation 3.1 is adopted which is known to provide good agreement with experiments for steel up to $\sigma_{0.2}$. However, for strains surpassing $\varepsilon_{t0.2}$ (total strains at $\sigma_{0.2}$), it predicts greater stresses in comparison to test data. Hence, for strains beyond $\varepsilon_{t0.2}$, modified Ramberg-Osgood model given by Gardner and Ashraf (2006) (Equation 3.2) and Rasmussen (2003) (Equation 3.3) are adopted for LDSS and DSS material respectively which were both developed from Mirambell and Real's multi-model (Mirambell and Real, 2000).

5.2.5 Validation of FE models

A verification study was carried out by validating the FE models using the experimental results on homogeneous LDSS stub columns conducted by Saliba and Gardner (2013a). These LDSS stub columns: I-200×140×12×8, I-200×140×10×8, I-200×140×8×6 and I-200×140×6×6 were validated by adopting the stainless steel properties (see Table 3.1). The average stress-strain values for 10 mm (Table 3.1a) and 8 mm (Table 3.1c) thickness tensile coupons were used to the lower halves (below neutral axis) of stub column at the flange and web respectively. Similarly, the average stress-strain values for 10 mm (Table 3.1d) and 8 mm (Table 3.1b) thickness compressive coupons were applied to the upper halves (above neutral axis) at the flange and web respectively (Saliba and Gardner, 2013a). Typical failure modes of FE and test model for LDSS stub column (I-200×140×10×8) are shown in Figure 5.3. Comparison of FE and experimental compressive load (P) with axial deformation (δ_L) of LDSS stub columns: I-200×140×10×8, I-200×140×12×8, I-200×140×8×6 and I-200×140×6×6 are shown in Figures 5.4, 5.5, 5.6 and 5.7 respectively. The percentage errors in column capacity seen in Figures 5.4, 5.5, 5.6 and 5.7 are ~1.9%, ~1.36%, ~2.60% and ~4.1% respectively and these errors may be considered as minimal. Therefore, the FE models show accurate prediction as compared to the experiments and

hence, can be adopted for parametric studies. In addition, hybrid and homogenous stainless steel stub columns having flange and web plates of different materials and thicknesses can be formed by welding. The same welding method adopted by Saliba and Gardner was used in this study (Saliba and Gardner, 2013a). The residual stress which may developed near the heat affected zone (HAZ), due to welding are ignored in the current study, because the influence of residual stress seen in the investigation of LDSS welded I-sections performed by Saliba and Gardner (2013a) was observed to be minor.

5.2.6 Parametric study

After validating the FE models successfully with test results, investigations were carried out using the validated FE models on the structural performance of stainless steel stub columns. For homogenous sections such as LDSS and DSS stub columns, the stainless steel properties provided in Tables 3.1a and 3.2 are used respectively. For HSS stub columns, DSS (Table 3.2) and LDSS (Table 3.1a) material properties are used in the flanges and web respectively. Whereas for HSS^{a} stub columns, the LDSS material (Table 3.1a) is used in the flanges and DSS material (see Table 3.2) is adopted in the web. For investigating the structural performance of HSS, HSS^{a}, LDSS and DSS stub columns, a total of ~ 310 models were analysed to cover the following parameters: (1) effect of t_f, (2) effect of t_w and (3) effect of flange width (b_f). The FE results were presented in terms of column resistance (P_u) and deformed shapes. Furthermore, a comparative study is presented between FE results and design specifications predicted by EN 1993-1-4 (2006 + A1, 2015) and DSM (Rossi and Rasmussen, 2012; AISI, 2016b; Arrayago *et al.*, 2017).

5.3 CURRENT DESIGN CODES

5.3.1 General

The applicability of the current design codes such as European code (EN 1993-1-4:2006 + A1, 2015) and Direct Strength Method (DSM) to LDSS, HSS, HSS[a] and DSS stub columns was assessed by comparing with the FE results. The FE results in the form of P_u are compared with unfactored design compression resistance predicted by European code (EN 1993-1-4:2006 + A1, 2015) and Direct Strength Method (DSM) (Rossi and Rasmussen, 2012; AISI, 2016b; Arrayago *et al.*, 2017). Comparison of FE results with design resistances are shown in Tables 5.1-5.4.

5.3.2 European code

The appropriateness of stainless steel design compression resistance provided in EN 1993-1-4 (2006 + A1, 2015) is checked for HSS and HSS[a] stub columns along with homogenous sections such as LDSS and DSS stub columns. The current study of stainless steel stub columns for internal compression elements (i.e. web) comprises of Class 1 ($c/t\varepsilon \leq 33$), Class 2 ($c/t\varepsilon \leq 35$), Class 3 ($c/t\varepsilon \leq 37$) and Class 4 ($c/t\varepsilon > 37$) cross-sections as per EN 1993-1-4 (2006 + A1, 2015) based on the slenderness of the most slender constituent plate elements ($c/t\varepsilon$, where c is the flat element length and t is the plate thickness). Furthermore, Class 1, 2 and 3 cross-sections are considered as 'stocky' cross-sections which are fully-effective and capable of attaining their yield load (P_y) (see Equation 3.23). On the other hand, Class 4 sections are considered as slender cross-sections which are incapable of achieving their yield load (P_y) due to the effect of local buckling (LB). Therefore, EN 1993-1-4 (2006 + A1, 2015) unfactored design compressive resistance (P_{EN}) for stainless steel sections is given in Equation 5.1.

$$P_{EN} = \begin{cases} A\sigma_{0.2} & \text{Class 1, 2 and 3 sections} \\ A_{eff}\sigma_{0.2} & \text{Class 4 sections} \end{cases} \quad (5.1)$$

where A and A_{eff} are the gross and effective cross-sectional areas respectively. In case of HSS and HSS[a] stub columns, the values of yield stress ($\sigma_{0.2}$) are calculated by their weighted average values (see Equation 3.18).

5.3.3 Direct strength method

The direct strength method (DSM) was first proposed by Schafer and Pekoz (1998) for the design of cold formed steel members. It is a simple non-iterative design method which is an alternative for the traditional 'effective width method'. Later, DSM was included in the North American Specification (NAS) AISI-S100-16 (AISI, 2016b) for design of cold-formed carbon steel structural members. DSM is calculated based on the elastic buckling load in local, global and distortional buckling modes. The DSM methods adopted in the current study utilizes the full cross-section slenderness ratio (λ_L) through the critical elastic local buckling load (P_{crl}) which can be obtained from software programs based on finite element and finite strip methods (Equation 5.2) (Arrayago *et al.*, 2017). The DSM design resistance for a concentrically loaded stub column is calculated based on Section E of AISI-S100-16 and is given in Equations 5.3-5.5. The DSM compression strength (P_v) is taken as the minimum of local buckling resistances (P_{nl}) and axial strength for yielding and global buckling (P_{ne}).

$$\lambda_L = \sqrt{\frac{P_{ne}}{P_{crl}}} \tag{5.2}$$

$$P_v = \min\left(P_{ne}, P_{nl}\right) \tag{5.3}$$

$$P_{ne} = \begin{cases} (0.658^{\lambda_c^2})P_y & for\,\lambda_c \le 1.5 \\ \left(\dfrac{0.877}{\lambda_c^2}\right)P_y & for\,\lambda_c > 1.5 \end{cases} \tag{5.4}$$

$$P_{nl} = \begin{cases} P_{ne} & for \lambda_L \le 0.776 \\ \left[1 - 0.15\left(\frac{P_{crl}}{P_{ne}}\right)^{0.4}\right]\left(\frac{P_{crl}}{P_{ne}}\right)^{0.4} P_{ne} & for \lambda_L > 0.776 \end{cases} \quad (5.5)$$

here $\lambda_c = \sqrt{P_y / P_{cre}}$; where P_{cre} ($=\pi^2 EA/(KL/r_y)^2$), K and r_y are the critical elastic buckling load in flexure buckling, effective length factor and radius of gyration of the cross-section about minor axis of buckling respectively.

5.3.4 Modified DSM

The original DSM provision implemented in NAS (AISI, 2016b) does not account for the effect of strain hardening. Although, it is known that stainless steel shows significant strain hardening (Gardner, 2005) which makes them different from carbon steel. Therefore, DSM predicted overly-conservative results for stainless steel members particularly for stocky cross-sections. To improve the column capacity prediction, Rossi and Rasmussen (2012) proposed an alternative DSM approach (DSM-RR) for stainless steel sections incorporating the strain hardening effect. Hence, an alternative modified DSM formulation ($P_{v,RR}$) given by Rossi and Rasmussen is given in Equation 5.6.

$$\frac{P_{v,RR}}{P_y} = \begin{cases} 1 + (1 - 2.11\lambda_L)\left(\frac{\sigma_u}{\sigma_{0.2}} - 1\right) & for \lambda_L \le 0.474 \\ \frac{0.95}{\lambda_L^{0.8}} - \frac{0.22}{\lambda_L^{1.6}} & for \lambda_L > 0.474 \end{cases} \quad (5.6)$$

Furthermore, Arrayago *et al.*, (2017) proposed a full-range DSM formulation ($P_{v,ARR}$) based on carbon steel strength curve following similar procedure given by Rossi and Rasmussen (2012) which is given in Equation 5.7. This proposed model was observed to predict accurately for stainless steel RHS and SHS members. For HSS and HSS[a] stub

columns, σ_u (Equation 3.19) and $\sigma_{0.2}$ (Equation 3.18) are taken as weighted average values in the DSM formulation given in Equations 5.6 and 5.7.

$$\frac{P_{v,ARR}}{P_y} = \begin{cases} 1+(1-1.29\lambda_L)\left(\dfrac{\sigma_u}{\sigma_{0.2}}-1\right) & for\,\lambda_L \le 0.776 \\ \dfrac{1}{\lambda_L^{0.8}} - \dfrac{0.15}{\lambda_L^{1.6}} & for\,\lambda_L > 0.776 \end{cases} \tag{5.7}$$

5.3.5 Reliability analysis

The applicability of current design standards including the proposed design equations are assessed by reliability analysis. The reliability analysis method given in the Commentary of the ASCE specifications for design of cold-formed stainless steel members (ASCE 8-02, 2002) was followed in the present study. The reliability index (β) was calculated using the Eq. C-2 given in the commentary of ASCE specification. A target reliability index (β_o) of 2.5 is adopted as a lower bound for stainless steel members. The FE results of stainless steel stub columns were compared with the design specifications of EN 1993-1-1 (2005), DSM in AISI standard (AISI, 2016b) and modified DSM (Rossi and Rasmussen, 2012; Arrayago *et al.*, 2017). These design predictions are considered to be reliable if the reliability index (β) is greater than or equal to 2.5. The values of P_m, V_p and β of the ratio of FE results to the design predictions for HSS, HSS^a, LDSS and DSS stub columns were computed and shown in Tables 5.1-5.4. The dead load (DL) to live load (LL) ratio of 1/5 was adopted, as recommended in AISI specification (AISI, 2016b). The load combination of 1.35 DL +1.5 LL and 1.2 DL + 1.6 LL were adopted for EC3 and DSM respectively following Zhu and Young (2012) . The resistance factor (φ) of 0.91 and 0.85 were adopted for EC3 and DSM respectively following earlier researchers such as (Zhu and Young, 2012; Arrayago *et al.*, 2017; Singh and Singh, 2017). The statistical parameters adopted in the current study includes the mean and coefficients of variation for

fabrication factors (F_m = 1.0 and V_F = 0.05) and material properties (M_m = 1.10, V_M = 0.10).

5.4 RESULTS AND DISCUSSIONS

5.4.1 Effect of t_f

Typical plots showing the effect of t_f are shown in the form of variation of compressive load (P) with axial deformation (δ_L). Figures 5.8 and 5.9 shows the variation of P-δ_L curve for HSS and HSS^a stub columns respectively covering a range of t_f/t_w = 0.5-3 by varying t_f ; keeping t_w and b_f as constant (i.e. t_w = 6 mm and b_f = 140 mm). It can be observed from Figures 5.8 and 5.9 that the column capacity (P_u) and axial deformation at ultimate load (δ_{Lu}) increases by increasing t_f. An increase in t_f (3-18 mm) or t_f/t_w (0.5-3) by 500% results in increase in P_u of ~381% and ~266% for HSS and HSS^a stub columns respectively. This clearly indicates that increase in flange thickness has significant enhancement on column capacity (i.e. P_u) for HSS stub columns as compared to HSS^a stub columns. Variation of P_u with t_f/t_w for constant t_w (i.e. t_w = 6 mm) is plotted in Figure 5.13 for HSS, HSS^a, LDSS and DSS stub columns. It can be seen that P_u increases with increase in t_f (i.e. t_f/t_w) for all stub columns. At thinner flange thickness (i.e. $t_f/t_w \leq 1$), all stub columns predicted almost similar column capacity with maximum variation of < 10%. However, in case of stocky flange sections (i.e. $t_f/t_w > 1$), significant improvement in P_u can be observed for DSS and HSS stub columns as compared to LDSS stub columns, as t_f increases. Whereas, for HSS^a stub column, very less improvement in P_u can be seen when compared to LDSS stub column with increase in t_f. Figure 5.10 shows variation of P-δ_L curve for LDSS, HSS, HSS^a and DSS stub columns for thinner flange sections (i.e. t_f = 3 mm) and thick flange sections (i.e. t_f = 18 mm). The value of P_u increases by ~13.4%, ~2.2%, ~9.4% for thin flange sections (i.e. t_f = 3 mm); and ~32%, ~29%, ~5% for thick flange sections (i.e. t_f = 18 mm) in DSS, HSS and HSS^a stub columns respectively when compared to LDSS

stub columns (i.e. LDSS stub columns predict minimum P_u). Figure 5.11 shows Von-Mises stress contours for HSS thinner flange sections (i.e. t_f = 3) and thick flange sections (i.e. t_f = 18) corresponding to δ_{Lu} and 2.5δ_{Lu}. The values of Von-Mises stress (hereafter referred to as stress) ≥ 652 MPa (i.e. $\sigma_{0.2f}$) are grey-coloured, showing areas which have crossed yield stress of flange (i.e. $\sigma_{0.2f}$). It can be observed from thinner flange sections (Figures 5.11a and b) that at δ_{Lu}, a larger area around the mid-height of the flanges has yielded and initiation of local buckling (LB) can be seen in the yielded area of the flanges. Whereas at post ultimate (i.e. at 2.5δ_{Lu}), LB can be seen in the yielded region of flanges and at mid-height of the web. For thicker flange sections (Figures 5.11c and d), it can be seen that at δ_{Lu}, the entire areas of flanges are yielded, indicating that the flanges are fully effective in resisting the axial load and further at 2.5δ_{Lu}, LB can be seen at two locations in the flange near the mid-height. Stress contours for thin flange sections (i.e. t_f = 3 mm) and thick flange sections (i.e. t_f = 18 mm) in HSS^a stub columns are shown in Figure 5.12. In thin flange sections (Figures 5.12a' and b'), it can be seen that at δ_{Lu}, large areas in the web have yielded (in contradiction to HSS stub columns) and initiation of LB can be observed in the flanges near the mid-height. Further at 2.5δ_{Lu}, few LB can be seen in the flanges and in the yielded region of web. In case of thick flange sections (Figures 5.12c' and d'), larger areas in the web compared to thin flange sections have yielded at δ_{Lu}, and further at 2.5 δ_{Lu}, LB can also be seen at few locations in the web and flanges similar to thin flange sections.

5.4.2 Effect of t_w

The effect of t_w is shown in the form of variation of P-δ_L curve for HSS and HSS^a stub columns in Figures 5.14 and 5.15 respectively covering a range of t_f /t_w = 0.33-2 by varying t_w ; keeping t_f and b_f as constant (i.e. t_f = 6 mm and b_f = 140 mm). It can be seen from Figures 5.14 and 5.15 that P_u and δ_{Lu} increases with decrease in t_f /t_w (i.e. by increasing t_w). At thinner web thickness (i.e.t_f /t_w = 2), the curve is relatively sharper around P_u, and as t_w increases, the curve becomes increasingly flatter for both HSS and

HSS[a] stub columns as shown in Figures 5.14 and 5.15 respectively. An increase in t_w (3-18 mm) or t_f/t_w (2-0.33) by 500% results in increase in P_u of ~170% and ~247% for HSS and HSS[a] stub columns respectively. This shows that increase in web thickness has improved the column capacity significantly for HSS[a] stub columns as compared with HSS stub columns (in contrast to effect of increase in t_f). Figure 5.13 shows the variation of P_u with t_f/t_w for constant t_f (i.e. t_f = 6 mm). It can be observed that P_u increases by decreasing t_f/t_w (i.e. by increasing t_w) for all stub columns. Also, it can be seen from Figure 5.10 that at thinner t_w (i.e. t_f/t_w = 2), HSS stub columns predicted higher P_u (i.e. ~13%) as compared to HSS[a] stub column and for thicker t_w (i.e. t_f/t_w = 0.33), P_u is observed to be higher for HSS[a] stub columns by ~15% compared with HSS stub column. Variation of P-δ_L curve for LDSS, HSS, HSS[a] and DSS stub columns for thinner web sections (i.e. t_w = 3 mm) and thick web sections (i.e. t_w = 18 mm) is shown in Figure 5.16. In comparison to homogenous LDSS stub columns, P_u increases by ~18%, ~15.3%, ~2% for thin web sections (i.e. t_w = 3 mm); and ~37%, ~13%, ~28% for thick web sections (i.e. t_w = 18 mm) in DSS, HSS and HSS[a] stub columns respectively. Figure 5.17 shows stress contours for HSS thinner web sections (i.e. t_w = 3 mm) and thick web sections (i.e. t_w = 18 mm) corresponding to δ_{Lu} and 2.5δ_{Lu}. It can be observed from thinner web section (Figures 5.17a and b) that at δ_{Lu}, small inclined area near the mid-height of the flanges has yielded and further at 2.5δ_{Lu}, the flange has completely yielded and few LB can be seen in the flanges and web near the mid-height. In case of thick web sections shown in Figure 5.17, the flange has completely yielded at δ_{Lu}, and multiple LB can be seen in the flanges at 2δ_{Lu}. Stress contours for thin (i.e. t_w = 3 mm) and thick (i.e. t_w = 18 mm) web sections in HSS[a] stub columns are shown in Figure 5.18. For thin web sections (Figures 5.14a' and b'), it can be seen that at δ_{Lu}, the web is yielded in few dispersed locations and further at 2.5δ_{Lu}, the yielded area has increased and LB can be seen at few locations in the flanges and web near the mid-height. In case of thick web sections (Figures 5.17c' and d'), it can be observed that the web is fully yielded at δ_{Lu} and multiple LB can be seen in the flanges at 2.5δ_{Lu}.

5.4.3 Effect of b_f

Variation of P-δ_L curve for HSS and HSS^a stub columns covering a range of b_f = 140-250 mm; keeping t_w and t_f as constant (i.e. t_w = 6 mm and t_f = 12 mm) can be seen in Figures 5.19 and 5.20 for HSS and HSS^a stub columns respectively. An increase in P_u can be observed with increase in b_f for HSS and HSS^a stub columns as shown in Figures 5.19 and 5.20 respectively. It can be seen that an increase in b_f (140-250 mm) by ~44% results in an improvement in P_u by ~58% and ~47% for HSS and HSS^a stub columns respectively. This shows that increase in flange width has more improvement on column capacity for HSS stub columns as compared to HSS^a stub columns. Also, in contrast to effect of increase in t_f or t_w, it can be seen that at higher flange width (i.e. b_f = 250 mm), the curve is relatively sharper around P_u, and as b_f decreases, the curve becomes increasingly flatter for both HSS and HSS^a stub columns. Figure 5.21 shows the variation of P-δ_L curve for smaller b_f (i.e. b_f = 140 mm) and higher b_f (i.e. b_f = 250 mm) stub columns. It can be seen that LDSS stub columns predicted minimum P_u. An improvement in P_u of ~30%, ~24%, ~8% for smaller b_f ; and ~29%, ~24%, ~6% for higher b_f can be seen in DSS, HSS and HSS^a stub columns respectively when compared with LDSS stub column. Figures 5.22 and 5.23 shows stress contours for smaller b_f (i.e. b_f = 140 mm) and wider b_f (i.e. b_f = 250 mm) sections in HSS and HSS^a stub columns respectively. For smaller b_f (Figures 5.22a and b), it can be seen that at δ_{Lu}, the flange is fully yielded and further at 2.5δ_{Lu}, LB can be seen at few locations in the flanges and web near the mid-height of the stub column. In case of wider b_f (Figures 5.22c and d), it can be observed that large areas in flange has yielded at δ_{Lu} and LB can be seen in the flanges at 2.5δ_{Lu}. In HSS^a stub columns of smaller b_f (Figures 5.23a' and b'), it can be seen that areas near the mid-height of web has yielded at δ_{Lu}, and further at 2.5δ_{Lu}, LB can be seen at few locations in the flange and web near the mid-height. In case of larger b_f (Figures 5.23c' and d'), it can be observed that areas near the mid-height of web have yielded at δ_{Lu} (similar to the pattern of smaller b_f HSS^a stub column) and further at 2.5δ_{Lu}, LB can be observed in flanges. In addition, effect of b_f is shown in the form of variation of P_u vs t_f keeping t_w as constant (i.e. t_w = 6 mm) for

HSS and HSS^a stub columns as shown in Figure 5.24. It can be seen that for thin flange sections (i.e. $t_f \leq 6$ mm), b_f has very less effect on P_u, whereas for $t_f > 6$mm, P_u significantly enhances with increase in b_f and t_f and this improvement in P_u is more effective in HSS stub columns as compared to HSS^a stub columns. This indicates that increase in b_f and t_f has more influence on HSS stub columns as compared to HSS^a stub columns. Figure 5.25 shows the effect of b_f in the form of variation of P_u vs t_w keeping t_f as constant (i.e. $t_f = 6$ mm) for HSS and HSS^a stub columns, it can be seen that for all stub columns, the rate of increase in P_u is almost similar for different range of t_w with increase in b_f. In addition, there is a slight improvement in P_u for HSS as compared with HSS^a stub columns with increase in b_f and t_w.

5.4.4 Comparison of FE results with European code

The FE results of LDSS, HSS, HSS^a and DSS stub columns are plotted in the form of $P_u/A\sigma_{0.2}$ vs the web slenderness ($c_w/t_w\varepsilon$) for web-critical section (i.e. internal web being the most slender constituent element) shown in Figure 5.26. It can be seen that the current European code (EN 1993-1-4:2006 + A1, 2015) that Class 3 limit for internal compression elements ($c_w/t_w\varepsilon$ = 37) is found to be safe and applicable for both homogenous (LDSS and DSS) and hybrid (HSS and HSS^a) stub columns. However, for the purpose of economic designs, the limit ($c_w/t_w\varepsilon$ = 48) is proposed for Class 3 limit for LDSS, HSS, HSS^a and DSS stub columns. The values of P_m, V_p and β for homogenous sections such as LDSS and DSS stub columns are found to be 1.19, 0.09, 2.95; and 1.19, 0.09, 2.95 respectively (see Tables 5.3 and 5.4). Also, for hybrid sections such as HSS and HSS^a stub columns (see Tables 5.1 and 5.2); the values of P_m, V_p and β are observed to be 1.18, 0.08, 2.92; and 1.17, 0.08, 2.91 respectively. Therefore, it can be seen that for all the stub columns, the reliability indices were found to be greater than the target reliability index (β_o=2.5) and hence it is seen to be reliable.

5.4.5 Comparison with DSM

This section assesses the applicability of DSM formulation (Equation 5.3) for the design of LDSS, HSS, HSS^a and DSS stub columns shown in Figure 5.27. Initially, the original DSM formulation (P_v) for a concentrically loaded stub column given in Equation 5.3 was plotted for all stainless steel stub columns as shown in Figure 5.27. It can be seen that this formulation predicted accurately for all sections such as LDSS, HSS, HSS^a and DSS stub columns. However, for stocky sections (i.e. λ_L < 0.7), the results predicted are too conservative. This may be due to the effect of strain hardening which was not incorporated in the original DSM and hence, for stainless steel stocky sections exhibiting significant strain hardening may predict over conservative results. The values of P_m, COV and β for LDSS, HSS, HSS^a and DSS stub columns are observed to be 1.08, 0.05, 3.13; 1.09, 0.06, 3.14; 1.10, 0.18, 2.61; and 1.10, 0.06, 3.14 respectively (see Tables 5.1-5.4). Hence, from the reliability analysis, the values of β for LDSS, HSS, HSS^a and DSS stub columns are found to be greater than the target reliability index (β_o= 2.5) and hence it is observed to be reliable.

5.4.6 Comparison with modified DSM

This section evaluates the applicability of modified DSM formulation (Equation 5.6) which incorporates the beneficial strain hardening effect proposed by Rossi and Rasmussen ($P_{v,RR}$) for HSS and HSS^a stub columns shown in Figures 5.28 and 5.29. It can be observed that this formulation predicted overly-conservative results for most data points (i.e. 0.4 < λ_L < 1.5) and also for few stocky sections (i.e. λ_L < 0.3), the FE results are found to be unsafe. Also, the values of P_m, COV and β for HSS and HSS^a stub columns are found to be 1.18, 0.07, 3.34; and 1.18, 0.18, 2.84 respectively (see Tables 5.1 and 5.2). Therefore, the values of β for HSS and HSS^a stub columns are observed to be greater than the target reliability index (β_o =2.5), and hence it is reliable.

The modified DSM formulation (DSM-ARR) based on carbon steel (Equation 5.7) given by Arrayago et al. ($P_{v,ARR}$) was also plotted for HSS and HSS^a stub columns

(Figures 5.28 and 5.29). It can be observed from Figure 5.28 that this formulation predicted accurate and conservative results for HSS stub columns since most of the data points fit accurately with the modified DSM curve given in Equation 5.7. However, for few stocky sections (i.e. λ_L < 0.3), this formulation is observed to be inapplicable. The value of P_m, COV and β for HSS stub columns are 1.03, 0.05 and 2.93 and hence it is reliable (see Table 5.1). In case of HSS^a stub columns (see Figure 5.29), it can be seen that this formulation also predicted fairly conservative results, but for stocky sections such as λ_L < 0.7, this formulation predicted unconservative results for HSS^a stub columns. It can be seen from Table 5.2 that the value of P_m, COV and β for HSS^a stub columns are 1.02, 0.2 and 2.30 respectively. Therefore, the value of β is found to be less than β_o and hence, it is found to be unreliable.

5.4.7 Proposed Direct strength method

A new DSM equation for HSS and HSS^a stub columns is proposed based on the modified DSM formulation for carbon steel given by Arrayago *et al.*, (2017). The proposed DSM formulation ($P_{v,P}$) for HSS and HSS^a stub columns is given in Equation 5.8 and they predicted accurate results for all data points as shown in Figures 5.28 and 5.29.

$$\frac{P_{v,P}}{P_y} = \begin{cases} 1+(0.46-0.63\lambda_L)\left(\dfrac{\sigma_u}{\sigma_{0.2}}-1\right) & for\ \lambda_L \le 0.776 \\ \dfrac{0.9}{\lambda_L^{0.8}}-\dfrac{0.08}{\lambda_L^{1.6}} & for\ \lambda_L > 0.776 \end{cases} \tag{5.8}$$

Also, the values of $\sigma_{0.2}$ and σ_u in the proposed equation (Equation 5.8) are replaced by their weighted average values which are given in Equations 3.18 and 3.19. In addition, the values of P_m, V_p and β for HSS and HSS^a stub columns are found to be 1.12, 0.07, 3.18; and 1.13, 0.20, 2.60 respectively (see Tables 5.1 and 5.2). The proposed DSM formulation ($P_{v,P}$) for HSS stub columns given in Equation 5.8 is found to be reliable (i.e. β > 2.5).

5.5 CONCLUSION

Numerical investigation on structural behaviour of stainless steel stub columns such as LDSS, HSS, HSS^a and DSS stub columns has been carried out through a parametric study such as: (1) flange-to-web thickness ratio (t_f/t_w) by varying t_f and t_w, (2) Effect of flange width (b_f) using the commercial finite element software, Abaqus. In addition, the FE results were further used to assess the applicability of current design specifications predicted by European code (EN 1993-1-4:2006 + A1, 2015) and Direct strength method (Rossi and Rasmussen, 2012; AISI, 2016b; Arrayago *et al.*, 2017). The conclusions achieved from the numerical investigations are presented below:

1) Increase in flange thickness (t_f) has significant improvement on P_u for HSS stub columns as compared to HSS^a stub columns. Also, increase in web thickness (t_w) is found to provide an enhancement in column capacity for HSS^a compared to HSS stub column.

2) An increase in flange thickness (b_f) has shown more effect on HSS stub columns as compared to HSS^a stub columns. Also, an increase in b_f has more influence for higher flange thickness (t_f) in all stub columns.

3) In general, EN 1993-1-4 Class 3 limit for internal webs in compression is found to be reliable and applicable for LDSS, HSS, HSS^a and DSS stub columns. In addition, for the purpose of efficient and economic designs, the limit ($c_w/t_w\varepsilon$ = 48) is proposed for Class 3 limit.

4) New DSM formulations for HSS and HSS^a stub columns have been proposed based on the full-range modified DSM specification for carbon steel.

Table 5.1: Comparison of FE results with design predictions for HSS stub columns

Section	P_u (kN)	P_{EN} (kN)	P_v (kN)	$P_{v,RR}$ (kN)	$P_{v,ARR}$ (kN)	$P_{v,P}$ (kN)	$\frac{P_u}{P_{EN}}$	$\frac{P_u}{P_v}$	$\frac{P_u}{P_{v,RR}}$	$\frac{P_u}{P_{v,ARR}}$	$\frac{P_u}{P_{v,P}}$
I-200×140×6×6	1573.4	1355.78	1529.11	1313.70	1546.70	1502.52	1.16	1.03	1.20	1.02	1.05
I-200×140×8×6	2063.65	1902.76	2022.74	1707.82	2043.91	2005.51	1.08	1.02	1.21	1.01	1.03
I-200×140×9×5.4	2182.1	1997.56	2089.11	1772.24	2109.66	2063.30	1.09	1.04	1.23	1.03	1.06
I-200×140×10×6	2437.5	2269.57	2406.73	2070.02	2466.51	2434.88	1.07	1.01	1.18	0.99	1.00
I-200×140×10×8	2891.86	2625.60	2604.23	2426.27	2820.95	2583.08	1.10	1.11	1.19	1.03	1.12
I-200×140×11×6.6	2876.25	2549.92	2647.40	2371.54	2789.19	2650.72	1.13	1.09	1.21	1.03	1.09
I-200×140×12×7.2	3065.54	2838.18	2888.08	2677.40	3112.73	2866.25	1.08	1.06	1.14	0.98	1.07
I-200×140×12×8	3361.96	2990.66	2967.13	2833.12	3263.56	2922.28	1.12	1.13	1.19	1.03	1.15
I-200×140×14×8.4	3860.48	3402.56	3369.44	3289.10	3759.49	3297.43	1.13	1.15	1.17	1.03	1.17
I-200×140×16×9.6	4467.47	3888.64	3850.81	3886.34	4405.39	3728.92	1.15	1.16	1.15	1.01	1.20
I-200×140×18×10.8	5040.11	4374.72	4332.18	4526.69	5050.90	4160.55	1.15	1.16	1.11	1.00	1.21
I-200×140×8.4×5	2034.36	1833.18	1855.01	1588.04	1873.23	1821.82	1.11	1.10	1.28	1.09	1.12
I-200×140×8.8×5.3	2122.68	1947.03	2021.92	1719.07	2041.83	1994.26	1.09	1.05	1.23	1.04	1.06
I-200×140×9.2×5.5	2260.89	2048.35	2159.15	1827.19	2180.37	2135.61	1.10	1.05	1.24	1.04	1.06
I-200×140×9.7×5.8	2422.81	2184.00	2332.55	1975.46	2364.80	2369.15	1.11	1.04	1.23	1.02	1.02
I-200×140×10.5×6.3	2712.37	2408.73	2527.06	2220.42	2628.01	2542.75	1.13	1.07	1.22	1.03	1.07
I-200×140×10.9×6.5	2829.43	2514.77	2619.38	2332.75	2748.82	2626.55	1.13	1.08	1.21	1.03	1.08

I-200×140×11.2×6.7	2949.31	2603.50	2693.56	2428.85	2850.29	2692.37	1.13	1.09	1.21	1.03	1.10
I-200×140×11.7×7	3099.09	2747.32	2813.90	2581.40	3011.80	2800.23	1.13	1.10	1.20	1.03	1.11
I-200×140×12.2×7.3	3279.88	2893.04	2934.24	2732.92	3172.20	2908.50	1.13	1.12	1.20	1.03	1.13
I-200×140×12.5×7.5	3369.3	2985.13	3008.42	2831.39	3274.95	2973.86	1.13	1.12	1.19	1.03	1.13
I-200×140×13×7.8	3547.5	3133.89	3128.76	2983.94	3436.12	3081.84	1.13	1.13	1.19	1.03	1.15
I-200×140×13.4×8	3677.64	3246.20	3221.08	3098.54	3557.91	3165.28	1.13	1.14	1.19	1.03	1.16
I-200×140×13.9×8.3	3818.07	3374.22	3341.42	3250.47	3719.15	3273.24	1.13	1.14	1.17	1.03	1.17
I-200×140×14.2×8.5	3926.65	3449.15	3415.60	3345.82	3820.25	3339.20	1.14	1.15	1.17	1.03	1.18
I-200×140×14.7×8.8	4084.12	3570.67	3535.94	3497.11	3982.12	3446.93	1.14	1.16	1.17	1.03	1.18
I-200×140×15×9	4177.85	3645.60	3610.12	3590.21	4082.33	3513.22	1.15	1.16	1.16	1.02	1.19
I-200×140×15.5×9.3	4325.61	3767.12	3730.47	3740.03	4244.74	3620.75	1.15	1.16	1.16	1.02	1.19
I-200×140×15.9×9.5	4437.2	3860.30	3822.79	3850.05	4365.61	3704.52	1.15	1.16	1.15	1.02	1.20
I-200×140×16.2×9.7	4523.71	3935.23	3896.97	3946.13	4466.49	3770.56	1.15	1.16	1.15	1.01	1.20
I-200×140×16.7×10	4655.99	4056.75	4017.31	4105.75	4627.50	3878.61	1.15	1.16	1.13	1.01	1.20
I-200×140×17.2×10.3	4809.08	4178.27	4137.65	4266.12	4788.98	3986.48	1.15	1.16	1.13	1.00	1.21
I-200×140×18.4×11	5146.44	4467.9	4424.5	4646.70	5172.74	4243.97	1.15	1.16	1.11	0.99	1.21
I-200×140×19.2×11.5	5378.11	4664.35	4619.03	4906.58	5434.25	4418.19	1.15	1.16	1.10	0.99	1.22
I-200×140×3x6	879.377	742.84	855.75	758.60	869.18	829.90	1.18	1.03	1.16	1.01	1.06
I-200×140×6×6	1573.4	1355.78	1529.11	1313.70	1546.71	1502.52	1.16	1.03	1.20	1.02	1.05
I-200×140×8×6	2063.65	1902.76	2022.74	1707.82	2043.91	2005.51	1.08	1.02	1.21	1.01	1.03

I-200×140×10×6	2437.5	2269.57	2406.73	2070.02	2466.51	2434.88	1.07	1.01	1.18	0.99	1.00
I-200×140×12×6	2936.47	2633.24	2769.44	2398.66	2850.85	2795.40	1.12	1.06	1.22	1.03	1.05
I-200×140×14×6	3374.46	2997.24	3132.08	2717.33	3226.88	3158.94	1.13	1.08	1.24	1.05	1.07
I-200×140×18×6	4234.49	3725.83	3857.24	3347.15	3972.83	3888.23	1.14	1.10	1.27	1.07	1.09
I-200×140×6×3	1161.19	973.27	915.48	817.91	924.11	874.28	1.19	1.27	1.42	1.26	1.33
I-200×140×6×6	1573.4	1355.78	1529.11	1313.70	1546.71	1502.52	1.16	1.03	1.20	1.02	1.05
I-200×140×6×8.5	1997.82	1779.55	1926.68	1675.25	1994.39	1952.00	1.12	1.04	1.19	1.00	1.02
I-200×140×6×9	2075.56	1832.89	1975.75	1749.00	2072.71	1992.92	1.13	1.05	1.19	1.00	1.04
I-200×140×6×12	2441.38	2152.28	2269.63	2145.56	2501.82	2253.29	1.13	1.08	1.14	0.98	1.08
I-200×140×6×14	2691.77	2364.76	2465.01	2367.55	2753.10	2439.40	1.14	1.09	1.14	0.98	1.10
I-200×140×6×18	3144.16	2789.24	2854.76	2780.63	3230.58	2820.59	1.13	1.10	1.13	0.97	1.11
I-200×200×3×6	925.394	764.03	813.56	731.81	818.80	769.61	1.21	1.14	1.26	1.13	1.20
I-200×200×6×6	1724.32	1431.01	1719.29	1497.75	1727.91	1657.15	1.20	1.00	1.15	1.00	1.04
I-200×200×8×6	2711.05	2059.34	2425.54	2071.42	2436.83	2366.00	1.32	1.12	1.31	1.11	1.15
I-200×200×10×6	3300.66	2802.84	3176.39	2663.89	3190.50	3131.97	1.18	1.04	1.24	1.03	1.05
I-200×200×12×6	3940.28	3569.65	3718.42	3183.85	3790.55	3740.18	1.10	1.06	1.24	1.04	1.05
I-200×200×14×6	4599.59	4090.33	4238.21	3639.66	4328.24	4259.33	1.12	1.09	1.26	1.06	1.08
I-200×200×18×6	5884.07	5132.21	5277.77	4546.14	5399.26	5299.20	1.15	1.11	1.29	1.09	1.11
I-200×250×3×6	991.983	776.70	802.36	727.32	805.38	751.66	1.28	1.24	1.36	1.23	1.32
I-200×250×6×6	1806.1	1468.93	1840.67	1619.69	1846.23	1756.87	1.23	0.98	1.12	0.98	1.03

I-200×250×8×6	2689.58	2134.87	2600.13	2254.42	2607.51	2504.82	1.26	1.03	1.19	1.03	1.07
I-200×250×10×6	3679.04	2939.87	3489.79	2974.61	3499.32	3397.59	1.25	1.05	1.24	1.05	1.08
I-200×250×12×6	4633.42	3860.75	4457.21	3734.36	4469.05	4384.96	1.20	1.04	1.24	1.04	1.06
I-200×250×14×6	5566.07	4873.67	5155.37	4409.15	5246.96	5176.01	1.14	1.08	1.26	1.06	1.08
I-200×250×18×6	7200.26	6304.82	6456.43	5529.19	6575.68	6479.57	1.14	1.12	1.30	1.09	1.11
I-200×200×6×3	1291.43	1039.27	1221.28	1086.23	1226.53	1159.92	1.24	1.06	1.19	1.05	1.11
I-200×200×6×6	1724.32	1431.01	1719.29	1497.75	1727.91	1657.15	1.20	1.00	1.15	1.00	1.04
I-200×200×6×8.5	2212.94	1863.52	2101.45	1807.46	2113.23	2043.92	1.19	1.05	1.22	1.05	1.08
I-200×200×6×12	2679.27	2241.51	2597.29	2205.99	2613.98	2549.37	1.20	1.03	1.21	1.02	1.05
I-200×200×6×14	2887.58	2456.03	2830.85	2397.79	2850.35	2785.34	1.18	1.02	1.20	1.01	1.04
I-200×200×6×18	3344.32	2883.02	3284.91	2772.09	3310.49	3244.07	1.16	1.02	1.21	1.01	1.03
I-200×250×6×3	1410.15	1071.09	1443.68	1284.82	1447.52	1366.86	1.32	0.98	1.10	0.97	1.03
I-200×250×6×6	1806.1	1468.93	1840.67	1619.69	1846.23	1756.87	1.23	0.98	1.12	0.98	1.03
I-200×250×6×8.5	2219.01	1907.56	2165.47	1890.72	2172.68	2078.42	1.16	1.02	1.17	1.02	1.07
I-200×250×6×12	2754.71	2290.20	2594.80	2247.54	2604.53	2505.01	1.20	1.06	1.23	1.06	1.10
I-200×250×6×14	3011.72	2506.80	2814.41	2431.39	2825.64	2722.60	1.20	1.07	1.24	1.07	1.11
I-200×250×6×18	3465.01	2936.89	3228.43	2779.99	3242.84	3131.96	1.18	1.07	1.25	1.07	1.11
I-200×140×3×3	493.41	366.86	477.97	433.33	483.47	453.56	1.34	1.03	1.14	1.02	1.09
I-200×140×4×4	757.924	636.02	779.99	694.75	788.97	748.94	1.19	0.97	1.09	0.96	1.01
I-200×140×2.5×2.5	379.034	257.87	349.78	319.88	353.81	329.95	1.47	1.08	1.18	1.07	1.15

I-200×140×2.7×2.7	424.906	299.34	398.96	363.60	403.55	377.23	1.42	1.07	1.17	1.05	1.13
I-200×140×2.2×2.2	310.944	201.13	281.53	258.77	284.77	264.64	1.55	1.10	1.20	1.09	1.17
I-200×140×2.3×2.3	334.652	219.31	304.46	279.34	307.97	286.56	1.53	1.10	1.20	1.09	1.17
I-200×140×2.4×2.4	354.928	238.22	325.58	298.30	329.33	306.73	1.49	1.09	1.19	1.08	1.16
I-200×140×20×20	6553.45	5667.20	5603.55	6433.12	6922.51	5257.88	1.16	1.17	1.02	0.95	1.25
I-200×140×25×25	8145.15	7084.00	7005.08	8298.82	8810.52	6515.72	1.15	1.16	0.98	0.92	1.25
I-200×140×30×30	9682.96	8500.80	8407.00	10113.17	10667.13	7784.86	1.14	1.15	0.96	0.91	1.24
I-200×140×50×50	16351.5	14168.00	14019.98	17185.00	17980.13	12902.24	1.15	1.17	0.95	0.91	1.27
I-200×140×80×80	26433.3	22668.80	22459.14	27812.23	28961.54	20574.02	1.17	1.18	0.95	0.91	1.28
No. of observations							**86**	**86**	**86**	**86**	**86**
Mean (P_m)							**1.18**	**1.09**	**1.18**	**1.03**	**1.12**
COV (V_p)							**0.08**	**0.06**	**0.07**	**0.05**	**0.07**
Resistance factor (φ)							**0.91**	**0.85**	**0.85**	**0.85**	**0.85**
Reliability index (β)							**2.92**	**3.14**	**3.34**	**2.93**	**3.18**

Table 5.2: Comparison of FE results with design predictions for HSS[a] stub columns

Section	P_u (kN)	P_{EN} (kN)	P_v (kN)	$P_{v,RR}$ (kN)	$P_{v,ARR}$ (kN)	$P_{v,P}$ (kN)	$\frac{P_u}{P_{EN}}$	$\frac{P_u}{P_v}$	$\frac{P_u}{P_{v,RR}}$	$\frac{P_u}{P_{v,ARR}}$	$\frac{P_u}{P_{v,P}}$
I-200×140×6×6	1541.77	1318.03	1481.36	1629.75	1497.80	1456.67	1.17	1.04	0.95	1.03	1.06
I-200×140×8×6	1892.07	1714.42	1892.88	1604.02	1920.91	1923.18	1.10	1.00	1.18	0.98	0.98
I-200×140×9×5.4	1944.12	1761.94	1936.63	1632.67	1954.01	1917.33	1.10	1.00	1.19	0.99	1.01
I-200×140×10×6	2224.96	1999.22	2174.09	1910.09	2270.40	2184.38	1.11	1.02	1.16	0.98	1.02
I-200×140×10×8	2628.73	2367.87	2430.05	2285.26	2668.24	2398.50	1.11	1.08	1.15	0.99	1.10
I-200×140×11×6.6	2534.19	2243.62	2391.50	2179.13	2568.26	2378.04	1.13	1.06	1.16	0.99	1.07
I-200×140×12×7.2	2814.76	2494.81	2608.91	2456.36	2871.89	2569.67	1.13	1.08	1.15	0.98	1.10
I-200×140×12×8	2964.68	2651.06	2711.37	2618.90	3041.20	2651.71	1.12	1.09	1.13	0.97	1.12
I-200×140×14×8.4	3391.61	3016.27	3043.74	2999.87	3471.82	2955.52	1.12	1.11	1.13	0.98	1.15
I-200×140×16×9.6	3965.34	3509.76	3478.58	3565.78	4083.86	3337.13	1.13	1.14	1.11	0.97	1.19
I-200×140×18×10.8	4507.94	3948.48	3913.42	4168.09	4690.07	3720.77	1.14	1.15	1.08	0.96	1.21
I-200×140×8.4×5	1850.3	1617.37	1723.69	1466.38	1739.12	1697.05	1.14	1.07	1.26	1.06	1.09
I-200×140×8.8×5.3	1892.77	1718.36	1874.96	1584.46	1891.81	1853.62	1.10	1.01	1.19	1.00	1.02
I-200×140×9.2×5.5	2012.99	1805.73	1997.60	1682.44	2016.98	2031.20	1.11	1.01	1.20	1.00	0.99
I-200×140×9.7×5.8	2137.58	1924.07	2106.30	1817.92	2169.09	2126.93	1.11	1.01	1.18	0.99	1.01
I-200×140×10×6	2224.94	1999.22	2174.09	1910.09	2270.40	2184.38	1.11	1.02	1.16	0.98	1.02
I-200×140×10.5×6.3	2377.37	2120.55	2282.79	2034.00	2409.99	2284.47	1.12	1.04	1.17	0.99	1.04

I-200×140×10.9×6.5	2491.57	2211.88	2364.63	2142.81	2528.87	2354.96	1.13	1.05	1.16	0.99	1.06
I-200×140×11.2×6.7	2578.9	2289.76	2432.42	2229.45	2623.86	2414.62	1.13	1.06	1.16	0.98	1.07
I-200×140×11.7×7	2722.51	2415.08	2541.13	2368.92	2776.44	2510.18	1.13	1.07	1.15	0.98	1.08
I-200×140×12.2×7.3	2830.74	2542.04	2649.83	2507.05	2927.74	2606.18	1.11	1.07	1.13	0.97	1.09
I-200×140×12.5×7.5	2954.16	2622.85	2717.62	2591.71	3020.79	2666.51	1.13	1.09	1.14	0.98	1.11
I-200×140×13×7.8	3102.53	2752.47	2826.33	2732.13	3174.53	2761.66	1.13	1.10	1.14	0.98	1.12
I-200×140×13.4×8	3214.27	2849.17	2908.17	2834.09	3287.35	2834.27	1.13	1.11	1.13	0.98	1.13
I-200×140×13.9×8.3	3348.99	2981.31	3016.88	2970.54	3438.62	2930.29	1.12	1.11	1.13	0.97	1.14
I-200×140×14.2×8.5	3445.76	3065.52	3084.66	3056.54	3534.23	2989.73	1.12	1.12	1.13	0.97	1.15
I-200×140×14.7×8.8	3592.84	3200.09	3193.37	3190.56	3684.87	3085.96	1.12	1.13	1.13	0.98	1.16
I-200×140×15×9	3668.22	3285.89	3261.16	3274.33	3779.62	3145.70	1.12	1.12	1.12	0.97	1.17
I-200×140×15.5×9.3	3795.75	3400.08	3369.87	3410.26	3929.28	3242.27	1.12	1.13	1.11	0.97	1.17
I-200×140×15.9×9.5	3928.43	3482.61	3451.71	3520.82	4041.82	3314.99	1.13	1.14	1.12	0.97	1.19
I-200×140×16.2×9.7	4015.44	3551.02	3519.50	3619.88	4139.40	3373.74	1.13	1.14	1.11	0.97	1.19
I-200×140×16.7×10	4156.82	3660.70	3628.21	3770.41	4290.93	3469.66	1.14	1.15	1.10	0.97	1.20
I-200×140×17.2×10.3	4273.7	3770.38	3736.92	3915.46	4439.10	3566.75	1.13	1.14	1.09	0.96	1.20
I-200×140×17.5×10.5	4367.6	3838.80	3804.71	4016.18	4537.70	3625.15	1.14	1.15	1.09	0.96	1.20
I-200×140×17.9×10.7	4472.6	3921.33	3886.55	4125.49	4649.47	3698.13	1.14	1.15	1.08	0.96	1.21
I-200×140×18.4×11	4612.61	4031.01	3995.26	4269.45	4796.98	3795.46	1.14	1.15	1.08	0.96	1.22
I-200×140×18.7×11.2	4696.67	4099.42	4063.05	4369.16	4894.96	3854.07	1.15	1.16	1.07	0.96	1.22

I-200×140×20×12	5040.23	4387.20	4348.27	4786.53	5306.15	4100.96	1.15	1.16	1.05	0.95	1.23
I-200×140×3×6	942.957	748.35	883.55	784.91	897.99	856.58	1.26	1.07	1.20	1.05	1.10
I-200×140×6×6	1541.77	1318.03	1481.36	1269.75	1497.77	1456.67	1.17	1.04	1.21	1.03	1.06
I-200×140×8×6	1892.07	1714.42	1892.88	1604.02	1920.91	1923.18	1.10	1.00	1.18	0.98	0.98
I-200×140×10×6	2224.96	1999.22	2174.09	1910.09	2270.40	2184.38	1.11	1.02	1.16	0.98	1.02
I-200×140×12×6	2557.47	2283.40	2455.10	2173.27	2579.97	2459.66	1.12	1.04	1.18	0.99	1.04
I-200×140×14×6	2850.19	2567.15	2735.99	2434.20	2887.68	2735.63	1.11	1.04	1.17	0.99	1.04
I-200×140×18×6	3448.78	3133.83	3297.59	2948.16	3496.07	3290.05	1.10	1.05	1.17	0.99	1.05
I-200×140×6×3	1028.37	914.40	362.01	337.64	365.07	335.07	1.12	2.84	3.05	2.82	3.07
I-200×140×6×6	1541.77	1318.03	1481.36	1269.75	1497.77	1456.67	1.17	1.04	1.21	1.03	1.06
I-200×140×6×8.5	1994.94	1804.57	1929.56	1680.97	2000.11	1953.97	1.11	1.03	1.19	1.00	1.02
I-200×140×6×9	2104.89	1916.40	1993.07	1764.96	2090.60	2010.54	1.10	1.06	1.19	1.01	1.05
I-200×140×6×12	2605.28	2325.62	2373.05	2230.85	2593.83	2363.89	1.12	1.10	1.17	1.00	1.10
I-200×140×6×14	2932.1	2595.99	2625.45	2504.52	2897.24	2610.83	1.13	1.12	1.17	1.01	1.12
I-200×140×6×18	3564.23	3138.13	3128.38	3010.96	3471.07	3116.56	1.14	1.14	1.18	1.03	1.14
I-200×200×3×6	975.303	737.32	813.56	731.81	818.80	769.61	1.32	1.20	1.33	1.19	1.27
I-200×200×6×6	1653.83	1345.20	1619.59	1405.53	1627.12	1563.93	1.23	1.02	1.18	1.02	1.06
I-200×200×8×6	2336.13	1907.73	2239.08	1898.85	2248.48	2191.97	1.22	1.04	1.23	1.04	1.07
I-200×200×10×6	2834.58	2556.54	2787.45	2388.90	2852.93	2802.39	1.11	1.02	1.19	0.99	1.01
I-200×200×12×6	3315.08	3012.47	3189.65	2813.30	3342.28	3179.35	1.10	1.04	1.18	0.99	1.04

I-200×200×14×6	3767.28	3416.90	3591.80	3184.23	3780.52	3574.10	1.10	1.05	1.18	1.00	1.05
I-200×200×18×6	4605.63	4225.07	4396.05	3916.15	4647.86	4366.79	1.09	1.05	1.18	0.99	1.05
I-200×250×3×6	1041.33	729.23	787.12	713.02	790.00	737.60	1.43	1.32	1.46	1.32	1.41
I-200×250×6×6	1746.72	1352.73	1705.65	1494.79	1710.33	1631.57	1.29	1.02	1.17	1.02	1.07
I-200×250×8×6	2537.83	1947.20	2547.17	2167.71	2553.57	2481.43	1.30	1.00	1.17	0.99	1.02
I-200×250×10×6	3265.65	2652.96	3123.86	2639.32	3131.27	3056.17	1.23	1.05	1.24	1.04	1.07
I-200×250×12×6	3956.64	3444.89	3797.73	3262.80	3895.72	3807.32	1.15	1.04	1.21	1.02	1.04
I-200×250×14×6	4472.33	4124.09	4300.87	3812.62	4527.85	4271.70	1.08	1.04	1.17	0.99	1.05
I-200×250×18×6	5583.67	5133.59	5307.10	4723.70	5608.57	5263.78	1.09	1.05	1.18	1.00	1.06
I-200×200×6×3	1175.88	954.67	1098.66	972.12	1102.77	1046.09	1.23	1.07	1.21	1.07	1.12
I-200×200×6×6	1653.83	1345.20	1619.59	1405.53	1627.12	1563.93	1.23	1.02	1.18	1.02	1.06
I-200×200×6×8.5	2150.82	1818.97	2044.66	1753.62	2055.68	1991.54	1.18	1.05	1.23	1.05	1.08
I-200×200×6×12	2703.38	2327.75	2604.44	2210.90	2621.18	2557.22	1.16	1.04	1.22	1.03	1.06
I-200×200×6×14	2999.69	2592.54	2882.27	2442.41	2902.47	2835.74	1.16	1.04	1.23	1.03	1.06
I-200×200×6×18	3576.39	3124.72	3411.82	2887.93	3439.64	3365.15	1.14	1.05	1.24	1.04	1.06
I-200×250×6×3	1236.1	971.22	1260.51	1117.76	1263.38	1195.56	1.27	0.98	1.11	0.98	1.03
I-200×250×6×6	1746.72	1352.73	1705.65	1494.79	1710.33	1631.57	1.29	1.02	1.17	1.02	1.07
I-200×250×6×8.5	2197.03	1817.56	2061.00	1794.27	2067.44	1981.20	1.21	1.07	1.22	1.06	1.11
I-200×250×6×12	2795.39	2316.87	2548.95	2204.29	2558.26	2462.87	1.21	1.10	1.27	1.09	1.14
I-200×250×6×14	3118.47	2577.14	2802.67	2419.51	2813.77	2712.34	1.21	1.11	1.29	1.11	1.15

I-200×250×6×18	3720.03	3101.06	3281.85	2829.20	3296.79	3181.97	1.20	1.13	1.31	1.13	1.17
I-200×140×3×3	467.826	359.82	467.51	423.03	472.69	443.90	1.35	1.00	1.11	0.99	1.05
I-200×140×4×4	729.22	622.17	760.26	675.72	768.69	730.53	1.21	0.96	1.08	0.95	1.00
I-200×140×2.5×2.5	353.897	253.24	339.92	310.48	343.69	320.70	1.45	1.04	1.14	1.03	1.10
I-200×140×2.7×2.7	397.595	293.81	389.63	354.51	393.95	368.56	1.40	1.02	1.12	1.01	1.08
I-200×140×2.2×2.2	280.758	197.65	273.63	251.22	276.67	257.24	1.47	1.03	1.12	1.01	1.09
I-200×140×2.3×2.3	304.061	215.47	295.57	270.87	298.84	278.21	1.46	1.03	1.12	1.02	1.09
I-200×140×2.4×2.4	332.26	234.00	316.42	289.55	319.93	298.14	1.47	1.05	1.15	1.04	1.11
I-200×140×20×20	6275.71	5430.40	5371.67	6225.37	6716.84	5017.27	1.20	1.17	1.01	0.93	1.25
I-200×140×25×25	7678.97	6788.00	6715.18	8039.59	8553.70	6215.76	1.17	1.14	0.96	0.90	1.24
I-200×140×30×30	9240.19	8145.60	8059.06	9799.31	10357.26	7426.05	1.17	1.15	0.94	0.89	1.24
I-200×140×50×50	15609	13576.00	13439.43	16663.99	17464.95	12304.92	1.19	1.16	0.94	0.89	1.27
I-200×140×80×80	25401.3	21721.60	21528.16	26991.70	28145.26	19616.58	1.21	1.18	0.94	0.90	1.29
No. of observations							**90**	**90**	**90**	**90**	**90**
Mean (P_m)							**1.17**	**1.10**	**1.18**	**1.02**	**1.13**
COV (V_p)							**0.08**	**0.18**	**0.18**	**0.20**	**0.20**
Resistance factor (φ)							**0.91**	**0.85**	**0.85**	**0.85**	**0.85**
Reliability index (β)							**2.92**	**2.61**	**2.84**	**2.30**	**2.60**

Table 5.3: Comparison of FE results with design predictions for LDSS stub columns

Section	P_u (kN)	P_{EN} (kN)	P_v (kN)	$P_{v,RR}$ (kN)	$P_{v,ARR}$ (kN)	$P_{v,P}$ (kN)	$\frac{P_u}{P_{EN}}$	$\frac{P_u}{P_v}$	$\frac{P_u}{P_{v,RR}}$	$\frac{P_u}{P_{v,ARR}}$	$\frac{P_u}{P_{v,P}}$
I-200×140×6×6	1445.07	1174.34	1367.28	1163.21	1380.93	1348.34	1.23	1.06	1.24	1.05	1.07
I-200×140×8×6	1771.17	1555.12	1718.40	1486.21	1777.19	1734.18	1.14	1.03	1.19	1.00	1.02
I-200×140×9×5.4	1834.83	1619.29	1799.43	1529.37	1832.05	1824.24	1.13	1.02	1.20	1.00	1.01
I-200×140×10×6	2066.45	1837.36	1999.37	1781.09	2121.45	1997.89	1.12	1.03	1.16	0.97	1.03
I-200×140×10×8	2373.42	2139.42	2197.51	2130.37	2504.71	2139.79	1.11	1.08	1.11	0.95	1.11
I-200×140×11×6.6	2337.04	2061.97	2199.31	2035.32	2410.01	2171.83	1.13	1.06	1.15	0.97	1.08
I-200×140×12×7.2	2592.76	2292.82	2399.25	2289.09	2697.28	2346.20	1.13	1.08	1.13	0.96	1.11
I-200×140×12×8	2716.19	2421.66	2478.55	2423.69	2846.26	2404.42	1.12	1.10	1.12	0.95	1.13
I-200×140×14×8.4	3110.84	2822.40	2799.14	2791.51	3272.83	2694.60	1.10	1.11	1.11	0.95	1.15
I-200×140×16×9.6	3641.54	3225.60	3199.03	3333.97	3847.74	3043.22	1.13	1.14	1.09	0.95	1.20
I-200×140×18×10.8	4033.55	3628.80	3598.92	3854.61	4392.23	3402.13	1.11	1.12	1.05	0.92	1.19
I-200×140×8.4×5	1684.43	1487.10	1623.80	1374.06	1637.27	1602.25	1.13	1.04	1.23	1.03	1.05
I-200×140×8.8×5.3	1790.44	1578.90	1761.43	1484.38	1779.52	1790.42	1.13	1.02	1.21	1.01	1.00
I-200×140×9.2×5.5	1875.39	1659.87	1837.44	1575.76	1885.91	1857.62	1.13	1.02	1.19	0.99	1.01
I-200×140×9.7×5.8	1975.83	1768.63	1937.41	1701.18	2030.29	1944.55	1.12	1.02	1.16	0.97	1.02
I-200×140×10×6	2066.53	1837.36	1999.37	1784.74	2125.17	1996.64	1.12	1.03	1.16	0.97	1.04
I-200×140×10.5×6.3	2193.03	1948.87	2099.34	1907.60	2265.37	2084.98	1.13	1.04	1.15	0.97	1.05

I-200×140×10.9×6.5	2299.97	2033.50	2175.35	2001.46	2372.13	2152.06	1.13	1.06	1.15	0.97	1.07
I-200×140×11.2×6.7	2385.84	2104.73	2237.32	2080.95	2462.01	2205.83	1.13	1.07	1.15	0.97	1.08
I-200×140×11.7×7	2517.99	2219.90	2337.29	2209.16	2606.92	2292.59	1.13	1.08	1.14	0.97	1.10
I-200×140×12.2×7.3	2641.13	2336.59	2437.26	2335.94	2750.58	2379.77	1.13	1.08	1.13	0.96	1.11
I-200×140×12.5×7.5	2732.91	2410.50	2499.22	2415.73	2841.05	2433.34	1.13	1.09	1.13	0.96	1.12
I-200×140×13×7.8	2854.43	2529.62	2599.20	2540.86	2983.88	2520.80	1.13	1.10	1.12	0.96	1.13
I-200×140×13.4×8	2960.43	2619.23	2675.21	2635.41	3092.38	2587.29	1.13	1.11	1.12	0.96	1.14
I-200×140×13.9×8.3	3067.12	2798.21	2775.18	2759.77	3236.02	2674.47	1.10	1.11	1.11	0.95	1.15
I-200×140×14.2×8.5	3167.27	2860.70	2837.14	2837.56	3326.55	2728.02	1.11	1.12	1.12	0.95	1.16
I-200×140×14.7×8.8	3302.66	2961.50	2937.12	2957.23	3467.11	2816.25	1.12	1.12	1.12	0.95	1.17
I-200×140×15×9	3391.57	3024.00	2999.08	3049.02	3560.45	2868.86	1.12	1.13	1.11	0.95	1.18
I-200×140×15.5×9.3	3483.87	3124.80	3099.06	3191.54	3704.12	2956.03	1.11	1.12	1.09	0.94	1.18
I-200×140×15.9×9.5	3604.51	3201.41	3175.07	3297.74	3812.02	3022.72	1.13	1.14	1.09	0.95	1.19
I-200×140×16.2×9.7	3687.41	3263.90	3237.03	3382.16	3898.69	3077.58	1.13	1.14	1.09	0.95	1.20
I-200×140×16.7×10	3823.62	3364.70	3337.01	3530.12	4045.70	3163.63	1.14	1.15	1.08	0.95	1.21
I-200×140×17.2×10.3	3945.68	3465.50	3436.98	3672.15	4189.08	3250.90	1.14	1.15	1.07	0.94	1.21
I-200×140×17.5×10.5	4017.52	3528.00	3498.95	3762.39	4279.31	3304.56	1.14	1.15	1.07	0.94	1.22
I-200×140×17.9×10.7	4108.99	3604.61	3574.96	3868.08	4386.90	3371.35	1.14	1.15	1.06	0.94	1.22
I-200×140×18.4×11	4229.79	3705.41	3674.94	4010.57	4530.55	3458.53	1.14	1.15	1.05	0.93	1.22
I-200×140×18.7×11.2	4302.92	3767.90	3736.90	4099.64	4620.07	3512.43	1.14	1.15	1.05	0.93	1.23

I-200×140×19.2×11.5	4418.51	3868.70	3836.88	4242.32	4763.85	3599.57	1.14	1.15	1.04	0.93	1.23
I-200×140×20×12	4614.27	4032.00	3998.82	4473.61	4996.85	3740.70	1.14	1.15	1.03	0.92	1.23
I-200×140×20.9×12.5	4818.76	4209.41	4174.81	4721.99	5248.23	3894.63	1.14	1.15	1.02	0.92	1.24
I-200×140×3×3	435.774	320.60	432.51	389.81	436.83	411.02	1.36	1.01	1.12	1.00	1.06
I-200×140×4×4	685.908	554.34	699.90	619.24	706.89	673.32	1.24	0.98	1.11	0.97	1.02
I-200×140×2.5×2.5	329.921	225.63	314.69	286.43	317.84	297.06	1.46	1.05	1.15	1.04	1.11
I-200×140×2.7×2.7	373.2	261.78	358.81	325.39	362.40	339.56	1.43	1.04	1.15	1.03	1.10
I-200×140×2.2×2.2	274.797	176.10	253.42	231.92	255.95	238.32	1.56	1.08	1.18	1.07	1.15
I-200×140×2.3×2.3	293.865	191.98	273.70	250.01	276.43	257.73	1.53	1.07	1.18	1.06	1.14
I-200×140×2.4×2.4	313.807	208.49	292.97	267.19	295.90	276.18	1.51	1.07	1.17	1.06	1.14
I-200×140×20×20	5558.44	4838.40	4791.20	5735.63	6220.78	4412.87	1.15	1.16	0.97	0.89	1.26
I-200×140×25×25	6806.94	6048.00	5989.47	7426.38	7933.00	5462.95	1.13	1.14	0.92	0.86	1.25
I-200×140×30×30	8204.81	7257.60	7188.04	9061.39	9611.15	6524.57	1.13	1.14	0.91	0.85	1.26
I-200×140×50×50	13812.4	12096.00	11986.24	15428.10	16217.75	10806.90	1.14	1.15	0.90	0.85	1.28
I-200×140×80×80	22376.6	19353.60	19198.14	25006.89	26145.22	17224.44	1.16	1.17	0.89	0.86	1.30
I-200×140×5×5	1092.66	841.16	1014.59	880.49	1024.72	988.24	1.30	1.08	1.24	1.07	1.11
I-200×140×5.5×5.5	1292.87	1002.39	1186.28	1019.43	1198.12	1162.60	1.29	1.09	1.27	1.08	1.11
I-200×140×5.8×5.8	1255.83	1104.33	1294.99	1106.01	1307.92	1274.01	1.14	0.97	1.14	0.96	0.99
I-200×140×4.8×4.8	1002.27	779.87	949.07	826.78	958.55	922.20	1.29	1.06	1.21	1.05	1.09
I-200×140×4.5×4.5	875.511	691.53	853.02	747.40	861.54	825.81	1.27	1.03	1.17	1.02	1.06

I-200×140×4.2×4.2	759.686	607.67	760.70	670.33	768.30	733.72	1.25	1.00	1.13	0.99	1.04
I-200×140×3.8×3.8	624.796	503.14	642.28	570.41	648.69	616.36	1.24	0.97	1.10	0.96	1.01
I-200×140×3.5×3.5	549.325	430.43	561.13	501.01	566.73	536.59	1.28	0.98	1.10	0.97	1.02
I-200×140×3.2×3.2	479.095	362.79	481.70	432.57	486.51	458.87	1.32	0.99	1.11	0.98	1.04
No. of observations							**61**	**61**	**61**	**61**	**61**
Mean (P_m)							**1.19**	**1.08**	**1.11**	**0.97**	**1.13**
COV (V_p)							**0.09**	**0.05**	**0.07**	**0.05**	**0.07**
Resistance factor (φ)							**0.91**	**0.85**	**0.85**	**0.85**	**0.85**
Reliability index (β)							**2.95**	**3.13**	**3.18**	**2.68**	**3.21**

Table 5.4: Comparison of FE results with design predictions for DSS stub columns

Section	P_u (kN)	P_{EN} (kN)	P_v (kN)	$P_{v,RR}$ (kN)	$P_{v,ARR}$ (kN)	$P_{v,P}$ (kN)	$\frac{P_u}{P_{EN}}$	$\frac{P_u}{P_v}$	$\frac{P_u}{P_{v,RR}}$	$\frac{P_u}{P_{v,ARR}}$	$\frac{P_u}{P_{v,P}}$
I-200×140×6×6	1652.71	1438.90	1640.40	1417.55	1661.03	1608.77	1.15	1.01	1.17	0.99	1.03
I-200×140×8×6	2273.29	2007.87	2143.63	1820.27	2167.77	2120.68	1.13	1.06	1.25	1.05	1.07
I-200×140×9×5.4	2306.38	2094.80	2194.50	1870.40	2217.48	2163.36	1.10	1.05	1.23	1.04	1.07
I-200×140×10×6	2697.03	2376.90	2580.97	2187.59	2617.58	2621.93	1.13	1.04	1.23	1.03	1.03
I-200×140×10×8	3128.95	2767.66	2836.15	2603.23	3022.01	2830.93	1.13	1.10	1.20	1.04	1.11
I-200×140×11×6.6	3050.72	2667.47	2839.08	2510.89	2956.71	2855.28	1.14	1.07	1.21	1.03	1.07
I-200×140×12×7.2	3416.42	2966.11	3097.18	2836.72	3294.53	3089.11	1.15	1.10	1.20	1.04	1.11
I-200×140×12×8	3586.54	3132.78	3199.32	3018.65	3464.93	3169.49	1.14	1.12	1.19	1.04	1.13
I-200×140×14×8.4	4090.84	3586.08	3613.39	3523.24	3992.63	3548.40	1.14	1.13	1.16	1.02	1.15
I-200×140×16×9.6	4782.22	4172.80	4129.61	4139.31	4647.76	4023.71	1.15	1.16	1.16	1.03	1.19
I-200×140×18×10.8	5437.98	4694.40	4645.84	4800.13	5324.26	4491.06	1.16	1.17	1.13	1.02	1.21
I-200×140×8.4×5	2096.42	1923.78	1949.73	1675.98	1970.10	1911.92	1.09	1.08	1.25	1.06	1.10
I-200×140×8.8×5.3	2232.84	2042.54	2123.92	1814.16	2146.19	2091.04	1.09	1.05	1.23	1.04	1.07
I-200×140×9.2×5.5	2376.55	2147.30	2268.10	1928.57	2291.83	2239.12	1.11	1.05	1.23	1.04	1.06
I-200×140×9.7×5.8	2573.34	2287.99	2470.16	2086.46	2496.00	2448.48	1.12	1.04	1.23	1.03	1.05
I-200×140×10×6	2697.03	2376.90	2580.97	2187.59	2617.58	2621.93	1.13	1.04	1.23	1.03	1.03
I-200×140×10.5×6.3	2845.00	2521.16	2710.03	2348.03	2786.79	2738.74	1.13	1.05	1.21	1.02	1.04

I-200×140×10.9×6.5	2995.33	2630.64	2808.16	2468.77	2913.81	2828.09	1.14	1.07	1.21	1.03	1.06
I-200×140×11.2×6.7	3129.95	2722.78	2888.14	2570.34	3019.32	2900.29	1.15	1.08	1.22	1.04	1.08
I-200×140×11.7×7	3322.61	2871.78	3017.20	2733.53	3188.49	3017.11	1.16	1.10	1.22	1.04	1.10
I-200×140×12.2×7.3	3491.52	3022.73	3146.25	2897.04	3357.42	3134.02	1.16	1.11	1.21	1.04	1.11
I-200×140×12.5×7.5	3554.53	3118.34	3226.23	3000.66	3463.58	3205.97	1.14	1.10	1.18	1.03	1.11
I-200×140×13×7.8	3776.71	3272.45	3355.29	3165.63	3633.23	3322.61	1.15	1.13	1.19	1.04	1.14
I-200×140×13.4×8	3912.98	3388.37	3453.42	3286.95	3759.38	3412.30	1.15	1.13	1.19	1.04	1.15
I-200×140×13.9×8.3	4099.44	3545.49	3582.47	3451.52	3928.99	3528.95	1.16	1.14	1.19	1.04	1.16
I-200×140×14.2×8.5	4213.99	3645.12	3662.46	3553.81	4034.52	3601.14	1.16	1.15	1.19	1.04	1.17
I-200×140×14.7×8.8	4361.45	3805.12	3791.51	3717.20	4204.06	3717.82	1.15	1.15	1.17	1.04	1.17
I-200×140×15×9	4478.72	3906.63	3871.50	3818.29	4309.38	3790.09	1.15	1.16	1.17	1.04	1.18
I-200×140×15.5×9.3	4652.93	4042.40	4000.56	3979.17	4478.33	3906.99	1.15	1.16	1.17	1.04	1.19
I-200×140×15.9×9.5	4724.58	4141.50	4098.69	4098.91	4605.42	3996.32	1.14	1.15	1.15	1.03	1.18
I-200×140×16.2×9.7	4857.40	4222.35	4178.68	4198.22	4710.88	4068.54	1.15	1.16	1.16	1.03	1.19
I-200×140×16.7×10	5019.95	4352.75	4307.74	4358.03	4880.06	4185.35	1.15	1.17	1.15	1.03	1.20
I-200×140×17.2×10.3	5175.45	4483.15	4436.79	4526.08	5049.18	4302.19	1.15	1.17	1.14	1.03	1.20
I-200×140×17.5×10.5	5280.00	4564.00	4516.78	4630.51	5154.18	4374.58	1.16	1.17	1.14	1.02	1.21
I-200×140×17.9×10.7	5397.82	4663.10	4614.92	4756.10	5281.41	4463.86	1.16	1.17	1.13	1.02	1.21
I-200×140×18.4×11	5554.02	4793.50	4743.98	4923.85	5450.34	4580.77	1.16	1.17	1.13	1.02	1.21
I-200×140×18.7×11.2	5645.22	4874.35	4823.97	5028.59	5555.54	4653.08	1.16	1.17	1.12	1.02	1.21

I-200×140×19.2×11.5	5802.33	5004.75	4953.03	5195.91	5724.21	4770.09	1.16	1.17	1.12	1.01	1.22
I-200×140×20×12	6048.45	5216.00	5162.08	5468.76	5998.55	4959.23	1.16	1.17	1.11	1.01	1.22
I-200×140×20.9×12.5	6307.23	5445.50	5389.28	5761.57	6294.39	5165.54	1.16	1.17	1.09	1.00	1.22
I-200×140×21.7×13	6575.79	5656.75	5598.33	6033.74	6568.32	5354.83	1.16	1.17	1.09	1.00	1.23
I-200×140×22.5×13.5	6829.10	5868.00	5807.39	6304.70	6841.51	5544.40	1.16	1.18	1.08	1.00	1.23
I-200×140×23.4×14	7034.52	6097.50	6034.59	6596.70	7136.85	5750.90	1.15	1.17	1.07	0.99	1.22
I-200×140×3×3	534.80	388.48	511.18	464.97	517.61	484.84	1.38	1.05	1.15	1.03	1.10
I-200×140×4×4	818.21	673.99	835.04	746.84	845.55	801.05	1.21	0.98	1.10	0.97	1.02
I-200×140×2.5×2.5	405.54	272.97	373.89	342.93	378.59	352.61	1.49	1.08	1.18	1.07	1.15
I-200×140×2.7×2.7	452.83	316.91	428.70	391.78	434.09	405.31	1.43	1.06	1.16	1.04	1.12
I-200×140×2.2×2.2	332.03	212.86	300.84	277.28	304.63	282.76	1.56	1.10	1.20	1.09	1.17
I-200×140×2.3×2.3	355.74	232.11	325.01	299.04	329.10	305.84	1.53	1.09	1.19	1.08	1.16
I-200×140×2.4×2.4	381.40	252.15	347.98	319.73	352.36	327.78	1.51	1.10	1.19	1.08	1.16
I-200×140×20×20	7283.91	6259.20	6182.50	6936.92	7427.17	5865.72	1.16	1.18	1.05	0.98	1.24
I-200×140×25×25	9207.82	7824.00	7728.89	8928.31	9441.18	7273.53	1.18	1.19	1.03	0.98	1.27
I-200×140×30×30	10830.00	9388.80	9275.77	10865.75	11422.20	8693.64	1.15	1.17	1.00	0.95	1.25
I-200×140×50×50	18202.0	15648.00	15469.62	18440.46	19239.30	14413.98	1.16	1.18	0.99	0.95	1.26
I-200×140×80×80	29289.80	25036.80	24784.12	29827.75	30980.36	22988.73	1.17	1.18	0.98	0.95	1.27
I-200×140×5×5	1205.95	1026.50	1213.86	1067.34	1229.13	1177.42	1.17	0.99	1.13	0.98	1.02
I-200×140×5.5×5.5	1474.45	1225.67	1421.24	1238.99	1439.11	1386.16	1.20	1.04	1.19	1.02	1.06

I-200×140×5.8×5.8	1625.18	1351.98	1537.08	1334.89	1556.41	1502.74	1.20	1.06	1.22	1.04	1.08
I-200×140×4.8×4.8	1116.51	950.97	1134.86	1001.21	1149.14	1098.43	1.17	0.98	1.12	0.97	1.02
I-200×140×4.5×4.5	989.34	842.31	1019.17	903.71	1031.99	983.20	1.17	0.97	1.09	0.96	1.01
I-200×140×4.2×4.2	881.70	739.36	908.11	809.31	919.54	873.18	1.19	0.97	1.09	0.96	1.01
I-200×140×3.8×3.8	757.72	611.31	778.30	697.37	788.10	745.71	1.24	0.97	1.09	0.96	1.02
I-200×140×3.5×3.5	670.34	522.43	668.59	602.81	677.00	637.93	1.28	1.00	1.11	0.99	1.05
I-200×140×3.2×3.2	586.02	439.89	573.46	519.69	580.67	545.28	1.33	1.02	1.13	1.01	1.07
No. of observations							**64**	**64**	**64**	**64**	**64**
Mean (P_m)							**1.19**	**1.10**	**1.15**	**1.02**	**1.13**
COV (V_p)							**0.09**	**0.06**	**0.06**	**0.03**	**0.07**
Resistance factor (φ)							**0.91**	**0.85**	**0.85**	**0.85**	**0.85**
Reliability index (β)							**2.95**	**3.14**	**3.36**	**2.93**	**3.25**

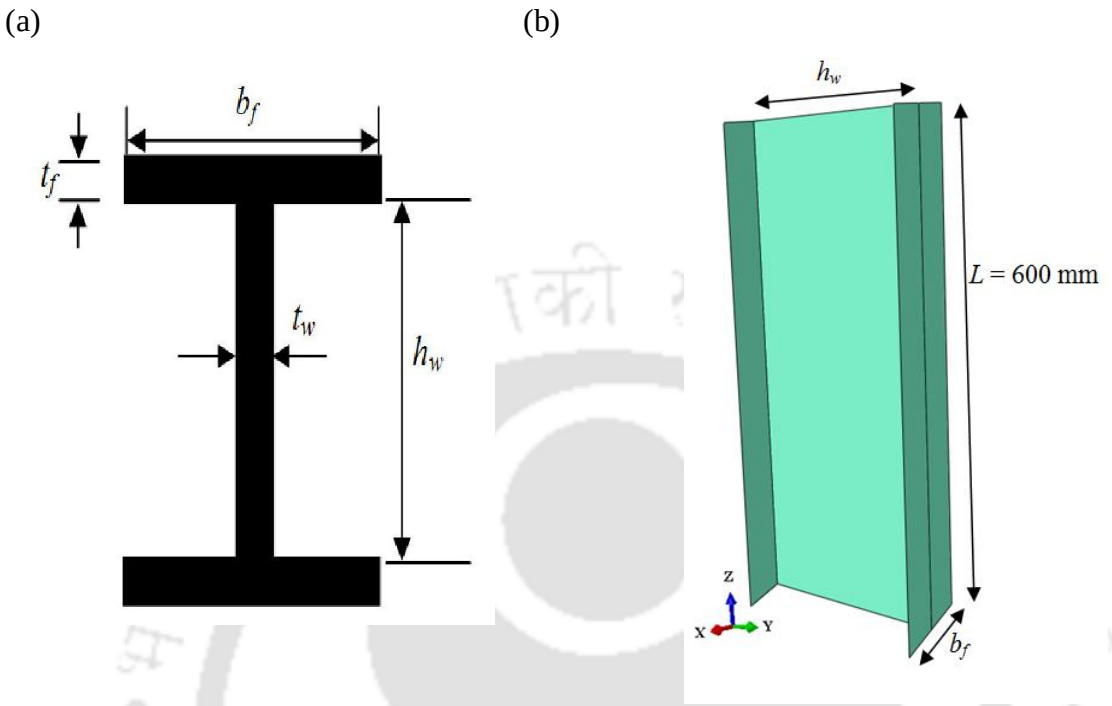

Figure 5.1: Schematic diagram showing (a) Cross-section notations (b) Geometry of stub column

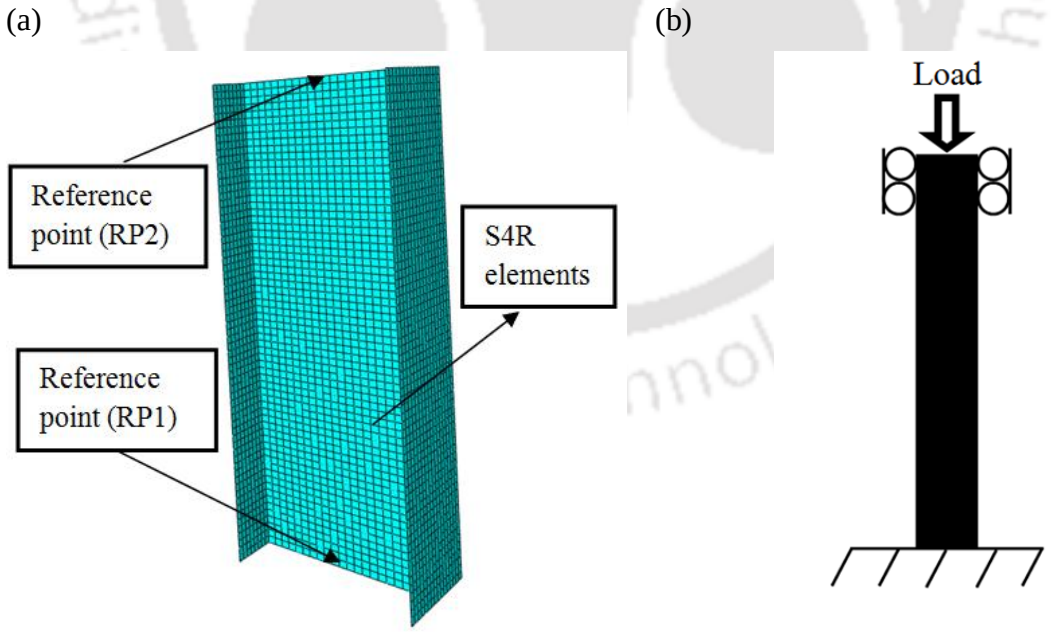

Figure 5.2: Schematic diagram showing (a) FE mesh (b) boundary condition of stub column

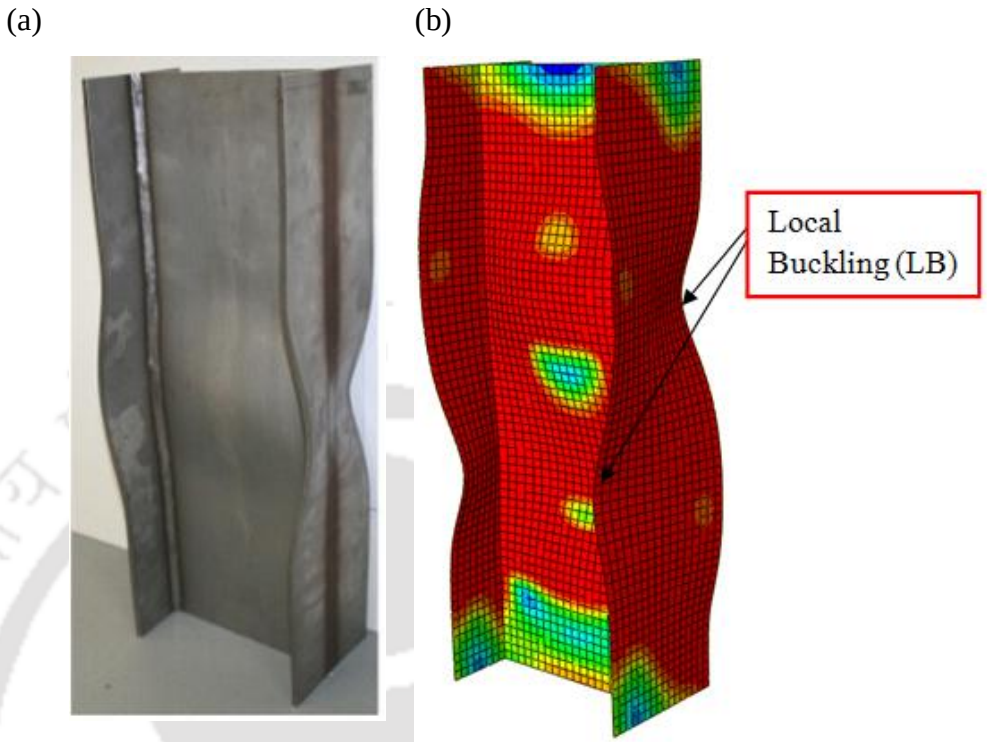

Figure 5.3: Typical failure mode of LDSS stub column (I-200×140×10×8) showing (a) Experiment (Saliba and Gardner, 2013a) (b) FE

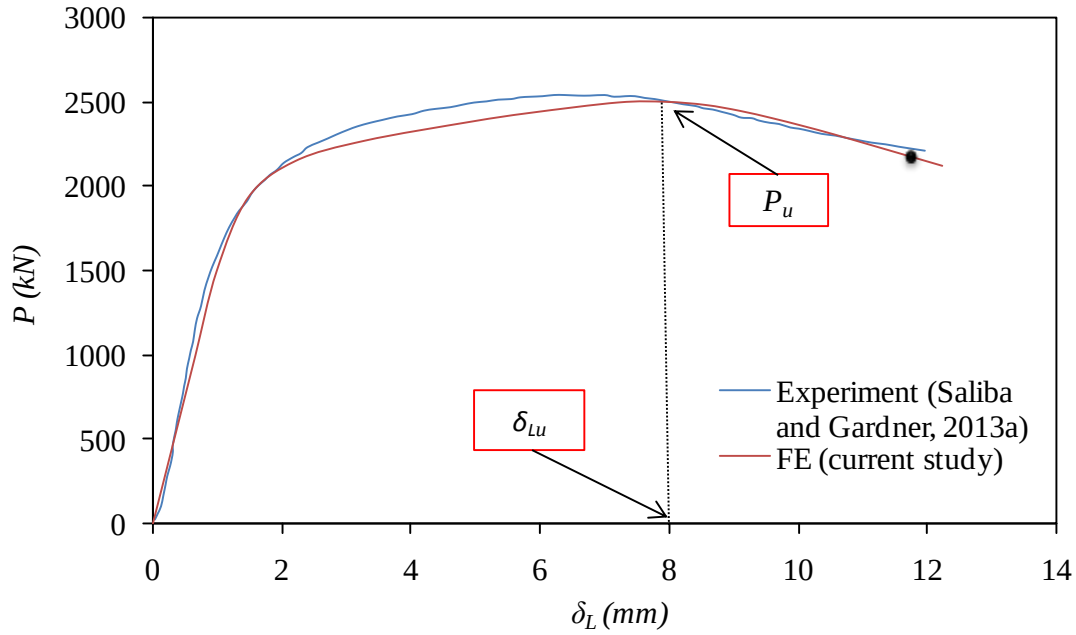

Figure 5.4: Comparison of experimental and FE results for LDSS stub columns (I-200×140×10×8)

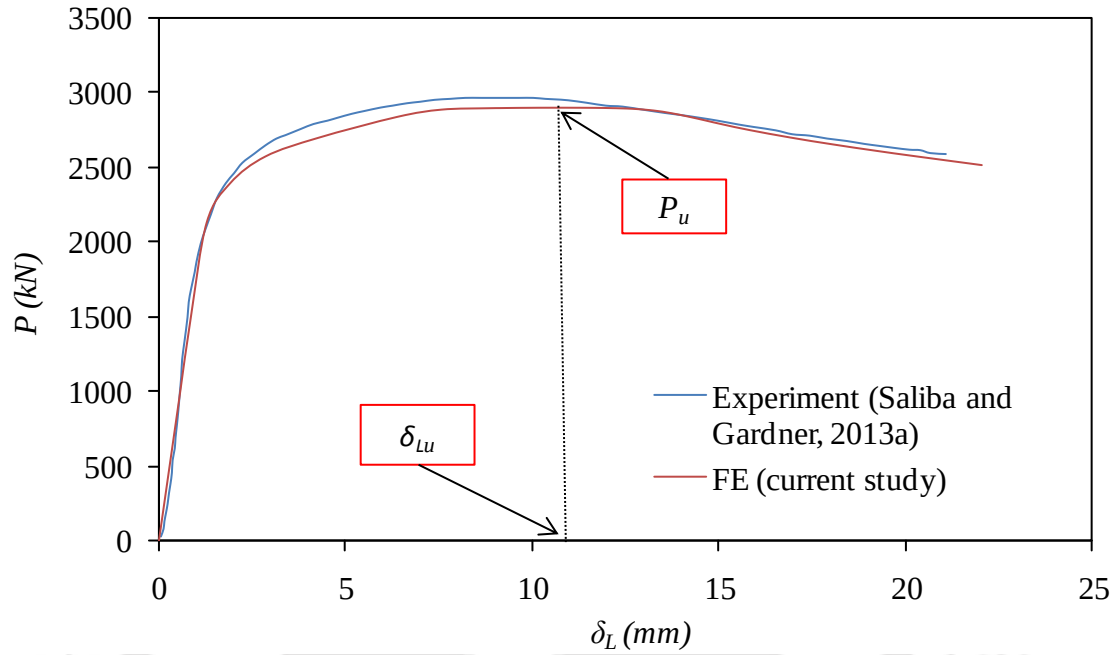

Figure 5.5: Comparison of experimental and FE results for LDSS stub columns (I-200×140×12×8)

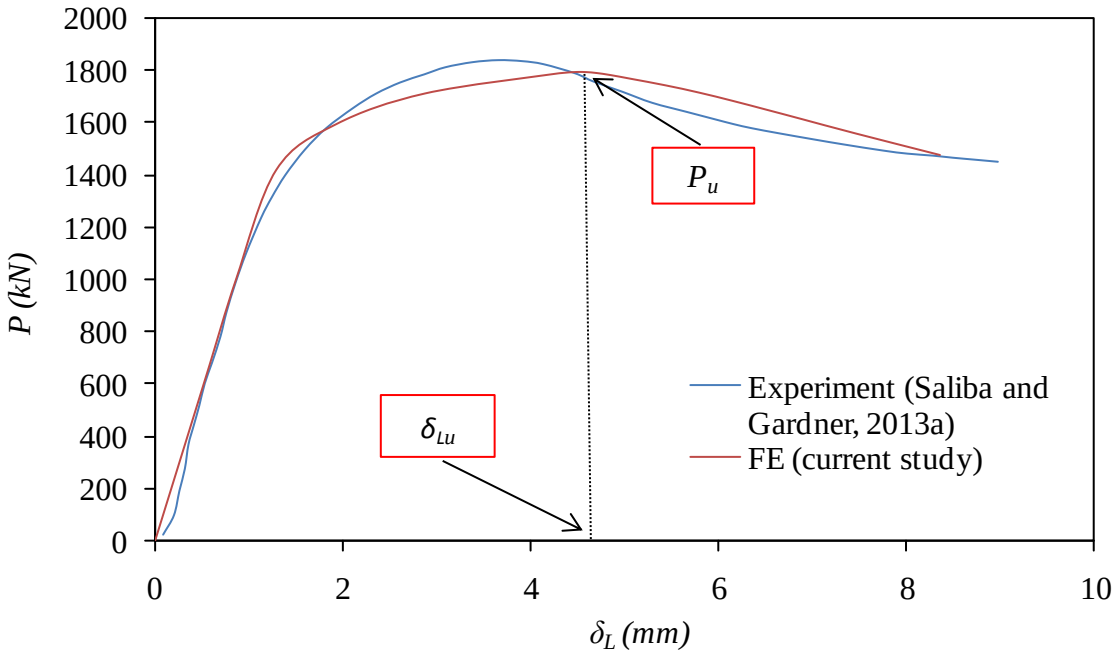

Figure 5.6: Comparison of experimental and FE results for LDSS stub columns (I-200×140×8×6)

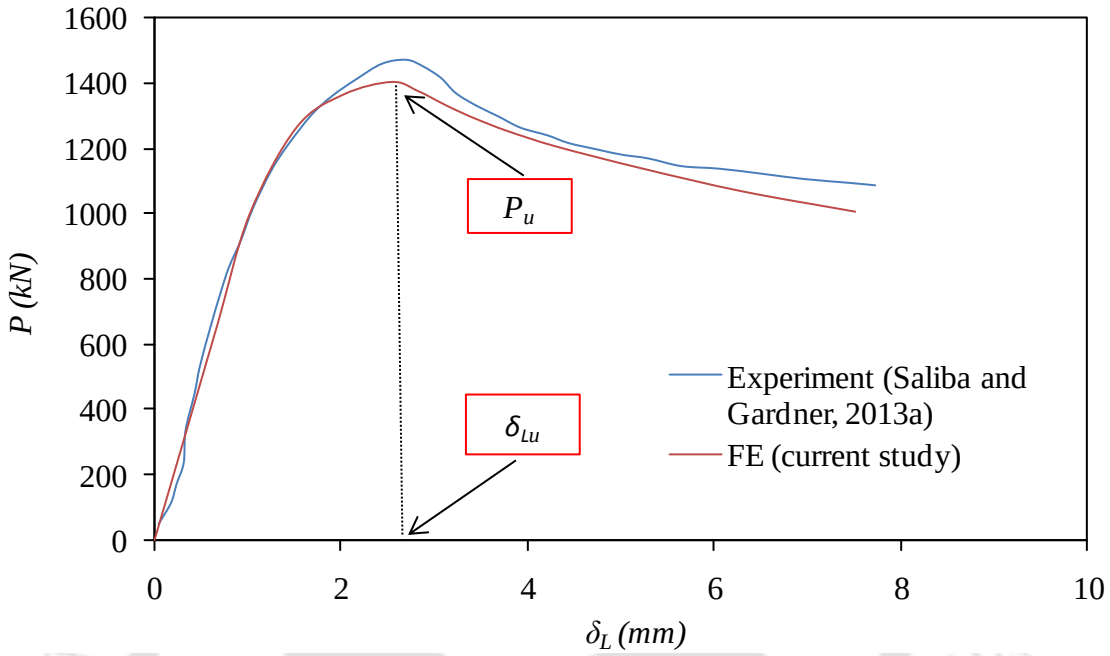

Figure 5.7: Comparison of experimental and FE results for LDSS stub column (I-200×140×6×6)

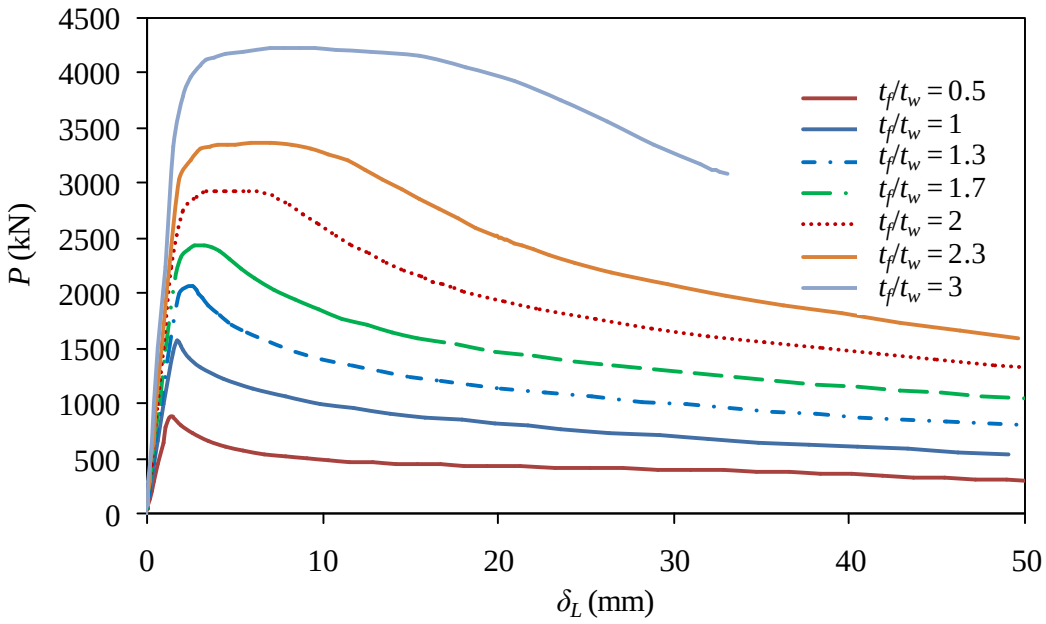

Figure 5.8: Variation of P vs δ_L by varying t_f (b_f = 140 mm, t_w = 6 mm) for HSS stub columns

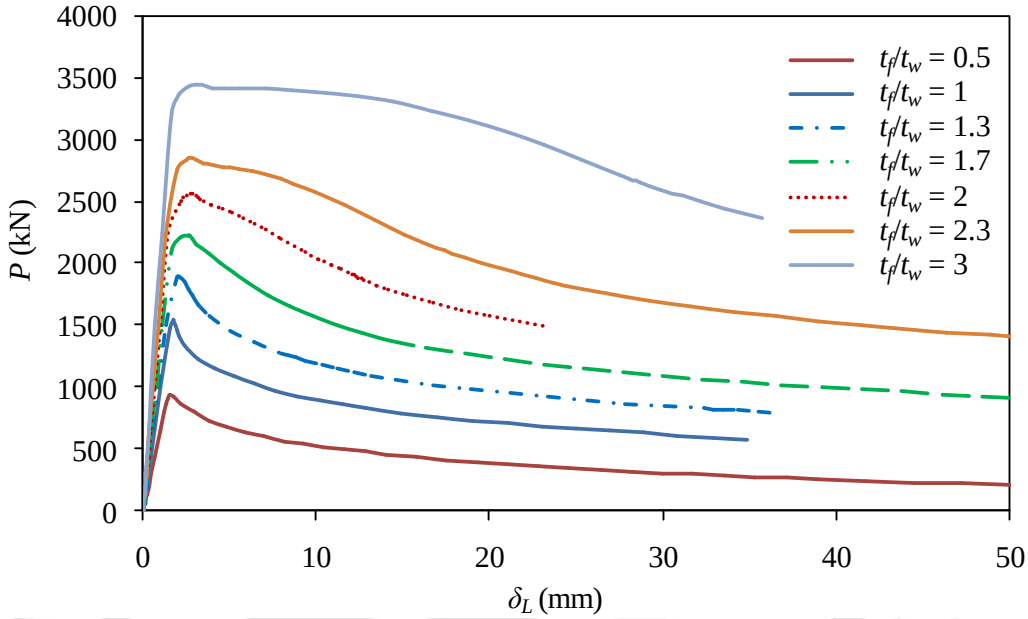

Figure 5.9: Variation of P vs δ_L by varying t_f (b_f = 140 mm, t_w = 6 mm) for HSS[a] stub columns

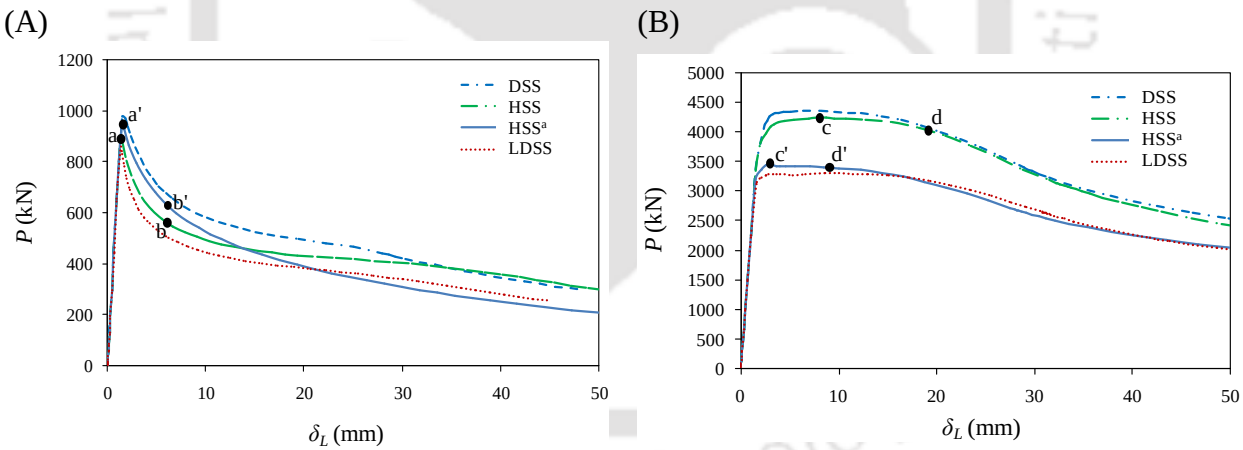

Figure 5.10: Variation of P vs δ_L by varying t_f: (A) I-200×140×3×6 (B) I-200×140×18×6

(a) $\delta_L = \delta_{L\,u}$ (b) $\delta_L = 2.5\ \delta_{Lu}$ (c) $\delta_L = \delta_{L\,u}$ (d) $\delta_L = 2.5\ \delta_{Lu}$

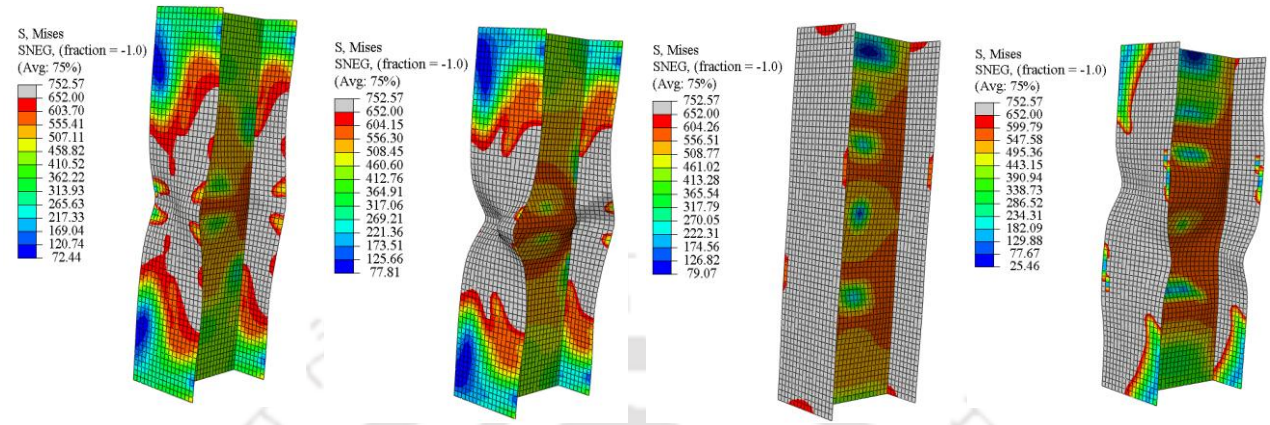

Figure 5.11: Schematic FE diagram of HSS stub columns: I-200×140×3×6 (a,b) and I-200×140×18×6 (c,d)

(a') $\delta_L = \delta_{L\,u}$ (b') $\delta_L = 2.5\ \delta_{Lu}$ (c') $\delta_L = \delta_{L\,u}$ (d') $\delta_L = 2.5\ \delta_{Lu}$

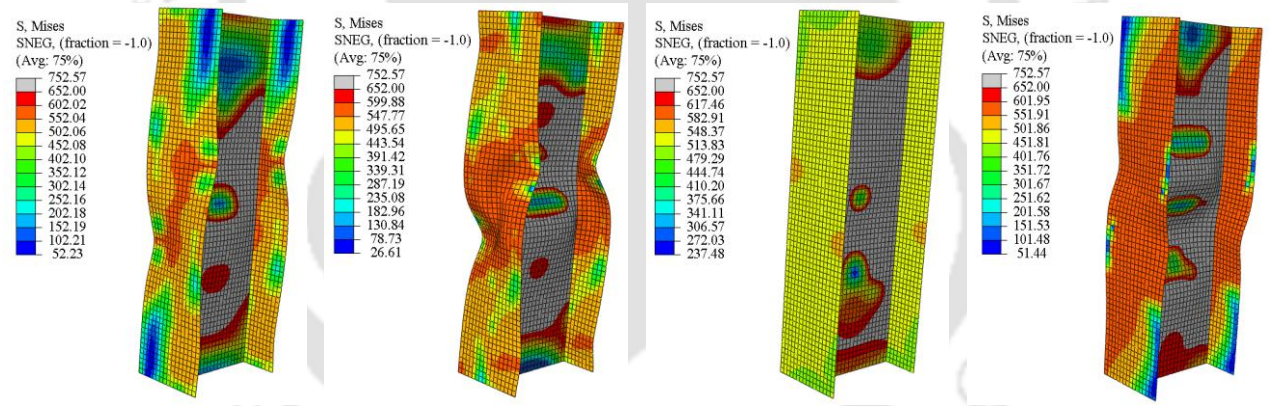

Figure 5.12: Schematic FE diagram of HSS[a] stub columns: I-200×140×3×6 (a',b') and I-200×140×18×6 (c',d')

(a) (b)

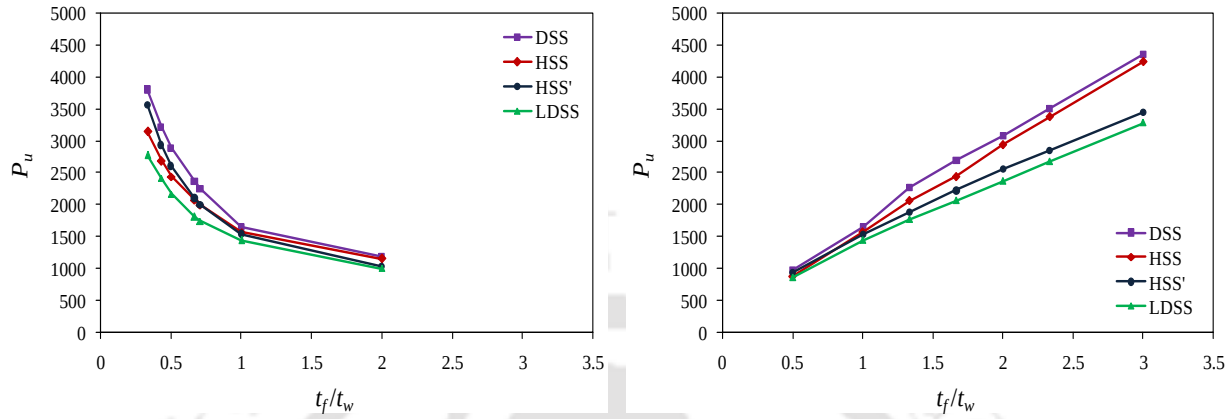

Figure 5.13: Variation of P_u with t_f/t_w by varying (a) t_w (t_f = 6 mm) (b) t_f (t_w = 6 mm)

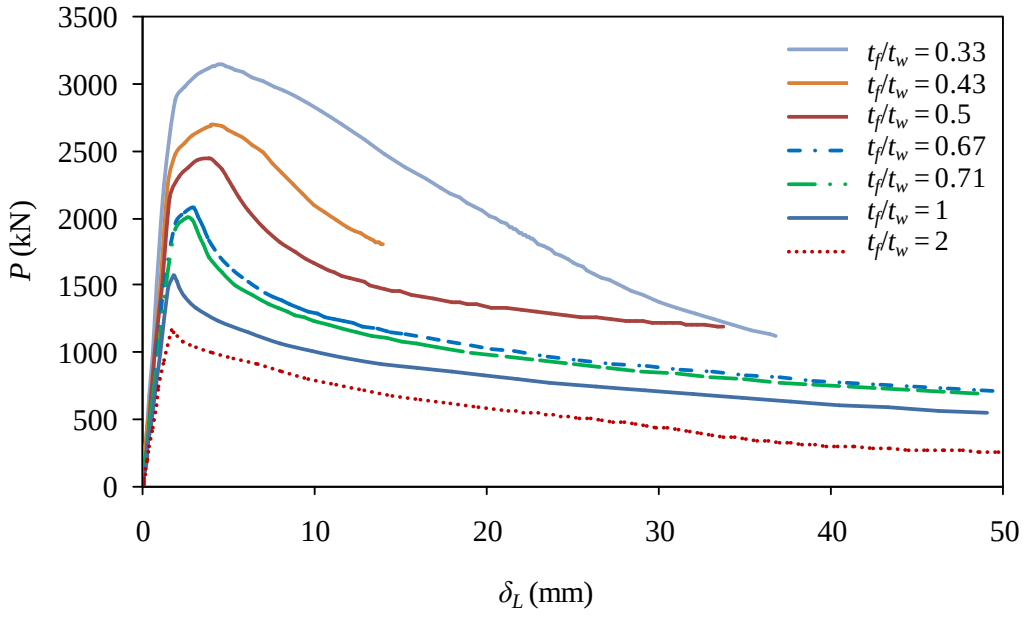

Figure 5.14: Variation of P vs δ_L by varying t_w (b_f = 140 mm, t_f = 6 mm) for HSS stub columns

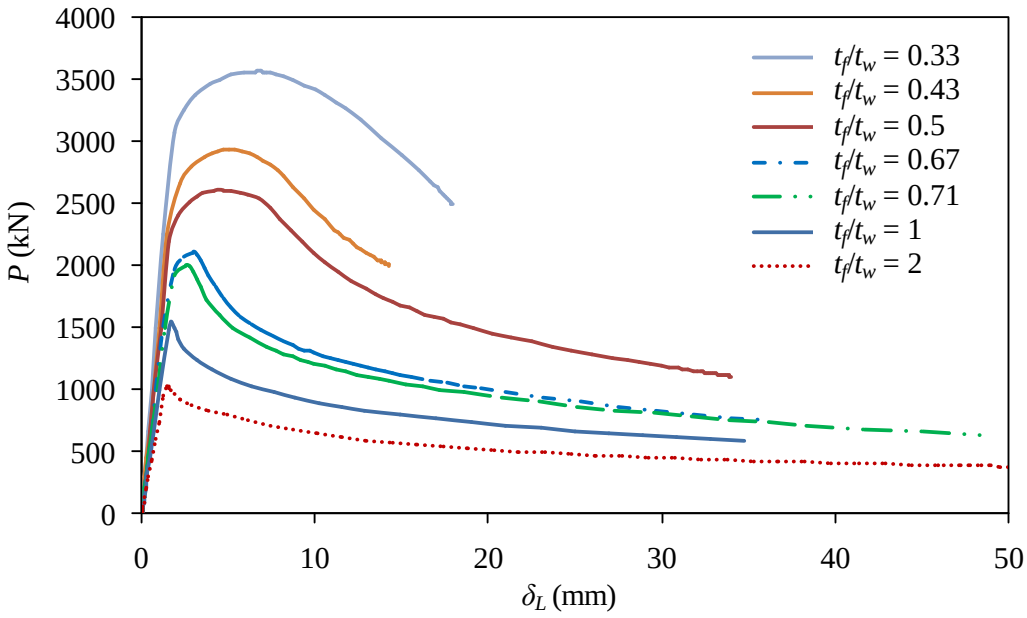

Figure 5.15: Variation of P vs δ_L by varying t_w (b_f = 140 mm, t_f = 6 mm) for HSS[a] stub columns

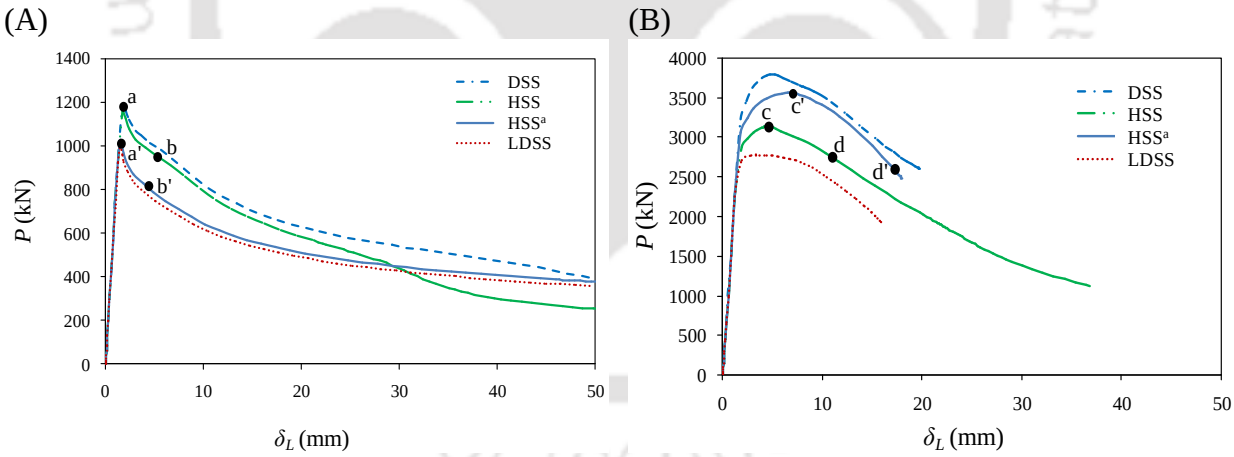

Figure 5.16: Variation of P vs δ_L by varying t_w: (A) I-200×140×6×3 (B) I-200×140×6×18

(a) $\delta_L = \delta_{L\,u}$ (b) $\delta_L = 2.5\,\delta_{Lu}$ (c) $\delta_L = \delta_{L\,u}$ (d) $\delta_L = 2.5\,\delta_{Lu}$

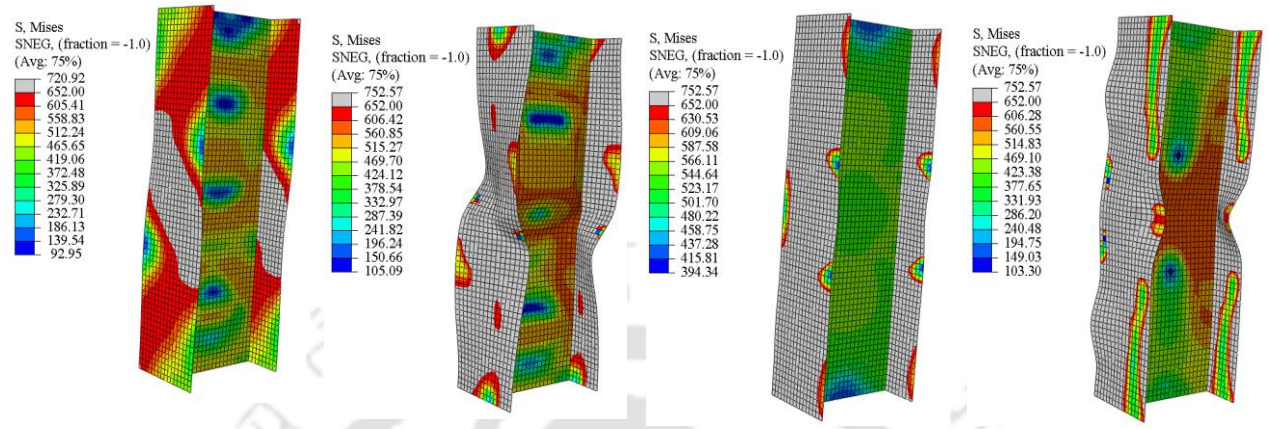

Figure 5.17: Schematic FE diagram of HSS stub columns: I-200×140×6×3 (a,b) and I-200×140×6×18 (c,d)

(a') $\delta_L = \delta_{L\,u}$ (b') $\delta_L = 2.5\delta_{L\,u}$ (c') $\delta_L = \delta_{L\,u}$ (d') $\delta_L = 2.5\delta_{L\,u}$

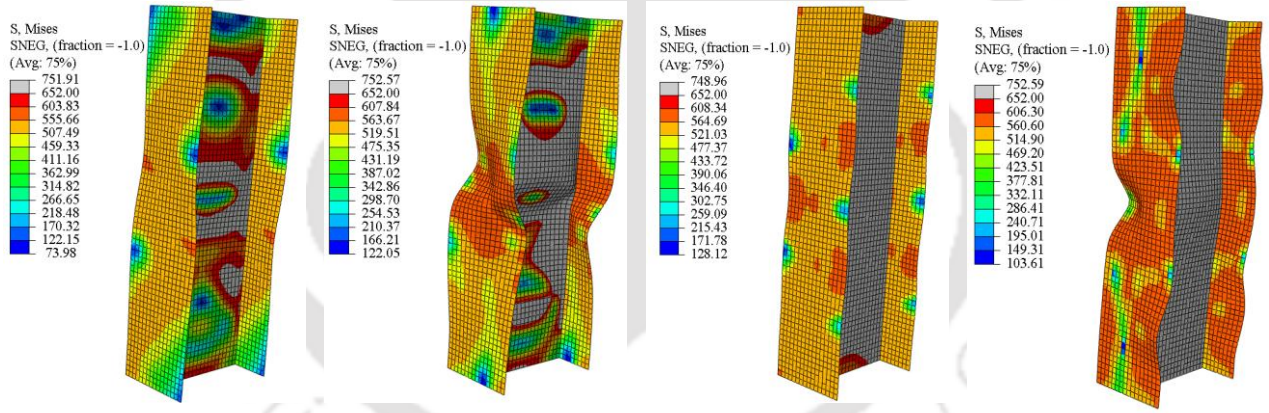

Figure 5.18: Schematic FE diagram of HSS[a] stub columns: I-200×140×6×3 (a',b') and I-200×140×6×18 (c',d')

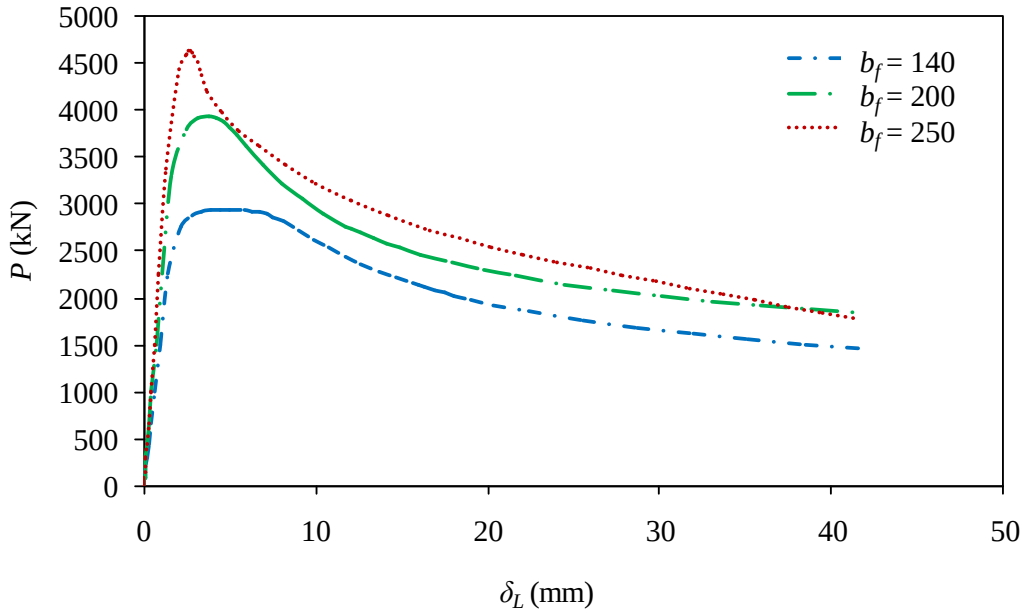

Figure 5.19: Variation of P vs δ_L by varying b_f (t_f = 12 mm, t_w= 6 mm) for HSS stub columns

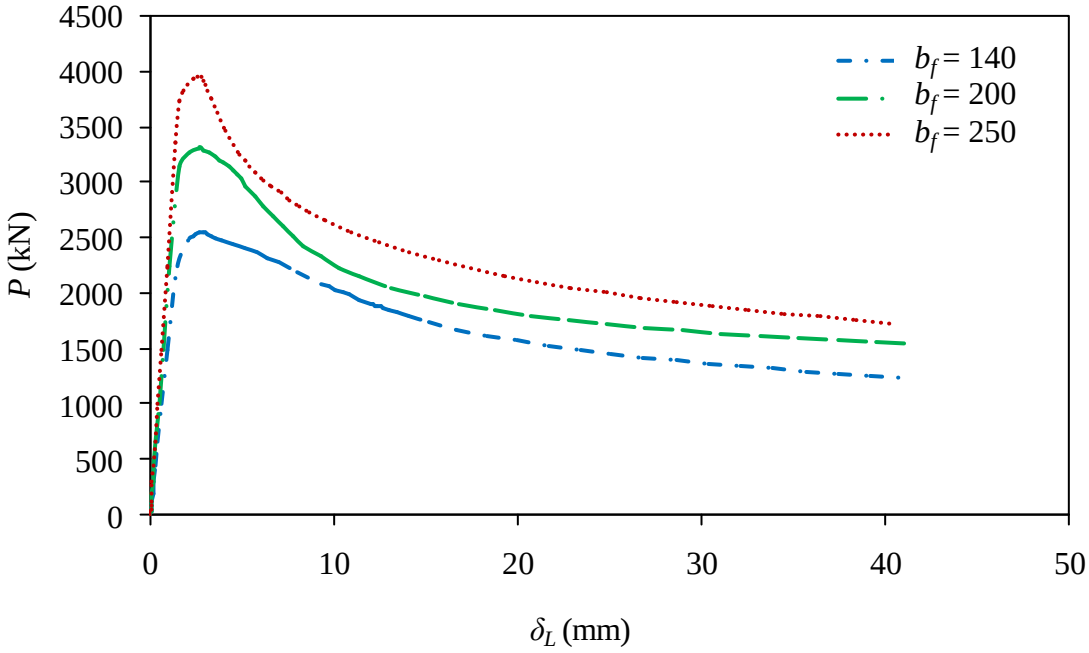

Figure 5.20: Variation of P vs δ_L by varying b_f (t_f = 12 mm, t_w= 6 mm) for HSS[a] stub columns

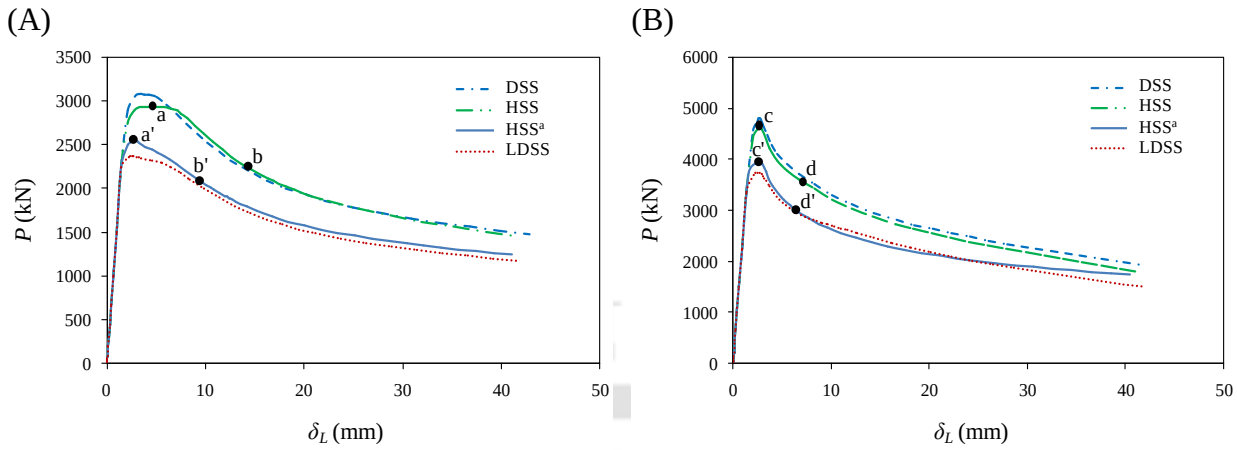

Figure 5.21: Variation of P vs δ_L by varying b_f: (A) I-200×140×12×6 (B) I-200×250×12×6

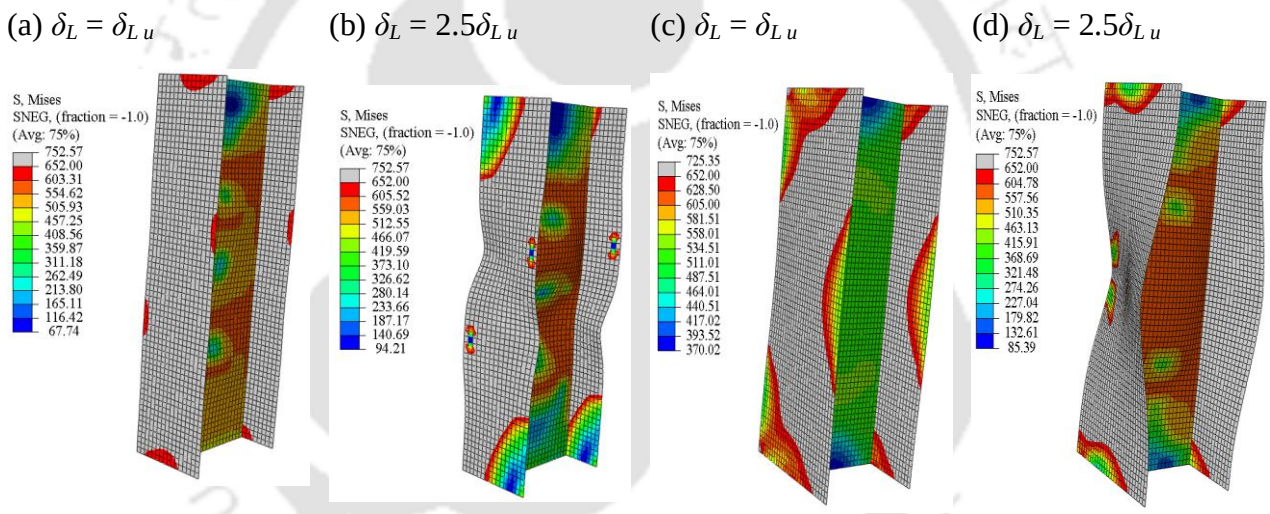

Figure 5.22: Schematic FE diagram of HSS stub columns: I-200×140×12×6 (a,b) and I-200×250×12×6 (c,d)

(a')) $\delta_L = \delta_{L\,u}$ (b')) $\delta_L = 2.5\delta_{L\,u}$ (c')) $\delta_L = \delta_{L\,u}$ (d')) $\delta_L = 2.5\delta_{L\,u}$

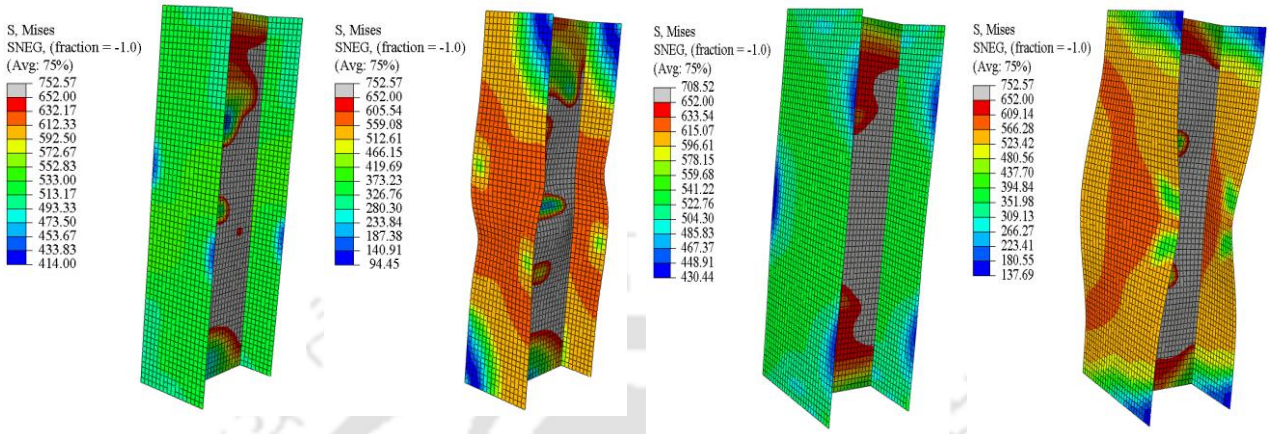

Figure 5.23: Schematic FE diagram of HSS[a] plate girders: I-200×140×12×6 (a',b') and I-200×250×12×6 (c',d')

(a) (b)

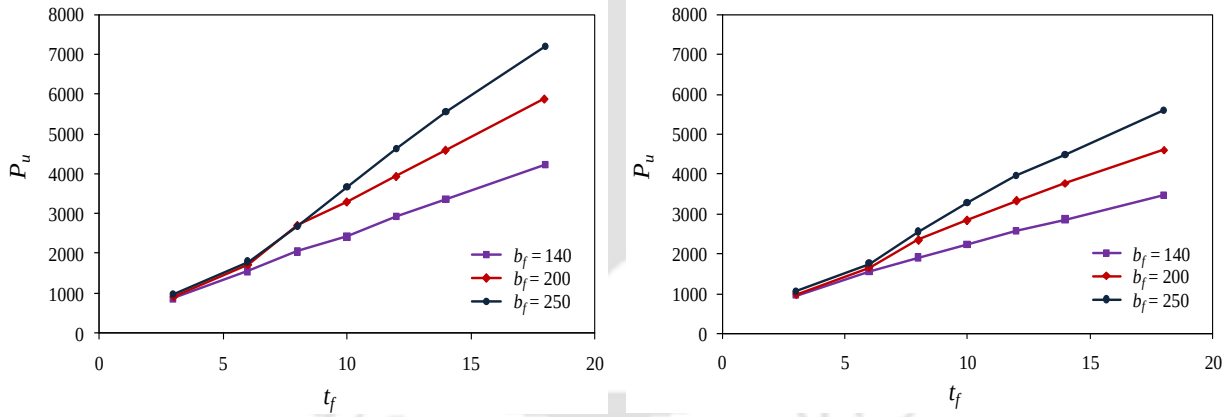

Figure 5.24: Variation of P_u with t_f by varying b_f (t_w = 6 mm) for (a) HSS (b) HSS[a] stub columns

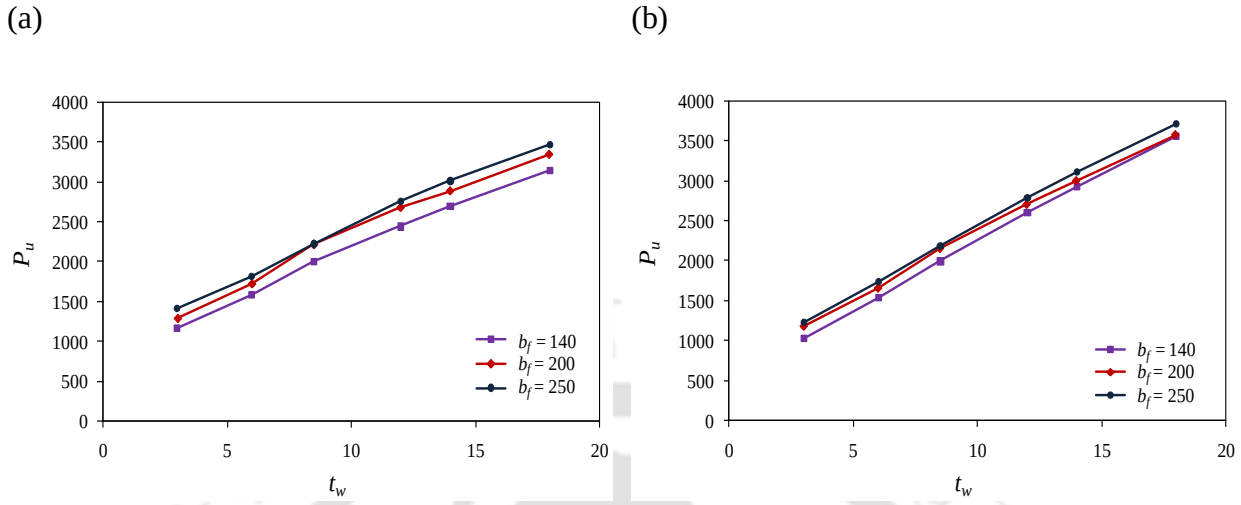

Figure 5.25: Variation of P_u with t_w by varying b_f (t_f = 6 mm) for (a) HSS (b) HSS^a stub columns

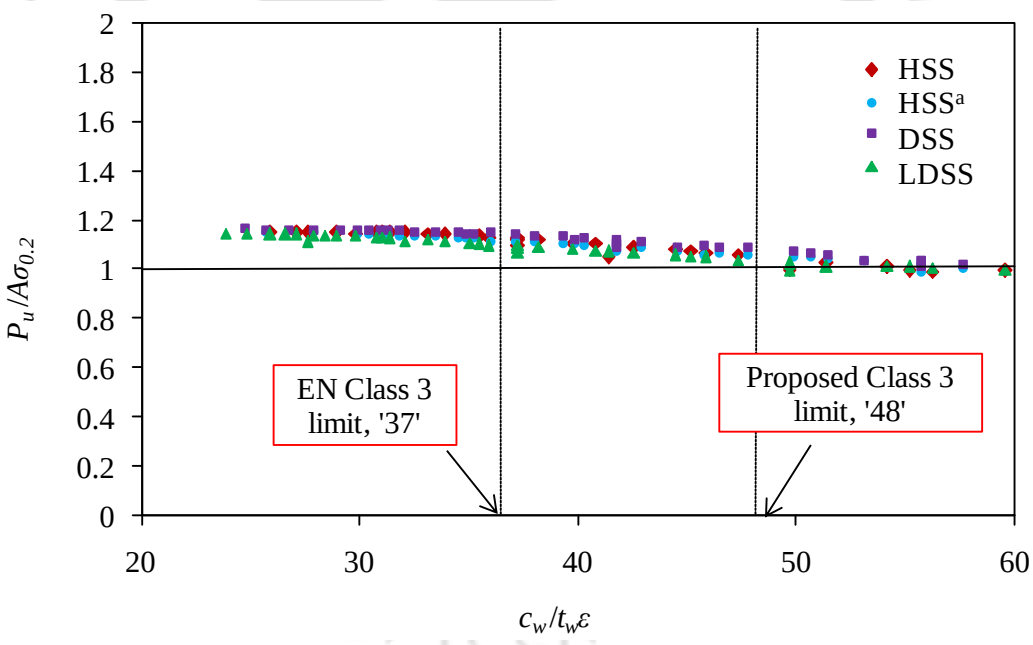

Figure 5.26: Assessment of Class 3 slenderness limits: LDSS, DSS, HSS and HSS^a stub columns

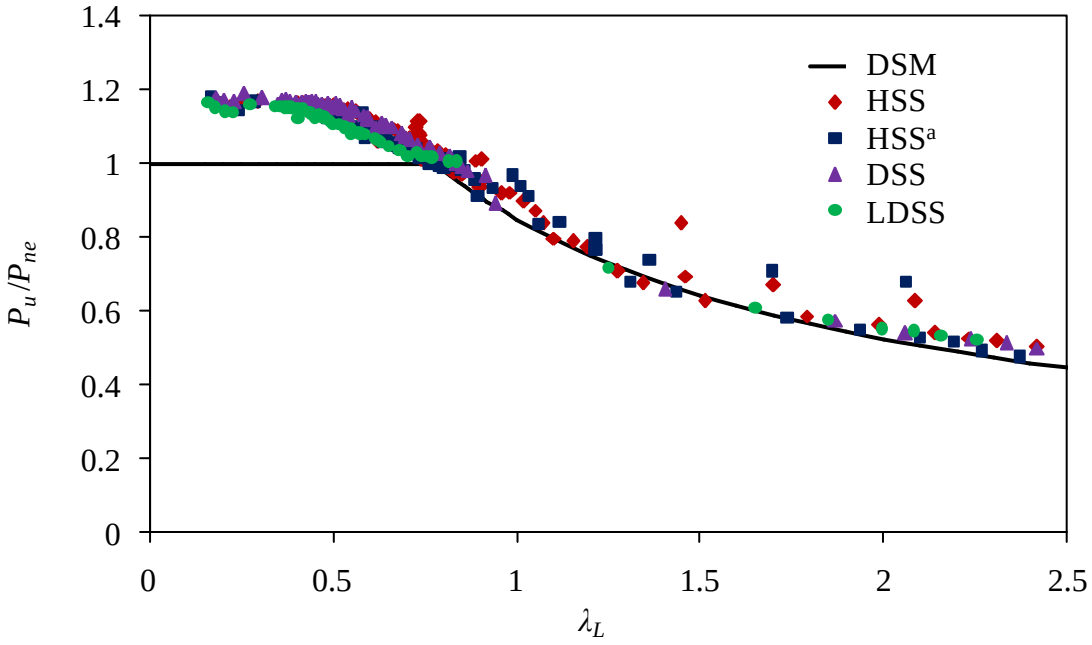

Figure 5.27: Assessment of DSM with LDSS, DSS, HSS and HSS[a] stub columns

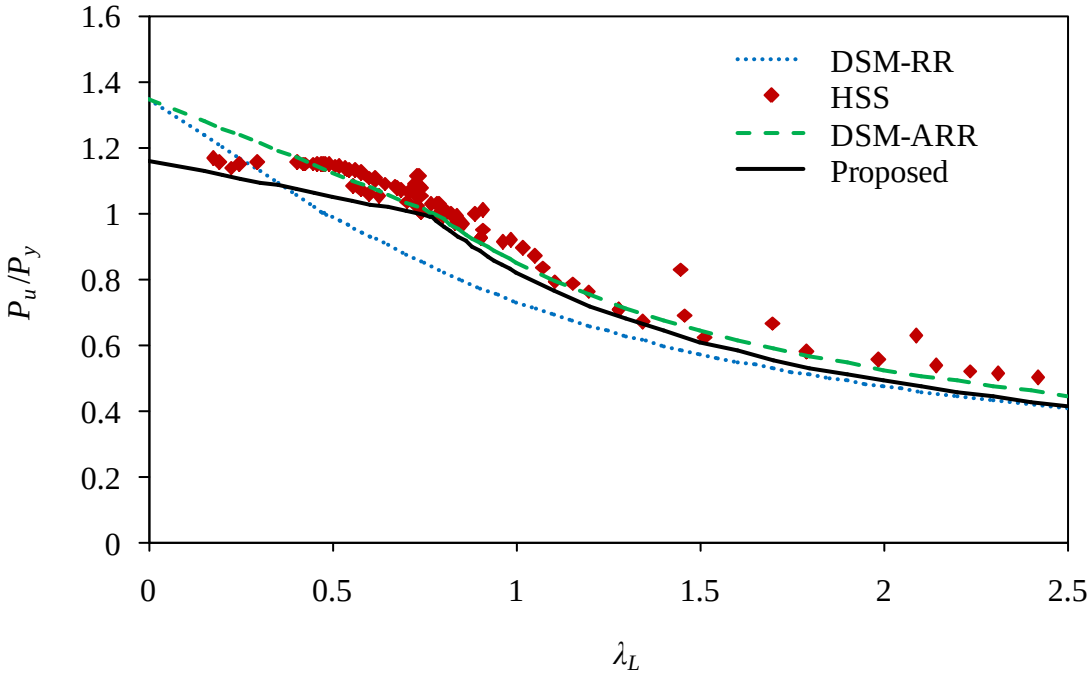

Figure 5.28: Assessment of modified DSM with HSS stub columns

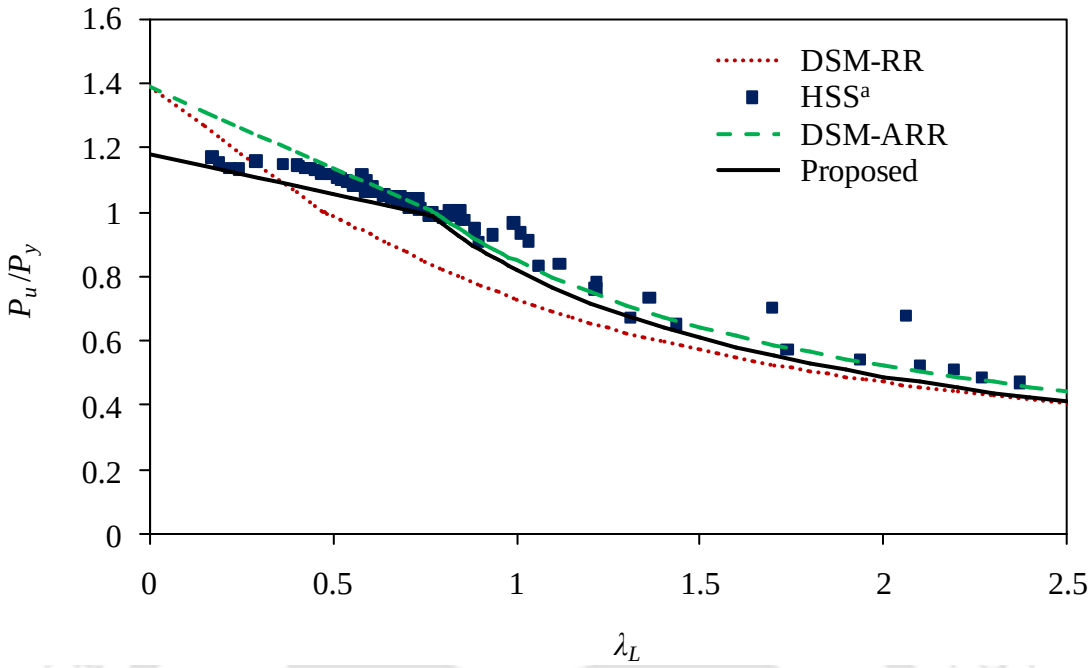

Figure 5.29: Assessment of modified DSM with HSS[a] stub columns

CHAPTER 6

6 CONCLUSIONS AND SUGGESTIONS FOR FUTURE WORK

6.1 INTRODUCTION

In this thesis, an attempt has been made to systematically investigate the structural behaviour of hybrid steel beams/girders adopting stainless steel as a primary structural material. Study has been conducted on the flexural and shear behaviours of Hybrid stainless steel (HSS) adopting LDSS and DSS in the web and flanges respectively. Also, the current study was further extended here to cover the structural behaviour of hybrid stainless steel stub columns under axial compression load. Important conclusions based on the current investigation along with the suggestions for future work are summarized below.

6.2 CONCLUSIONS

6.2.1 Flexural behaviour of hybrid stainless steel I-beams

An investigation on the flexural behaviour of HSS I-beams along with LDSS and DSS I-beams for both flange-critical and web-critical sections were conducted by varying flange thickness (t_f) and web thickness (t_w) respectively, using finite element (FE) analysis, *via* Abaqus. The FE results were used to evaluate the applicability of the

current design rules predicted by European code (EN 1993-1-4:2006 + A1, 2015) and Direct Strength Method (DSM) (Becque *et al.*, 2008; Rossi and Rasmussen, 2012; Arrayago *et al.*, 2017). Hence, the conclusions drawn from the FE investigations are presented below:

1) Rotation capacity (R) was observed to be maximum for LDSS I-beams as compared to HSS and DSS I-beams.

2) Significant improvement in flexural capacity (M_u) can be observed for of HSS I-beams although the proportion of DSS material is maintained in HSS I-beams.

3) In general, it can be seen that 3PB specimens predicted higher bending strength (M_u) as compared to 4PB specimens.

4) An increase in slenderness of the cross-section (i.e. flange and web slenderness), it can be seen that the rotation capacity (R) of the section decreases.

5) In general, EN 1993-1-4 is found to be reliable and applicable for LDSS, HSS and DSS I-beams. For flange-critical and web-critical section, the slenderness limits given in EN 1993-1-4 are observed to predict overly-conservative results and hence, to allow for economic design, new slenderness limits were proposed for Class 1, Class 2 and Class 3 limits respectively.

6) The original DSM formulation was found to be safe and applicable for LDSS, DSS and HSS I-beams, however they predicted too conservative results. Also, the modified DSM formulation given by Rossi and Rasmussen predicted overly conservative results for HSS and DSS I-beams. However, it was observed that this modified formulation presents accurate predictions for LDSS I-beams.

7) The modified DSM formulation given by Arrayago *et al.* was found to predict accurate results for DSS I-beams. Moreover, new DSM equations for HSS I-beams have been proposed based on the full-range modified DSM formulation for carbon steel given by Arrayago *et al.*

6.2.2 Shear behaviour of hybrid stainless steel plate girders

Shear performance of HSS plate girders along with homogenous sections such as LDSS and DSS plate girders have been conducted through a parametric study such as: (1) flange-to-web thickness ratio (t_f/t_w) by varying t_f and t_w, (2) flange slenderness (b_f/t_f) by varying b_f using FE analyses. The FE results in the form of shear capacity (V_u) are compared with the unfactored design shear resistances given by European code (EN 1993-1-4:2006 + A1, 2015) and Direct Strength Method (DSM) (Keerthan and Mahendran, 2015; AISI, 2016b) for HSS plate girders. The conclusions obtained from the FE studies are given below:

1) Three failure modes were seen in the FE models such as: shear dominant failure mode (i.e. indicating diagonal tension band), bending dominant failure mode (i.e. showing plastic hinge at mid span compression flange) and combined shear and bending dominant failure mode indicating both shear and bending failure modes.

2) Shear dominant failure modes are generally observed in HSS plate girders of thick flange with relatively thinner web (i.e. $t_f/t_w > 2$). Also, bending dominant failure mechanisms are observed in specimens having lower flange thickness as compared to web thickness (i.e. $t_f / t_w \leq 1$).

3) Shear capacity was found to increase by increasing flange thickness. An increase in t_f (4-20 mm) or t_f/t_w (1-5) by 400% keeping t_w as constant has been

found to result in an increase in shear capacity (V_u) of ~50% for HSS plate girders.

4) Significant improvement in shear capacity can be seen by increasing the web thickness. An increase in t_w (4-12 mm) or t_f/t_w (3-1.2) by 200% keeping t_f as constant has been seen to significantly enhance shear capacity (V_u) of ~270%.

5) Shear capacity (V_u) has been seen to increase with increasing the flange width (b_f). An increase in b_f (150-300 mm) or b_f/t_f (12.5-25) by ~100% resulted in increase in V_u by ~ 18%.

6) In general, European code (EN 1993-1-4:2006 + A1, 2015) is found to be applicable and safe for most of the sections. For thin sections (i.e. $\bar{\lambda}_w > 1.5$), EN 1993-1-4 predicted overly-conservative results and for thicker sections (i.e. $\bar{\lambda}_w \leq 0.65$), FE results are found to be not safe. Hence, for the purpose of economic and efficient design, an improved design expression similar to EN 1993-1-4 (2006 + A1, 2015) has been proposed for rigid end post HSS plate girders.

7) The original DSM (AISI, 2016b) has been seen to predict very conservative results for HSS plate girders. Also, the modified DSM given by Keerthan and Mahendran (2015) has been observed to predict more accurate results as compared to original DSM, although few specimens have found to be unsafe. Therefore, for enhancing the efficiency, modified DSM formulations have been proposed for HSS plate girders.

6.2.3 Hybrid stainless steel stub columns under pure compression

Numerical study on the structural performance of HSS and HSS[a] stub columns along with homogenous sections such as LDSS and DSS stub columns have been investigated through a parametric study such as: (1) flange-to-web thickness ratio (t_f/t_w) by varying

t_f and t_w, (2) effect of flange width (b_f) using the commercial FE software, Abaqus. Also, the FE results were further used to check the appropriateness of current design specifications predicted by European code (EN 1993-1-4:2006 + A1, 2015) and Direct strength method (Rossi and Rasmussen, 2012; AISI, 2016b; Arrayago *et al.*, 2017). The conclusions obtained from the FE investigations are presented below:

1) Increase in flange thickness (t_f) has been seen to have significant improvement on P_u for HSS stub columns as compared to HSS^a stub columns. An increase in t_f (3-18 mm) or t_f/t_w (0.5-3) by 500% resulted in increase in P_u of ~381% and ~266% for HSS and HSS^a stub columns respectively.

2) In contrast to effect of t_f, increase in web thickness has been seen to enhance the column capacity significantly for HSS^a stub columns as compared to HSS stub columns. An increase in t_w (3-18 mm) or t_f/t_w (2-0.33) by 500% resulted in increase in P_u of ~170% and ~247% for HSS and HSS^a stub columns respectively.

3) Increase in flange width has been found to have more improvement on column capacity for HSS stub columns as compared to HSS^a stub columns. An increase in b_f (140-250 mm) by ~44% resulted in an improvement in P_u by ~58% and ~47% for HSS and HSS^a stub columns respectively.

4) In addition, for thin flange sections (i.e. $t_f \leq 6$ mm), b_f has been observed to have very less effect on P_u, whereas for $t_f > 6$mm, P_u significantly enhanced with increase in b_f and t_f and this improvement in P_u has been found to be more effective in HSS stub columns as compared to HSS^a stub columns.

5) In general, Class 3 limit for internal compression element (i.e. web) in EN 1993-1-4 has been found to be reliable and applicable for LDSS, HSS, HSS^a

and DSS stub columns. Therefore, for the purpose of efficient and economic designs, the limit ($c_w/t_w\varepsilon$ = 48) has been proposed for Class 3 limit.

6) The original DSM formulation (AISI, 2016b) has been found to applicable for most of the stub columns (i.e. LDSS, HSS, HSS^a and DSS stub columns). However, this formulation has been observed to predict too conservative results for stocky sections.

7) In addition, new DSM equations for HSS and HSS^a stub columns have been proposed based on the full-range modified DSM specification for carbon steel.

6.3 SUGGESTIONS FOR FUTURE WORK

In this thesis, although, significant number of FE analyses (approximately ~600 models) have been undertaken, considering various relevant geometrical parameters; to understand the structural behaviour of hybrid I-sections under bending, shear and axial compression load (i.e. stub columns); ample scopes for its expansion are available. These extensions can be in the form of changing the materials, considerations of various perforations, loading types, etc., via both FE and experimental approaches. Some possible extensions are presented in the following sections.

6.3.1 Structural material

The structural behaviour of hybrid stainless I-sections may be further extended by adopting different material combinations such as adopting other stainless steel grades *viz.* austenitic and ferritic stainless steel. Also, it can be further extended adopting different material combinations such as stainless steel and carbon steel.

6.3.2 Effect of perforations

Structural performance of hybrid stainless I-sections can be conveniently extended by incorporating the effect of perforations. The perforation study can include various shapes of perforations such as circular, square, rectangular, elliptical, oval, rhombus etc. and sizes. In addition, instead of single perforations, double or multiple perforations may also be considered.

6.3.3 Loading conditions

The present study is limited to bending, shear and axial compression load. Hence, the study can be extended by considering cyclic loading, torsion, etc. In addition, the effect of extreme loading cases such as impact, blast and fire may also be investigated.

REFERENCES

AASHTO, L. (2004) 'bridge design specifications AASHTO', *Washington (DC)*.

Abaqus (2009) 'Abaqus/Standard user's manual volumes I-III and ABAQUS CAE manual. Version 6.9-EF1, Dassault Systemes Simulia Corp., Providence, RI, USA.'

Afshan, S. and Gardner, L. (2013) 'The continuous strength method for structural stainless steel design', *Thin-Walled Structures*. Elsevier, 68, pp. 42–49.

AISC 360-10 (2010) 'Specifications for Structural Steel Buildings. Chicago'.

AISI (2007) 'Commentary on North American Specification for the Design of Cold-Formed Steel Structural Members. AISI S100-2007-C. North American Cold-formed steel specification. American Iron and Steel Institute, Washington, DC'.

AISI (2016a) 'Commentary on North American Specification for the Design of Cold-Formed Steel Structural Members, American Iron and Steel Institute (AISI), Washington, DC, S100-16C'.

AISI (2016b) 'North American Specification for the Design of Cold-Formed Steel Structural Members, Am. Iron Steel Inst. (AISI), Washington, DC', pp. S100-16.

Aoki, T. and Ji, B. (2000) 'Experimental study on buckling strength of tri-tube steel members', in *Coupled Instabilities In Metal Structures: CIMS'2000*. World Scientific, pp. 283–290.

Arrayago, I., Rasmussen, K.J.R. and Real, E. (2017) 'Full slenderness range DSM approach for stainless steel hollow cross-sections', *Journal of Constructional Steel Research*. Elsevier, 133, pp. 156–166.

Arrayago, I. and Real, E. (2016) 'Experimental study on ferritic stainless steel simply supported and continuous beams', *Journal of Constructional Steel Research*, 119, pp. 50–62.

Arrayago, I., Real, E. and Gardner, L. (2015) 'Description of stress–strain curves for stainless steel alloys', *Materials & Design*. Elsevier, 87, pp. 540–552.

AS/NZS (2001) 'Cold-formed stainless steel structures. AS/NZS 4673, Australian/New Zealand Standard, Standards Australia. Sydney, Australia.'

ASCE 8-02 (2002) 'Specification for the design of cold-formed stainless steel structural members, American Society of Civil Engineers'.

Ashraf, M., Gardner, L. and Nethercot, D.A. (2006a) 'Compression strength of stainless steel cross-sections', *Journal of Constructional Steel Research*, 62(1), pp. 105–115.

Ashraf, M., Gardner, L. and Nethercot, D.A. (2006b) 'Finite element modelling of structural stainless steel cross-sections', *Thin-walled structures*. Elsevier, 44(10), pp. 1048–1062.

Ashraf, M., Gardner, L. and Nethercot, D.A. (2008) 'Resistance of stainless steel CHS columns based on cross-section deformation capacity', *Journal of Constructional Steel Research*. Elsevier, 64(9), pp. 962–970.

Azizinamini, A., Hash, J.B., Yakel, A.J. and Farimani, R. (2007) 'Shear capacity of hybrid plate girders', *Journal of Bridge Engineering*. American Society of Civil Engineers, 12(5), pp. 535–543.

Baddoo, N.R. (2008) 'Stainless steel in construction: A review of research, applications, challenges and opportunities', *Journal of Constructional Steel Research*. Elsevier, 64(11), pp. 1199–1206.

Barth, K.E. and White, D.W. (1998) 'Finite element evaluation of pier moment-rotation

characteristics in continuous-span steel I Girders', *Engineering Structures*. Elsevier, 20(8), pp. 761–778.

Becque, J., Lecce, M. and Rasmussen, K.J.R. (2008) 'The direct strength method for stainless steel compression members', *Journal of Constructional Steel Research*, 64(11), pp. 1231–1238.

Bredenkamp, P.J. and Van den Berg, G.J. (1995) 'The strength of stainless steel built-up I-section columns', *Journal of Constructional Steel Research*. Elsevier, 34(2–3), pp. 131–144.

Carvalho, E.C.G., Van den Berg, G.J. and Van der Merwe, P. (1990) 'Local shear buckling in cold-formed stainless steel beam webs', in *Proceedings of the annual technical session, Structural Stability Research Council. April 10-11. St Louis, Missouri, USA*.

Chacón, R., Bock, M. and Real, E. (2011) 'Longitudinally stiffened hybrid steel plate girders subjected to patch loading', *Journal of Constructional Steel Research*. Elsevier, 67(9), pp. 1310–1324.

Cruise, R.B. and Gardner, L. (2006) 'Measurement and prediction of geometric imperfections in structural stainless steel members', *Structural Engineering and Mechanics*. Taejon, Korea: Techno-Press, c1993-, 24(1), pp. 63–90.

Dawson, R.G. and Walker, A.C. (1972) 'Post-buckling of geometrically imperfect plates', *Journal of the Structural Division*. ASCE, 98(1), pp. 75–94.

Ellobody, E., Feng, R. and Young, B. (2013) *Finite element analysis and design of metal structures*. Elsevier.

Ellobody, E. and Young, B. (2005) 'Structural performance of cold-formed high strength stainless steel columns', *Journal of Constructional Steel Research*, 61, pp. 1631–1649.

EN 10088-4 (2009) 'Stainless steels-Part 4: Technical delivery conditions for sheet/plate and strip of corrosion resisting steels for general purposes.' CEN.

EN 1993-1-1 (2005) 'Eurocode 3: Design of steel structures, Part 1.1: General rules and rules for buildings. British Standard-BS EN 1993-1-1:2005'.

EN 1993-1-4 (2006) 'Eurocode 3: Design of steel structures–Part 1.4: General rules–Supplementary rules for stainless steels. CEN.'

EN 1993-1-4:2006 + A1 (2015) 'Eurocode 3: Design of steel structures–Part 1.4: General rules–Supplementary rules for stainless steels.'

EN 1993-1-5 (1997) 'Eurocode 3: Design of steel structures–Part 1-5: General rules-supplementary rules for planar plated structures without transverse loading. Brussels.'

EN 1993-1-5 (2007) 'Eurocode 3: Design of steel structures–Part 1-5: Plated Structural Elements. CEN.'

ENV 1993-1-4 (1996) 'Eurocode 3: Design of steel structures–Part 1.4: General rules–Supplementary rules for stainless steels. Brussels.'

Estrada, I., Real, E. and Mirambell, E. (2007a) 'General behaviour and effect of rigid and non-rigid end post in stainless steel plate girders loaded in shear. Part I: Experimental study', *Journal of constructional steel research*. Elsevier, 63(7), pp. 970–984.

Estrada, I., Real, E. and Mirambell, E. (2007b) 'General behaviour and effect of rigid and non-rigid end post in stainless steel plate girders loaded in shear. Part II: Extended numerical study and design proposal', *Journal of Constructional Steel Research*. Elsevier, 63(7), pp. 985–996.

Frost, R.W. and Schilling, C.G. (1964) 'Behavior of hybrid beams subjected to static loads', *Journal of the Structural Division*. ASCE, 90(3), pp. 55–88.

Gardner, L. (2002) 'A new approach to structural stainless steel design'. Imperial College London (University of London).

Gardner, L. (2005) 'The use of stainless steel in structures', *Progress in Structural Engineering and Materials*. Wiley Online Library, 7(2), pp. 45–55.

Gardner, L. and Ashraf, M. (2006) 'Structural design for non-linear metallic materials', *Engineering Structures*. Elsevier, 28(6), pp. 926–934.

Gardner, L., Bu, Y. and Theofanous, M. (2016) 'Laser-welded stainless steel I-sections: Residual stress measurements and column buckling tests', *Engineering Structures*. Elsevier, 127, pp. 536–548.

Gardner, L. and Cruise, R.B. (2009) 'Modeling of residual stresses in structural stainless steel sections', *Journal of Structural Engineering*. American Society of Civil Engineers, 135(1), pp. 42–53.

Gardner, L., Insausti, A., Ng, K.T. and Ashraf, M. (2010) 'Elevated temperature material properties of stainless steel alloys', *Journal of Constructional Steel Research*. Elsevier, 66(5), pp. 634–647.

Gardner, L. and Nethercot, D.A. (2001) 'Numerical modelling of cold-formed stainless steel sections', in *Proceedings of the ninth nordic steel construction conference*, pp. 781–789.

Gardner, L. and Nethercot, D.A. (2004) 'Numerical modeling of stainless steel structural components—a consistent approach', *Journal of structural Engineering*. American Society of Civil Engineers, 130(10), pp. 1586–1601.

Gardner, L., Talja, A. and Baddoo, N.R. (2006) 'Structural design of high-strength austenitic stainless steel', *Thin-walled structures*. Elsevier, 44(5), pp. 517–528.

GB/T1591 (2008) 'Chinese standard for High Strength Low alloy Structural Steels. Beijing, China'.

GB50017 (2003) 'National Standard of the People's Republic of China. Code for Design of Steel Structures, Beijing, China'.

Gkantou, M., Kokosis, G., Theofanous, M. and Dirar, S. (2019) 'Plastic design of stainless steel continuous beams', *Journal of Constructional Steel Research*. Elsevier, 152, pp. 68–80.

Greco, N. (2000) 'Cross-sectional compactness and bracing requirements for hybrid hps girders. Master Dissertation, University of Pittsburgh, Pennsylvania'.

Greco, N. and Earls, C.J. (2003) 'Structural ductility in hybrid high performance steel beams', *Journal of Structural Engineering*. American Society of Civil Engineers, 129(12), pp. 1584–1595.

Green, P.S., Sause, R. and Ricles, J.M. (2002) 'Strength and ductility of HPS flexural members', *Journal of Constructional Steel Research*. Elsevier, 58(5–8), pp. 907–941.

Haaijer, G. (1957) 'Plate buckling in the strain-hardening range', *Transactions of the American Society of Civil Engineers*. ASCE, 124(1), pp. 117–148.

Haaijer, G. and Thürlimann, B. (1958) 'On inelastic buckling in steel', *Journal of the Engineering Mechanics Division*. ASCE, 84(2), pp. 1–48.

Hassanein, M.F. (2010) 'Imperfection analysis of austenitic stainless steel plate girders failing by shear', *Engineering Structures*, 32(3), pp. 704–713.

Hassanein, M.F. (2011) 'Finite element investigation of shear failure of lean duplex stainless steel plate girders', *Thin-Walled Structures*. Elsevier, 49(8), pp. 964–973.

Hassanein, M.F. and Silvestre, N. (2013) 'Flexural behavior of lean duplex stainless steel girders with slender unstiffened webs', *Journal of Constructional Steel Research*. Elsevier, 85, pp. 12–23.

Heidarpour, A., Cevro, S., Song, Q.-Y. and Zhao, X.-L. (2013) 'Behaviour of

innovative stub columns utilising mild-steel plates and stainless steel tubes at ambient and elevated temperatures', *Engineering Structures*. Elsevier, 57, pp. 416–427.

Hill, H.N. (1944) 'Determination of stress-strain relations from "offset" yield strength values. Technical note no 927, National Advisory Committee for Aeronautics, Washigton.'

Höglund, T. (1971) 'Behaviour and strength of the web of thin plate I-girders. Bulletin no 93', in *Division of building statics and structural engineering*. The Royal Institute of Technology, Stockholm, Sweden.

Höglund, T. (1973) *Design of thin plate I girders in shear and bending with special reference to web buckling. Bulletin no. 94*. Division of building statics and structural engineering. Royal Institute of Technology, Stockholm, Sweden.

Höglund, T. (1997) 'Shear Buckling Resistance of Steel and Aluminium Plate Girders', *Thin-Walled Structures*, 29, pp. 1–4.

Huang, Y. and Young, B. (2012) 'Material properties of cold-formed lean duplex stainless steel sections', *Thin-Walled Structures*.

Huang, Y. and Young, B. (2013) 'Experimental and numerical investigation of cold-formed lean duplex stainless steel flexural members', *Thin-Walled Structures*, 73, pp. 216–228.

Huang, Y. and Young, B. (2014) 'Structural performance of cold-formed lean duplex stainless steel columns', *Thin-Walled Structures*. Elsevier, 83, pp. 59–69.

Javidan, F., Heidarpour, A., Zhao, X.-L., Hutchinson, C.R. and Minkkinen, J. (2016) 'Effect of weld on the mechanical properties of high strength and ultra-high strength steel tubes in fabricated hybrid sections', *Engineering Structures*, 118, pp. 16–27.

Joint ASCE-AASHO Committee on Flexural Members (1968) 'Design of hybrid steel beams, report of the Subcommittee 1 on hybrid beams and girders', *Journal of*

Structural Division. ASCE, 94(6), pp. 1397–1426.

Keerthan, P. and Mahendran, M. (2011) 'New design rules for the shear strength of LiteSteel beams', *Journal of Constructional Steel Research*. Elsevier, 67(6), pp. 1050–1063.

Keerthan, P. and Mahendran, M. (2015) 'Improved shear design rules of cold-formed steel beams', *Engineering Structures*. Elsevier, 99, pp. 603–615.

Kemp, A.R. (1985) 'I Interaction of Plastic Local and Lateral Buckling', *Journal of Structural Engineering*. American Society of Civil Engineers, 111(10), pp. 2181–2196.

Kiymaz, G. (2005) 'Strength and stability criteria for thin-walled stainless steel circular hollow section members under bending', *Thin-walled structures*. Elsevier, 43(10), pp. 1534–1549.

Kouhi, J., Talja, A., Salmi, P. and Ala-Outinen, T. (2000) 'Current R&D work on the use of stainless steel in construction in Finland', *Journal of Constructional Steel Research*. Elsevier, 54(1), pp. 31–50.

Kuhlmann, U. (1989) 'Definition of flange slenderness limits on the basis of rotation capacity values', *Journal of Constructional Steel Research*. Elsevier, 14(1), pp. 21–40.

Kuwamura, H. (2003) 'Local buckling of thin-walled stainless steel members', *Steel Structures*, 3(3), pp. 191–201.

Lin, S.-H., Yu, W.-W. and Galambos, T. V (1992) 'ASCE LRFD method for stainless steel structures', *Journal of Structural Engineering*. American Society of Civil Engineers, 118(4), pp. 1056–1070.

Liu, Y. and Young, B. (2003) 'Buckling of stainless steel square hollow section compression members', *Journal of Constructional Steel Research*. Elsevier, 59(2), pp. 165–177.

McDermott, J.F. (1969) 'Plastic bending of A514 steel beams', *Journal of the Structural Division*. ASCE, 95(9), pp. 1851–1871.

Mirambell, E. and Real, E. (2000) 'On the calculation of deflections in structural stainless steel beams: an experimental and numerical investigation', *Journal of Constructional Steel Research*. Elsevier, 54(1), pp. 109–133.

Nagarajarao, N.R., Marek, P. and Tall, L. (1972) 'Welded hybrid steel columns', *Welding Journal*, 51(9), pp. 4625–4725.

Narendra, P.V.R. and Singh, K.D. (2016) 'Structural performance of elliptical hollow section (EHS) steel tubular braces under extremely low cycle fatigue loading-a finite element study', *Thin-Walled Structures*. Elsevier, 109, pp. 202–216.

NAS (2001) 'North American Specification for the Design of Cold-Formed Steel Structural Members, American Iron and Steel Institute, Washington, D.C. USA'.

Nguyen, C.T., Joo, H.-S., Moon, J. and Lee, H.-E. (2012) 'Flexural-torsional buckling strength of I-girders with discrete torsional braces under various loading conditions', *Engineering Structures*. Elsevier, 36, pp. 337–350.

Olsson, A. (2001) 'Stainless steel plasticity: material modelling and structural applications. PhD Thesis. Lulea University of Technology, Sweden.'

Patton, M.L. and Singh, K.D. (2012) 'Numerical modeling of lean duplex stainless steel hollow columns of square , L- , T- , and +- shaped cross sections under pure axial compression', *Thin-Walled Structures*. Elsevier, 53, pp. 1–8.

Pham, C.H. and Hancock, G.J. (2012) 'Direct strength design of cold-formed C-sections for shear and combined actions', *Journal of Structural Engineering*. American Society of Civil Engineers, 138(6), pp. 759–768.

Pham, S.H., Pham, C.H. and Hancock, G.J. (2014) 'Direct strength method of design for shear including sections with longitudinal web stiffeners', *Thin-Walled Structures*.

Elsevier, 81, pp. 19–28.

Ramberg, W. and Osgood, W.R. (1943) 'Description of stress-strain curves by three parameters, Technical Note No. 902, National Advisory Committee for Aeronautics, Washington, DC'.

Rasmussen, K.J.R. (2003) 'Full-range stress–strain curves for stainless steel alloys', *Journal of constructional steel research*. Elsevier, 59(1), pp. 47–61.

Rasmussen, K.J.R. and Hancock, G.J. (1993) 'Design of cold-formed stainless steel tubular members. II: Beams', *Journal of Structural Engineering*. American Society of Civil Engineers, 119(8), pp. 2368–2386.

Real, E. and Mirambell, E. (2005a) 'Flexural behaviour of stainless steel beams', *Engineering Structures*, 27, pp. 1465–1475. doi: 10.1016/j.engstruct.2005.04.008.

Real, E. and Mirambell, E. (2005b) 'Flexural behaviour of stainless steel beams', *Engineering Structures*. Elsevier, 27(10), pp. 1465–1475.

Real, E., Mirambell, E. and Estrada, I. (2007) 'Shear response of stainless steel plate girders', *Engineering Structures*. Elsevier, 29(7), pp. 1626–1640.

Rossi, B. and Rasmussen, K.J.R. (2012) 'Carrying capacity of stainless steel columns in the low slenderness range', *Journal of Structural Engineering*. American Society of Civil Engineers, 139(6), pp. 1088–1092.

Sachidananda, K. and Singh, K.D. (2015) 'Numerical study of fixed ended lean duplex stainless steel (LDSS) flat oval hollow stub column under pure axial compression', *Thin-Walled Structures*. Elsevier, 96, pp. 105–119.

Sachidananda, K. and Singh, K.D. (2017) 'Structural behaviour of fixed ended stocky Lean Duplex Stainless Steel (LDSS) flat oval hollow column under axial compression', *Thin-Walled Structures*. Elsevier, 113, pp. 47–60.

Saliba, N. and Gardner, L. (2013a) 'Cross-section stability of lean duplex stainless steel welded I-sections', *Journal of Constructional Steel Research*, 80, pp. 1–14.

Saliba, N. and Gardner, L. (2013b) 'Experimental study of the shear response of lean duplex stainless steel plate girders', *Engineering Structures*. Elsevier, 46, pp. 375–391.

Saliba, N., Real, E. and Gardner, L. (2014) 'Shear design recommendations for stainless steel plate girders', *Engineering Structures*, 59, pp. 220–228.

Schafer, B.W. (2008) 'The direct strength method of cold-formed steel member design', *Journal of constructional steel research*. Elsevier, 64(7–8), pp. 766–778.

Schafer, B.W. and Pekoz, T. (1998) 'Direct strength prediction of cold-formed steel members using numerical elastic buckling solutions'. University of Missouri--Rolla.

Schilling, C.G. (1988) 'Moment-rotation tests of steel bridge girders', *Journal of Structural Engineering*. American Society of Civil Engineers, 114(1), pp. 134–149.

SCI-P413 (2017) *Design manual for structural stainless steel*. 4th edn. Edited by N. R. Baddoo. Silwood Park, Ascot, Berkshire, UK: SCI (The Steel Construction Institute).

Shokouhian, M. and Shi, Y. (2014) 'Investigation of ductility in hybrid and high strength steel beams', *International Journal of Steel Structures*, 14(2), pp. 265–279.

Shokouhian, M. and Shi, Y. (2015) 'Flexural strength of hybrid steel I-beams based on slenderness', *Engineering Structures*. Elsevier, 93, pp. 114–128.

Shokouhian, M., Shi, Y. and Head, M. (2016) 'Interactive buckling failure modes of hybrid steel flexural members', *Engineering Structures*, 125, pp. 153–166.

Sieurin, H., Sandström, R. and Westin, E.M. (2006) 'Fracture toughness of the lean duplex stainless steel LDX 2101', *Metallurgical and materials transactions A*. Springer, 37(10), pp. 2975–2981.

Silvestre, N., Pires, T. and Duarte, A.P.C. (2013) 'Numerical analysis of semi-elliptical

hollow section columns', *Proceedings of the Institution of Civil Engineers-Structures and Buildings*. Thomas Telford Ltd, 166(8), pp. 424–433.

Singh, T.G. and Singh, K.D. (2017) 'Structural performance of YSt–310 cold–formed tubular steel stub columns', *Thin-Walled Structures*. Elsevier, 121, pp. 25–40.

Sonu, J.K. and Singh, K.D. (2017) 'Shear characteristics of Lean Duplex Stainless Steel (LDSS) rectangular hollow beams', *Structures*. Institution of Structural Engineers, 10, pp. 13–29.

Theofanous, M., Chan, T.M. and Gardner, L. (2009a) 'Flexural behaviour of stainless steel oval hollow sections', *Thin-Walled Structures*. Elsevier, 47(6–7), pp. 776–787.

Theofanous, M., Chan, T.M. and Gardner, L. (2009b) 'Structural response of stainless steel oval hollow section compression members', *Engineering Structures*.

Theofanous, M. and Gardner, L. (2008) 'Discrete and continuous treatment of local buckling in stainless steel elements', *Journal of Constructional Steel Research*, 64, pp. 1207–1216.

Theofanous, M. and Gardner, L. (2009) 'Testing and numerical modelling of lean duplex stainless steel hollow section columns', *Engineering Structures*, 31, pp. 3047–3058.

Theofanous, M. and Gardner, L. (2010) 'Experimental and numerical studies of lean duplex stainless steel beams', *Journal of Constructional Steel Research*. Elsevier, 66(6), pp. 816–825.

Theofanous, M., Liew, A. and Gardner, L. (2012) 'Ultimate capacity of stainless steel RHS subjected to combined compression and bending', in *Proceedings of the 14th International Symposium on Tubular Structures, London, UK*, pp. 423–430.

Topkaya, C. (2006) 'A numerical study on linear bifurcation web buckling of steel I-beams in the sidesway mode', *Engineering structures*. Elsevier, 28(7), pp. 1028–1037.

Veljkovic, M. and Johansson, B. (2004) 'Design of hybrid steel girders', *Journal of Constructional Steel Research*. Elsevier, 60(3–5), pp. 535–547.

Wasserman, E.P., Pate, W.H. and Huff, T. (2003) 'The Evolution of Best Practices with High Performance Steel for Bridges'.

White, D.W. (2004) 'Unified provisions for flexural capacity of steel bridge I-sections', *School of Civil and Environmental Engineering, Georgia Institute of Technology, Atlanta, GA*.

White, D.W. and Jung, S.-K. (2007) 'Effect of web distortion on the buckling strength of noncomposite discretely-braced steel I-section members', *Engineering structures*. Elsevier, 29(8), pp. 1872–1888.

Wilkerson, S. (2005) 'A smooth shear strength function for steel flexural members', *Engineering structures*. Elsevier, 27(8), pp. 1268–1277.

Yamada. and Kato (1988) 'Strength and deformation of H-shaped stainless steel beams. Japanese Institution of Archirtecture', *Journal of the Kanto Branch*.

Yuan, H.X., Wang, Y.Q., Shi, Y.J. and Gardner, L. (2014a) 'Residual stress distributions in welded stainless steel sections', *Thin-Walled Structures*. Elsevier, 79, pp. 38–51.

Yuan, H.X., Wang, Y.Q., Shi, Y.J. and Gardner, L. (2014b) 'Stub column tests on stainless steel built-up sections', *Thin-Walled Structures*, 83, pp. 103–114.

Zhao, X.L., Al-Mahaidi, R. and Tao, Z. (2004) 'Stub column tests of fabricated square and triangular sections utilizing very high strength steel tubes', *Journal of Constructional Steel Research*, 60(11), pp. 1637–1661.

Zhou, F. and Young, B. (2005) 'Tests of cold-formed stainless steel tubular flexural members', *Thin-walled structures*. Elsevier, 43(9), pp. 1325–1337.

Zhu, J.H. and Young, B. (2012) 'Design of cold-formed steel oval hollow section columns', *Journal of Constructional Steel Research*. Elsevier, 71, pp. 26–37.

APPENDIX A

DESIGN SAMPLE OF HSS I-beams

Flexural capacity calculation for HSS I-beams under 3PB (I-200×140×12×7.2)

A1 ***Classification of cross-section elements (Table 5.2 of EN 1993-1-4 (2006+A1, 2015)***

a) ***Web***

Material properties

$\sigma_{0.2tw}$ = 525.5 MPa, $\sigma_{0.2bw}$ = 504 MPa, $\sigma_{utw} = \sigma_{ubw}$ 727.5 MPa

c_w/t_w = 200/7.2 = 27.8, 72ε = 47.52

$c_w/t_w < 72\varepsilon$, therefore it is Class 1

b) ***Flange***

Material properties

$\sigma_{0.2tf}$ = 652 MPa, $\sigma_{0.2tf}$ = 652 MPa, $\sigma_{utf} = \sigma_{ubf}$ = 854 MPa

c_f = (140-7.2)/2 = 66 mm, c_f/t_f = 66/12 = 5.5, 9ε = 5.55

$c_f/t_f < 9\varepsilon$, therefore it is Class 1

A2 ***Eurocode (EN 1993-1-4 (2006+A1, 2015)) Design calculation***

A2.1 ***Effective widths in Class 4 cross-section***

a)***Web***

There is no reduction due to local buckling since this section is not a slender section (i.e. Class 4).

b) *Flange*

There is no reduction due to local buckling since this section is not a slender section (i.e. Class 4).

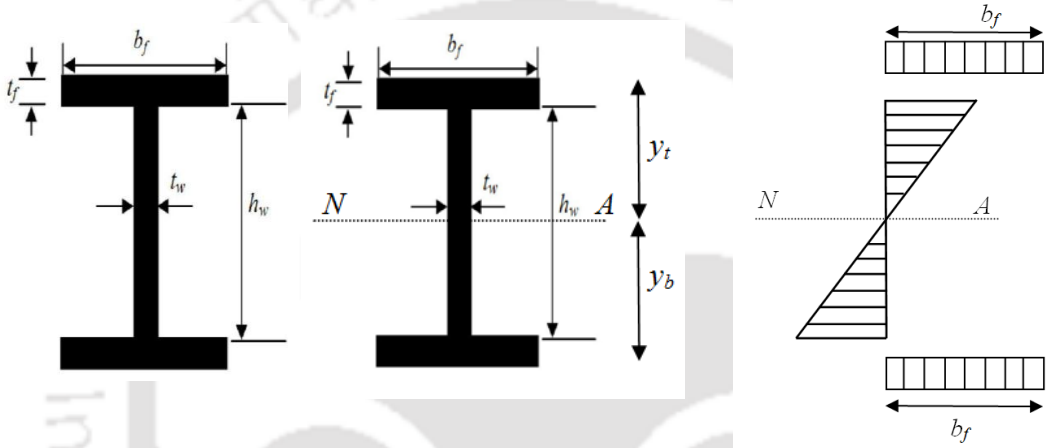

A2.2 *Calculation of neutral axis*

Neutral axis depth from bottom edge of tension flange is denoted by y_b. Taking moment of area about bottom edge of the tension flange:

$$y_b = \frac{\left(b_f \times t_f \times \left(t_f + h_w + 0.5 \times t_f\right)\right) + \left(h_w \times t_w \times \left(t_f + 0.5 \times h_w\right)\right) + \left(b_f \times t_f \times \left(0.5 \times t_f\right)\right)}{A}$$

$$y_b = \frac{\left(140 \times 12\left(12 + 200 + 6\right)\right) + \left(200 \times 7.2 \times \left(12 + 100\right)\right) + \left(140 \times 12 \times \left(0.5 \times 12\right)\right)}{140 \times 12 \times 2 + 200 \times 7.2} = 112 \text{ mm}$$

$$y_t = y_b = 112 \text{ mm}$$

$$A = 140 \times 2 \times 12 + 200 \times 7.2 = 4800 \text{ mm}^2$$

A2.3 *Calculation of effective moment capacity*

$$M_{EN} = \begin{cases} M_p & M_p = W_{pltf}\sigma_{0.2tf} + W_{plbf}\sigma_{0.2bf} + W_{pltw}\sigma_{0.2tw} + W_{plbw}\sigma_{0.2bw} \\ M_{el} & M_{el} = W_{eltf}\sigma_{0.2tf} + W_{elbf}\sigma_{0.2bf} + W_{eltw}\sigma_{0.2tw} + W_{elbw}\sigma_{0.2bw} \\ M_{eff} & M_{eff} = W_{efftf}\sigma_{0.2tf} + W_{elbf}\sigma_{0.2bf} + W_{efftw}\sigma_{0.2tw} + W_{elbw}\sigma_{0.2bw} \end{cases}$$

Hence, $M_{EN} = M_p$ (Class 1 sections)

$$M_p = \{(140\times12(112-0.5\times12))\times2\times652\} + \{(100\times7.2\times50)\times525.5\} + \{(100\times7.2\times50)\times504\}$$

M_p = 269.28 kNm

M_{EN} = 269.28 kNm; M_u = 301.43 kNm

$$\frac{M_u}{M_{EN}} = 1.12$$

A3 *Flexural capacity based on Direct Strength Method (DSM)*

$$\lambda_l = \sqrt{\frac{M_{el}}{M_{crl}}} = 0.298$$

M_{crl} is the elastic local buckling capacity determined from FE

$$M_{el} = W_{eltf}\sigma_{0.2tf} + W_{elbf}\sigma_{0.2bf} + W_{eltw}\sigma_{0.2tw} + W_{elbw}\sigma_{0.2bw}$$

$$M_{el} = \frac{\left\{\left(\frac{140\times12^3}{12} + \left(140\times12(112-0.5\times12)^2\right)\right)\times2\times652\right\} + \left\{\left(\frac{7.2\times100^3}{12} + \left(100\times7.2(112-12-50)^2\right)\right)\times525.5\right\} + \left\{\left(\frac{7.2\times100^3}{12} + \left(100\times7.2(112-12-50)^2\right)\right)\times504\right\}}{112}$$

M_{el} = 244.72 kNm

Hence, DSM flexural capacity,

$M_v = M_{el}$ = 244.72 kNm (since $\lambda_l \leq 0.474$)

Modified DSM equation ($M_{v,RR}$) for estimation of moment capacity given by Rossi and Rasmussen, $M_{v,RR} = \left\{1+\left(1-2.11\lambda_l\right)\left(\frac{\sigma_u}{\sigma_{0.2}}-1\right)\right\}M_{el}$

$$M_{v,RR} = \left\{1+\left(1-2.11\times 0.298\right)\left(\frac{816.1}{610.82}-1\right)\right\}\times 244.72 = 275.38 \text{ kNm}$$

$$\sigma_{0.2} = \frac{A_{tf}\sigma_{0.2tf} + A_{bf}\sigma_{0.2bf} + A_{tw}\sigma_{0.2tw} + A_{bw}\sigma_{0.2bw}}{A}$$

$$\sigma_{0.2} = \frac{140\times 12\times 652\times 2 + 100\times 7.2\times 525.5 + 100\times 7.2\times 504}{4800} = 610.82 \text{ MPa}$$

$$\sigma_u = \frac{A_{tf}\sigma_{utf} + A_{bf}\sigma_{ubf} + A_{tw}\sigma_{utw} + A_{bw}\sigma_{ubw}}{A}$$

$$\sigma_{0.2} = \frac{140\times 12\times 854\times 2 + 100\times 7.2\times 727.5 + 100\times 7.2\times 727.5}{4800} = 816.10 \text{ MPa}$$

Proposed DSM formulation, $M_{v,P} = \frac{1}{P_y}\left[\begin{matrix}\left\{2A_f\sigma_{uf} + 2.58\lambda_l\left(A_f\sigma_{0.2f} - A_f\sigma_{uf}\right)\right\}+ \\ \left\{A_w\sigma_{uw} + 1.29\lambda_l\left(A_w\sigma_{0.2w} - A_w\sigma_{uw}\right)\right\}\end{matrix}\right]M_{el}$

$$P_y = 2A_f\sigma_{0.2f} + A_w\sigma_{0.2w} = 2\times 140\times 12\times 652 + 200\times 7.2\times 515 = 2932320 \text{ N}$$

$$\left[\left\{2\times 140\times 12\times 854 + 2.58\times 0.298\left(140\times 12\times 652 - 140\times 12\times 854\right)\right\}+\right.$$

$$M_{v,P} = \{200\times 7.2\times 727.5 + 1.29\times 0.298(200\times 7.2\times 515 - 200\times 7.2\times 727.5)\}]\frac{244.72}{2932320}$$

$M_{v,P}$ = 295.42 kNm; M_u = 301.43 kNm

$$\frac{M_u}{M_v} = 1.23;\ \frac{M_u}{M_{v,RR}} = 1.09;\ \frac{M_u}{M_{v,P}} = 1.02$$

APPENDIX B

DESIGN SAMPLE OF HSS PLATE GIRDERS

Shear capacity calculation for HSS plate girder I-600×200×12×4

B1 ***Classification of cross-section elements (Table 5.2 of EN 1993-1-4 (2006+A1, 2015))***

a) ***Web***

Material properties

E = 203000 MPa, $\sigma_{0.2w}$ = 504 MPa, σ_{uw} = 727.5 MPa

c_w/t_w = 600/4 = 150 mm, $\varepsilon = \left[\frac{235}{\sigma_{0.2}} \times \frac{E}{210000}\right]^{0.5} = \left[\frac{235}{504} \times \frac{203000}{210000}\right]^{0.5} = 0.67, 90\varepsilon = 60.3$

$c_w/t_w > 90\varepsilon$, therefore it is Class 4

b) ***Flange***

Material properties

E = 2088000 MPa, $\sigma_{0.2f}$ = 652 MPa, σ_{uf} = 854 MPa

c_f = (200-4)/2 = 98 mm, c_f/t_f = 98/12 = 8.17,

$\varepsilon = \left[\frac{235}{\sigma_{0.2}} \times \frac{E}{210000}\right]^{0.5} = \left[\frac{235}{652} \times \frac{208800}{210000}\right]^{0.5} = 0.59, 14\varepsilon = 14\times0.59 = 8.26, 10\varepsilon = 5.9$

$14\varepsilon > c_f/t_f > 10\varepsilon$, therefore it is Class 3

B2 *Eurocode (EN 1993-1-4 (2006+A1, 2015)) Design calculation*

B2.1 *Effective widths in Class 4 cross-section*

a)*Web*

Reduction factor due to local buckling *(According to Equation 5.1 from Clause 5.2.3 of EN 1993-1-4 (2006+A1, 2015))* is

$$\rho = \frac{0.772}{\bar{\lambda}_p} - \frac{0.079}{\bar{\lambda}_p^2} \text{ but } \leq 1$$

Element slenderness *(According to Equation 5.1 from Clause 5.2.3 of EN 1993-1-4 (2006+A1, 2015))* is

$$\bar{\lambda}_p = \frac{\bar{b}/t}{28.4\varepsilon\sqrt{k_\sigma}} = \frac{600/4}{28.4 \times 0.67 \times \sqrt{23.9}} = 1.61$$

$$\rho = \frac{0.772}{1.61} - \frac{0.079}{1.61^2} = 0.45$$

t = relevant thickness, $\bar{b} = h_w$

k_σ is the buckling factor corresponding to the stress ratio ψ and boundary conditions (Table 5.1 or Table 5.2 in EN 1993-1-5) as appropriate

ψ = -1; k_τ = 23.9

$$h_{w,eff} = \frac{\rho h_w}{(1-\psi)} = \frac{0.45 \times 600}{2} = 135 \text{ mm}$$

$h_{w,eff1} = 0.4h_{w,eff}$ = 54 mm, $h_{w,eff2} = 0.6h_{w,eff}$ = 81 mm

Non-effective height of web, $h_{w,non\text{-}eff}$ = 300-(81+54) = 165 mm

b) *Flange*

There is no reduction due to local buckling since this section is not a slender section (i.e. Class 4).

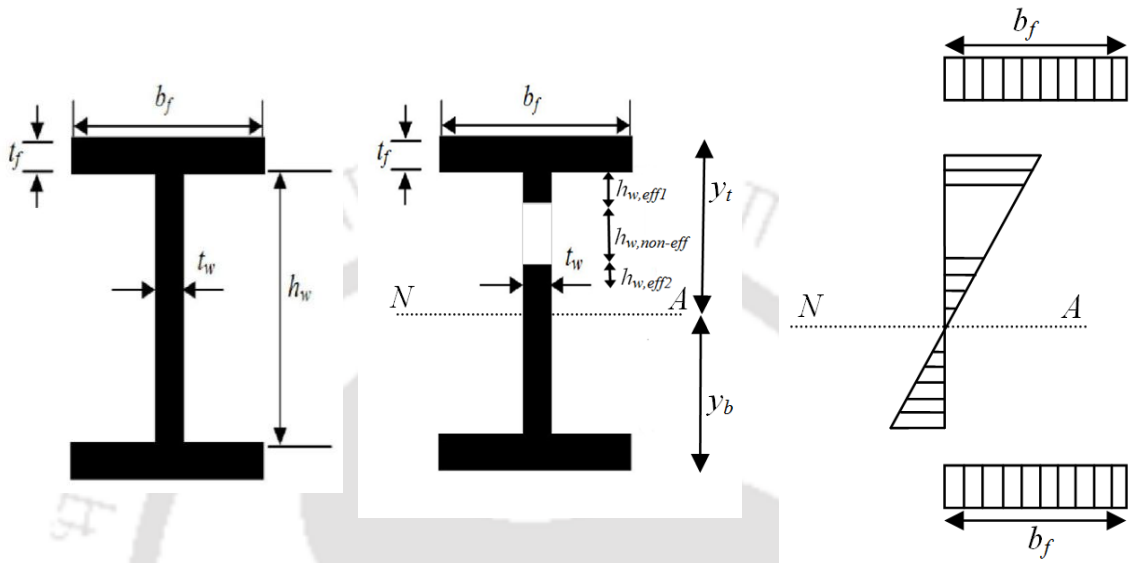

B2.2 ***Calculation of neutral axis***

Neutral axis depth from bottom edge of tension flange is denoted by y_b. Taking moment of area about bottom edge of the tension flange:

$$\left(b_f \times t_f \times \left(t_f + h_w + 0.5 \times t_f\right)\right) + \left(h_{w,eff\,1} \times t_w \times \left(t_f + h_w - 0.5 \times h_{w,eff\,1}\right)\right) + \left(h_{w,eff\,2} \times t_w \times \left(t_f +\right.\right.$$

$$y_b = \frac{\left.\left.0.5 \times h_w + 0.5 \times h_{w,eff\,2}\right)\right) + \left(0.5 \times h_w \times t_w \times \left(t_f + 0.5 \times 0.5 \times h_w\right)\right) + \left(b_f \times t_f \times \left(0.5 \times t_f\right)\right)}{A_{eff}}$$

$$\left(200 \times 12 \times \left(12 + 600 + 0.5 \times 12\right)\right) + \left(54 \times 4 \times \left(12 + 600 - 0.5 \times 54\right)\right) + \left(81 \times 4 \times \left(12 + 0.5 \times 600\right.\right.$$

$$y_b = \frac{\left.\left. + 0.5 \times 81\right)\right) + \left(0.5 \times 600 \times 4 \times \left(12 + 0.5 \times 0.5 \times 600\right)\right) + \left(200 \times 12 \times \left(0.5 \times 12\right)\right)}{6540}$$

y_b = 295.5 mm

$y_t = h_w + 2t_f - y_b = 600 + 2\times12 - 295.5 = 328.5$ mm

Effective Area, $A_{eff} = 200\times12\times2 + 54\times4 + 81\times4 + 300\times4 = 6540$ mm^2

B2.3 ***Calculation of effective bending strength***

$$W_{eff} = \frac{Moment\ of\ inertia}{y_{\max}} = \frac{Moment\ of\ inertia}{y_t}$$

$$W_{eff} = \frac{\begin{aligned}&\left\{\left(\frac{b_f\times t_f^3}{12}\right) + b_f\times t_f\times\left(y_t - 0.5\times t_f\right)^2\right\} + \left\{\left(\frac{t_w\times h_{w,eff\,1}^3}{12}\right) + t_w\times h_{w,eff\,1}\times\left(y_t - t_f - 0.5\times h_{w,eff\,1}\right)^2\right\} + \\ &\left\{\left(\frac{t_w\times h_{w,eff\,2}^3}{12}\right) + t_w\times h_{w,eff\,2}\times\left(y_t - t_f - h_{w,eff\,1} - h_{w,non-eff} - 0.5\times h_{w,eff\,2}\right)^2\right\} + \left\{\left(\frac{t_w\times(0.5\times h_w)^3}{12}\right)\right. \\ &\left. + t_w\times0.5\times h_w\times\left(y_b - t_f - 0.5\times0.5\times h_w\right)^2\right\} + \left\{\left(\frac{b_f\times t_f^3}{12}\right) + b_f\times t_f\times(y_b - 0.5\times t_f)^2\right\}\end{aligned}}{y_t}$$

$$W_{eff} = \frac{\begin{aligned}&\left\{\left(\frac{200\times12^3}{12}\right) + 200\times12\times\left(328.5 - 0.5\times12\right)^2\right\} + \left\{\left(\frac{4\times54^3}{12}\right) + 4\times54\times\left(328.5 - 12 - 0.5\times54\right)^2\right\} + \\ &\left\{\left(\frac{4\times81^3}{12}\right) + 4\times81\times\left(328.5 - 12 - 54 - 165 - 0.5\times81\right)^2\right\} + \left\{\left(\frac{4\times(0.5\times600)^3}{12}\right)\right. \\ &\left. + 4\times0.5\times600\times\left(295.5 - 12 - 150\right)^2\right\} + \left\{\left(\frac{200\times12^3}{12}\right) + 200\times12\times(295.5 - 0.5\times12)^2\right\}\end{aligned}}{328.5}$$

$W_{eff} = 1523863.70$ mm^3

Effective bending strength,

$$M_{eff,Rd} = \frac{Z_{eff}\times\sigma_{0.2avg}}{\gamma_{mo}} = \frac{1523863.70\times602.67}{1.0} = 918.38\ \text{kNm}$$

$$\sigma_{0.2avg} = \frac{2\sigma_{0.2f}A_f + \sigma_{0.2w}A_w}{2A_f + A_w} = \frac{2\times 652\times 12\times 200 + 504\times 4\times 600}{2\times 200\times 12 + 4\times 600} = 602.67 \text{ MPa}$$

B2.4 ***Calculation of design plastic moment capacity***

$$W_{pl} = (200\times 12\times(312-6)\times 2) + (300\times 4\times(312-12-150)\times 2) = 1828800 \text{ mm}^3$$

$$M_{pl,Rd} = \frac{\{(200\times 12\times(312-6)\times 2) + (300\times 4\times(312-12-150)\times 2)\}\times 602.67}{1.0}$$

$M_{pl,Rd}$ = 1102.16 kNm

B2.5 ***Calculation of design plastic moment of flanges***

$$M_{f,Rd} = \frac{\{(200\times 12\times(328.65-6)) + (200\times 12\times(295.5-6))\}\times 652}{1.0} = 957.89 \text{ kNm}$$

B2.6 ***Calculation of web slenderness***

$$\lambda_w = \frac{h_w}{37.4t_w\varepsilon\sqrt{k_\tau}} = \frac{600}{37.4\times 4\times 0.67\times\sqrt{9.34}} = 1.96$$

k_τ is the minimum shear buckling co-efficient for the web panel

$$k_\tau = 5.34 + 4.00\left(\frac{h_w}{a}\right) \quad \text{when} \left(\frac{a}{h_w}\right) \geq 1$$

$$= 4.00 + 5.34\left(\frac{h_w}{a}\right) \quad \text{when} \left(\frac{a}{h_w}\right) < 1$$

a is the clear span

Therefore, $k_\tau = 5.34 + 4.00\left(\frac{600}{600}\right) = 9.34$

B2.7 ***Calculation of design shear resistances***

The shear design resistance ($V_{b,Rd}$) is the total shear contribution from the web ($V_{bw,Rd}$) and flanges ($V_{bf,Rd}$), therefore

$$V_{b,Rd} = V_{bf,Rd} + V_{bw,Rd} \le \frac{\eta \sigma_{0.2w} h_w t_w}{\sqrt{3}\gamma_{M1}}$$

Shear contribution from web, $V_{bw,Rd} = \frac{\chi_w \sigma_{0.2w} h_w t_w}{\sqrt{3}\gamma_{M1}}$

χ_w is the web buckling reduction factor for rigid end post (*Clause 5.6 of EN 1993-1-4 ()*),

$$\chi_w = \frac{1.56}{0.91 + \bar{\lambda}_w} = \frac{1.56}{0.91 + 1.96} = 0.544 \qquad \text{for } \lambda_w \ge 0.65$$

$$\chi_{w,P} = \frac{4}{4.5 + \bar{\lambda}_w} = \frac{4}{4.5 + 1.96} = 0.62 \qquad \text{for } \lambda_w > 1.5$$

$$V_{bw,Rd} = \frac{0.54 \times 504 \times 600 \times 4}{\sqrt{3} \times 1.0} = 380.15 \text{ kN} \; ; \; V_{bw,Rd,P} = \frac{0.62 \times 504 \times 600 \times 4}{\sqrt{3} \times 1.0} = 432.70 \text{ kN}$$

Shear contribution from flange, $V_{bf,Rd} = \left(\frac{b_f t_f^2 \sigma_{0.2f}}{c \gamma_{M1}} \right) \left(1 - \left(\frac{M_{Ed}}{M_{f,Rd}} \right)^2 \right)$

M_{ed} and $M_{f,Rd}$ are the design bending resistance and plastic moment of flanges respectively; and c is the width of tension band,

$$c = \left(0.17 + \frac{3.5 b_f t_f^2 \sigma_{0.2f}}{t_w h_w^2 \sigma_{0.2w}} \right) a = \left(0.17 + \frac{3.5 \times 200 \times 12^2 \times 652}{4 \times 600^2 \times 504} \right) \times 600 = 156.33 \text{ mm}$$

$M_{ed} = V_{u,FE} \times 0.6 = 565 \times 0.6 = 339$ kNm

$$V_{bf,Rd} = \left(\frac{200 \times 12^2 \times 652}{156.33 \times 1.0} \right) \left(1 - \left(\frac{339}{957.89} \right)^2 \right) = 105.06 \text{ kN}$$

$$V_{b,Rd} = V_{bf,RD} + V_{bw,RD} \le \frac{\eta \sigma_{0.2w} h_w t_w}{\sqrt{3}\gamma_{M1}}$$

$V_{b,Rd} = 105.06 + 380 = 485.06$ kN; $V_{b,Rd,P} = 105.06 + 432.98 = 538.04$ kN

$$\frac{\eta \sigma_{0.2w} h_w t_w}{\sqrt{3}\gamma_{M1}} = \frac{1.2 \times 504 \times 600 \times 4}{\sqrt{3} \times 1.0} = 838.04 \text{ kN}$$

Therefore, $V_{b,Rd} \leq \frac{\eta \sigma_{0.2w} h_w t_w}{\sqrt{3}\gamma_{M1}}$ (OK)

B2.8 ***Calculation of shear-moment (M-V) interaction***

Shear-Moment interaction occurs when design shear force exceeds 50% of web shear resistance, when $V_{ED} < 50\%\ V_{bw,Rd}$, interaction is ignored.

$V_{u,FE}$ = 565 kN; 50% $V_{bw,Rd}$ = 0.5×380.15 = 190 kN

Since $V_{u,FE} \geq 50\%\ V_{bw,Rd}$, hence, interaction should be considered.

$$\bar{\eta}_1 + \left(1 - \frac{M_{f,Rd}}{M_{pl,Rd}}\right)\left(2\bar{\eta}_3 - 1\right)^2 \leq 1.0 \qquad \text{for } \bar{\eta}_1 \geq \frac{M_{f,Rd}}{M_{pl,Rd}}$$

$$\bar{\eta}_1 = \frac{M_{Ed}}{M_{pl,Rd}}; \quad \bar{\eta}_3 = \frac{V_{Ed}}{V_{bw,Rd}}; \quad \frac{M_{f,Rd}}{M_{pl,Rd}} = \frac{957.89}{1102.16} = 0.87$$

Table A1 M-V interaction from EN 1993-1-4 (*2006+A1, 2015*)

M_{Ed}	$V_{bf,Rd}$	$V_{b,Rd} = V_{bf,Rd} + V_{bf,Rd}$	$M_{Ed}/M_{c,Rd}$	$V_{Ed}/V_{b,Rd}$
0	120.12	500.12	0.00	1.32
50	119.79	499.79	0.05	1.32
100	118.81	498.81	0.09	1.31
150	117.17	497.17	0.14	1.31
200	114.88	494.88	0.18	1.30
250	111.93	491.93	0.23	1.29
300	108.33	488.33	0.27	1.29
350	104.08	484.08	0.32	1.27
400	99.17	479.17	0.36	1.26
450	93.61	473.61	0.41	1.25
500	87.39	467.39	0.45	1.23
550	80.52	460.52	0.50	1.21
600	72.99	452.99	0.54	1.19
650	64.81	444.81	0.59	1.17
700	55.97	435.97	0.64	1.15
730	50.35	430.35	0.66	1.13
750	46.48	426.48	0.68	1.12
800	36.33	416.33	0.73	1.10
850	25.53	405.53	0.77	1.07
900	14.08	394.08	0.82	1.04
950	1.97	381.97	0.86	1.01
957.89	0.00	380.00	0.87	1.00

980			0.89	0.96
1000			0.91	0.92
1030			0.93	0.85
1060			0.96	0.77
1090			0.99	0.65
1102			1.00	0.52
1102.16			1.00	0.50

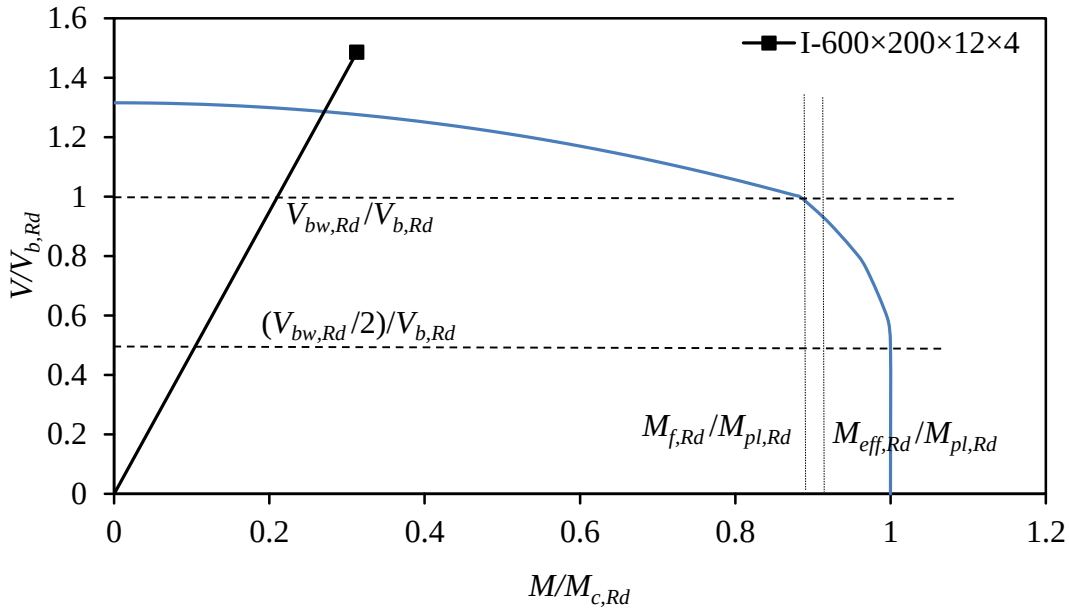

$V_u = 565$ kN; $\frac{V_u}{V_{EN}} = \frac{565}{380.15} = 1.49$; $\frac{V_u}{V_{EN,P}} = \frac{565}{432.70} = 1.31$

B3 ***Shear resistance based on Direct Strength Method (DSM)***

$$\lambda_l = \sqrt{\frac{V_{yw}}{V_{cr}}} = \sqrt{\frac{725.76}{377.80}} = 1.386$$

$$V_{yw} = \frac{\sigma_{0.2w} h_w t_w}{\sqrt{3}} = 0.6 \times 504 \times 600 \times 4 = 725.76 \text{ kN}$$

V_{cr} is the elastic shear buckling capacity determined from FE.

B3.1 ***Calculation of DSM without post buckling***

DSM shear resistance (V_v) without post buckling is calculated as:

$$V_v = \frac{V_{yw}}{\lambda_l^2} = \frac{725.76}{1.386^2} = 377.88 \text{ kN}$$

B3.2 ***Calculation of DSM with inclusion of post buckling***

DSM shear capacity ($V_{v,KM}$) including the effect of post-buckling strength proposed by Keerathan and Mahendran (2015)

$$V_{v,KM} = V_{yw}\left\{\frac{1}{\lambda_l^2} + 0.25\left(1 - \frac{1}{\lambda_l^2}\right)\right\} = 725.76\left\{\frac{1}{1.386^2} + 0.25\left(1 - \frac{1}{1.386^2}\right)\right\} = 464.86 \text{ kN}$$

Proposed DSM shear resistance, $V_{v,P} = V_{yw}\left\{\frac{0.9}{\lambda_l^2} + 0.35\left(1 - \frac{1}{\lambda_l^2}\right)\right\}$

$$V_{v,P} = 698.36\left\{\frac{0.9}{1.386^2} + 0.35\left(1 - \frac{1}{1.386^2}\right)\right\} = 461.85 \text{ kN}$$

$V_u = 565$ kN; $\frac{V_u}{V_v} = \frac{565}{377.88} = 1.50$; $\frac{V_u}{V_{v,KM}} = \frac{565}{464.86} = 1.22$;

$$\frac{V_u}{V_{v,P}} = \frac{565}{461.85} = 1.22$$

APPENDIX C

DESIGN SAMPLE OF HSS STUB COLUMNS

Compression resistance calculation for HSS stub column I-200×140×8×6

C1 ***Classification of cross-section elements (Table 5.2 of EN 1993-1-4 (2006+A1, 2015))***

a) ***Web***

Material properties

E = 203000 MPa, $\sigma_{0.2w}$ = 504 MPa, σ_{uw} = 727.5 MPa

$c_w/t_w = 200/6 = 33.33,\ \varepsilon = \left[\frac{235}{\sigma_{0.2}} \times \frac{E}{210000}\right]^{0.5} = \left[\frac{235}{504} \times \frac{203000}{210000}\right]^{0.5} = 0.67, 37\varepsilon = 24.79$

$c_w/t_w > 37\varepsilon$, therefore it is Class 4

b) ***Flange***

Material properties

E = 208800 MPa, $\sigma_{0.2f}$ = 652 MPa, σ_{uf} = 854 MPa

c_f = (140-6)/2 = 67 mm, c_f/t_f = 67/12 = 8.38,

$\varepsilon = \left[\frac{235}{\sigma_{0.2}} \times \frac{E}{210000}\right]^{0.5} = \left[\frac{235}{652} \times \frac{208800}{210000}\right]^{0.5} = 0.59, 14\varepsilon = 14 \times 0.59 = 8.26,$

$c_f/t_f > 14\varepsilon$, therefore it is Class 4

C2 ***Eurocode (EN 1993-1-4 (2006+A1, 2015)) Design calculation***

C2.1 ***Effective widths in Class 4 cross-section***

a)*Web*

Reduction factor due to local buckling *(According to Equation 5.1 from Clause 5.2.3 of EN 1993-1-4 (2006+A1, 2015))* is

$$\rho = \frac{0.772}{\bar{\lambda}_p} - \frac{0.079}{\bar{\lambda}_p^2} \text{ but} \leq 1$$

Element slenderness *(According to Equation 5.1 from Clause 5.2.3 of EN 1993-1-4 (2006+A1, 2015))* is

$$\bar{\lambda}_p = \frac{\bar{b}/t}{28.4\varepsilon\sqrt{k_\sigma}} = \frac{200/4}{28.4 \times 0.67 \times \sqrt{4}} = 0.87$$

$$\rho = \frac{0.772}{0.87} - \frac{0.079}{0.87^2} = 0.78$$

t = relevant thickness; $\bar{b} = h_w$

k_σ is the buckling factor corresponding to the stress ratio ψ and boundary conditions (Table 5.1 or Table 5.2 in EN 1993-1-5) as appropriate

ψ = 1; k_τ = 4

$$A_{w,eff} = \rho A_w = 0.78 \times 200 \times 6 = 935.30 \text{ mm}^2$$

a) *Flange*

Reduction factor due to local buckling *(According to Equation 5.1 from Clause 5.2.3 of EN 1993-1-4 (2006+A1, 2015))* is

$$\rho = \frac{1}{\bar{\lambda}_p} - \frac{0.188}{\bar{\lambda}_p^2} \text{ but} \leq 1$$

Element slenderness *(According to Equation 5.1 from Clause 5.2.3 of EN 1993-1-4 (2006+A1, 2015))* is

$$\bar{\lambda}_p = \frac{\bar{b}/t}{28.4\varepsilon\sqrt{k_\sigma}} = \frac{(140-6)/(8\times 2)}{28.4\times 0.59\times\sqrt{0.43}} = 0.75$$

$$\rho = \frac{1}{0.75} - \frac{0.188}{0.75^2} = 0.99$$

t = relevant thickness; $\bar{b} = \frac{b_f - t_w}{2t_f}$

k_σ is the buckling factor corresponding to the stress ratio ψ and boundary conditions (Table 5.1 or Table 5.2 in EN 1993-1-5) as appropriate

$\psi = 1$; $k_\tau = 0.43$

$$A_{f,eff} = 2\rho A_f = 2\times 0.99\times 140\times 8 = 2234 \text{ mm}^2$$

Therefore total effective area is given by $A_{eff} = A_{w,eff} + A_{f,eff}$ = 935.30 +2234 = 3169.30 mm^2

C2.2 ***Calculation of design resistances***

The design compression resistance (P_{EN}) is calculated as

$$P_{EN} = \begin{cases} A\sigma_{0.2} & \text{Class 1, 2 and 3 sections} \\ A_{eff}\sigma_{0.2} & \text{Class 4 sections} \end{cases}$$

For HSS stub columns, $\sigma_{0.2}$ is taken as their weighted average values, hence

$$\sigma_{0.2} = \frac{A_f\sigma_{0.2f} + A_w\sigma_{0.2w}}{A_f + A_w} = \frac{2\times 140\times 8\times 652 + 200\times 6\times 504}{2\times 140\times 8 + 200\times 6} = 600.37 \text{ MPa}$$

P_{EN} = 3169.30 × 600.37 = 1902.76 kN; P_u = 2063.65 kN

$$\frac{P_u}{P_{EN}} = \frac{2063.65}{1902.76} = 1.08$$

C3 *Column capacity based on Direct Strength Method (DSM)*

The critical elastic load in flexure buckling, $P_{cre} = \frac{\pi^2 EA}{\left(KL/r_y\right)^2}$

$$r_y = \sqrt{\frac{I_{\min}}{A}} = \sqrt{\frac{\left(2\times 8\times 140^3/12\right)+\left(200\times 6^3/12\right)}{3440}} = 32.63 \text{ mm}$$

$$A = 2\times 140\times 8 + 200\times 6 = 3440 \text{ mm}^2$$

$$E = \frac{2\times 140\times 8\times 208800 + 200\times 6\times 203000}{2\times 140\times 8 + 200\times 6} = 206777 \text{ MPa}$$

$$P_{cre} = \frac{\pi^2 EA}{\left(KL/r_y\right)^2} = \frac{\pi^2\times 206777\times 3440}{\left(0.5\times 600/32.63\right)^2} = 83039.192 \text{ kN}$$

$$\lambda_c = \sqrt{P_y/P_{cre}} = \sqrt{2065.28/83039.19} = 0.158$$

$$P_y = 2A_f\sigma_{0.2f} + A_w\sigma_{0.2w} = 2\times 140\times 8\times 652 + 200\times 6\times 504 = 2065.28 \text{ kN}$$

$$P_{ne} = \left(0.658^{\lambda_c^2}\right)P_y = 0.658^{0.158^2}\times 2065.28 = 2043.89 \text{ kN}$$

$$\lambda_L = \sqrt{\frac{P_{ne}}{P_{crl}}} = \sqrt{\frac{2043.89}{3283.90}} = 0.789$$

P_{crl} is the elastic local buckling capacity determined from FE

$$P_{nl} = \left[1 - 0.15\left(\frac{P_{crl}}{P_{ne}}\right)^{0.4}\right]\left(\frac{P_{crl}}{P_{ne}}\right)^{0.4} P_{ne}$$

$$P_{nl} = \left[1 - 0.15\left(\frac{3283.9}{2043.89}\right)^{0.4}\right]\left(\frac{3283.9}{2043.89}\right)^{0.4} 2043.89 = 2022.74 \text{ kN}$$

DSM compression resistance, $P_v = \min(P_{ne}, P_{nl}) = 2022.74$ kN

Modified DSM equation ($P_{v\text{-}RR}$) for estimation of column capacity given by Rossi and Rasmussen, $P_{v,RR} = \left(\frac{0.95}{\lambda_L^{0.8}} - \frac{0.22}{\lambda_L^{1.6}}\right)P_y = \left(\frac{0.95}{0.789^{0.8}} - \frac{0.22}{0.789^{1.6}}\right) \times 2065.28 = 1707.82$ kN

Modified DSM formulation ($P_{v,ARR}$) for determination of column strength proposed by Arrayago *et al.*, $P_{v,ARR} = \left(\frac{1}{\lambda_L^{0.8}} - \frac{0.15}{\lambda_L^{1.6}}\right)P_y = \left(\frac{1}{0.789^{0.8}} - \frac{0.15}{0.789^{1.6}}\right) \times 2065.28 = 2043.91$ kN

Proposed DSM formulation, $P_{v,P} = \left(\frac{0.9}{\lambda_L^{0.8}} - \frac{0.08}{\lambda_L^{1.6}}\right)P_y = \left(\frac{0.9}{0.789^{0.8}} - \frac{0.08}{0.789^{1.6}}\right) \times 2065.28$

$$P_{v,P} = \left(\frac{0.9}{0.789^{0.8}} - \frac{0.08}{0.789^{1.6}}\right) \times 2065.28 = 2005.51 \text{ kN}$$

$P_u = 2063.65$ kN

$$\frac{P_u}{P_v} = \frac{2063.65}{2022.74} = 1.02; \quad \frac{P_u}{P_{v,RR}} = \frac{2063.65}{1707.82} = 1.21; \quad \frac{P_u}{P_{v,ARR}} = \frac{2063.65}{2043.91} = 1.01$$

$$\frac{P_u}{P_{v,P}} = \frac{2063.65}{2005.51} = 1.03$$

LIST OF PUBLICATIONS

A) Journals

Lalthazuala, R. and Singh, K. D., 2019. Investigations on structural performance of hybrid stainless steel I-beams based on slenderness. *Thin-Walled Structures*, 137, 197-212.

Lalthazuala, R. and Singh, K. D., 2019. Structural performance of hybrid stainless steel plate girders under shear. *Thin-Walled Structures*, 143, 106214.

Lalthazuala, R. and Singh, K. D., 2019. Structural behaviour of hybrid stainless steel stub columns under axial compression. (under review)

B) Conferences

Lalthazuala, R. and Singh, K. D., 2019. Shear behaviour of hybrid stainless steel plate girders. *Ninth International conference on Steel and Aluminium Structures (ICAS19). University of Bradford, UK* .